Universitat Autònoma de Barcelona

Impact of Ocean Warming and Acidification on Coccolithophore Ecology and Calcification in the North Pacific

Anaid Rosas-Navarro

Impact of Ocean Warming and Acidification on Coccolithophore Ecology and Calcification in the North Pacific

DOCTORAL THESIS by

Anaid Rosas–Navarro

submitted for the degree of
Doctor of Environmental Science and Technology

PhD directors: Dr. Patrizia Ziveri and Dr. Gerald Langer

UNIVERSITAT AUTÒNOMA DE BARCELONA
Institut de Ciència i Tecnologia Ambientals (ICTA)
PhD programme in Environmental Science and Technology

Barcelona, 2018

"Nuestra lealtad es para las especies y el planeta. Nuestra obligación de sobrevivir no es sólo para nosotros mismos sino también para ese cosmos, antiguo y vasto, del cual derivamos." Carl Sagan (1934–1996)

Creo que un mundo mejor se puede lograr si cada uno se enfoca en superarse disfrutando el proceso sin hacer daño a los demás, esto último incluye no hacer cosas que dañen el futuro del mundo. Anaid Rosas-Navarro

Abstract

Coccolithophores are cosmopolitan unicellular calcifying phytoplankton involved in important biogeochemical global cycles. This PhD thesis focuses on the impacts of ocean warming and acidification on the morphology and calcification of coccolithophores, with special attention to the cosmopolitan and dominant species *Emiliania huxleyi*. The study includes temperature experiments using three strains of *E. huxleyi* isolated in the NW Pacific Ocean, and the analysis of water samples collected along a transect covering the Gulf of California and NE Pacific margin waters. This type of work is timely since global warming and the rapid increase in anthropogenic atmospheric CO_2 have remarkable consequences on the marine environment.

To clarify discrepancies featuring in the literature about the calcification response to temperature changes, we compared three strains of *E. huxleyi* grown under non-limiting nutrient and light conditions, at 10, 15, 20 and 25 °C of temperature. All three strains displayed similar growth rate versus temperature relationships, with an optimum at 20–25 °C. Over the sub-optimum to optimum temperature range (10–25 °C), elemental production (particulate inorganic carbon (PIC), particulate organic carbon (POC), total particulate nitrogen (TPN)), coccolith mass, coccolith size, width of the tube element cycle, number of attached coccoliths per coccosphere, coccosphere mass, individual sinking velocity, individual cell PIC : POC ratio, and coccolith production rate, were positively correlated with temperature. The correlation between PIC production and coccolith mass/size supports the notion that coccolith mass can be used as a proxy for PIC production in sediment samples. We found that incompleteness of coccoliths is not due to time shortage at high PIC production. Sub-optimal growth temperatures lead to an increase in the percentage of malformed coccoliths in a strain-specific fashion. The PIC : POC ratio showed a minimum at optimum growth temperature in all investigated strains. In the context of climate change, global warming might cause a decline in coccolithophore's PIC contribution to the rain ratio, as well as improved fitness in some genotypes due to fewer coccolith malformations; our data also point to an important influence of global warming on sinking velocities.

Given that warming, acidification, and lowered nutrient availability might occur simultaneously under climate change scenarios, there is the question about what the net effect of different influential factors will be. Therefore, we analysed 68 summertime samples along a transect at different stations and depths, giving a large range of conditions. The studied regions are expected to be particularly susceptible to both warming and acidification, and are characterized by high seasonal primary production through upwelling events. We focused the study on the coccosphere standing stock variations of the main morphotypes and morphological variations of the species *E. huxleyi* and on the different species of the genus *Gephyrocapsa*. We found that *E. huxleyi* type O is a colder morphotype enhanced by higher ammonium concentrations and is more tolerant to lower pH values than the morphotype A. The over-calcified *E. huxleyi* type A shared niche with the morphotype O. The observed morphological aberrations and the under-calcified morphology were associated to unfavorable conditions for the cell such as low (though not the lowest) nutrient concentrations. The PIC contribution per liter of *G. oceanica* was higher than that of *E. huxleyi*, in third place was that of *G. muellerae*. *Gephyrocapsa oceanica* presented the highest affinity to warmer waters with lower nutrient concentrations, and *G. muellerae* the highest tolerance to lower pH. In the context of climate change, *G. oceanica* and *G. muellerae* might increase their relative abundance with subsequent changes in the coccolithophore PIC production.

List of publications derived from this work

- Rosas-Navarro, A., Langer, G., and Ziveri, P.: Temperature affects the morphology and calcification of *Emiliania huxleyi* strains, Biogeosciences, 13, 2913–2926, doi:10.5194/bg-13-2913-2016, URL http://www.biogeosciences.net/13/2913/2016/, 2016.

- Rosas-Navarro, A., Langer, G., and Ziveri, P.: Temperature effects on sinking velocity of different *Emiliania huxleyi* strains, PloS one, 13, e0194 386, URL https://doi.org/10.1371/journal.pone.0194386, 2018.

- Wolhowe, M. D., Prahl, F. G., White, A. E., Popp, B. N., and Rosas-Navarro, A.: A biomarker perspective on coccolithophorid growth and export in a stratified sea, Progress in Oceanography, 122, 65 – 76, doi:10.1016/j.pocean.2013.12.001, URL http://www.sciencedirect.com/science/article/pii/S0079661113002292, 2014.

Resumen

Los cocolitofóridos son fitoplancton calcificante unicelular cosmopolita involucrado en importantes ciclos biogeoquímicos globales. Esta tesis doctoral se centra en los impactos del calentamiento del océano y la acidificación sobre la morfología y la calcificación de los cocolitofóridos, con especial atención a la especie cosmopolita y dominante *Emiliania huxleyi*. El estudio incluye experimentos de temperatura usando tres cepas de *E. huxleyi* aisladas en el noroeste del océano Pacífico, y el análisis de muestras de agua colectadas a lo largo de un transecto que cubre aguas del Golfo de California y del margen NE del oceáno Pacífico. Este tipo de trabajo es oportuno dado que el calentamiento global y el rápido aumento del CO_2 antropogénico en la atmósfera tienen consecuencias notables en el medio marino.

Para aclarar discrepancias que aparecen en la literatura sobre la respuesta de la calcificación a los cambios de temperatura, comparamos tres cepas de *E. huxleyi* cultivadas bajo condiciones no limitantes de nutrientes ni de luz, a 10, 15, 20 y 25 °C de temperatura. Las tres cepas mostraron tasas de crecimiento similares en función de la temperatura, con un óptimo en los 20–25 °C. Se correlacionaron positivamente con la temperatura: la producción de elementos particulados (carbono inorgánico particulado (PIC), carbono orgánico particulado (POC), nitrógeno particulado total (TPN)), la masa del cocolito, el tamaño del cocolito, el ancho del ciclo de elementos del tubo de los cocolitos, el número de cocolitos unidos a la cocosfera, la masa de la cocosfera, la velocidad de hundimiento de los individuos, la relación PIC : POC de las células individuales, y la tasa de producción de cocolitos. La correlación entre la producción de PIC y la masa/tamaño del cocolito apoya la noción de que la masa del cocolito se puede usar como proxy para la producción de PIC en muestras de sedimentos. Encontramos que la incompletitud de los coccolitos no se debe a la escasez de tiempo a altas producciones de PIC. Las temperaturas de crecimiento subóptimas aumentan el porcentaje de coccolitos malformados de manera específica en algunas cepas. La relación PIC : POC mostró un mínimo a la temperatura óptima de crecimiento en todas las cepas investigadas. En el contexto del cambio climático, el calentamiento global podría causar una disminución en la contribución del PIC exportado de los cocolitofóridos, podría ser una conveniencia en algunos genotipos debido a una menor cantidad de malforma-

ciones de cocolitos y podría influir de manera importante sobre las velocidades de hundimiento.

Dado que el calentamiento, la acidificación y la menor disponibilidad de nutrientes pueden ocurrir simultáneamente en los escenarios de cambio climático, existe la pregunta sobre cuál será el efecto neto de los diferentes factores de influencia. Por lo tanto, analizamos 68 muestras de verano colectadas en diferentes sitios y profundidades a lo largo de un transecto, dando una amplia gama de condiciones. Se espera que las regiones estudiadas sean particularmente susceptibles tanto al calentamiento como a la acidificación, y se caracterizan por una alta producción primaria estacional a través de eventos de surgencia. Enfocamos el estudio en las principales variaciones morfológicas y de morfotipo de la especie *E. huxleyi*, y también en las diferentes especies del género *Gephyrocapsa*. Descubrimos que *E. huxleyi* tipo O es un morfotipo más frío potenciado por concentraciones más altas de amonio y es más tolerante a valores de pH más bajos que el morfotipo A. El morfotipo A sobre-calcificado compartió el nicho con el morfotipo O. Las aberraciones morfológicas observadas y la morfología sub-calcificada se asociaron a condiciones desfavorables para la célula, tales como bajas (aunque no las más bajas) concentraciones de nutrientes. La contribución de PIC por litro de *G. oceanica* fue más alta que la de *E. huxleyi*, en tercer lugar fue la de *G. muellerae*. *Gephyrocapsa oceanica* presentó la mayor afinidad a las aguas más cálidas con menores concentraciones de nutrientes, y *G. muellerae* la mayor tolerancia a un pH más bajo. En el contexto del cambio climático, *G. oceanica* y *G. muellerae* podrían aumentar su abundancia relativa, generando cambios en la producción de PIC.

Lista de publicaciones derivadas de este trabajo

- Rosas-Navarro, A., Langer, G., and Ziveri, P.: Temperature affects the morphology and calcification of *Emiliania huxleyi* strains, Biogeosciences, 13, 2913–2926, doi:10.5194/bg-13-2913-2016, URL http://www.biogeosciences.net/13/2913/2016/, 2016.

- Rosas-Navarro, A., Langer, G., and Ziveri, P.: Temperature effects on sinking velocity of different *Emiliania huxleyi* strains, PloS one, 13, e0194 386, URL https://doi.org/10.1371/journal.pone.0194386, 2018.

- Wolhowe, M. D., Prahl, F. G., White, A. E., Popp, B. N., and Rosas-Navarro, A.: A biomarker perspective on coccolithophorid growth and export in a stratified sea, Progress in Oceanography, 122, 65 – 76, doi:10.1016/j.pocean.2013.12.001, URL http://www.sciencedirect.com/science/article/pii/S0079661113002292, 2014.

Acknowledgements

Technical support

Thanks to the researchers and technicians at the Institute of Environmental Science and Technology from the Autonomous University of Barcelona (ICTA-UAB), where most of the research was done, and at the Alfred Wegener Institute for Polar and Marine Research (AWI), where the laboratory experiments were developed. Thanks to Dr. Michael Grelaud for his advice on the use of the software SYRACO and his scientific feedbacks. Thanks to Dr. Yannick Alan de Icaza Astiz and Dr. Roberto De Jesus León Montiel for their scientific feedback and their support in the use of the LATEX editing program. Thanks to the anonymous referees and the editors from the journals Biogeosciences and PlosOne, for the constructive comments that greatly helped to improve the manuscript of Chapter 2(published in Biogeosciences) and Chapter 3 (published in PlosOne). Thanks to the people involved in the GoCAL4 fieldwork, specially to Dr. Debora Simon for collecting and organizing the coccolithophore samples; thanks to Dr. Fred G. Prahl, Dr. Brian N. Popp, the 14 scientists, and the crew aboard the RV New Horizon, for collecting and analyzing the chemical samples. Special thanks to my PhD thesis directors Dr. Patrizia Ziveri and Dr. Gerald Langer.

Personal support

What I liked the most about my PhD, what I will most remember and appreciate, will be all the nice people, places and experiences that I knew thanks to this PhD. Although I believe that a PhD is achieved through effort, dedication, decision and self-confidence, those wonderful people who were along this path to the PhD, all places and experiences, both inside and outside of work, are what allowed me to bring a smile throughout this process.

I want to start by thanking all those who allowed me to start this journey: Thanks to Patrizia Ziveri, for giving me the opportunity to work with her and

introducing me to the world of coccolithophores; thanks for the constant motivation and great kindness. Thanks to my family, in particular to my parents Mario Alberto and María Eugenia, and my brother Mario, because they helped me get the professional and emotional training necessary to reach the point of making the jump to another continent. Thanks to my aunt María Elena Navarro, my husband Yannick de Icaza, and my thesis director Patrizia Ziveri, for motivating me and helping me financially to start this journey. And thanks to the government of Spain for the FPU scholarship, without it this path would have been practically impossible.

During this PhD I learned that stays abroad improve you professionally and personally. Finding yourself in a new place, with new people and with different traditions, is very exciting; the possible fear becomes excitement and effort which make you grow. A stay limited in time, far from the known, makes you take care of solving at the moment all the new difficulties that arise since you do not have a lot of time to think about whether or not you will do certain things. All this makes you alert, basically the new experience fills you with adrenaline which makes you remember many details of the experience, such as the smells, sights and sensations of the place, and of course also the acquired or reinforced knowledge. This situation makes you live and work to the fullest. The stays abroad change your perspective; they make you grow in every way.

I want to thank everyone involved in my stay at the AWI. I thank all the researchers, technicians and colleagues who made my stay a stage of great professional and personal growth. Thanks to the Spanish government for the scholarship for the stay that helped me to focus on achieving with enthusiasm the scientific and professional objectives. Especially thanks to my co-director of the thesis Gerald Langer, who since then became a key person for my advancement in the doctorate thanks to his guidance, help and motivation; he is an example of a researcher and a wonderful person. I thank the dear friends who made me feel at home: Jelle Bijma, Hannah Kleyer, Niko Hoch, Laura Schmidt, Martin Brokof, Anne Thonig, Leo Elettra, Yohannes Kidane, Conor Purcell, and Tim Eberlein. I learned a lot there, I achieved a lot and I was very happy with everyone, thanks AWI.

I thank my research group at ICTA and the members of ICTA (researchers, students and administrators), for making the institute a place to want to go to every day. I specially thank my entire research group for the scientific discussions, talks, snacks and parties, and the happy moments full of anecdotes; I thank you above all for your friendship. I thank: Laura Rodriguez, Angela Oviedo, Barbara D'Amario, Michael Grelaud, Anna Ripoll, Rahiman Abdullah, Ana Claudia Popartan, Paty Jimenez, Luis Rodriguez, Sonia Chaabane, Gianluca Marino, Marlene Parari, Lukas Jonkers, Marcello Passaro, Kelsey Dyez , Marilisa Cagnetti, and of course Graham Mortyn, Patrizia Ziveri and Rainer Zahn.

During this stage of growth as a PhD student there were important people for me, who although outside my research group, accompanied me on this journey and with their scientific and non-scientific conversations, they helped me to advance better and with more motivation. To all of them, mostly icfonians (from ICFO), thank you. The list is long, but I want to thank my dear friends Roberto León, Adiv Gonzalez, Isabel Caicedo, Luis José Salazar, Jiri Svozilik, Ramaiah Badarla, Rafa Betancur, Alejandro Zamora and Luis Dominguez. Thanks also to Daryia, Alex, Hermes and Beatriz, and to the new friends I have made in the city of Terrassa for their support and friendship.

Thanks to all my family, including my husband's family, for the motivation and support despite the distance. Thanks also to my old Mexican friends who give me strength with their friendship. Special thanks to my dear friends Mariana, Daisy, Axini, Pale, Jaime, Mario, Gustavo and Alex.

To finish, I want to especially thank my husband Yannick. Thank you for supporting me financially once my scholarship was over. Thank you especially for accompanying me and supporting me in all the ups and downs of this PhD project, for always being present to help me get ahead and finish it. Thank you for the love, support and understanding throughout this project. Thank you for being my listener and for giving me feedback on technical and scientific aspects of this project.

Agradecimientos

Soporte técnico

Gracias a los investigadores y técnicos del Instituto de Ciencia y Tecnología Ambientales de la Universidad Autónoma de Barcelona (ICTA-UAB), donde se realizó la mayor parte de la investigación, y del Instituto Alfred Wegener de Investigación Polar y Marina (AWI), donde se desarrollaron los experimentos de laboratorio. Gracias al Dr. Michael Grelaud por su asesoramiento sobre el uso del software SYRACO y su retroalimentación científica. Gracias al Dr. Yannick Alan de Icaza Astiz y al Dr. Roberto De Jesus León Montiel por las discusiones científicas y por su apoyo en el uso del programa de edición de LATEX. Gracias a los árbitros anónimos y a los editores de las revistas Biogeosciences y PlosOne, por los comentarios constructivos que contribuyeron enormemente a mejorar el manuscrito del Capítulo 2 (publicado en Biogeosciences) y el Capítulo 3 (publicado en PlosOne). Gracias a las personas involucradas en el trabajo de campo GoCAL4, especialmente a la Dra. Debora Simon por colectar y organizar las muestras de cocolitóforos; gracias al Dr. Fred G. Prahl, al Dr. Brian N. Popp, al resto de investigadores, y a la tripulación a bordo del RV New Horizon, por colectar y analizar las muestras químicas. Un agradecimiento especial a los directores de mi tesis doctoral, la Dra. Patrizia Ziveri y el Dr. Gerald Langer.

Soporte personal

Lo que más me gustó de mi doctorado, lo que más recordaré y agradeceré, serán todas las personas, los lugares y experiencias que conocí gracias a este doctorado. Aunque creo que un doctorado se logra gracias al esfuerzo, dedicación, decisión y confianza en uno mismo, esas maravillosas personas que estuvieron a lo largo de este camino hacia el doctorado, todos los lugares y experiencias tanto laborales como personales, son los que me permitieron llevar una sonrisa a lo largo de este proceso.

Quiero empezar agradeciendo a todos aquellos que me permitieron iniciar este recorrido: Gracias a Patrizia Ziveri, por darme la oportunidad de trabajar con ella y presentarme el mundo de los cocolitóforos; gracias por la constante motivación y su gran amabilidad. Gracias a mi familia, en particular a mis padres Mario Alberto y María Eugenia, y a mi hermano Mario, porque me ayudaron a conseguir la formación profesional y emocional necesaria para llegar al punto de dar el salto hacia otro continente. Gracias a mi tía María Elena Navarro, a mi esposo Yannick de Icaza, y a mi directora de tesis Patrizia Ziveri, por su motivación y por ayudarme económicamente a iniciar este camino. Y gracias al gobierno de España por la beca FPU, sin ella este camino recorrido habría sido prácticamente imposible.

Durante este doctorado aprendí que las estancias te hacen mejor profesional y mejor persona. Encontrarte en un lugar nuevo, con gente nueva y con costumbres distintas, es muy emocionante, el posible miedo se convierte en emoción y esfuerzo que te hacen crecer. Una estancia limitada en el tiempo, lejos de lo conocido, te hace ocuparte de resolver al momento todas las nuevas dificultades que se presentan dado que no tienes mucho tiempo para pensar si harás o no tal cosa. Todo ello te vuelve alerta, básicamente la experiencia nueva te llena de adrenalina, lo cual te hace recordar posteriormente muchos detalles de lo vivido, desde olores, vistas y sensaciones, hasta los conocimientos adquiridos o reforzados, básicamente te hace vivir en un estado que te lleva a trabajar y vivir el lugar al máximo. Las estancias te cambian la perspectiva, te hacen crecer en todos sentidos.

Quiero agradecer a todos los involucrados en mi estancia en el AWI. Agradezco a todos los investigadores, técnicos y colegas que hicieron de mi estancia una etapa de gran crecimiento profesional y personal. Al gobierno de España por la beca para la estancia que me ayudó a enfocarme a lograr con entusiasmo los objetivos científicos y profesionales. Muy especialmente a mi codirector de tesis Gerald Langer, que desde ese momento se convirtió en una persona clave para mi avance en el doctorado gracias a su guía, ayuda y motivación; es un ejemplo de investigador y una maravillosa persona. Agradezco a los queridos amigos que me hicieron sentir como en casa: Jelle Bijma, Hannah Kleyer, Niko Hoch, Laura Schmidt, Martin Brokof, Anne Thonig, Elettra Leo, Yohannes Kidane, Conor Purcell, y Tim Eberlein. Aprendí mucho ahí, logré mucho y fui muy feliz con todos, gracias AWI.

Durante este gran recorrido para llegar a la meta, mi grupo de investigación en el ICTA fue cambiando así como los integrantes mismos del ICTA. Les agradezco a todos los de mi grupo las discusiones científicas, charlas, meriendas y fiestas, tuvimos momentos felices y llenos de anécdotas, les agradezco sobretodo su amistad. Agradezco a: Laura Rodríguez, Angela Oviedo, Barbara D'Amario, Michael Grelaud, Anna Ripoll, Rahiman Abdullah, Ana Claudia Popartan, Paty Jimenez, Luís Rodriguez, Sonia Chaabane, Gianluca Marino, Marlen Parari, Lukas Jonkers, Marcello Passaro, Kelsey Dyez, Marilisa Cagnetti, y por supuesto Graham Mortyn,

Patrizia Ziveri y Rainer Zahn. Agradezco también a investigadores, estudiantes y administrativos del ICTA, por hacer del instituto un lugar al cual querer ir cada día.

Durante esta etapa de crecimiento como estudiante de doctorado hubo personas importantes para mí, que aunque ajenas a mi grupo de investigación, me acompañaron en esta travesía y con sus conversaciones científicas y no científicas, me ayudaron a avanzar mejor y con más motivación. A todos ellos, en su mayoría icfonianos (del ICFO), gracias. La lista es larga, pero quiero agradecer especialmente a mis queridos amigos Roberto León, Adiv Gonzalez, Isabel Caicedo, Luis José Salazar, Jiri Svozilik, Ramaiah Badarla, Rafa Betancur, Alejandro Zamora y Luis Dominguez. Gracias también a Daryia, Alex, Hermes y Beatriz por su bella amistad y apoyo. Gracias a los nuevos amigos que he hecho en la ciudad de Terrassa por su apoyo y amistad.

Gracias a toda mi familia, incluida la familia de mi esposo, por motivarme y estar al pendiente de mí a pesar de la distancia. Gracias también a mis viejos amigos mexicanos que con su amistad me dan fortaleza. Gracias especialmente a mis queridas amigas Mariana, Daisy, Axini y Pale, y a mis queridos amigos Jaime, Mario, Gustavo y Alex.

Para terminar, quiero agradecer especialmente a mi esposo Yannick. Gracias por apoyarme económicamente una vez terminada mi beca. Gracias sobre todo por acompañarme y apoyarme en todas las subidas y bajadas de este proyecto de doctorado, por estar siempre presente de principio a fin para ayudarme a salir adelante y terminarlo. Gracias por el cariño, apoyo y comprensión a lo largo de todo este proyecto. Gracias por ser mi escucha y retroalimentarme en lo técnico y científico de este proyecto.

Table of contents

Chapter 1

Introduction

Coccolithophores are cosmopolitan unicellular calcifying marine phytoplankton (McIntyre and Bé, 1967; Brown, 1995; Brownlee and Taylor, 2004) involved in important biogeochemical global cycles (Robertson et al., 1994; Buitenhuis et al., 1996; Ridgwell and Zeebe, 2005; Findlay et al., 2011). They are important marine primary producers. It is generally acknowledged that global climate change will impact marine phytoplankton at every ecological level, so the impact will be observed in the coccolithophore individuals, populations and communities, affecting the marine primary production, their biogeography, and the carbon and carbonate cycles (e.g., Harada et al., 2012). Given that warming, acidification, and lowered nutrient availability might occur simultaneously under climate change scenarios (Rost and Riebesell, 2004; Cermeño et al., 2008; Feely et al., 2008; Doney et al., 2009), there is the question about what the net effect of different influential factors will be. In order to understand the possible effects of climate change on coccolithophores and the possible feedbacks from coccolithophores on the environment, both experiments and field studies are necessary.

This PhD thesis focuses on the impacts of ocean warming and acidification on the morphology and calcification of coccolithophores, with special attention to the cosmopolitan and dominant species *Emiliania huxleyi*. The study includes temperature experiments using three strains of *E. huxleyi* isolated in the NW Pacific Ocean (core chapters: 2 and 3), and the analysis of water samples collected along a transect covering the Gulf of California (G. Cal) and NE Pacific margin waters (core chapters: 5 and 6). This type of work is timely since global warming and the rapid increase in anthropogenic atmospheric CO_2 have remarkable consequences on the marine environment.

Chapters 2 and 3 are based on a culture experiment in which three different strains of the species *E. huxleyi* were grown at different temperatures corresponding to their sub-optimal to optimal temperature range. Chapter 2 is focused on

the temperature effects on the calcification and morphology of the studied strains. Chapter 3 is focused on the effects of the mentioned temperature range on the individual sinking velocity calculated from the coccosphere architecture. Chapters 2 and 3 correspond to the published articles by Rosas-Navarro et al. (2016) and by Rosas-Navarro et al. (2018), respectively.

Chapters 5 and 6 are based on water samples collected along a transect in the Gulf of California and the NE Pacific margin, spanning a large range of environmental conditions measured *in situ*. Chapter 5 is focused on the environmental effects on the morphotypes and morphological variations of *E. huxleyi*. Chapter 6 is focused on the environmental conditions associated with the different species within the genus *Gephyrocapsa* and on the calcite contribution estimated on *E. huxleyi* and the *Gephyrocapsa* spp. The standing stocks of *E. huxleyi* and the *Gephyrocapsa* spp. were used in the published article by Wolhowe et al. (2014) to estimate cellular production rate (cells L^{-1} d^{-1}) using alkenones as biomarkers.

Coccolithophore distribution, productivity and calcification are controlled by parameters such as water carbonate chemistry, temperature, salinity, nutrients, and light, which in turn are influenced by other factors such as latitude, ocean currents, water masses and seasonality (Okada and Honjo, 1973; Winter and Siesser, 1994; Baumann et al., 1999). There are still many unknowns about the coccolithophore responses on the morphology, calcification and primary production of different morphotypes and species, which in turn make it difficult to increase the certainty of future predictions. To improve the knowledge it is important to make field studies spanning a large range of conditions, and to make laboratory experiments including different strains and species grown at single and combined conditions.

1.1 Coccolithophores

The coccolithophores (phylum Haptophyta, class Prymnesiophyceae) include all haptophyte algae possessing calcified scales (coccoliths) at some stage of their lives. The Prymnesiophyceae also feature non-calcifying organisms (Edvardsen et al., 2000; Thierstein and Young, 2004). They are widely distributed (Winter and Siesser, 1994) and can form large blooms detectable by satellites (Brown and Yoder, 1994). They first appeared in the late Triassic ($\sim$ 225 Ma) sediments (Bown et al., 2004). The coccolith calcareous deposits are the major constituent of chalk. Coccoliths are useful fossils in both stratigraphic and paleoceanographic studies for paleoclimatic reconstructions; they are common tools for age determinations in oil exploration. Of the approximately 300 haptophytes in modern oceans, about 200 are coccolithophores (Jordan and Kleijne, 1994; Jordan and Green, 1994; Jordan and Chamberlain, 1997; Bown, 1998). Their assemblages in sediment samples

can be used as proxies, for example for productivity and water column stratification (Baumann et al., 1999; Álvarez et al., 2010a,b). The more we understand the relationship between the environmental conditions and the distribution of coccolithophores, the more we will be able to predict/reconstruct.

Coccolithophores are an important group of oceanic primary producers, they represent 10% of the global phytoplankton biomass (Tyrrell and Young, 2009). Their coccoliths make up about half of the open ocean vertical flux of inorganic carbon (Tyrrell and Young, 2009). They are important in the marine carbon and carbonate cycles (Westbroek et al., 1993; Thierstein and Young, 2004). They are also important in the sulfur cycle, they are one of the principal producers of dimethyl sulfide (DMS) which is the dominant precursor for cloud formation.

The ratio of particulate inorganic carbon (PIC, contained in the calcite of coccoliths) and particulate organic carbon (POC), influences surface water–atmosphere gas exchange as well as the composition of matter exported from surface waters to the deep ocean (Ridgwell and Zeebe, 2005; Findlay et al., 2011). The study of the response of PIC and POC production and their ratio to the different controlling environmental factors is necessary to understand the possible impact of coccolithophores on global biogeochemical cycles.

Coccolithophores are on average more successful (in terms of diversity and fraction of the total phytoplankton community) in warm, oligotrophic, low-latitude waters (Winter and Siesser, 1994). This is in contrast to diatom blooms, which mainly form when the upper ocean is deeply mixed (Richardson et al., 1983). Up to 83% of global particulate organic carbon (POC) fluxes are associated with calcium carbonate, possibly because $CaCO_3$ is denser than opal and more abundant than terrigenous material (Klaas and Archer, 2002).

1.2 Coccolith morphology in heterococcoliths

Heterococcoliths are the most common group of calcareous structure plates (coccoliths) formed by haptophytes (Young et al., 1999). Heterococcoliths are composed of an oval organic base plate with a distal rim of interlocking calcite ($CaCO_3$) crystals. Crystals of two distinct forms alternate about the rim (Marsh (1999); Young et al. (1999). A single segment consists of two crystal units, a peg-like V unit, and a complex R unit consisting of several superficially discrete elements. The interlocking crystals form two parallel discs known as the distal and proximal shield elements, and the vertical or sub-vertical structures linking the shields are known as tube elements (Young et al., 1997). The concave surface is directed toward the cell and so is termed proximal or lower (Young et al., 1999). Coccoliths are strongly birefringent placoliths. A group of interlocked coccoliths surrounding the

cell form the coccosphere. Coccospheres can present multiple layers of coccoliths (Young et al., 2003).

Culture experiments have shown that the strains do not change morphotype but do show variation in certain aspects of coccolith morphology, especially size and degree of calcification (Young and Westbroek, 1991). The morphological variation has been linked to environmental factors, such as salinity (Paasche et al., 1996; Bollmann et al., 2009), temperature (Watabe and Wilbur, 1966), temperature and phosphate (Satoh et al., 2009), or nutrient availability (Young and Westbroek, 1991; Young, 1994; Paasche, 1998). Decreases in size during the logarithmic growth phase of cultures, and between pre-bloom and bloom samples, suggest an effect reflected in a change from a slow reproducing population with cells in varying physiological states to a more homogeneous rapidly growing population (Thierstein and Young, 2004).

1.3 Coccolithophore calcification

Calcification involves the precipitation of calcite ($CaCO_3$) from calcium (Ca^{2+}) and carbonate (CO_3^{2-}) ions in solution (Thierstein and Young, 2004).

Particulate organic carbon production and biogenic calcification are generally described by the overall reactions (Zondervan et al., 2002):

$$6CO_2 + 12H_2O \longrightarrow C_6H_{12}O_6 + 6O_2 + 6H_2O, \tag{1.1}$$

and

$$Ca^{2+} + 2HCO_3^- \longrightarrow CaCO_3 + CO_2 + H_2O. \tag{1.2}$$

Base plates of calcifying coccolithophores acquire calcitic rims in the coccolith vesicle, a mineralizing vesicle derived from Golgi elements (de Vrind-de Jong and de Vrind, 1997). During mitosis, the coccolith vesicle disappears and is rebuilt in the newly divided cells (van Emburg et al., 1986; Linschooten et al., 1991), suggesting that dividing cells are mechanistically incapable of calcifying (Müller et al., 2008). The vesicle is connected to the reticular body, a labyrinthine membrane system, which is thought to be suitable for the rapid transport of large quantities of mineral ions into the vesicle in order to provide and maintain a supersaturated solution during calcite nucleation and growth (Müller et al., 2008). From studies in the species *E. huxleyi*, it is suggested that a galacturonomannan, known as the coccolith polysaccharide, localized in the vesicle (van Emburg et al., 1986), is part of the machinery that regulates the growth and shaping of calcite crystals

(Fichtinger-Schepman et al., 1981; Marsh et al., 2002), through site-specific interaction with the calcite surface, with a preferential interaction of CP with acute surface sites (Henriksen et al., 2004). Experiments suggest that calcification occurs only during the G1 (assimilation) cell cycle phase, as seen by a correlation between the percentage of cells in G1 and calcification, during the dark period (Müller et al., 2008).

As photosynthetic organisms, they shift the seawater carbonate system towards $[CO_3^{2-}]$, but as calcifiers they shift the seawater carbonate system towards $[CO_2]$. This last is because during the process of calcification is released CO_2; however, through the photosynthesis and coccoliths sinking to depth, coccolithophores cause a net draw down of CO_2 from the atmosphere into the ocean and modify upper-ocean alkalinity (Rost and Riebesell, 2004).

Coccoliths may have an ecological/evolutionary significance (Henriksen et al., 2003; Langer et al., 2011). Their function is not fully clear but has mostly been associated with protection and with light or buoyancy control (Young, 1994; Paasche, 2001; Guan and Gao, 2010). Supporting the light protection hypothesis, light saturation for growth is comparably high in *E. huxleyi* compared with diatoms (Richardson et al., 1983). Exposed to high irradiances, diatoms are often photoinhibited, whereas *E. huxleyi* appears to be resistant to photoinhibition (Nielsen, 1997). Guan and Gao (2010) showed that increased coccolith thickness ameliorate the photoinhibition of PSII photochemical efficiency caused by UVR, therefore coccoliths may play a certain role in reducing solar UV radiation (UVR, 280–400 nm) protecting the cells from being harmed. The coccolith cover reduced more UVA (320–400 nm) than UVB (280–315 nm), leading to less inhibition per energy at the UVA band (Guan and Gao, 2010).

The morphological variation in response to environmental parameter changes might represent a survival advantage (Dixon, 1900; Young, 1994). A possible role is the control of the individuals sinking velocity, using the coccoliths as ballast stones, due to the comparatively high density of calcite, influencing the position of the living cells in the water column Eppley et al. (1969); Ziveri et al. (2007); Bach et al. (2012b). This is part of the topic studied in Chapter 3, published by Rosas-Navarro et al. (2018).

1.4 *Emiliania huxleyi*

Emiliania huxleyi is the best-studied coccolithophore species, although it cannot be regarded as a typical coccolithophore in terms of phylogeny (Sáez et al., 2003). The dominant phase is diploid, non-motile and usually heterococcolith-bearing,

although naked mutants often occur in culture. The alternate phase is haploid, scale-bearing and motile. There is no holococcolith stage (Young et al., 2003).

Emiliania huxleyi is the most abundant coccolithophore in the oceans, distributed worldwide apart from the polar regions (Winter and Siesser, 1994). The ecological success of *E. huxleyi* has been attributed to the plasticity of its genome; there is significant genetic variation in populations collected from different waters and even within the populations obtained from the same site (Medlin et al., 1996; IglesiasRodríguez et al., 2002). *Emiliania huxleyi* thrives even in the relatively cold waters such as the North Atlantic south of Iceland, the Patagonian Shelf and even the Barents Sea (Smyth et al., 2004). An uncommon trait of *E. huxleyi* is its ability to form extensive blooms (Brown and Yoder, 1994; Young et al., 2003) with densities up to 10^7 cells L^{-1} (Holligan et al., 1993). The blooms are advancing into colder regions and have been correlated with positive temperature/negative salinity anomalies, therefore global warming is expected to increase the frequency of coccolithophore blooms at higher latitudes.

1.5 Hypotheses and objectives

Global warming, the related deepening of the nutricline (Cermeño et al., 2008), and ocean acidification (Doney et al., 2009), might reduce the distribution of coccolithophores in the most affected areas, constraining them to specific water layers where the conditions allow them to survive. One of the most important factors controlling their global distribution is temperature. Despite the importance of temperature there are still many doubts about its effect on the morphology of coccolithophores and about the temperature optimum for many of the species, and many more doubts about the combined effects with other environmental variables.

We believe that the coccolithophore distribution in warm regions highly affected by climate change, might be pushed down in the water column due to the high temperature and low nutrient concentration of surface waters, and that the upward migrations of the calcite saturation horizons in the photic zone, will restrict their vertical distribution even more, probably restricting the vertical coccolithophore distribution into narrower water layers; ultimately these changes might affect the primary production and the PIC : POC ratio. The effect of the different environmental factors on the coccolith morphology and level of calcification, could affect their resilience, adaptation and even survival while alive; but also, when liberated and transported to the sea floor, could make the coccoliths more prone to dissolution or could affect the properties of their aggregates.

Through a laboratory culture experiment testing *E. huxleyi* in its sub-optimum to optimum temperature range, we expect to find answers about the effect of tem-

perature on the morphology and calcification of *E. huxleyi*, pointing to possible effects on other coccolithophore species and on the PIC : POC ratio. And through the study of water samples we expect to unravel some of the main effects of the combined natural conditions, spanning a large range of conditions, on the morphology and calcification of dominant coccolithophore species. The water samples include highly stratified temperate waters, which have conditions that resemble some of those expected by climate change.

With the aim of improving the understanding of the effects related to climate change on the morphology and calcification of coccolithophores, the main specific objectives of this thesis are:

- Determine the effects of temperature, in the range of suboptimal to optimal, on the morphology and calcification of *E. huxleyi*.
- Determine the effects of such temperature range on the individual sinking velocity calculated from the coccosphere architecture.
- Determine the main factors controlling the vertical and horizontal distribution of *E. huxleyi* morphotypes A and O in Gulf of California and NE Pacific margin waters.
- Determine the main factors controlling the morphology of *E. huxleyi* in Gulf of California and NE Pacific margin waters.
- Determine the main factors controlling the vertical and horizontal distribution of the different species of *Gephyrocapsa* present in waters from the Gulf of California and NE Pacific margin .
- Estimate the PIC contribution per liter and the PIC production of *E. huxleyi* and the different species of *Gephyrocapsa* found in the studied waters from the Gulf of California and NE Pacific margin.

After this study we expect to have a more detailed knowledge about the effect of temperature on the morphology of the dominant species *E. huxleyi*, about the effect of combined environmental factors on its distribution and morphology, about the effect of combined environmental factors on the coccolithophore distribution, and about the PIC contribution of *E. huxleyi* and the *Gephyrocapsa* spp. in highly stratified temperate waters. With the new information about the environmental effects on coccolith morphology we expect to understand which conditions can be detrimental for them possibly affecting their resilience/adaptation to future climate scenarios, and possibly affecting their feedbacks on the biogeochemical cycles. With the new findings about the environmental control on distribution, together with the PIC contribution of different dominant species, we expect to improve the knowledge about coccolithophore's PIC contribution to the rain ratio, which will help improve future predictions involving coccolithophores.

Chapter 2

Temperature affects the morphology and calcification of *Emiliania huxleyi* strains

This chapter corresponds to the published article by Rosas-Navarro et al. (2016), the supplementary figures found in Appendix A.1 are also found at http://www.biogeosciences.net/13/2913/2016/bg-13-2913-2016-supplement.pdf and the data of the supplementary tables in Appendix A.2 can also be found at https://doi.pangaea.de/10.1594/PANGAEA.860214.

2.1 Abstract

The global warming debate has sparked an unprecedented interest in temperature effects on coccolithophores. The calcification response to temperature changes reported in the literature, however, is ambiguous. The two main sources of this ambiguity are putatively differences in experimental setup and strain specificity. In this study we therefore compare three strains isolated in the North Pacific under identical experimental conditions. Three strains of *Emiliania huxleyi* type A were grown under non-limiting nutrient and light conditions, at 10, 15, 20 and 25 °C. All three strains displayed similar growth rate versus temperature relationships, with an optimum at 20–25 °C. Elemental production (particulate inorganic carbon (PIC), particulate organic carbon (POC), total particulate nitrogen (TPN)), coccolith mass, coccolith size, and width of the tube element cycle were positively correlated with temperature over the sub-optimum to optimum temperature range. The correlation between PIC production and coccolith mass/size supports the notion that coccolith mass can be used as a proxy for PIC production in sediment

samples. Increasing PIC production was significantly positively correlated with the percentage of incomplete coccoliths in one strain only. Generally, coccoliths were heavier when PIC production was higher. This shows that incompleteness of coccoliths is not due to time shortage at high PIC production. Sub-optimal growth temperatures lead to an increase in the percentage of malformed coccoliths in a strain-specific fashion. Since in total only six strains have been tested thus far, it is presently difficult to say whether sub-optimal temperature is an important factor causing malformations in the field. The most important parameter in biogeochemical terms, the PIC : POC ratio, shows a minimum at optimum growth temperature in all investigated strains. This clarifies the ambiguous picture featuring in the literature, i.e. discrepancies between PIC : POC–temperature relationships reported in different studies using different strains and different experimental setups. In summary, global warming might cause a decline in coccolithophore's PIC contribution to the rain ratio, as well as improved fitness in some genotypes due to fewer coccolith malformations.

2.2 Introduction

Emiliania huxleyi (Lohmann) Hay and Mohler is a cosmopolitan (McIntyre and Bé, 1967; Brown, 1995), genetically diverse (Medlin et al., 1996; Schroeder et al., 2005; Iglesias-Rodríguez et al., 2006; Hagino et al., 2011; Read et al., 2013), morphologically variable (Hagino et al., 2005; Hagino and Okada, 2006; Cubillos et al., 2007) marine photosynthetic and calcifying (Brownlee and Taylor, 2004) unicellular haptophyte algae species and the most abundant of the coccolithophores. It produces calcite ($CaCO_3$) plates called coccoliths which cover the cell. As a photosynthetic organism, *E. huxleyi* shifts the seawater carbonate system towards $[CO_3^{2-}]$, but as a calcifier it shifts the seawater carbonate system towards $[CO_2]$. Therefore, part of the interest in *E. huxleyi* derives from its role in the global carbon cycle. In particular, extensive blooms (Westbroek et al., 1993; Paasche, 2001) might impact air–sea gas exchange (Robertson et al., 1994; Buitenhuis et al., 1996). Climate-change-induced surface water stratification was shown to trigger *E. huxleyi* blooms (Harada et al., 2012).

The ratio of particulate inorganic carbon (PIC) and particulate organic carbon (POC) influences surface water–atmosphere gas exchange as well as the composition of matter exported from surface waters to the deep ocean (Ridgwell and Zeebe, 2005; Findlay et al., 2011). The response of PIC and POC production and their ratio in the prolific species *E. huxleyi* to temperature is a necessary first step towards an understanding of its possible impact on global biogeochemical cycles.

The relationship of PIC production/PIC : POC and temperature in *E. huxleyi* is not clear. De Bodt et al. (2010) found that PIC production was higher at lower

temperatures in a strain grown at 13 and 18 °C, while Sett et al. (2014) found the opposite in another strain grown at 10, 15 and 20 °C. De Bodt et al. (2010) found higher PIC : POC ratios at lower temperatures for a strain of *E. huxleyi* and Gerecht et al. (2014) found a similar relationship for a strain of the species *Coccolithus pelagicus*. Sett et al. (2014), however, found a different relationship for the PIC : POC ratio in another strain of *E. huxleyi*, which is not supported by the experiment of Langer et al. (2007) on the same strain. Feng et al. (2008) did not find differences in the PIC : POC ratio in another strain grown at 20 and 24 °C. These discrepancies between studies might stem from different experimental setups and a lack of knowledge of the optimum growth temperature or indeed strain-specific differences (Hoppe et al., 2011). Therefore, it is necessary to test more than one strain for its temperature response under otherwise identical conditions. This we have done in the present study.

Apart from biogeochemical considerations, global warming might also be of interest in terms of the ecological success of coccolithophores, because different groups of organisms might be differently affected by warming and therefore ecological succession patterns, grazing pressure, etc., might change. The latter was proposed to depend on coccolith morphology more than it does on PIC production (Langer et al., 2011). The effect of temperature on coccolith morphogenesis is evident in field observations (Bollmann, 1997; Ziveri et al., 2004) and is best assessed with respect to the optimum growth temperature in laboratory experiments. While the effect of supra-optimal temperature is unequivocally detrimental (Watabe and Wilbur, 1966; Langer et al., 2010), it is not clear whether there is an effect of sub-optimal temperature at all (Watabe and Wilbur, 1966; Langer et al., 2010; De Bodt et al., 2010). A temperature increase in the sub-optimal range is probably what most coccolithophore clones will experience in the course of global warming (this study Buitenhuis et al., 2008; Langer et al., 2009; Heinle, 2014), and therefore this temperature range is particularly interesting. In the present study we focus on coccolith morphology under sub-optimal temperature, doubling the amount of data currently available, and thereby clarifying whether sub-optimal temperatures can cause malformations. We selected three strains of *E. huxleyi* from a single area, the Japanese coast in the North Pacific Ocean, in order to assess the plasticity within strains originating from a particular environmental setting.

2.3 Materials and methods

2.3.1 Pre-culture and batch culture experiments

Clonal cultures of *Emiliania huxleyi* were obtained from the Roscoff Culture Collection. We selected three strains of *E. huxleyi*, two from the Japanese coast in the North Pacific Ocean (RCC1710 – synonym of NG1 and RCC1252 – synonym of AC678 and MT0610E) and a third strain from the same region but of unknown exact origin and strain name, named here IAN01. Strain RCC1710 was collected off Nagasaki at Tsushima Strait (Japan) and RCC1252 at Tsugaru Strait (Japan); both places are strongly influenced by the Tsushima warm current. Additional information about the strain RCC1252 can be found at `http://roscoff-culture-collection.org/`.

The culture media was sterile-filtered North Sea water (filtered through 0.2 μm pore size sterile Sartobran 300 filter cartridges, Sartorius, Germany) supplemented with nutrients (nitrate and phosphate), metals and vitamins according to Guillard and Ryther (1962). Cell densities were determined using a Multisizer 3 Coulter Counter (Beckman Coulter for particle characterization). To prevent significant changes in seawater carbonate chemistry, maximum cell densities were limited to $\approx 1 \times 10^5$ cells mL^{-1} (e.g. Oviedo et al., 2014). We used a 16/8 light/dark cycle, and an irradiance of $\approx 300\,\mu$mol photons s^{-1} m^{-2}. The three strains were grown for at least 20 generations.

The dilute batch culture experiments were conducted in triplicate, for the strains RCC1710 and RCC1252 at 10, 15, 20 and 25 °C of temperature, and for IAN01 at 15, 20 and 25 °C. The strains were grown in 2 L of sea water within transparent sterilized 2.3 L glass bottles. Cell density at inoculation was 500 to 1000 cells mL^{-1}, and at harvest it was a maximum of 1×10^5cells mL^{-1}. Harvesting was done 9 h after the onset of the light period.

Growth rate was calculated from exponential regression according to

$$\mu = (\ln c_1 - \ln c_0)\Delta t^{-1}, \tag{2.1}$$

where c_1 and c_0 are the final cell concentration and the initial cell concentration, respectively, and Δt is the duration of incubation in days. Averages of triplicates and SD were used in tables and figures (Table 2.3 and Fig. 2.4a).

2.3.2 Carbonate chemistry

The seawater carbonate system was monitored because temperature and coccolithophore production alter the system. We employed the dilute batch method (Langer et al., 2013) to minimize production effects.

During the harvesting, samples for total alkalinity (TA) measurements were sterile-filtered (0.2 μm pore size) and stored for less than 2 months prior to measurement in 25 mL borosilicate flasks at 4 °C. TA was calculated from linear Gran plots (Gran, 1952) after potentiometric titration (in duplicate) (Bradshaw et al., 1981; Brewer et al., 1986).

Samples for dissolved inorganic carbon (DIC) were sterile-filtered (0.2 μm pore size) with gentle pressure using cellulose-acetate syringe filters and stored bubble-free for less than 2 months prior to measurement at 4 °C in 5 mL borosilicate flasks. DIC was measured, in triplicate, using a Shimadzu TOC 5050A.

The carbonate system was calculated from temperature, salinity (32 ‰), TA and DIC, using the program CO2SYS (Lewis and Wallace, 1998), applying the equilibrium constants from Mehrbach et al. (1973), refitted by Dickson and Millero (1987). For an overview of carbonate chemistry final conditions in all treatments, see Table 2.1.

Table 2.1: The carbonate system final values. Standard deviation of the triplicates in parentheses.

Strain	T [°C]	TA [μmol kg^{-1}]	DIC [μmol kg^{-1}]	pH (total scale)	pCO_2 [μatm]	HCO_3^- [μmol kg^{-1}]	CO_3^{2-} [μmol kg^{-1}]	Omega calcite
RCC1710	10	2138 (23)	2012 (3)	7.95 (0.07)	482 (74)	1893 (14)	98 (15)	2.38 (0.36)
RCC1710	15	2167 (14)	2023 (12)	7.92 (0.01)	530 (13)	1893 (11)	111 (3)	2.69 (0.07)
RCC1710	20	2291 (25)	2110 (4)	7.92 (0.06)	571 (84)	1953 (19)	139 (18)	3.39 (0.45)
RCC1710	25	2306 (24)	2123 (7)	7.86 (0.03)	688 (55)	1961 (4)	142 (11)	3.51 (0.28)
RCC1252	10	2249 (8)	2095 (12)	8.02 (0.03)	427 (30)	1959 (16)	117 (6)	2.84 (0.15)
RCC1252	15	2219 (57)	2065 (6)	7.94 (0.12)	533 (136)	1925 (21)	119 (32)	2.90 (0.78)
RCC1252	20	2212 (20)	2043 (15)	7.91 (0.01)	571 (10)	1896 (11)	129 (4)	3.15 (0.09)
RCC1252	25	2229 (8)	2052 (10)	7.85 (0.04)	670 (64)	1896 (19)	137 (11)	3.37 (0.26)
IAN01	15	2206 (9)	2064 (16)	7.92 (0.02)	551 (33)	1932 (19)	111 (4)	2.70 (0.11)
IAN01	20	2249 (28)	2106 (6)	7.84 (0.05)	698 (86)	1969 (5)	115 (14)	2.80 (0.34)
IAN01	25	2243 (2)	2066 (4)	7.85 (0.01)	677 (13)	1910 (5)	137 (2)	3.37 (0.05)

2.3.3 Particulate organic and inorganic carbon, particulate nitrogen and calcite

Duplicate samples for the determination of total particulate carbon (TPC) and total particulate nitrogen (TPN) were filtered onto pre-combusted (500 °C; 12 h) 0.6 μm nominal pore size glass fibre filters (Whatman GF/F), placed in pre-combusted Petri dishes (500 °C; 12 h), oven-dried (60 °C 24 h) and stored at −20 °C. Before analysis, TPC and TPN samples were dried for 24 h in a drying cabinet at 60 °C prior to measurement. All samples were then measured on a Euro EA analyser (Euro Vector).

Particulate inorganic carbon (PIC) was calculated measuring calcium content of samples with 3.6×10^6 *E. huxleyi* cells filtered onto 47 mm polycarbonate (PC) filters (0.8 μm pore size). PC filters were immersed overnight in an acid solution of 1 % HNO_3 to dissolve calcite. Calcium was determined by analysing an aliquot of the samples using an inductively coupled plasma mass spectrometer (ICP-MS, Agilent model 7500ce). Cellular PIC was calculated from the molecular mass of calcite, using the following equations:

$$\mathrm{PIC}_{\mathrm{cell}^{-1}} = \frac{\mathrm{PIC_s}}{c \cdot V_\mathrm{s}}, \quad \text{where} \quad \mathrm{PIC_s} = \frac{[\mathrm{Ca}^{2+}]_\mathrm{s} \cdot 12.0107}{40.078}, \tag{2.2}$$

where $\mathrm{PIC}_{\mathrm{cell}^{-1}}$ is the cellular PIC (in pg), $\mathrm{PIC_s}$ is the PIC sampled contained in the filter (in pg), c is the cell concentration (in cells L^{-1}), V_s is the volume sampled (in L), $[\mathrm{Ca}^{2+}]_\mathrm{s}$ is the calcium content in the sample (in pg), 12.0107 corresponds to the relative atomic mass of carbon, and 40.078 corresponds to the relative atomic mass of calcium. Particulate organic carbon (POC) was calculated as the difference between TPC and PIC. PIC, POC and TPN production (P_PIC, P_POC, P_TPN) were estimated as the product of cellular PIC, POC or TPN, and growth rate. Calcite ($CaCO_3$) per cell (concomitant of PIC) can also be estimated, substituting in Eq. (2.2) the calcium carbonate molecular mass (100.0869) in place of the relative atomic mass of carbon. The ratio between PIC and POC (PIC : POC) and the ratio between POC and TPN (POC : TPN) were also calculated.

2.3.4 Coccolith morphology – by scanning electron microscopy

Thirty millilitres of culture was filtered onto polycarbonate filters (0.8 μm pore size) and dried at 60 °C for 24 h. A small portion ($\sim 0.7\,\mathrm{cm}^2$) of each filter was mounted on an aluminium stub and coated with gold (EMITECH K550X sputter coater). Images were captured along random transects using a ZEISS-EVO MA10 scanning electron microscope (SEM).

Emiliania huxleyi SEM images were used to measure and categorize 300 coccoliths per sample (e.g. Langer et al., 2009); the coccoliths were on coccospheres. The tube width (width of the tube elements cycle) of each coccolith (Fig. 2.1c) was the average of the tube width measured on the two semi-minor axes (along the coccolith width) on the distal view of the coccolith. Tube width measurements were manually taken using the program Gimp-2.8. Examples of the tube width variations in the three different strains are shown in Fig. 2.1. The 300 coccoliths were classified as normal, malformed or incomplete (e.g. Langer et al., 2011), as described in Table 2.2, with examples in Figs. 2.2 and 2.3.

Table 2.2: Morphological categorization of coccoliths (from SEM images) of *E. huxleyi* used in this study.

Morphological category	Description
Normal	Regular coccolith in shape, with well-formed distal shield elements aligned forming a symmetric rim. Considered normal when nil or only two malformations were present.
Malformed	Irregular coccolith in shape or size of individual elements and a general reduction in the degree of radial symmetry shown; teratological malformation (Young and Westbroek, 1991). Considered malformed when three or more malformations were present in the coccolith.
Incomplete	Coccolith with variations in its degree of completion according to its normal growing order, with no malformations. Primary calcification variation (Young, 1994).

2.3.5 Coccolith length and mass – by polarized light microscopy

Between 10 and 30 mL of culture was filtered with $\sim$200 mbar onto cellulose nitrate filters (0.2 μm pore size) and dried at 60 °C for 24 h. A radial piece of filter was embedded and made transparent in immersion oil on microscope slides (e.g. Ziveri et al., 1995).

Images were taken at a magnification of 1000× with a Leica DM6000B cross-polarized light microscope (LM) equipped with a SPOT Insight camera (e.g. Bach et al., 2012a; Horigome et al., 2014). Between 50 and 200 image frames from each sample were taken along radial transects and analysed using SYRACO software

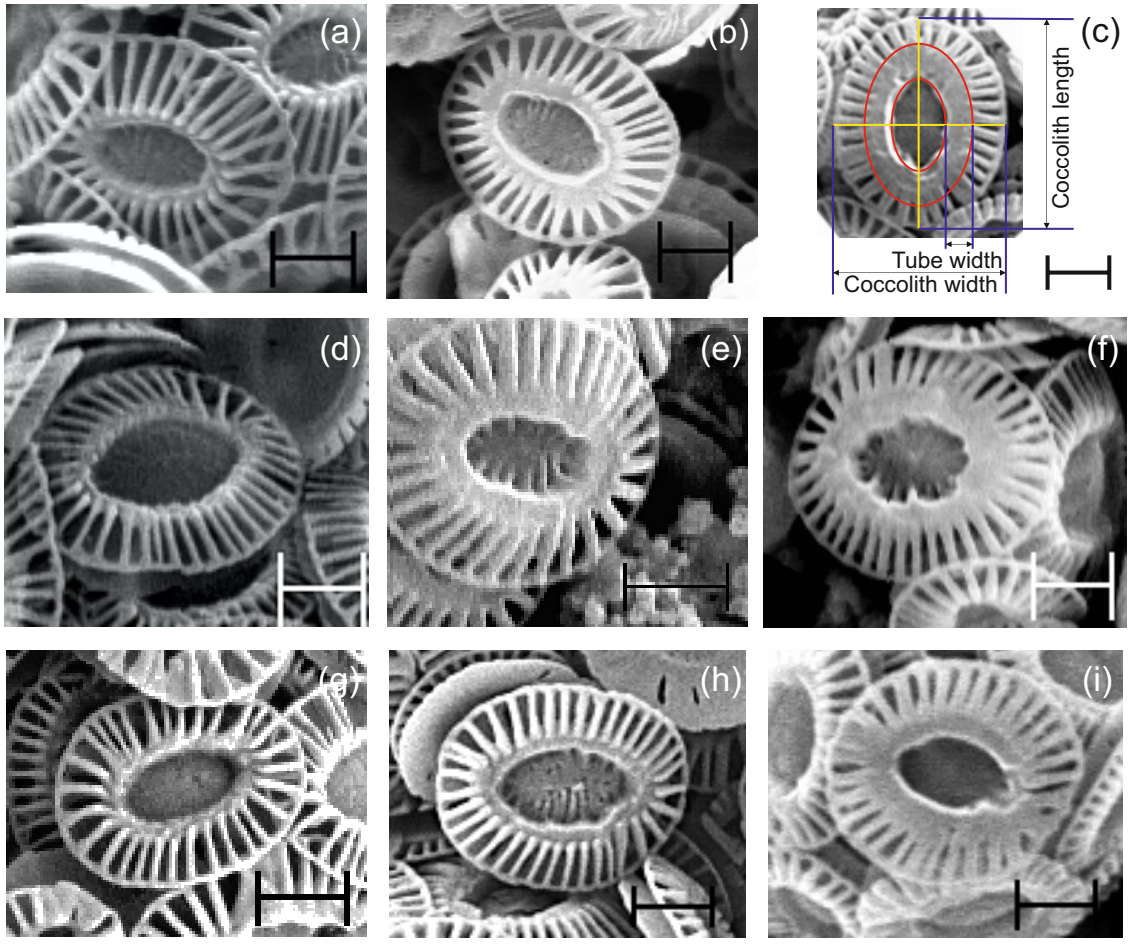

Figure 2.1: Examples of tube width variations observed in *E. huxleyi* RCC1710 (a-c), RCC1252 (d-f), and IAN01 (g-i) coccoliths. Tube width (c) was measured along the two semi-minor axes (along the coccolith width) of each coccolith and averaged. Scale bar equal to 1 μm.

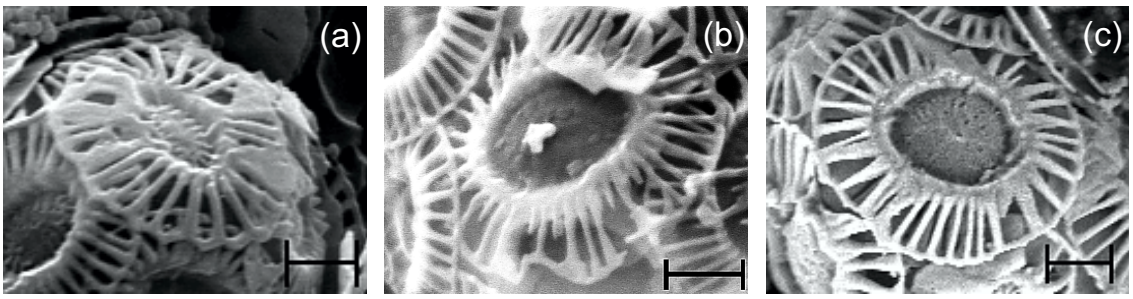

Figure 2.2: Examples of malformed coccoliths found in *E. huxleyi* RCC1710 (a), RCC1252 (b), and IAN01 (c). Scale bar equal to 1 μm.

(Dollfus and Beaufort, 1999; Beaufort and Dollfus, 2004). A minimum of 300 coccolith images were automatically identified by the software and measured in pixels. The software also automatically measures the grey level for each pixel by a birefringence method based on the coccolith brightness when viewed in cross-polarized

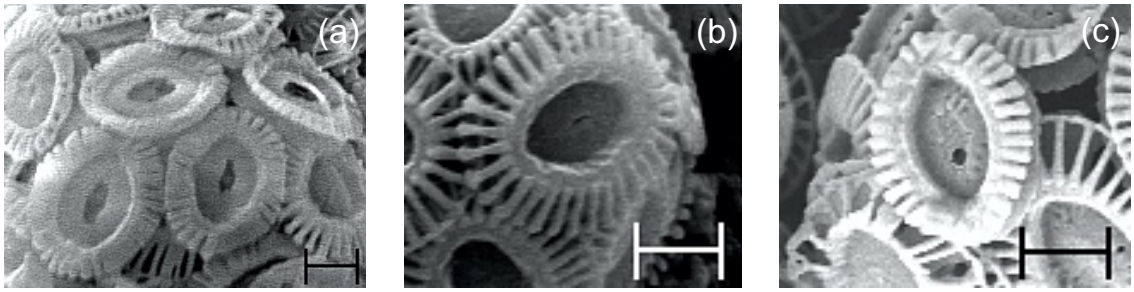

Figure 2.3: Examples of incomplete coccoliths of *E. huxleyi* RCC1710 (a), RCC1252 (b), and IAN01 (c). Scale bar equal to 1 μm.

light (Beaufort, 2005). Coccolith length and mass were subsequently calculated from the pixels and from the measured grey level, respectively, following Horigome et al. (2014) and Beaufort (2005). Therefore, coccolith length was converted from pixels to micrometres, where 832 pixels correspond to 125 μm, and coccolith mass was converted from grey level units to picograms, where 2275.14 grey level units were equivalent to 1 pg of calcite.

2.3.6 Statistics

For the three *E. huxleyi* strains together, ANOVA (two-factor with replication) was used to test whether a response variable (i.e. growth rate, element variables, morphological variables and mass) presented significant ($p < 0.05$) differences between the temperature treatments, to test whether the effect was strain-independent or strain-specific ($p < 0.05$), and to test whether there were significant differences in the interaction between treatment and strain ($p < 0.05$) and therefore whether the different strains respond similarly or not regardless of whether they were presenting differences between them. If the temperature effect was strain-specific, further ANOVA was used for pairs of strains.

If a response variable presented significant differences between the temperature treatments, and the variable also presented a significant strain-independent response to temperature, or at least the same response on two of the strains, the variable for the similar strains was analysed with simple and multiple linear regressions, including CO_2 partial pressure (pCO_2), CO_3^{2-} concentration and pH, in order to find the useful coefficients (t statistics, $p < 0.05$) of the significant equation (F test, $p < 0.05$) that would estimate the assessed variable value, e.g. the single or combined variables significantly estimating growth rate.

2.4 Results

2.4.1 Population growth

The three strains of *E. huxleyi* presented a stable growth rate (per day) that changed with temperature (Fig. 2.4a, Table 2.3), with significant differences between the temperature treatments ($F = 244.11$, $p = 0.000$). The strains RCC1710 and RCC1252 presented similar growth rates, not statistically different from one another ($F = 0.372$, $p = 0.550$). From 15 to 25 °C, the IAN01 growth rate was significantly different from the other two *E. huxleyi* strains ($F = 4.53$, $p = 0.025$), but there was no significant difference in the interaction between treatment and strain ($F = 0.71$, $p = 0.597$), so the three strains behaved significantly similarly. The optimum temperature for the three strains was 25 °C. When RCC1710 and RCC1252 were analysed together, changes in growth rate only depended significantly on temperature (linear regression: $R^2 = 0.91$, $F = 229.58$, $p = 0.000$); the carbonate system variables (Table 2.1) did not much increase the coefficient of determination (maximum to an $R^2 = 0.92$) and none of them were significantly useful in predicting growth rate when used together with temperature (t statistics: $p > 0.05$). According to Eq. (2.1), on the three strains, a minimum of one duplication per day was obtained from 15 to 27.5 °C.

Table 2.3: Growth rate and cellular PIC, POC, and TPN content and production, of the three strains of *E. huxleyi* at different temperatures. Standard deviation of the triplicates in parentheses. Measured growth rates for extra temperatures from the pre-experiments are included, but PIC, POC and TPN were not measured for these temperatures.

Strain	T [°C]	Growth rate (μ)	PIC [pg cell^{-1}]	POC [pg cell^{-1}]	TPN [pg cell^{-1}]	P_{PIC} [pg cell^{-1} day^{-1}]	P_{POC} [pg cell^{-1} day^{-1}]	P_{TPN} [pg cell^{-1} day^{-1}]
RCC1710	6.5	0.19						
RCC1710	10	0.26 (0.00)	15.31 (0.15)	8.91 (0.29)	1.54 (0.07)	3.98 (0.03)	2.32 (0.08)	0.40 (0.01)
RCC1710	15	0.75 (0.01)	14.07 (0.40)	9.90 (0.11)	1.47 (0.01)	10.55 (0.41)	7.42 (0.16)	1.10 (0.01)
RCC1710	20	1.15 (0.02)	11.47 (0.09)	12.05 (0.79)	1.71 (0.06)	13.16 (0.15)	13.82 (0.63)	1.98 (0.04)
RCC1710	25	1.24 (0.01)	10.80 (0.24)	9.30 (0.80)	1.38 (0.04)	13.34 (0.33)	11.48 (0.99)	1.70 (0.06)
RCC1710	27.5	1.04						
RCC1710	30	0.23						
RCC1252	6.5	0.18						
RCC1252	10	0.26 (0.04)	8.29 (0.49)	6.35 (0.11)	1.16 (0.03)	2.15 (0.39)	1.64 (0.23)	0.30 (0.04)
RCC1252	15	0.73 (0.00)	9.92 (0.32)	8.64 (0.29)	1.34 (0.03)	7.22 (0.23)	6.29 (0.22)	0.97 (0.02)
RCC1252	20	1.15 (0.14)	9.89 (0.28)	8.75 (0.71)	1.35 (0.07)	12.01 (0.74)	9.99 (1.13)	1.56 (0.26)
RCC1252	25	1.22 (0.02)	12.20 (0.21)	10.19 (0.75)	1.41 (0.02)	14.84 (0.38)	12.39 (0.86)	1.72 (0.02)
RCC1252	27.5	1.02						
RCC1252	30	0.00						
IAN01	6.5	0.12						
IAN01	15	0.81 (0.01)	10.18 (0.30)	9.89 (0.43)	1.47 (0.08)	8.20 (0.19)	7.97 (0.30)	1.18 (0.06)
IAN01	20	1.17 (0.00)	8.12 (0.21)	8.95 (0.43)	1.75 (0.09)	9.46 (0.25)	10.43 (0.51)	2.04 (0.11)
IAN01	25	1.32 (0.03)	11.21 (0.36)	9.95 (0.11)	1.46 (0.01)	14.84 (0.49)	13.17 (0.22)	1.94 (0.03)
IAN01	27.5	1.01						
IAN01	30	-0.11						

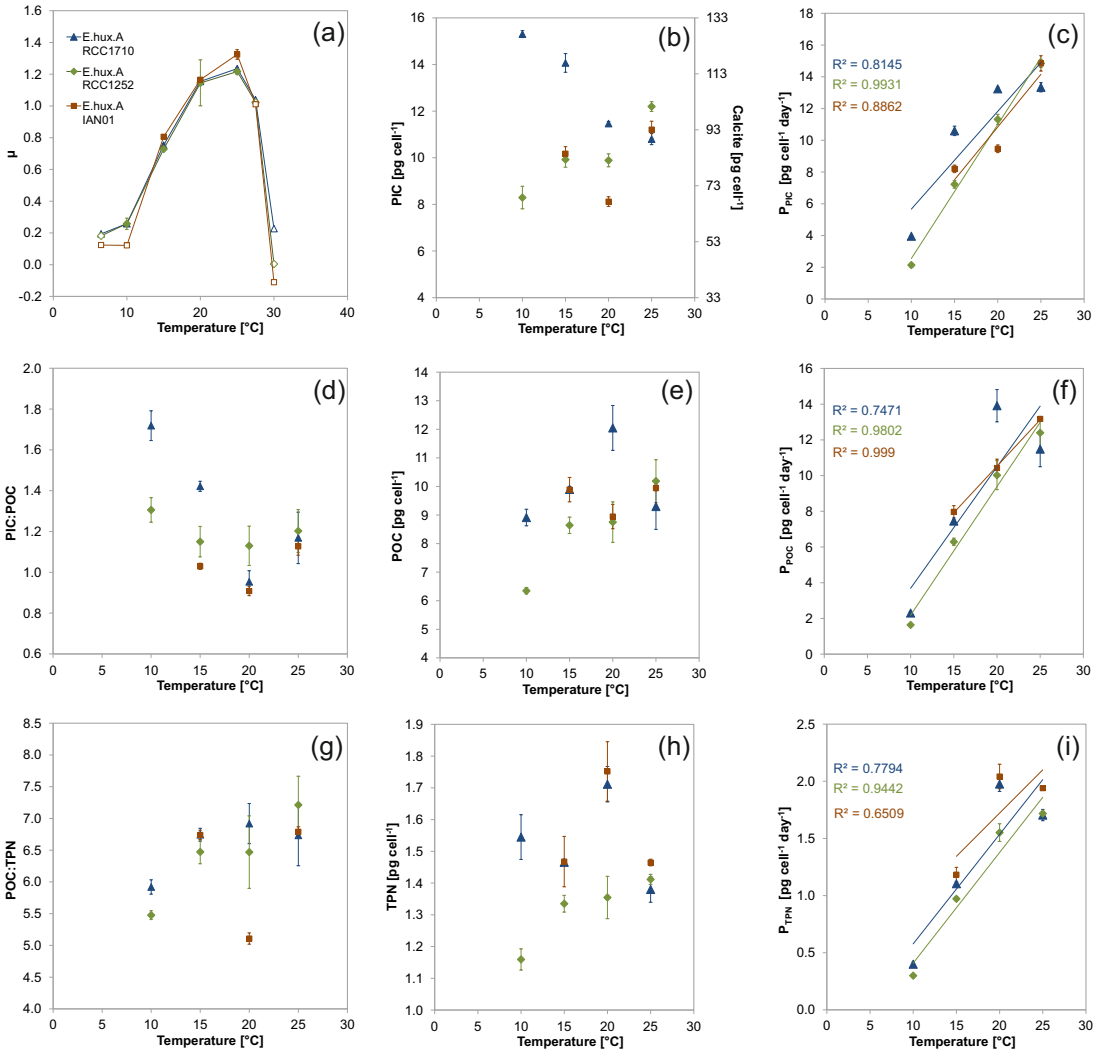

Figure 2.4: Results at different temperatures. Growth rate (a) (extra temperatures from pre-experiments are included and shown as empty symbols); cellular PIC and its concomitant calcite (b), POC (e) and TPN (h) content; PIC (c), POC (e) and TPN (i) production (linear trend lines and r-squared values are shown); and PIC : POC ratio (d) and POC : TPN ratio (g). Standard deviations of the triplicate experiment results are shown. Three different strains of *E. huxleyi* were used.

2.4.2 Element measurements, ratios and production

Cellular PIC (and its concomitant calcite), POC and TPN (pg cell^{-1}) did not show a consistent trend related to temperature when comparing the three strains of *E. huxleyi* (Fig. 2.4b, e, h; Table 2.3). When cellular PIC and TPN response to temperature (from 15 to 25 °C) were statistically analysed (ANOVA), significant differences were found between treatments ($F = 113.42$, $p = 0.000$ and $F = 36.52$, $p = 0.000$, respectively), but these were not strain-independent ($F = 182.86$, $p = 0.000$ and $F = 33.32$, $p = 0.000$, respectively). Cellular POC, conversely,

did not show significant differences between strains ($F = 1.71$, $p = 0.209$), nor did between the temperature treatments ($F = 0.09$, $p = 0.908$). There was no consistent explanatory variable for cellular PIC, POC, and TPN when analysing the three strains independently.

In the three strains, production of PIC (and its concomitant calcite), POC and TPN (pg cell^{-1}day^{-1}) showed a positive relationship with temperature (Fig. 2.4c, f, i; Table 2.3). Highest PIC and POC production was in general reached at 25 °C, except for RCC1710, which reached it at 20 °C. From the statistical analysis, PIC and POC production response to temperature, when comparing the three strains of *E. huxleyi* together, was significantly different between the temperature treatments ($F = 8.36$, $p = 0.003$) and the response was strain-independent ($F = 0.89$, $p = 0.428$). Highest TPN production was in general reached at 20 °C, except for RCC1252, which reached it at 25 °C. The latest was supported statistically, as TPN production response, with significant differences between temperature treatments ($F = 499.96$, $p = 0.000$), was strain-specific ($F = 65.92$, $p = 0.000$) when comparing the three strains of *E. huxleyi* together, and yet still the strains RCC1710 and IAN01 presented a similar interaction between treatment and strain ($F = 3.52$, $p = 0.062$); thus, the two strains had a similar behaviour in the TPN production response despite the different values between the strains ($F = 19.02$, $p = 0.000$).

Changes in PIC production on the three strains of *E. huxleyi* mostly depended on temperature (linear regression: $R^2 = 0.89$, $F = 217.36$, $p = 0.000$); pCO_2 with $[CO_3^{2-}]$, when used together with temperature, only slightly increased the coefficient of determination ($R^2 = 0.93$). Changes in POC production on the three strains of *E. huxleyi* only depended significantly on temperature (linear regression: $R^2 = 0.85$, $F = 157.71$, $p = 0.000$).

The PIC : POC ratio decreased from 10 to 20 °C in the three strains of *E. huxleyi* (Fig. 2.4d). POC was higher than PIC only in the strains RCC1710 and IAN01 at 20 °C. From the statistical analyses, the only significant similitude obtained was in the interaction between treatment and strain for RCC1252 and IAN01 ($F = 2.12$, $p = 0.163$), which means that the PIC : POC ratio behaves similarly towards temperature in these two strains.

The POC : TPN ratio (Fig. 2.4h) relationship with temperature was strain-specific ($F = 9.59$, $p = 0.001$). The differences between the temperature treatments were significant ($F = 16.95$, $p = 0.000$). There were no significant differences between the strains RCC1710 and RCC1252 ($F = 2.71$, $p = 0.119$), in which the lowest POC : TPN ratio was found at 10 °C; however, there were significant differences in the interaction between treatment and strain ($F = 3.52$, $p = 0.039$), as observed in the different temperatures at which maximum POC : TPN ratios were found for each strain (20 and 25 °C, respectively). The strain IAN01 showed

a much different relationship with temperature, with a minimum POC : TPN ratio found at 20 °C.

2.4.3 Coccolith morphology and mass

Although there was great variation between replicates, mean tube width of coccoliths (Fig. 2.5a, Table 2.4) presented a positive trend with temperature, independent of the strain of *E. huxleyi* ($F = 1.73$, $p = 0.204$). Changes in tube width on the three strains of *E. huxleyi* only depended on temperature (linear regression: $R^2 = 0.47$, $F = 28.09$, $p = 0.000$); pCO_2 and $[CO_3^{2-}]$ did not much increase the coefficient of determination ($R^2 = 0.51$) and none of them were significantly useful in predicting tube width when used together with temperature (t statistics: $p > 0.05$).

Table 2.4: Coccoliths morphology and mass. Standard deviation of the triplicates is shown in parentheses.

Strain	T [°C]	Tube width [μm]	Coccolith length [μm]	Coccolith mass [pg]	Malformed [%]	Incomplete [%]
RCC1710	10	0.20 (0.02)	2.03 (0.06)	0.99 (0.11)	33.18 (2.02)	2.39 (0.75)
RCC1710	15	0.22 (0.03)	2.12 (0.03)	1.63 (0.25)	29.19 (4.50)	2.38 (2.36)
RCC1710	20	0.26 (0.02)	2.05 (0.04)	1.75 (0.09)	33.66 (5.85)	8.60 (4.51)
RCC1710	25	0.28 (0.02)	2.16 (0.05)	2.48 (0.16)	37.75 (7.90)	20.10 (5.24)
RCC1252	10	0.21 (0.04)	2.06 (0.00)	1.61 (0.00)	56.39 (3.54)	1.22 (0.51)
RCC1252	15	0.26 (0.05)	2.15 (0.09)	1.97 (0.07)	7.65 (5.29)	1.28 (1.25)
RCC1252	20	0.28 (0.04)	2.27 (0.03)	2.49 (0.30)	10.09 (3.21)	7.09 (5.01)
RCC1252	25	0.27 (0.02)	2.30 (0.03)	3.00 (0.18)	9.09 (3.67)	5.08 (4.85)
IAN01	15	0.22 (0.03)	2.15 (0.06)	2.02 (0.19)	52.13 (8.41)	2.58 (0.66)
IAN01	20	0.25 (0.03)	2.24 (0.00)	2.63 (0.00)	47.09 (2.92)	3.05 (1.78)
IAN01	25	0.27 (0.02)	2.26 (0.02)	2.66 (0.27)	41.18 (4.01)	8.95 (3.01)

Coccolith length (Fig. 2.5b, Table 2.4) showed a positive trend with temperature, especially on strains RCC1252 and IAN01. The positive trend in strain RCC1710 was not so clear; however, minimum length was also found at 10 °C and maximum length also at 25 °C. Strains RCC1252 and IAN01 were analysed together in a multiple linear regression analysis, as they did not present significant differences between them ($F = 2.12$, $p = 0.171$); temperature gave the highest coefficient of determination ($R^2 = 0.62$, $F = 24.03$, $p = 0.000$) and was the only useful coefficient in estimating coccolith length when making any combination with pCO_2, $[CO_3^{2-}]$ or pH. The strain RCC1710 was analysed independently of the other two strains: temperature presented a low and non-significant coefficient of determination ($R^2 = 0.28$, $F = 3.55$, $p = 0.092$); instead, pH presented the highest coefficient of determination ($R^2 = 0.65$, $F = 16.87$, $p = 0.002$).

The positive relationship of the mean tube width with temperature reflects the increased coccolith calcite quota at higher temperature. Coccolith mass and coccolith size are positively correlated. Why coccolith mass or size should increase with temperature cannot be decisively answered based on our data.

Regardless of the strain, coccolith calcite mass (Fig. 2.5c, Table 2.4) showed a positive trend with temperature; significant differences were found between treatments ($F = 35.59$, $p = 0.000$) and no significant differences were found in the interaction between treatment and strain ($F = 2.53$, $p = 0.08$). The strains RCC1252 and IAN01 were analysed together as they did not show significant differences between them ($F = 0.65$, $p = 0.425$). Temperature presented the highest coefficient of determination for RCC1252 and IAN01 ($R^2 = 0.75$, $F = 45.93$, $p = 0.000$) and also for RCC1710 ($R^2 = 0.87$, $F = 58.58$, $p = 0.000$), and adding other coefficients was not significantly useful in estimating coccolith mass. On average, coccolith mass increased with temperature $\sim$2.2× from 10 to 25 °C, $\sim$1.5× from 15 to 25 °C, and $\sim$1.2× from 20 to 25 °C; on average, coccolith mass increased 1.28× (or 0.45 pg) each 5 °C.

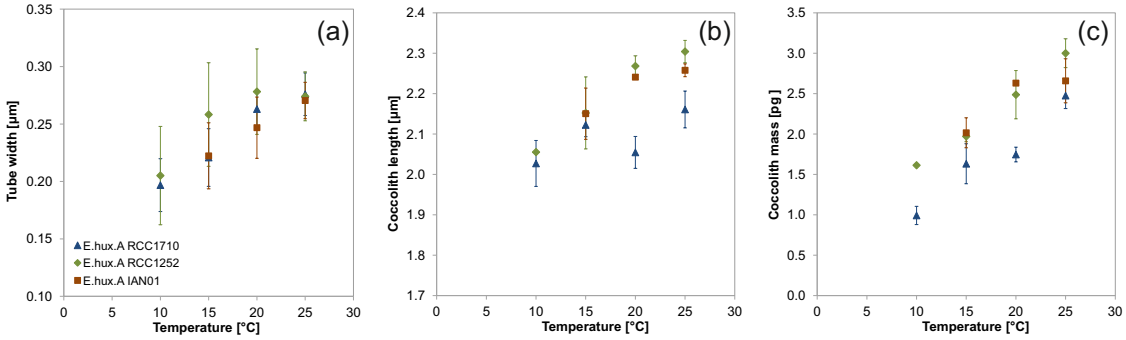

Figure 2.5: Changes in coccolith morphometry (a and b) and mass (c), at different temperatures. Standard deviations of the triplicate experiment results are shown. Three different strains of *E. huxleyi* were used.

The percentage of malformed coccoliths per sample (Fig. 2.6a, Table 2.4) did not show a consistent trend with temperature when comparing the three strains of *E. huxleyi* ($F = 113.21$, $p = 0.000$). Only one strain (RCC1252) presented significant differences between the temperature treatments, with higher percentage at the lowest experimented temperature.

Only in strain RCC1710, the percentage of incomplete coccoliths presented a significant increase with temperature (Fig. 2.6b, Table 2.4). Higher percentages of incomplete coccoliths in strain RCC1710 were found at 25 °C. ANOVA results showed that, between the three strains, there were no significant differences between only the strains RCC1252 and IAN01 ($F = 0.06$, $p = 0.810$) and their interaction between treatment and strain ($F = 2.33$, $p = 0.139$), though in this case (analysed from 15 to 25 °C) there were also no significant differences between the

temperature treatments ($F = 3.78$, $p = 0.053$). Significant strain-independent and strain-specific responses of *E. huxleyi* to temperature, found in the three strains of this study, are summarized in Table 2.5. Supplementary figures and tables are found in the appendices A.1 and A.2 respectively.

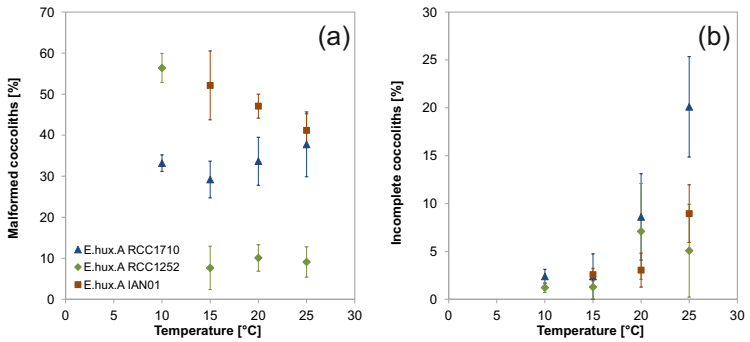

Figure 2.6: Percentage of malformed (a) and incomplete (b) coccoliths, in three *E. huxleyi* strains grown at different temperatures. Standard deviations of the triplicate experiment results are shown.

2.5 Discussion

2.5.1 Growth rate, elemental production and incomplete coccoliths

All three *E. huxleyi* strains investigated here displayed similar growth rate versus temperature relationships, with an optimum at 20–25 °C (Fig. 2.4a). This is a typical range for many *E. huxleyi* strains (e.g. Watabe and Wilbur, 1966; Van Rijssel and Gieskes, 2002; Sorrosa et al., 2005; De Bodt et al., 2010; Langer et al., 2009). We expect that strains isolated, for example, in the Arctic will have a lower temperature optimum, though. Also not untypical, elemental production (PIC, POC, TPN) increased with temperature over the sub-optimum to optimum temperature range (Fig. 2.4; Langer et al., 2007; Sett et al., 2014). It is intuitive that, approaching optimum, higher temperature increases elemental production, because biochemical rates are temperature-dependent. It is also intuitive that the percentage of incomplete coccoliths should increase with higher P_{PIC}, as indeed observed in RCC1710 (Fig. 2.6b). The idea underlying this intuition is that less time is taken to produce one coccolith and that the production process is stopped before the coccolith is fully formed. A comparison of RCC1710 and RCC1252 shows how wrong this idea is (Table 2.6). The percentage of incomplete coccoliths increases in the former only. While it is true that coccolith production time in RCC1710 decreases from 31 min at 10 °C to 22 min at 25 °C, this decrease is even more pronounced in RCC1252 (from 88 to 23 min). Hence, RCC1252 should show

Table 2.5: Significant strain-independent and strain-specific responses of *E. huxleyi* to temperature, found in the three strains of this study.

Strain-independent responses	Strain-specific responses
• Growth rate optimum temperature was 25 °C. • Highest PIC, POC, and TPN production values were found at 20 or 25 °C. • The PIC:POC ratio decreased from 10 to 20 °C. • Tube width increased with temperature, from ∼ 0.20 μm at 10 °C to ∼ 0.27 μm at 25 °C. • Maximum coccolith length was found at 25 °C. • Coccolith mass increased with temperature (∼ 2.2 times from 10 to 25 °C, ∼ 1.5 times from 15 to 25 °C, and ∼ 1.2 times from 20 to 25 °C; on average, 0.45 pg each 5 °C).	• Cellular PIC, POC and TPN (pg per cell). • POC:TPN ratio. However, in the two strains tested at 10 °C (RCC1710 and RCC1252), the POC:TPN ratio was lowest at 10 °C. • Percentage of malformed coccoliths per sample. • Percentages of incomplete coccoliths. • Coccolith length, although in strains RCC1252 and IAN01 was positively correlated with temperature.

a steeper increase in incompleteness than RCC1710. This is not the case. Please note that the increase in incompleteness in RCC1252 (Fig. 2.6b) is not significant, because the increase is well below 10 % and the error bars overlap (see also Langer et al., 2013, for a discussion of this criterion). Another piece of evidence which does not fit the "premature release of coccoliths because of time shortage" idea is that both RCC1710 and RCC1252 manage to produce heavier coccoliths in a shorter time at higher temperature (Tables 2.4 and 2.6). We do not know why the stop signal for coccolith growth is affected by temperature in RCC1710. Nothing is known about the biochemical underpinning of that stop signal, so it is unfortunately impossible to speculate about the mechanism of a temperature effect. It was, however, argued that the processes involved in the stop signal are different from those producing teratological malformations (Young and Westbroek,

1991; Langer et al., 2010, 2011). This is supported by our data, because there is no correlation between incompleteness and malformations (Fig. 2.6). We will discuss malformations in Sect. 2.5.3.

Table 2.6: Coccolith production time. Standard deviation of the triplicates is shown in parentheses. Lith: coccolith, d: day, h: hour, min: minutes.

Strain	T [°C]	pgPIC · lith^{-1}	Lith · cell^{-1}	Lith · cell^{-1} · d^{-1}	Lith · cell^{-1} · h^{-1}	Min · lith^{-1}	pgPIC · h^{-1}
RCC1710	10	0.12 (0.01)	121 (2)	31 (0)	2.0 (0.0)	31 (0)	0.25 (0.00)
RCC1710	15	0.20 (0.03)	74 (14)	55 (10)	3.4 (0.6)	18 (3)	0.66 (0.03)
RCC1710	20	0.21 (0.01)	53 (0)	61 (1)	3.8 (0.1)	16 (0)	0.82 (0.01)
RCC1710	25	0.30 (0.02)	36 (2)	45 (2)	2.8 (0.1)	22 (1)	0.83 (0.03)
RCC1252	10	0.19 (0.00)	43 (2)	11 (2)	0.7 (0.1)	88 (18)	0.13 (0.02)
RCC1252	15	0.24 (0.01)	42 (1)	31 (1)	1.9 (0.1)	31 (1)	0.45 (0.01)
RCC1252	20	0.30 (0.04)	35 (6)	42 (4)	2.6 (0.2)	23 (2)	0.75 (0.05)
RCC1252	25	0.36 (0.02)	34 (3)	41 (3)	2.6 (0.2)	23 (2)	0.93 (0.02)
IAN01	15	0.24 (0.02)	42 (3)	34 (2)	2.1 (0.2)	28 (2)	0.51 (0.01)
IAN01	20	0.32 (0.00)	26 (1)	30 (1)	1.9 (0.0)	32 (1)	0.59 (0.02)
IAN01	25	0.32 (0.03)	35 (5)	47 (6)	2.9 (0.4)	21 (3)	0.93 (0.03)

Interestingly coccolith mass is positively correlated with temperature (and P_{PIC}) in all strains tested here. The positive correlation of coccolith mass and P_{PIC} was also observed by Bach et al. (2012a) in a carbonate chemistry manipulation experiment and is the basis of using coccolith mass as a proxy for P_{PIC} (Beaufort et al., 2011). This is an interesting option, because in field samples coccolith mass might be a promising indicator of P_{PIC}. There are only few proxies available to reconstruct past coccolithophore P_{PIC}, the traditional one being the calcite Sr / Ca ratio, established at the turn of the millennium (Stoll and Schrag, 2000). Analysing Sr / Ca, however, requires either a sizable sample or comparatively sophisticated secondary ion mass spectrometry (SIMS) measurements (Stoll et al., 2007; Prentice et al., 2014). Recently, coccosphere diameter and coccolith quota were introduced as growth rate proxies (Gibbs et al., 2013). However, complete coccospheres are the exception rather than the rule in sediment samples, so it is important to have a proxy based on individual coccoliths. Hence, coccolith mass and size (which are correlated; Fig. 2.5, Table 2.4) are an option which it is worthwhile exploring in the future.

2.5.2 *Emiliania huxleyi* PIC : POC response

As detailed in the introduction there is considerable variability in the PIC : POC response of *E. huxleyi* to temperature changes. This variability cannot be traced back to strain-specific features, but it might partly reflect the fact that different temperature ranges were investigated, mostly without the knowledge of the optimum temperature. Other experimental conditions, such as light intensity and

nutrient concentrations, varied and might have also played a role (Hoppe et al., 2011). In this study we ran three strains under identical conditions and, for the first time, are presented with a coherent picture. All three strains display a bell-shaped curve with lowest PIC : POC close to the optimum growth temperature (Fig. 2.4d). Although our data on the right-hand side of the PIC : POC minimum are not conclusive for RCC1252, the bell-shaped curve is discernible in the latter strain. This finding seems to fit data on other *E. huxleyi* strains (De Bodt et al., 2010; Sett et al., 2014) and on *C. pelagicus* (Gerecht et al., 2014). This comparison is, however, not straightforward since two of the studies (De Bodt et al., 2010; Gerecht et al., 2014) employed two temperatures, one of the studies employed three temperatures (Sett et al., 2014), only without determining the optimum temperature in all three studies. Be that as it may, based on our data, we might conclude that *E. huxleyi* tends to show the lowest PIC : POC close to its optimum growth temperature. In the context of global warming, that would mean that, in the future, *E. huxleyi* and possibly coccolithophore PIC : POC will tend to decrease because most strains live at sub-optimal temperatures in the field (Buitenhuis et al., 2008; Langer et al., 2009; Heinle, 2014). This trend might be pronounced because global warming is accompanied by lower surface water nutrient levels and ocean acidification (Cermeño et al., 2008; Doney et al., 2009). All these changes apparently cause a decrease in *E. huxleyi*'s PIC : POC (our data; Hoppe et al., 2011; Oviedo et al., 2014). A marked decline in coccolithophore PIC : POC will have implications for long-term carbon burial and might even affect surface water carbonate chemistry on short timescales, i.e. 1 year (Barker et al., 2003; Ridgwell and Zeebe, 2005; Cermeño et al., 2008).

2.5.3 Coccolith malformations

The coccolith shaping machinery is, besides the ion transport machinery, an essential part of coccolith formation (for an overview see Holtz et al., 2013). The latter commences with heterogeneous nucleation on an organic template, the so-called base plate. The nucleation determines crystal axis orientation. Crystal growth proceeds in principle inorganically, with the notable exception that crystal shape is strongly modified by means of a dynamic mould, which essentially consists in the coccolith vesicle shaped by cytoskeleton elements and polysaccharides inside the coccolith vesicle. Malformations can be due to an abnormal base plate which would affect crystal axis orientation, aberrations in the composition or structure of the polysaccharides, and disturbance of cytoskeleton functionality. The last of these would most likely also cause a decline in growth rate, which is why this mechanism was disregarded in the case of carbonate-chemistry-induced malformations (Langer et al., 2011). By the same reasoning, temperature-induced malformations might be due to cytoskeleton disturbance, because temperature does also alter growth rate (Fig. 2.4a). However, it is not straightforward to see why lower than opti-

mum temperature should disturb cytoskeleton functionality (see also Langer et al., 2010). At any rate, coccolith malformations are most likely detrimental to fitness, because malformed coccoliths result in fragile coccospheres, which are regarded as instrumental in coccolithophore fitness (Dixon, 1900; Young, 1994; Langer and Bode, 2011; Langer et al., 2011). One of the many hypotheses concerning function of calcification is that the coccosphere confers mechanical protection (Dixon, 1900; Young, 1994). After more than a century of research, it still remains the most plausible hypothesis.

Coccolith malformations, i.e. disturbances of the coccolith shaping machinery, occur in both field and culture samples, but usually more so in the latter (Langer et al., 2006, 2013). The causes of malformations are only partly known. In cultured samples, artificial conditions (not present in the field) such as cell densities of 10^6cells mL^{-1}, cells sitting on the bottom of the culture flask, stagnant water, and confinement in a culture flask play a role in inducing the surplus of malformations compared to field samples (Langer et al., 2013; Ziveri et al., 2014). However, in the field malformations do occur, and sometimes in considerable percentages (Giraudeau et al., 1993; Ziveri et al., 2014). The environmental conditions leading to elevated levels of malformations have long since been disputed. Besides nutrient limitation (Honjo, 1976), temperature and carbonate chemistry are conspicuous candidates. Although the range of temperatures used here exceeds 2100 projections (IPCC, 2013), we used it not only on physiological grounds but also for ecological reasons. Over the course of the year, coccolithophores in the North Pacific experience the whole range of temperatures used here (http://disc.sci.gsfc.nasa.gov/giovanni/, Fig. 2.7). In a seminal experimental study it was shown that moving away from the optimal growth temperature increases malformations in *E. huxleyi* (Watabe and Wilbur, 1966). This result was confirmed for higher than optimum temperature in another strain (Langer et al., 2010) but could not be confirmed for sub-optimal temperature in two strains (De Bodt et al., 2010; Langer et al., 2010). The sub-optimal temperature range is of particular interest because most clones live at sub-optimal temperatures in the field. Here we investigated sub-optimum to optimum temperatures in three further strains. While RCC1710 showed no change in the percentage of malformations and IAN01 featured a shallow gradual increase from 25 to 15 °C, RCC1252 was insensitive over the latter range but displayed a steep increase in malformations at 10 °C (Fig. 2.6). Based on our own and the literature data, we conclude that the sub-optimal temperature effect on morphogenesis is strain-specific. The fact that the base level of malformations in cultured coccolithophores differs between species and strains (and also varies with time) has been recognized for many years and is now well documented (e.g. Langer and Benner, 2009; Langer et al., 2011, 2013). Also, the response of the morphogenetic machinery to environmental factors is strain-specific (Langer et al., 2011). We currently do not have enough accessory information to formulate a hypothesis why exactly one strain differs from another.

The fact that they do indeed differ, however, probably reflects the high genetic diversity in *E. huxleyi*.

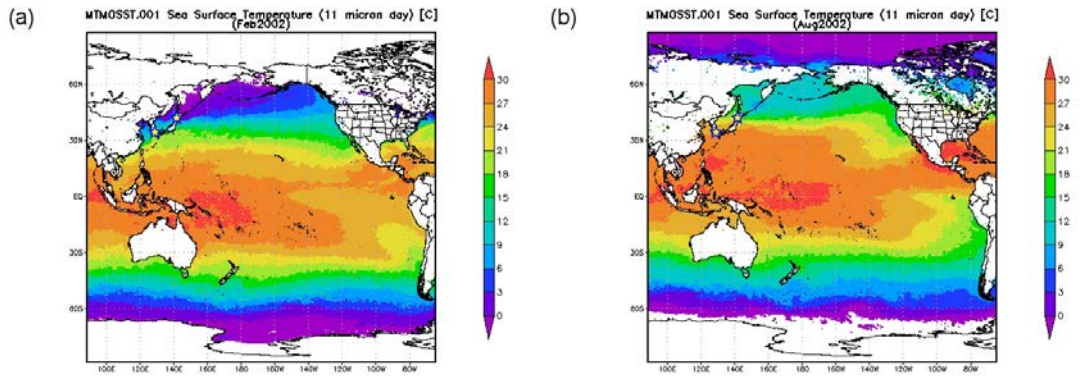

Figure 2.7: Sea surface temperatures in the North Pacific in February and August 2002 (http://disc.sci.gsfc.nasa.gov/giovanni/), the year in which the strain RCC1252 was collected. Regions of origin of the RCC1710 and RCC1252 strains in the Japanese coast are marked (stars).

Can we see a pattern in this strain specificity? It is intriguing that *E. huxleyi* clones fall into two distinct groups characterized by their temperature preference: the warm-water and the cool-water group (Hagino et al., 2011). Of the strains analysed for morphology, the following belong to the warm-water group: BT-6 (Watabe and Wilbur, 1966), RCC1710, RCC1252, and possibly RCC1238 (Langer et al., 2010). The latter was unfortunately not included in the study by Hagino et al. (2011). Since these strains display different responses to temperature, their being part of the warm-water group does unfortunately not help finding common features of sensitive strains. However, only a few strains have been studied so far, and it might be worthwhile testing a statistical number from the warm-water and the cool-water group.

2.6 Conclusions

1. Temperature, PIC production, coccolith mass, and coccolith size are positively correlated. Since the positive correlation between coccolith mass and PIC production was observed in response to seawater carbonate chemistry changes as well (Bach et al., 2012a), it can be hypothesized that coccolith mass might be a good proxy for PIC production independent of the environmental parameter causing the change in PIC production.

2. Sub-optimal growth temperature was identified as one of the potential causes of coccolith malformations in the field. Since the effect of sub-optimal temperature on coccolith morphogenesis is strain-specific, a statistically relevant

number of strains have to be tested in order to clarify whether this effect is indeed ecologically relevant.

3. We consistently showed for the first time that *E. huxleyi* features a PIC : POC minimum under optimum growth temperature. Taken together with literature data, this finding suggests that global environmental change will lead to a marked decrease in PIC : POC of *E. huxleyi* and possibly coccolithophores as a group.

Chapter 3

Temperature affects the individual sinking velocity of *Emiliania huxleyi* strains

This chapter corresponds to the published article by Rosas-Navarro et al. (2018).

3.1 Abstract

The sinking properties of three strains of *Emiliania huxleyi* in response to temperature changes were examined. We used a recently proposed approach to calculate sinking velocities from coccosphere architecture Hoffmann et al. (2015), which has the advantage to be applicable not only to culture samples, but also to field samples including fossil material. Our data show that temperature in the sub-optimal range impacts sinking velocity of *E. huxleyi*. This response is widespread among strains isolated in different locations and moreover comparatively predictable, as indicated by the similar slopes of the linear regressions. Sinking velocity was positively correlated to temperature as well as individual cell PIC : POC ratio over the sub-optimum to optimum temperature range in all strains. In the context of climate change our data point to an important influence of global warming on sinking velocities. It has recently been shown that seawater acidification has no effect on sinking velocity of a Mediterranean *E. huxleyi* strain, while nutrient limitation seems to have a small negative effect on sinking velocity Bach et al. (2012b); Pantorno et al. (2013); Milner et al. (2016). Given that warming, acidification, and lowered nutrient availability will occur simultaneously under climate change scenarios, the question is what the net effect of different influential factors will be. For example, will the effects of warming and nutrient limitation cancel? This ques-

tion cannot be answered conclusively but analyses of field samples in addition to laboratory culture studies will improve predictions because in field samples multifactor influences and even evolutionary changes are not excluded. As mentioned above, the approach of determining sinking rate followed here is applicable to field samples. Future studies could use it to analyse not only seasonal and geographic patterns but also changes in sinking velocity over geological time scales.

3.2 Introduction

It is generally acknowledged that global climate change will impact marine phytoplankton in terms of physiology. These physiological changes are usually considered in isolation. However, physiological changes might also have secondary effects, which can themselves feedback on physiology. An example of such a secondary effect is sinking velocity, which influences the position in the water column in which the cells reside. Sinking of the biogeochemically important coccolithophores is strongly influenced by their calcareous shell, the coccosphere. The comparatively high density of calcite makes the coccosphere act as ballast stones Eppley et al. (1969); Ziveri et al. (2007); Bach et al. (2012b). Although surface ocean mixing rates are high compared to coccolithophore sinking rates, some of the bigger species such as *Coccolithus pelagicus* are exported as individual cells Broerse et al. (2000); Young and Ziveri (2000); Ziveri and Thunell (2000); Monteiro et al. (2016). This is counter intuitive because the sinking velocity of e.g. *C. pelagicus* is ca. 6 m/d Gerecht et al. (2015) and slow compared to surface ocean mixing rates of ca. 100 m/d Young (1994). Calculations combining *E. huxleyi* growth rates, sinking rates, and surface ocean mixing rates suggest that individual cell sinking in this species is relatively unimportant whereas it might be relevant in heavier species such as *C. pelagicus* and *Calcidiscus leptoporus* Monteiro et al. (2016). However, our choice of *E. huxleyi* was not primarily motivated by the ecological relevance of its sinking. We chose *E. huxleyi* to make this study maximally comparable to previous studies using the same equations to calculate individual cell density and sinking rate (see below).

Moreover, climate change will result in a more pronounced stratification of the water column, thereby increasing the significance of sinking. Stratification will also lead to nutrient depletion in the photic zone where coccolithophores thrive. It has traditionally been assumed that nutrient limitation enhances calcification, and increases sinking velocities Baumann et al. (1978); Linschooten et al. (1991); Young (1994); Lecourt et al. (1996). This mechanism was regarded as a means to reach deeper, nutrient rich water layers. The slim, currently available, evidence however, does not support this view Bach et al. (2012b); Pantorno et al. (2013); Gerecht et al. (2015). Climate change induced nutrient depletion will be accompanied by seawater acidification and a rise in temperature Levitus et al. (2000);

Cermeño et al. (2008); Doney et al. (2009); Lyman et al. (2010); Bopp et al. (2013). Hence, in order to assess future sinking behaviour of coccolithophores, these factors also have to be considered. A recent study analysed sinking velocities of *E. huxleyi* in response to acidification and temperature increase Milner et al. (2016). While acidification had no effect on sinking velocity, a temperature increase had a profound effect, increasing sinking velocity. This suggests that in the context of climate change temperature might be an important factor influencing sinking velocity. However, the study by Milner et al. (2016) is of somewhat limited evidential strength, because only one strain of *E. huxleyi* was analysed at two different temperatures. Moreover, the temperature optimum for this strain is unknown, although it is fair to assume that the sub-optimal temperature range was studied Milner et al. (2016). In this study we analyse the sinking velocity response to temperature of three further *E. huxleyi* strains in the sub-optimal temperature range. In the context of global climate change, the sub-optimal temperature range is of particular interest because global warming over the next century will result in surface ocean temperatures which are still sub-optimal for most coccolithophore clones Buitenhuis et al. (2008); Langer et al. (2009); Heinle (2014); Rosas-Navarro et al. (2016). In terms of cell physiology the distinction between sub-optimal and supra-optimal temperatures is important because the latter usually have dramatic effects which can be attributed to heat-damage of e.g. proteins Langer et al. (2010). Sub-optimal temperatures, by contrast, generally produce less obvious effects and it is by no means straightforward to predict whether an effect will be observable or not Rosas-Navarro et al. (2016). That is why we analysed sinking velocities in response to sub-optimum to optimum temperatures here. Our analyses are not based on direct measurements of sinking rate. Instead, we employ a recently introduced method of calculating sinking rates from coccosphere architecture Hoffmann et al. (2015). This approach yields *E. huxleyi* sinking rates which tally well with directly measured rates, and has the advantage of being applicable to culture samples and field samples including fossil material. Hence there is the potential for comparative culture-field studies. The first calculations by Hoffmann et al. (2015) were based on FIB-SEM data, the production of which is technically difficult and time consuming. Subsequent studies, however, used data based on conventional SEM, light microscopy, and cell counters, which are readily available in the framework of a culture experiment Gerecht et al. (2015); Milner et al. (2016). We followed this latter approach to make our data and calculations comparable to the ones by Milner et al. Milner et al. (2016), because it was the aim of this study to build upon their initial sinking rate-temperature data. We used three different *E. huxleyi* strains to test for strain specificity, and four different temperatures, the highest of which representing the optimum temperature of these strains.

3.3 Materials and methods

In this chapter, with the main objective of calculating the sinking velocity of individual cells of three strains of *E. huxleyi* grown at different temperatures, under non-limiting conditions of light and nutrients, we used the Stokes' law Hoffmann et al. (2015). To use the Stokes' law formula the following four measurements were needed: number of observed attached coccoliths, coccosphere diameter, protoplast diameter, and coccolith calcite mass. The first two were measured from scanning electronic microscopy (SEM) images and the protoplast diameter with a Coulter Counter. The coccolith calcite mass variable results of the experiment are already analysed by Rosas-Navarro et al. (2016). Temperature and salinity were necessary to calculate the water density and the dynamic viscosity of water, both required variables to calculate the sinking velocity. The experiment was performed by triplicate.

Another objective of the present study was to compare the particulate inorganic carbon (PIC) in individual cells (that is the PIC in the attached coccoliths) with the bulk PIC (that is the PIC in both attached and detached coccoliths). The bulk PIC was chemically derived and was analysed by Rosas-Navarro et al. (2016).

We also calculated a geometrically derived particulate organic carbon (POC) and compared it with the chemically derived POC; this last one was analysed by Rosas-Navarro et al. (2016). Similarly, we calculated and compared individual PIC : POC ratios using the individual PIC and the geometrically and chemically derived results for POC. We compared the individual PIC : POC ratio with the bulk PIC : POC ratio. Throughout the text we use the word "individual" to make clear that the PIC or calcite of the attached coccoliths was used, as opposed to bulk PIC including loose coccoliths.

3.3.1 Pre-culture and batch culture experiments

Clonal cultures of *Emiliania huxleyi* were obtained from the Roscoff Culture Collection. We selected three strains of *E. huxleyi*, two from the Japanese coast in the North Pacific Ocean (RCC1710 – synonym of NG1 and RCC1252 – synonym of AC678 and MT0610E) and a third strain from the same region but of unknown exact origin and strain name, named here IAN01. Strain RCC1710 was collected off Nagasaki at Tsushima Strait (Japan) and RCC1252 at Tsugaru Strait (Japan); both places are strongly influenced by the Tsushima warm current. Additional information about the strain RCC1252 can be found at `http://roscoff-culture-collection.org/`.

The culture media was sterile-filtered North Sea water (filtered through 0.2 μm pore size sterile Sartobran 300 filter cartridges, Sartorius, Germany) supplemented with nutrients (nitrate –882.5 μM– and phosphate –36.25 μM), metals and vitamins according to Guillard and Ryther (1962). Cell densities, called here cell concentration to prevent confusion with the individual density, and cell diameter were determined using a Multisizer 3 Coulter Counter (Beckman Coulter for particle characterization). To prevent significant changes in seawater carbonate chemistry, maximum cell densities were limited to $\approx 1 \times 10^5$ cells ml^{-1} (e.g. Oviedo et al., 2014). We used a 16/8 light/dark cycle, and an irradiance of $\approx 300\,\mu$mol photons s^{-1} m^{-2} in an incubator, where transparent culture flasks during the acclimation, and latter the transparent glass bottles during the experiment, were located in the incubator so that they would not block the path of light. For acclimation to the different temperatures of the experiment before harvesting, the three strains were grown at the different temperatures in 200 ml culture media solution in polycarbonate culture flasks of 250 ml volume, at initial densities of 4000 cells per millilitre, with daily observation and quantification for at least 20 generations. The frequency of inoculation in new flasks varied depending on the cell concentration or the amount of water remaining (since it was subtracted for the measurements) so therefore depending on each growth rate.

The dilute batch culture experiments were conducted in triplicate, i.e. in three different incubation bottles, for the strains RCC1710 and RCC1252 at 10, 15, 20 and 25 °C of temperature, and for IAN01 at 15, 20 and 25 °C. The strains were grown in 2 L of sea water within transparent sterilized 2.3 L glass bottles. Cell concentration at inoculation was 500 to 1000 cells ml^{-1}, and at harvest it was a maximum of 1×10^5cells ml^{-1}. Harvesting was done 9 h after the onset of the light period, lasting between 1 and two hours.

3.3.2 Coccosphere's number of attached coccoliths and diameter

Thirty millilitres of culture was filtered onto polycarbonate filters (0.8 μm pore size) and dried at 60 °C for 24 h. A small portion (~ 0.7 cm^2) of each filter was mounted on an aluminium stub and coated with gold (EMITECH K550X sputter coater). Images were captured along random transects using a ZEISS-EVO MA10 SEM.

The SEM images were used to analyse ~ 50 complete coccospheres per sample by counting the number of attached coccoliths observed in each coccosphere (including those observed below other coccoliths in multi-layered coccospheres). The number of attached coccoliths per coccosphere was estimated dividing the number of visible attached coccoliths per coccosphere by 0.75 (Hoffmann et al., 2015).

As coccospheres were mostly oval and in some cases irregular, their diameter was calculated using the surface area of the coccosphere in the formula for area of a circle. The surface area of the coccospheres was manually measured on the SEM images using the program ImageJ. Measurements in pixels were transformed to micrometres according to the corresponding scale of the SEM images.

3.3.3 Individual density and sinking velocity

Individual density was estimated dividing the total individual mass by the total individual volume (Hoffmann et al., 2015). Cell (protoplast) diameter was recorded from the Multisizer 3 Coulter Counter data and was used to calculate the cell volume and to estimate the cell mass assuming a density of 1.05 g cm^3 for the organic cell matter (Paasche, 2002). Coccosphere calcite mass was calculated as the product of coccolith mass (results from Chapter 2 and in Rosas-Navarro et al. (2016)) by the number of attached coccoliths per cell. Coccosphere calcite volume was estimated assuming a density for calcite of 2.7 g cm^3 (Paasche, 2002). Total individual volume was calculated from the measured coccosphere diameter. For the total individual mass were considered the spaces between coccoliths presumably filled with seawater. Hence, volume of seawater was calculated from the difference of the total individual volume minus the sum of the volumes of the organic (protoplast) plus the inorganic (calcite) cellular components. Seawater mass was estimated from a calculated seawater density for each temperature (Table 3.1). Seawater density was calculated for each temperature treatment, for a measured salinity of 32‰ and at atmospheric pressure, according to Millero et al. (1980). Therefore, individual density was estimated dividing the sum of the three masses (protoplast, calcite, and seawater) by the total volume estimated from the measured coccosphere diameter.

Table 3.1: Seawater density and seawater dynamic viscosity. Used for the estimation of the individual sinking velocity at the different temperature T treatments.

T [°C]	Water density [g cm^{-3}]	Dynamic viscosity [g cm^{-1} s^{-1}]
10	1.025	0.014
15	1.024	0.012
20	1.022	0.011
25	1.021	0.010

According to Stokes' law, individual sinking velocity was calculated according to:

$$v_s = \frac{2(\rho_i - \rho_{sw}) \cdot g \cdot R^2}{9 \cdot \nu_{sw}}, \tag{3.1}$$

where v_s is the individual sinking velocity (in $m\,d^{-1}$) (vertically downwards if $\rho_i > \rho_{sw}$), g is the gravitational acceleration (in $m\,d^{-2}$), R is the radius of the coccosphere (in m), ρ_i is the individual density (in $g\,m^{-3}$), ρ_{sw} is seawater's density (in $g\,m^{-3}$) and ν_{sw} is the dynamic viscosity of seawater (in $g\,m^{-1}\,d^{-1}$). Dynamic viscosity was calculated for each temperature (Table 3.1), for a salinity of 32‰ and at atmospheric pressure, according to Sharqawy et al. (2010).

3.3.4 Geometrically derived PIC in individual cells

Particulate inorganic carbon in individual cells, i.e. PIC in the attached coccoliths per coccosphere, was calculated using SEM and light microscopy (LM) results. It was calculated using the measured PIC per coccolith derived from LM coccolith mass measurements Rosas-Navarro et al. (2016), and the number of attached coccoliths per coccosphere obtained from SEM counts.

Geometrically derived PIC in individual cells was then calculated as follows:

$$\mathrm{PIC}_{\mathrm{cell}^{-1}} = \frac{M_c \cdot 12.0107 \cdot C_{\mathrm{sph}^{-1}}}{100.0869}, \tag{3.2}$$

where $\mathrm{PIC}_{\mathrm{cell}^{-1}}$ = cellular PIC (in pg), M_c = coccolith calcite mass (in pg), 12.0107 corresponds to the relative atomic mass of carbon, 100.0869 corresponds to the relative molecular mass of calcite, $C_{\mathrm{sph}^{-1}}$ = attached coccoliths per coccosphere. Calculations were made for each replicate.

3.3.5 Theoretical number of detached coccoliths

The theoretical number of detached coccoliths per cell and the loose PIC per cell were calculated using the chemically derived bulk PIC per cell, the PIC per coccolith measured through microscopy techniques (both variables from the results in Chapter 2 published by Rosas-Navarro et al., 2016), and the counted number of attached coccoliths per coccosphere. The calculation for the theoretical number of detached coccoliths per cell was: total coccoliths per cell (from chemically measured cellular PIC divided by the LM derived PIC per coccolith) minus attached coccoliths per coccosphere (from SEM counts). We got the loose PIC per cell multiplying the number of detached coccoliths per cell by the measured PIC per coccolith. The calculations were done for each replicate.

3.3.6 Geometrically derived cellular POC

Geometrically derived cellular POC quota was calculated following Menden-Deuer and Lessard (2000) as in Hoffmann et al. (2015), according to the following equation:

$$\mathrm{POC}_{\mathrm{cell}^{-1}} = 0.216 \cdot {V_{\mathrm{cell}}}^{0.939} \tag{3.3}$$

where $\mathrm{POC}_{\mathrm{cell}^{-1}}$ = cellular POC (in pg), V_{cell} = cell (protoplast) volume (in $\mu\mathrm{m}^3$) calculated from the cell diameter measured with the Coulter Counter, 0.216 and 0.939 correspond to constants for plankton (Menden-Deuer and Lessard, 2000; Hoffmann et al., 2015). Calculations were made for each replicate.

The PIC : POC ratio for individual cells, i.e. only considering the attached coccoliths and not the detached coccoliths, was calculated using the geometrically derived cellular PIC quota in the ratio instead of the chemically derived PIC quota. A purely geometrically derived PIC : POC ratio was also calculated using the geometrically derived cellular PIC and POC quotas.

3.3.7 Statistics

For the three *E. huxleyi* strains together, ANOVA (two-factor with replication) was used to test whether a response variable (e.g. individual sinking velocity) presented significant ($p < 0.05$) differences between the temperature treatments, to test whether the effect was strain-independent or strain-specific ($p < 0.05$), and to test whether there were significant differences in the interaction between treatment and strain ($p < 0.05$) and therefore whether the different strains respond similarly or not regardless of whether they were presenting differences between them. Degrees of freedom are given as subscripts of F. For the different methods used for calculating the cellular POC and the individual cell PIC : POC ratio, a t-Test (two-tail) was used to test the null hypothesis that the means of the two methods are equal ($alpha = 0.05$).

Each measured variable, for each of the tripled bottles, came from a statistically big number of samples (of ~ 50 for the case of SEM samples, of minimum ~ 300 for the LM samples, and of $\sim 50\,000$ for the Coulter Counter samples), reducing the standard errors and therefore strengthening the statistical analysis. Except for the regressions reported in the figures which used the mean values of the triplicates, the rest of statistical analysis used the values of each replicate. In the results we report the means and the standard deviations of the triplicates. For the case of the calculated individual sinking velocity, to strengthen the results due to the involvement of several variables each one with its own standard error, we

calculated the error propagation of the individual sinking velocity calculation for each replicate (three replicates per temperature treatment and strain). The errors used for the error propagation calculation were the standard errors of the four measured variables (number of observed attached coccoliths, protoplast diameter, coccolith calcite mass, and coccosphere diameter), the errors of the variables water density and dynamic viscosity which were calculated using the errors derived from the maximum variation found for temperature and salinity during the experiment (0.5 °C and 0.5‰ respectively), and the error for the gravitational acceleration based on the maximum and minimum values that can be found on Earth. These results are more detailed in the Appendix B.2.

Finally, the biotic variables analysed in this chapter and in Chapter 2 (published by Rosas-Navarro et al., 2016) were analysed through a correlation matrix (Table B.1 in Appendix B.1). The analysis was carried out using PRIMER-E v.6.0., following the methods described by Clarke and Gorley (2006).

3.4 Results

3.4.1 Coccosphere morphology and mass, and cell diameter

Independently of the strain, the number of attached coccoliths per coccosphere increased linearly with temperature (Fig. 3.2b and Table 3.2). There were no significant differences in the interaction between treatment and strain of the three strains ($F = 0.37$, $p = 0.824$), so there were no significant differences between their slopes, even though the number of attached coccoliths of the strain IAN01 was lower than that of the other two strains. There were no significant differences between strains RCC1710 and RCC1252 ($F = 1.05$, $p = 0.321$). On average, the number of attached coccoliths increased with temperature $\sim$ 5.5 coccoliths from 10 to 25 °C, $\sim$ 3.6 coccoliths from 15 to 25 °C, and $\sim$ 2.2 coccoliths from 20 to 25 °C; on average, coccospheres had 1.9 coccoliths more (or 1.1 times more) each 5 °C. Representative images of two coccospheres of the strain RCC1252 grown at 10 and 25 °C are shown in Fig. 3.1.

Coccosphere calcite mass (Fig. 3.2c and Table B.3), calculated from coccolith mass and number of attached coccoliths per coccosphere, increased linearly from 10 to 25 °C in the three strains. It presented significant differences between the treatments ($F = 64.34$, $p = 0.000$), also between the strains ($F = 12.66$, $p = 0.000$), but there were no significant differences in the interaction between treatment and strain ($F = 2.29$, $p = 0.099$). Coccosphere calcite mass increased on average 41% or 12.75 pg each 5 °C.

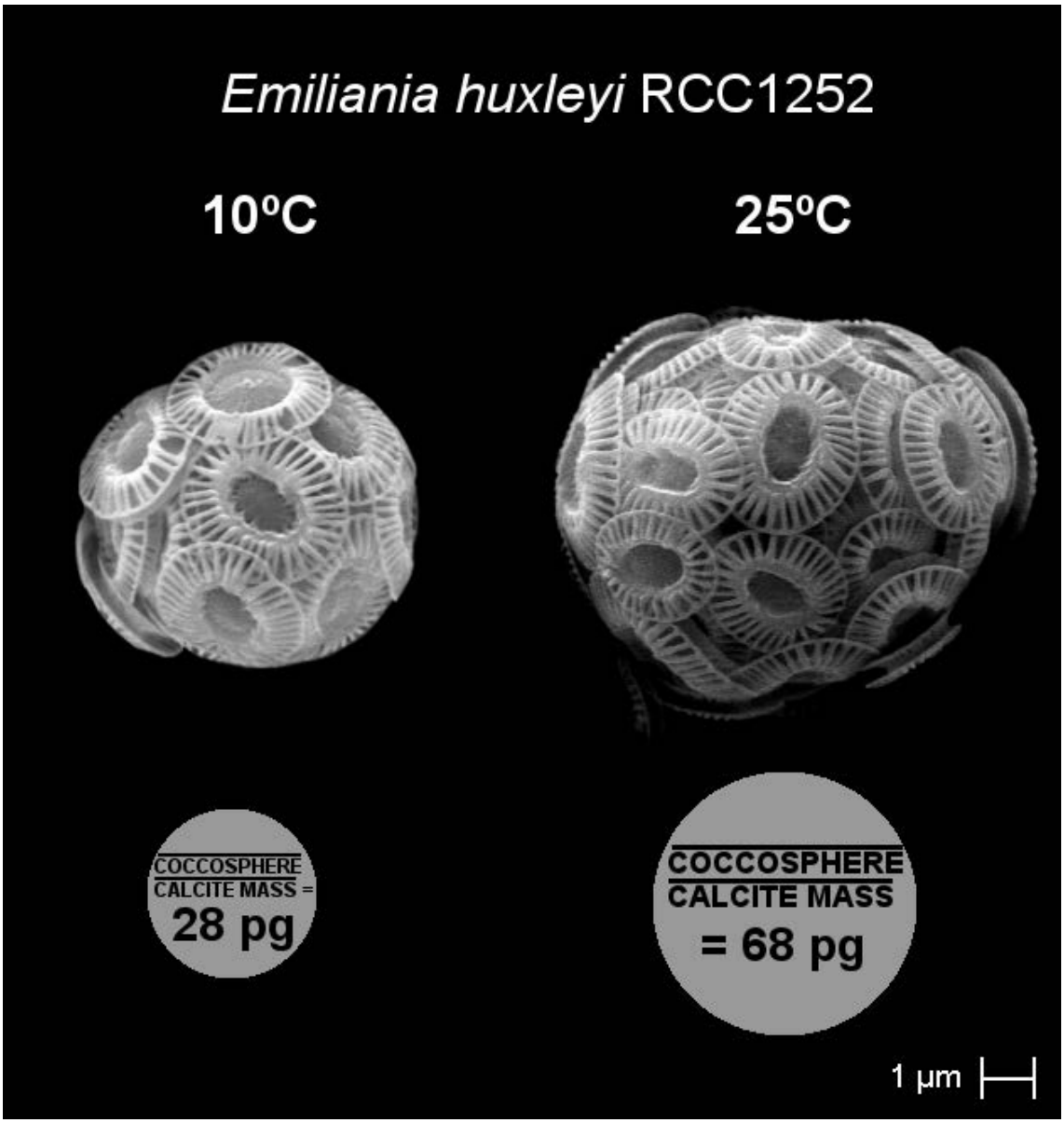

Figure 3.1: Examples of two coccospheres of the strain RCC1252 grown at 10 and 25 °C. The average coccosphere calcite mass for the strain at both temperatures is shown in circles (circle areas are proportional to the average mass). Scale bar equal to 1 μm.

Coccosphere diameter results (Fig. 3.3a and Table 3.2) showed statistically significant differences between the three strains ($F = 42.01$, $p = 0.000$) but were found significant differences between the treatments in which the three strains presented smaller coccospheres at lower experimental temperatures and larger coccospheres at higher experimental temperatures.

Cell diameter (Fig. 3.3b and Table 3.2) did not show any strain-independent or strain-specific trend related with temperature or any other variable.

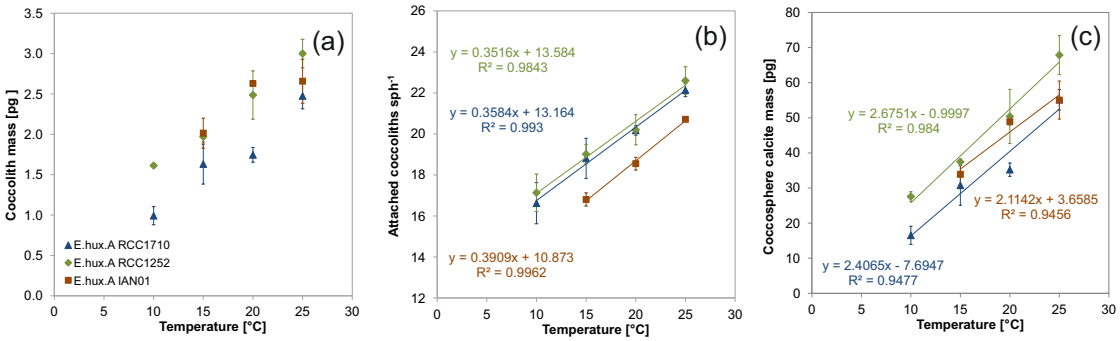

Figure 3.2: Changes in the coccosphere calcite mass (c) calculated from the coccolith mass (a; results from Chapter 2) and the number of attached coccoliths per coccosphere (b), at different temperatures. Standard deviations of the triplicate experiment results are shown. Some linear trend lines and r-squared values are shown (b, c). Three different strains of *E. huxleyi* were used.

Table 3.2: Protoplast and coccosphere diameter, number of attached and detached coccoliths per cell, PIC per coccolith, and loose PIC per cell. Standard deviation of the triplicates is shown in parentheses. Sph: coccosphere.

Strain	T [°C]	Protoplast diameter [μm]	Sph diameter [μm]	Attached coccoliths sph^{-1}	Detached coccoliths cell^{-1}	PIC/coccolith [pg]	Loose PIC/cell [pg]
RCC1710	10	4.80 (0.01)	6.44 (0.16)	16.62 (1.00)	103.87 (2.84)	0.12 (0.01)	13.16 (0.06)
RCC1710	15	5.24 (0.17)	6.91 (0.22)	18.81 (0.98)	54.35 (14.48)	0.20 (0.03)	10.29 (0.54)
RCC1710	20	4.99 (0.01)	6.98 (0.26)	20.17 (0.23)	32.99 (0.57)	0.21 (0.01)	7.12 (0.03)
RCC1710	25	4.78 (0.06)	6.95 (0.07)	22.14 (0.32)	13.79 (1.26)	0.30 (0.02)	4.09 (0.11)
RCC1252	10	4.60 (0.05)	6.27 (0.39)	17.13 (0.91)	25.79 (2.64)	0.19 (0.00)	4.98 (0.52)
RCC1252	15	4.86 (0.03)	6.75 (0.14)	19.02 (0.48)	22.97 (0.70)	0.24 (0.01)	5.43 (0.23)
RCC1252	20	4.47 (0.02)	6.82 (0.19)	20.20 (0.74)	14.63 (7.36)	0.30 (0.04)	4.06 (1.47)
RCC1252	25	4.89 (0.00)	7.51 (0.07)	22.60 (0.67)	11.38 (3.00)	0.36 (0.02)	4.06 (0.87)
IAN01	15	4.53 (0.05)	6.07 (0.19)	16.81 (0.32)	25.44 (3.10)	0.24 (0.02)	6.11 (0.17)
IAN01	20	4.51 (0.01)	5.92 (0.11)	18.55 (0.31)	7.13 (0.63)	0.32 (0.00)	2.26 (0.20)
IAN01	25	4.58 (0.05)	6.66 (0.38)	20.71 (0.09)	14.74 (4.70)	0.32 (0.03)	4.60 (1.00)

Table 3.3: *Emiliania huxleyi* estimated individual density and estimated individual sinking velocity. Calculated masses and volumes involved in the estimations are shown. Standard deviation of the triplicates is shown in parentheses. Cell: protoplast; Sph: coccosphere; SW: extracellular matrix seawater.

Strain	T [°C]	Cell mass [pg]	Cell volume [μm^3]	Sph. calcite mass [pg]	Sph. calcite volume [μm^3]	SW mass [pg]	SW volume [μm^3]	Individual mass [pg]	Individual volume [μm^3]	Individual density [g · cm^{-3}]	Individual sinking velocity [m · d^{-1}]
RCC1710	10	60.75 (0.29)	57.86 (0.28)	16.53 (2.59)	6.12 (0.96)	77.64 (10.15)	75.78 (9.91)	154.93 (10.66)	139.76 (10.04)	1.11 (0.01)	0.12 (0.02)
RCC1710	15	79.48 (7.70)	75.69 (7.34)	30.77 (5.68)	11.39 (2.10)	87.86 (24.25)	85.83 (23.69)	198.10 (16.60)	172.91 (16.16)	1.15 (0.02)	0.23 (0.04)
RCC1710	20	68.38 (0.49)	65.12 (0.47)	35.23 (1.91)	13.05 (0.71)	102.37 (19.30)	100.12 (18.88)	205.97 (21.70)	178.29 (20.05)	1.16 (0.01)	0.29 (0.00)
RCC1710	25	59.89 (2.43)	57.04 (2.32)	55.15 (2.91)	20.43 (1.08)	99.13 (6.89)	97.08 (6.75)	215.21 (6.29)	175.76 (5.58)	1.23 (0.02)	0.49 (0.03)
RCC1252	10	53.65 (1.57)	51.10 (1.50)	27.64 (1.47)	10.24 (0.55)	70.49 (23.85)	68.80 (23.28)	151.78 (25.94)	130.13 (24.44)	1.17 (0.02)	0.19 (0.00)
RCC1252	15	62.99 (1.20)	59.99 (1.14)	37.45 (0.79)	13.87 (0.29)	89.07 (10.29)	87.01 (10.05)	189.51 (9.99)	160.87 (10.04)	1.18 (0.01)	0.27 (0.01)
RCC1252	20	49.03 (0.67)	46.69 (0.64)	50.38 (7.71)	18.66 (2.85)	103.43 (13.08)	101.16 (12.79)	202.84 (18.16)	166.51 (14.08)	1.22 (0.02)	0.40 (0.05)
RCC1252	25	64.10 (0.14)	61.05 (0.13)	67.85 (5.56)	25.13 (2.06)	138.89 (8.10)	136.02 (7.93)	270.84 (5.14)	222.20 (6.55)	1.22 (0.02)	0.55 (0.05)
IAN01	15	51.19 (1.55)	48.75 (1.47)	33.91 (3.72)	12.56 (1.38)	57.10 (11.05)	55.78 (10.79)	142.19 (13.18)	117.09 (11.34)	1.21 (0.02)	0.27 (0.02)
IAN01	20	50.30 (0.29)	47.90 (0.28)	48.80 (0.82)	18.07 (0.30)	43.96 (6.73)	43.00 (6.58)	143.06 (5.97)	108.97 (6.33)	1.31 (0.02)	0.45 (0.02)
IAN01	25	52.91 (1.89)	50.39 (1.80)	55.05 (5.42)	20.39 (2.01)	86.71 (28.07)	84.92 (27.49)	194.67 (31.34)	155.70 (27.61)	1.25 (0.02)	0.51 (0.02)

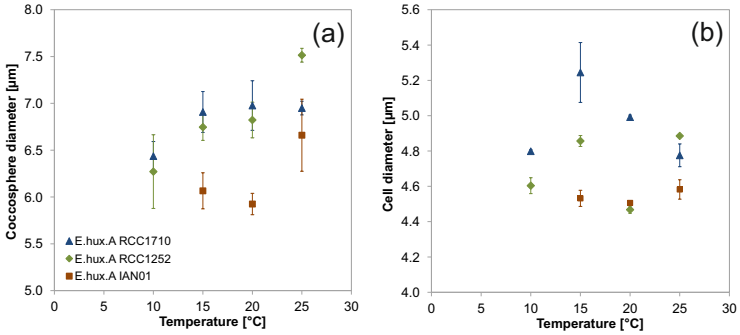

Figure 3.3: Changes in the coccosphere (a) and cell (b) diameters at different temperatures. Standard deviations of the triplicate experiment results are shown. Three different strains of *E. huxleyi* were used.

3.4.2 Individual density and sinking velocity

Individual density was calculated considering the organic and inorganic components of the cell and the spaces between the coccoliths presumably filled with seawater (Table B.3); total mass (Fig. 3.4a) was divided by the individual volume which was calculated from the coccosphere diameter (Fig. 3.3a and Table 3.2). Individuals density was lowest at the lowest temperature treatment independently of the strain (Fig. 3.4b). The treatments presented significant differences ($F = 21.71$, $p = 0.000$), but there were also significant differences between the three strains and in the interaction between treatment and strain. Highest differences between intervals of 5 °C, were found between 15 and 20 °C in strains RCC1252 and IAN01, and between 20 and 25 °C in strain RCC1710. Individual density changes were on average 2% higher each 5 °C.

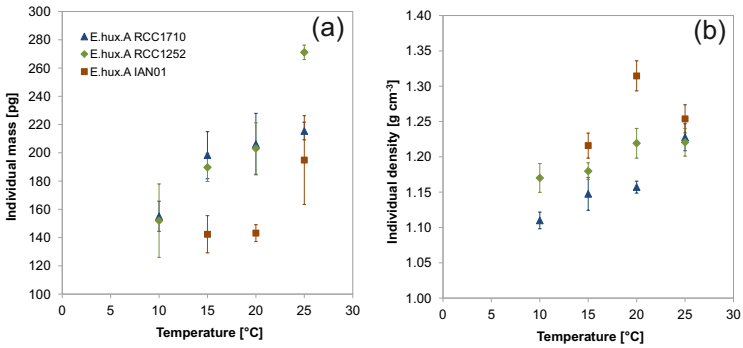

Figure 3.4: Changes in the individual mass (a) and density (b) at different temperatures. Individual results consider changes in the the cell organic matter, in the coccosphere calcite –from attached coccoliths–, and in the seawater presumably filling the spaces between the coccoliths. Standard deviations of the triplicate experiment results are shown. Three different strains of *E. huxleyi* were used.

Individual sinking velocity (Fig. 3.5 and Table B.3) presented significant differences between treatments ($F = 133.45$, $p = 0.000$), it was significantly positively correlated with temperature, independently of the strain, and the carbonate system variations did not improve the correlation significantly. The calculated velocities with their error propagation showed a positive trend with temperature in the three strains (see Appendix B.2). No significant differences were found between strains RCC1252 and IAN01, neither in their interaction between treatment and strain. Strain RCC1710 presented significant differences with the other two strains but no significant difference with the strain RCC1252 in the interaction between treatment and strain ($F = 1.43$, $p = 0.271$). The increase in velocity each 5 °C was of $\sim$ 50%. Maximum individual sinking velocity in the three strains was found at 25 °C and was of $\sim$ 0.5 m d^{-1}.

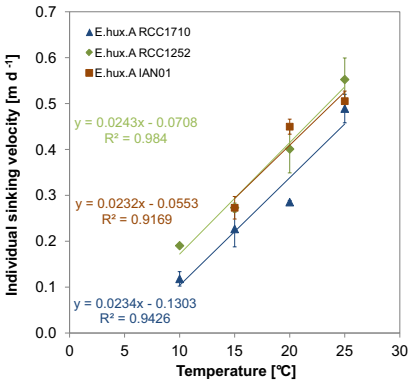

Figure 3.5: Changes in the individual sinking velocity calculated for three different strains of *E. huxleyi* grown at different temperatures. Strain RCC1710 (triangle symbols), strain RCC1252 (diamond symbols), and strain IAN01 (square symbols). Standard deviations of the triplicate experiment results, linear trend lines, corresponding equations, and r-squared values are shown.

3.4.3 Detached coccoliths and loose PIC

The theoretical numbers of detached coccoliths per cell (Table 3.2) were significantly different between the temperature treatments, between the strains and in the interaction between treatment and strain. Part of the variation is due to the errors of the variables involved in the calculation which presented low standard errors as they were obtained with statistically large sample sizes (minimum of 50 which was the case of the SEM samples) and part could be due to a possible change in the percentage of calcifying cells which unfortunately we do not know. Another part of the variation could be due to detaching because of the sampling procedure, to minimize it, careful management of the samples was always taken, for example the mixing of the cultures to avoid sedimentation was always performed with a very gentle rotation and the pressure of the pump during filtration limited to 200

mbar. Maximum numbers of detached coccoliths were found at 10 °C in strain RCC1710 with ∼ 100 detached coccoliths per cell and minimum numbers in all strains were on average ∼ 11 detached coccoliths per cell.

Maximum values of loose PIC per cell were found at 10 °C in strain RCC1710, they were of 13 pg per cell, and minimum values were on average of 3.5 pg per cell. The linear correlation between the loose PIC per cell (Table 3.2) and the number of detached coccoliths per cell had an R of 0.97.

3.4.4 Chemically and geometrically derived PIC and POC

The geometrically derived PIC quota for individuals cells is proportional to the coccosphere calcite mass (Fig. 3.2c) (the individual PIC gives the carbon (C) of the calcite ($CaCO_3$) in the coccosphere), they increased linearly from 10 to 25 °C independently of the strain.

The results obtained from the different methods used for calculating the cellular POC (geometrical or chemical, Table B.4 and Fig. 3.6) and the individual cell PIC : POC ratio (geom:geom or geom:chem in Table B.4) do not present significant differences (two-tail t-Test, $alpha = 0.05$). The POC ratio data (ratio calculated from the chemically derived POC divided by the geometrically derived POC) fits a normal distribution (Fig. 3.6) and has a mean value of 0.99 with a standard deviation of 0.05.

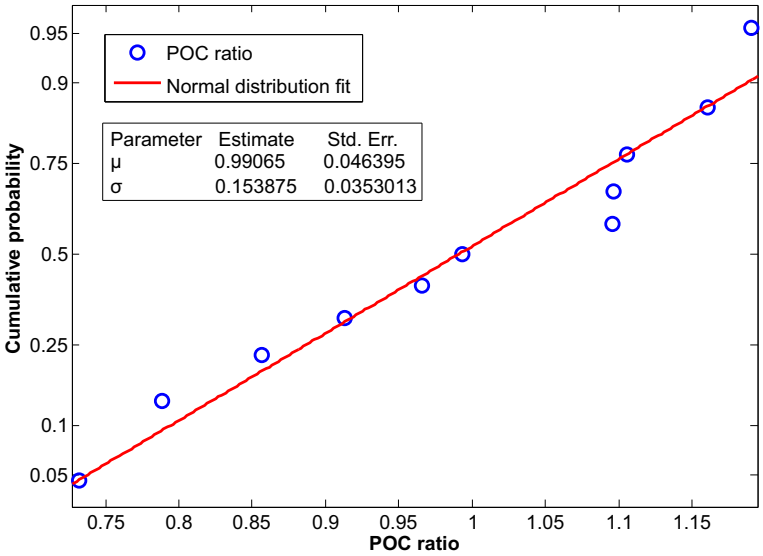

Figure 3.6: Cumulative probability of the particulate organic carbon (POC) ratio data. The POC ratio was calculated from the chemically derived POC and the geometrically derived POC. The plot shows that the data (circle symbols) fit a normal distribution (solid line). In a box are shown the mean and the standard deviation values with their corresponding standard errors.

Table 3.4: Chemically (chem) and geometrically (geom) derived PIC and POC. The chemical PIC corresponds to the bulk PIC, that is the PIC in the attached and in the detached coccoliths, while the geometrical PIC corresponds to the individual cell PIC. Standard deviation of the triplicates is shown in parentheses. Sph: coccosphere.

Strain	T [°C]	PIC (chem) [pg cell^{-1}]	PIC (geom) [pg sph^{-1}]	POC (chem) [pg cell^{-1}]	POC (geom) [pg cell^{-1}]	PIC : POC ratio (chem : chem)	PIC : POC ratio (geom : geom)	PIC : POC ratio (geom : chem)	POC ratio (chem : geom)
RCC1710	10	15.31 (0.15)	1.98 (0.31)	8.91 (0.29)	9.76 (0.04)	1.72 (0.07)	0.2 (0.03)	0.24 (0.03)	0.92 (0.03)
RCC1710	15	14.07 (0.4)	3.69 (0.68)	9.9 (0.11)	12.55 (1.14)	1.42 (0.02)	0.29 (0.05)	0.38 (0.09)	0.83 (0.04)
RCC1710	20	11.47 (0.09)	4.23 (0.23)	12.05 (0.79)	10.9 (0.07)	0.95 (0.05)	0.39 (0.02)	0.36 (0.01)	1.1 (0.07)
RCC1710	25	10.8 (0.24)	6.62 (0.35)	9.3 (0.8)	9.63 (0.37)	1.17 (0.13)	0.68 (0.06)	0.68 (0.07)	0.96 (0.05)
RCC1252	10	8.29 (0.49)	3.31 (0.17)	6.35 (0.11)	8.68 (0.24)	1.31 (0.06)	0.38 (0.02)	0.52 (0.03)	0.73 (0.02)
RCC1252	15	9.92 (0.32)	4.49 (0.1)	8.64 (0.29)	10.09 (0.18)	1.15 (0.07)	0.45 (0.01)	0.52 (0.03)	0.86 (0.04)
RCC1252	20	9.89 (0.28)	6.05 (0.92)	8.75 (0.71)	7.98 (0.1)	1.13 (0.1)	0.76 (0.12)	0.7 (0.16)	1.1 (0.08)
RCC1252	25	12.2 (0.21)	8.14 (0.67)	10.19 (0.75)	10.26 (0.02)	1.2 (0.1)	0.79 (0.07)	0.8 (0.02)	0.99 (0.07)
IAN01	15	10.18 (0.3)	4.07 (0.45)	9.89 (0.43)	8.31 (0.24)	1.03 (0.02)	0.49 (0.04)	0.41 (0.03)	1.19 (0.03)
IAN01	20	8.12 (0.21)	5.86 (0.11)	8.95 (0.43)	8.17 (0.04)	0.91 (0.02)	0.72 (0.01)	0.66 (0.03)	1.09 (0.05)
IAN01	25	11.21 (0.36)	6.61 (0.65)	9.95 (0.11)	8.57 (0.29)	1.13 (0.04)	0.77 (0.1)	0.66 (0.06)	1.16 (0.05)

3.4.5 Highly linearly correlated biotic variables

From a correlation matrix (Table B.1 in Appendix B.1) including all the biotic variables analysed in this chapter and in Chapter 2 (published by Rosas-Navarro et al., 2016)), we highlight the following linear correlations. Individual sinking velocity is highly correlated with coccosphere mass (concomitant with coccosphere volume and with PIC per individual cell)($R = 0.98$) and with coccolith mass ($R = 0.97$). Coccosphere mass, besides with individual sinking velocity, is mainly correlated with coccolith mass ($R = 0.97$). Detached and total number of coccoliths present a correlation of 0.99. The number of attached coccoliths per coccosphere is mainly correlated with individual mass ($R = 0.89$), secondly with tube width ($R = 0.88$), and thirdly with coccosphere mass ($R = 0.87$). The geometrically derived PIC : POC ratio is mainly correlated with coccolith mass ($R = 0.97$) and individual sinking velocity ($R = 0.95$). Regarding the relationship with temperature, growth rate (μ) was the highest linearly correlated variable with temperature ($R = 0.96$).

Table 3.5 lists and briefly describes the significant strain-independent and strain-specific responses to temperature found in this study.

3.5 Discussion

Our calculated sinking rates match data based on direct measurements of another *E. huxleyi* strain Bach et al. (2012b). On average, our sinking rates are by a factor of 1.3 lower than the ones reported by Bach et al. (2012b). Considering that RCC1710 has a 1.2 times lower sinking rate than the other two strains (Table B.3), the difference between our sinking rates and the ones reported by Bach

Table 3.5: Significant strain-independent and strain-specific responses of *E. huxleyi* to temperature, found in this study.

Strain-independent responses	Strain-specific responses
• The number of attached coccoliths per coccosphere increased linearly with temperature (on average 2 coccoliths more each 5 °C). • Coccosphere calcite mass increased linearly from 10 to 25 °C, on average 12.75 pg each 5 °C. • Smaller coccospheres were found at lower experimental temperatures and larger coccospheres at higher experimental temperatures. • Individual density lowest values were found at the lowest temperature treatment. • Individual sinking velocity increased linearly with temperature, from 10 to 25 °C. Velocity at 25 °C was of $\sim 0.5\ \mathrm{m \cdot d^{-1}}$. • Higher numbers of detached coccoliths per cell were found at the lowest temperature treatments. • Higher numbers of total number of coccoliths per cell were found at the lowest temperature treatments.	• Cell diameter. • Coccosphere diameter. Though a positive trend with temperature is observed in the three strains.

et al. (2012b) could be due to strain differences. This shows that our calculations are a useful way of estimating sinking rate. In the study by Bach et al. Bach et al. (2012b), however, cells were grown at 15 °C only. Therefore it remains an open question whether the response to changing temperature would show the same pattern when comparing measured and calculated sinking rates. Hence it is worthwhile to conduct a comparative study in the future, in which direct measurements are put alongside calculations as presented here.

The sinking velocity of all three strains of *E. huxleyi* was positively correlated to temperature. These results suggest that the effect of temperature in the suboptimal temperature range on sinking velocity of *E. huxleyi* is widespread among strains isolated in different locations and moreover comparatively predictable, as indicated by the similar slopes of the linear regressions. This means that there probably is little if any clone specificity in *E. huxleyi*'s temperature response pattern. In total four strains were tested (one by Milner et al., 2016, and three in this study), which might seem a small number but clone specificity was conspicuous when testing four clones for their responses to seawater carbonate chemistry Langer et al. (2009). Therefore we are confident that if responses were highly variable we would have detected that. Little inter-clone variability is a prerequisite for predicting the behaviour of natural populations. These populations are typically comprised of many different clones Medlin et al. (1996) and a relatively

uniform response pattern is therefore central to any prediction. However, predicting the behaviour of natural populations on the basis of laboratory results is not straightforward for another reason. In a laboratory experiment one single physicochemical factor can be varied and the response of a particular clone monitored. In the field, potentially many factors change simultaneously and an accurate prediction would require knowledge about the effects of all influential factors. In the course of climate change, a temperature increase will be accompanied by reduced nutrient availability and reduced seawater pH Boyd and Doney (2002); Caldeira and Wickett (2003); Rost et al. (2008), which will be discussed below.

Our data and the ones by Milner et al. (2016) show an increase in sinking rate with temperature. This effect has two components. First, a physical component which consists in the decrease in seawater density and dynamic viscosity (Table 3.1). Whereas the change in seawater density can account for a negligible increase in sinking rate of 0.4%, the change in dynamic viscosity causes an increase in sinking rate of ca. 28%. By contrast, our calculations yield an increase in sinking rate of ca. 70%. This difference is due to the second component, which is biological, i.e. related to changes in the individual cell density and cell size. Both individual cell density and cell size increase with temperature thus contributing to the increase in sinking rate. The changes in individual cell density are positively correlated to the individual cell PIC : POC. Therefore sinking rate correlates well with individual cell PIC : POC. This is driven by an increase in coccosphere size; not by a decrease in protoplast size. With increasing temperature there are more coccoliths in a coccosphere and the individual coccolith is heavier. In other words, the biological effect consists in the cell's putting on more and heavier ballast stones.

It is interesting to compare the bulk PIC : POC and the individual cell PIC : POC in response to temperature changes. While the bulk PIC : POC decreases with increasing temperature, the individual cell PIC : POC increases (Fig. 3.7). This highlights the need to consider individual cell PIC : POC, not bulk PIC : POC, as an indicator of sinking velocity in *E. huxleyi* (Fig. 3.8). In species which do not shed many coccoliths, e.g. *C. pelagicus*, this is of minor importance Gerecht et al. (2015). As an interesting methodological aside, we would like to emphasize that POC quota as determined by sample combustion tallies well with POC quota calculated from cell diameter (Fig. 3.6). Consequently the PIC : POC vs sinking velocity relationship holds, regardless of whether geometrically derived or directly measured POC quota is used (Fig. 3.8). This is important because using calculated POC quota renders it possible to determine PIC : POC vs sinking velocity relationships of fossil samples such as the exceptionally well preserved material described by Gibbs et al. (2013). While the positive correlation between PIC : POC and sinking velocity seems to be robust, the correlation between PIC : POC and individual cell density is slightly less reliable. Although a positive correlation between PIC : POC and individual cell density can be seen clearly in two of our three investigated strains (Fig. 3.9) and is also present in the one studied by Milner et al.

(2016) as well as in *C. pelagicus* Gerecht et al. (2015), one strain (IAN01) shows a less convincing correlation, which was also the case in the study by Hoffmann et al. (2015). This might simply be due to too few data points.

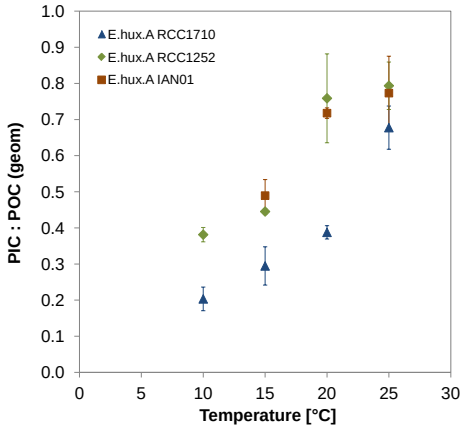

Figure 3.7: Geometrically derived PIC : POC changes in the individual cells of three different strains of *E. huxleyi* grown at different temperatures. Standard deviations of the triplicate experiment results are shown.

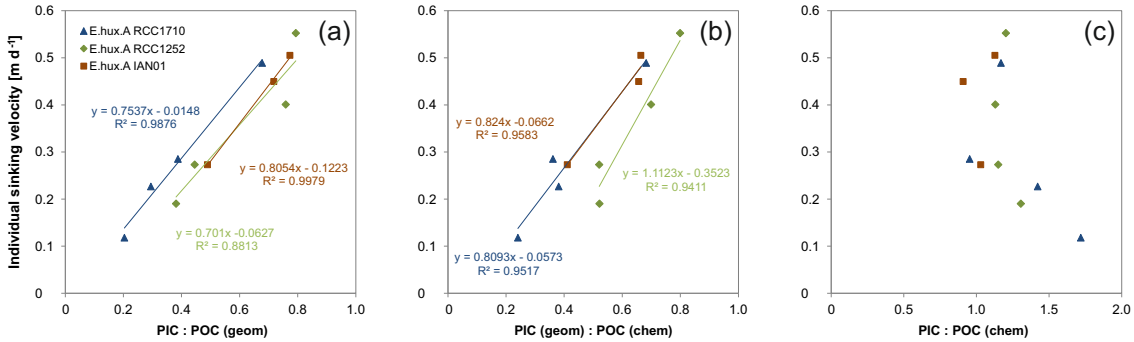

Figure 3.8: Geometrically derived PIC : POC in **(a)**, geometrically derived PIC and chemically derived POC in **(b)**, and chemically derived PIC : POC in **(c)**, versus the individual sinking velocity. PIC : POC in **(a)** and **(b)** correspond to the individual cell ratio, while in **(c)** the PIC of the ratio corresponds to the PIC in the attached plus the detached coccoliths, not only the attached as the PIC for the ratios in **(a)** and **(b)**. Obtained for three different strains of *E. huxleyi* grown at different temperatures. Linear trend lines and r-squared values are shown in **(a)** and **(b)**.

On the whole, there seems to be a strong impact of temperature on *E. huxleyi* sinking rates in laboratory cultures. In the context of climate change that would mean that global warming will increase sinking rates. However, global warming does not occur in isolation but will be accompanied by seawater acidification and reduced nutrient supply. A Mediterranean *E. huxleyi* strain showed no change in sinking rate in response to seawater acidification Milner et al. (2016). Should this response be representative for *E. huxleyi* as a species, the influence of ocean acidification can be ignored. Nutrient limitation has long since been regarded as a calcification stimulus and it was therefore thought that ballasting and sinking

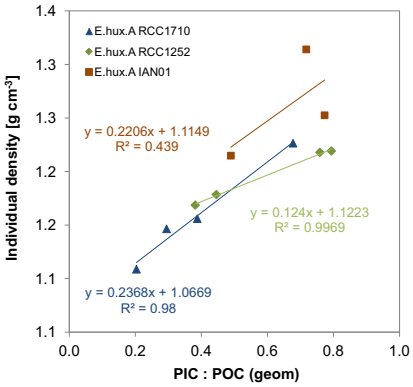

Figure 3.9: Geometrically derived PIC : POC versus the individual cell density. Obtained in three different strains of *E. huxleyi* grown at different temperatures. Linear trend lines and r-squared values are shown.

rate will increase under limiting conditions Baumann et al. (1978); Benner (2008). Recent laboratory experiments on *E. huxleyi* and *C. pelagicus*, however, showed slightly decreased sinking rates in response to macro-nutrient limitation Bach et al. (2012b); Pantorno et al. (2013); Gerecht et al. (2015). If that was a general pattern, the effects of nutrient limitation and warming would work in opposite directions. The net effect observed in the field will depend partly on the local situation, because nutrient limitation is more likely in already oligotrophic areas. Hence predicting *E. huxleyi*'s sinking rate behaviour under climate change conditions is difficult even if only ocean acidification and nutrient limitation are considered as secondary influences (considering temperature the primary one). And of course there might be more, as yet unknown, secondary influences. Therefore it would be interesting to calculate sinking rates of different coccolithophores from field samples. This is feasible using the calculations employed here, given that coccospheres are preserved. Field studies could not only analyse extant species over seasonal and geographical temperature changes, but also fossil material over major geological climate events such as the PETM. This would provide important information on multi-factor influences in the field, and moreover include evolutionary changes in case of geological timescales. This type of information is needed for any prediction of coccolithophore sinking behaviour under future climate change.

3.6 Conclusions

We demonstrate that the PIC : POC vs sinking velocity relationship can be determined based on geometrically derived PIC and POC quotas using raw data other than the FIB-SEM-approach Hoffmann et al. (2015). This is important because FIB sectioning of coccospheres is so time consuming that it would be practically impossible to produce a dataset such as the one presented here.

Although a direct comparison between calculated and measured sinking rate using the same strain is still missing, our calculated sinking rates tally well with measured sinking rates of another strain grown at one of the temperatures used in the present study. Our sinking rate calculations are based on coccosphere architecture alone and therefore have the advantage of being applicable to field samples including fossil material. This opens up the possibility of comparative culture-field studies which are impossible using direct measurements of sinking rate. Well preserved fossil coccospheres could be used to gain information of sinking behaviour over geological timescales and major climate events such as the PETM.

Bulk PIC data includes inorganic carbon from both individual cell and loose coccoliths. The bulk PIC : POC decreases with increasing temperature but the individual cell PIC : POC increases, emphasizing the need of considering individual cell PIC : POC, not bulk PIC : POC, as an indicator of sinking velocity in *E. huxleyi*.

Our study suggests that global warming will exert the foremost influence on coccolithophore sinking behaviour as opposed to ocean acidification and nutrient limitation. Calcification temperature in the sub-optimal range is driving the sinking velocity of individual cells of *E. huxleyi* and might lead to significant changes in eco-physiological terms. If cells sink faster under global warming conditions they might, for instance, experience light limitation earlier.

Chapter 4

Summary of Chapters 5 and 6

Chapters 5 and 6 are based on the same water samples collected along a transect in the Gulf of California and the NE Pacific margin. Chapter 5 is focused on *Emiliania huxleyi*'s morphotypes and morphological calcification variations, and Chapter 6 is focused on the different species within the genus *Gephyrocapsa* and on calcite estimations of both *E. huxleyi* and the *Gephyrocapsa* spp. Here we present a summary of both chapters.

In general, the main controlling hydrographic parameters in the G. Cal and NE Pacific margin waters are the low pH limiting in the deeper waters, the temperature limiting in the shallower waters due to temperatures above the optimum, and the nutrients mainly enhancing the standing stocks to maximum values (except for the species *G. oceanica*) in the corresponding station. The values at which the different species or morphologies are controlled are specific to each one.

Emiliania huxleyi type O is a colder morphotype more akin with higher ammonium concentrations and more tolerant to lower pH values than the morphotype A. The over-calcified *E. huxleyi* type A shared niche with the morphotype O. Despite the mentioned shared niche, the over-calcified *E. huxleyi* type A is probably really a morphological variation in the type A related to the hydrographic conditions and not a different genotype. The morphotype O might be indicative of the input of northern cold water transported by the CCS.

Here we found that unfavorable conditions for the cell such as the combination of phosphate, nitrate and nitrite low concentrations (though not the lowest concentrations), as well as low salinity and high coccolithophore/phytoplankton cell densities, are probably responsible for the collapsed morphology observed in the species *E. huxleyi* and *G. oceanica*. The under-calcified morphology, similarly to the collapsed morphology, seems mostly enhanced by unfavorable nutrient conditions.

Gephyrocapsa oceanica, the species with the highest coccosphere calcite mass of the species studied here, is the warmest species and the most tolerant and even akin to nutrient depleted waters. *Gephyrocapsa ornata* and *G. ericsonii* are less warmer species than *G. oceanica*, *G. ornata* additionally prefers less saline waters than the rest of the *Gephyrocapsa* species. *Gephyrocapsa muellerae*, the second species with high coccosphere calcite mass, was the coldest *Gephyrocapsa* species and the most tolerant to lower pH.

The stratification of the summertime analysed samples gave a large range of conditions allowing the distinction of different ecological niches. Ordinations using either the standing stocks of the morphotypes and morphogenesis of *E. huxleyi*, or the latter together with the *Gephyrocapsa* species, can give a very certain clustering of the sampling zonation; as different hydrographic conditions can be associated to the clusters according to the species ecological preferences, the mentioned biotic data can be used as proxies to delimit different hydrographic zones and to associate the hydrographic conditions corresponding to each zone. The cluster analysis showed that with only five different biotic variables it is possible to obtain a very certain zonation.

In the context of global warming, the related deepening of the nutricline (Cermeño et al., 2008), and ocean acidification, in highly stratified temperate waters we might find in the upper water layers a relative increase in the species/morphologies tolerant to higher temperatures and lower nutrient concentrations such as the species *G. oceanica*, while in the subsurface waters once reaching the nutricline, we might find a relative increase in the species/morphologies tolerant to lower temperatures and lower pH such as the species *G. muellerae*, the over-calcified morphology of *E. huxleyi* type A, and *E. huxleyi* type O. In this same context, we expect to find a lower contribution of *E. huxleyi* type A to the calcium carbonate production in the upper warmer nutrient-depleted water layers despite the increase of the multi-layer morphology in those layers. Therefore, heavy species such as *G. oceanica* and *G. muellerae* might be favored by climate change conditions and a subsequent increase in the coccolithophore PIC production might occur. Likewise, warm species/morphologies might expand poleward while the cold ones might be more restricted to poleward regions.

Chapter 5

Environmental conditions controlling *Emiliania huxleyi* morphology

5.1 Abstract

Coccolithophores have an important role in the global carbon cycle as calcium carbonate producers and photosynthesizers. The dominant coccolithophore species *Emiliania huxleyi* is known for its large morphological plasticity and its response to environmental change. Its response might affect the primary production as well as biogeochemical cycles. We focused this study on the controlling environmental factors of the morphotypes and morphological variations of *E. huxleyi*. We analysed summertime photic zone samples along a transect covering the Gulf of California and NE Pacific margin waters, spanning a large range of environmental conditions and depths. *Emiliania huxleyi* largely dominated the coccolithophore community in this region as in general in the modern ocean. The morphotypes of *E. huxleyi* present in the region were the morphotypes A and O. The morphotype O was a colder morphotype more akin with higher ammonium concentrations and more tolerant to lower pH values than the morphotype A. The over-calcified *E. huxleyi* type A shared niche with the morphotype O. The observed morphological aberrations (coccoliths with "collapsed" distal elements) were related to low concentration (though not minimum) of phosphate, nitrate and nitrite, also to low salinity and to high chlorophyll-*a*. The under-calcified morphology was mainly associated with low nutrient concentrations, specially of phosphate. In the context of climate change, elevated temperatures as well as a nutricline deepening on highly stratified temperate waters might restrict *E. huxleyi* morphotypes A and O to lower depths in the euphotic zone, while the lowering of pH due to upward

migrations of the calcite saturation horizons might restrict them from lower water layers.

5.2 Introduction

Climate change is driving marine food web processes including the ones controlled by phytoplankton at its base. The observed increase in CO_2 entails three of the main climate-derived changes which photosynthetic marine organisms have to deal with, which are the rising temperatures, the lowering of pH known as ocean acidification, and the increase of the upper-ocean thermal stratification with the reduction in surface nutrient concentrations (Rost and Riebesell, 2004; Cermeño et al., 2008; Doney et al., 2009). Coccolithophores are an important cosmopolitan unicellular calcifying phytoplankton involved in the ocean carbon cycle (Westbroek et al., 1993). The impact on coccolithophores can be at different ecological levels (e.g. individual, population, community, etc.) and on none of them the impact is clear. The dominant coccolithophore species *Emiliania huxleyi* has shown the ability to adapt to combined high temperatures and high CO_2 concentrations at controlled laboratory growing conditions (Schlüter et al., 2014), however in nature coccolithophores experience large temporal and spatial changes in their growing conditions with complex multiple effects of environmental parameters and species to community interaction that in some regions, such as the ones with upwelling, are very pronounced Feely et al. (2008). Moreover, in both laboratory and field studies, they have shown variations in their morphology and malformations when grown at different conditions (Triantaphyllou et al., 2010; Ziveri et al., 2014; Rosas-Navarro et al., 2016).

Emiliania huxleyi presents a high intra-specific variation in coccolith morphology, varying in degree of completion, degree of calcification, size, malformation and genotypic variation (Young and Westbroek, 1991; Hagino et al., 2011; Rosas-Navarro et al., 2016). Coccoliths may have an ecological/evolutionary significance (Henriksen et al., 2003; Langer et al., 2011), their function is not fully clear but has mostly been associated with protection and with light or buoyancy control (Young, 1994; Paasche, 2001; Guan and Gao, 2010). The morphological variation in response to environmental parameter changes might represent a survival advantage (Dixon, 1900; Young, 1994).

The different morphological responses in *E. huxleyi* might affect the species specific individual mass contribution and possibly their carbonate export, altering ocean processes in which it is involved. For example, their morphology might affect the "rain" ratio of calcium carbonate to organic carbon, also described as the PIC : POC (particulate inorganic carbon to particulate organic carbon) rain ratio, by which biogenic particles sink down from the ocean surface (Hutchins,

2011). Aberrant coccoliths have been found both in field samples and commonly in laboratory culture experiments (Young, 1994; Ziveri et al., 2014; Rosas-Navarro et al., 2016). It is not clear if aberrant coccoliths are more likely to dissolve than non-aberrant coccoliths, but there is an observed kind of aberration in coccoliths, the "collapsed" aberration, in which different elements of the coccoliths are lost (Young, 1994). Curiously, this kind of aberration has only been described in field water samples and not in sediments (Kleijne, 1990; Henderiks et al., 2012) since it is likely that malformed coccoliths are easily fragmented during the sinking and sedimentation processes. These observations suggest that processes such as the rain ratio might be affected by the coccolith morphology and therefore, in order to predict such processes, it is important to understand how is coccolith morphology affected by different water conditions.

There is a major lack of information about the morphological response of the species *E. huxleyi* to environmental parameters measured *in situ* and even less including the carbonate chemistry. This last has gained more attention in the last decade due to the ongoing ocean acidification and to its influence in coccolithophore morphology (Beaufort et al., 2008, 2011; Meier et al., 2014; Bolton et al., 2016), which however is not clear. The lack of clearness is due to the variability between and within the coccolithophore species (e.g., Langer et al., 2009; Rosas-Navarro et al., 2016) and to the high correlation between many of the environmental variables which can make it difficult to identify the main driving force (e.g., Charalampopoulou et al., 2016).

The main objective of this study is to determine the main factors controlling *E. huxleyi* morphotype and morphology in Gulf of California and NE Pacific margin waters, spanning a large range of environmental conditions measured *in situ*, using 68 summertime water samples collected at different stations and depths (0–100 m). We specially focus on finding the environmental factors controlling: (1) *E. huxleyi* morphotype A and O (2) the level of calcification of coccoliths including a particular over-calcified morphology which has presented a different behavior associated with pH declines (Beaufort et al., 2011; Smith et al., 2012), and (3) the "collapsed" morphology which has been usually described as a malformation despite that Young (1994) argued it was possibly a kind of dissolution.

The morphotype O is known to be a "cold" morphotype (subarctic type in Okada and Honjo, 1973), but was separated from other morphotypes until the molecular phylogenetic study by Hagino et al. (2011). Regarding the over-calcified morphology, it has been observed a kind of gradient in the level of morphological "over-calcification", but the causes are still unclear as well as if it consists in a shift of genotype or phenotype (Smith et al., 2012). Regarding the "collapsed" morphology, the observed aberrations in the coccoliths are mostly restricted to the tube elements, in some cases being completely lost causing the collapse of the distal elements on the proximal shield, which suggest that the morphology is

originated by a malformation followed by a secondary effect presumably a kind of dissolution as could be grazing. Although not always with that name, the collapsed morphology has been previously reported in different regions (Okada and Honjo, 1975; Verbeek, 1989; Kleijne, 1990; Giraudeau et al., 1993; Young, 1994; Ziveri et al., 2014), but its cause is not conclusive. Therefore, with this study spanning a large range of conditions, we pretend to find the detonators and drivers of *E. huxleyi* morphology. Apart from all of the above, the morphotype/morphology data could be useful as a proxy to detect for example the nutricline depth, the water hydrographic conditions or even water currents, specially in stratified regions where coccolithophores are expected to dominate more than diatoms (Cermeño et al., 2008).

5.3 Materials and methods

5.3.1 Physical oceanography

The samples for this study were taken throughout the upper 100 m in locations along a transect from the Gulf of California (G. Cal) to the northeastern Pacific margin (NE Pacific). The G. Cal is connected to the Pacific Ocean through its southern opening between 20°N and 23°N, it is the region that we call here the entrance zone (EZ).

The physical oceanography of the region studied is mainly controlled by the California Current System (CCS), the Gulf of California waters and the Equatorial system (Fig. 5.1). The NE Pacific waters are mainly defined by the CCS. The EZ is a region where a portion of the Equatorial system branches to the north transporting warmer water from the south and where a transition zone of the North Pacific Ocean coincides with the entrance to the G. Cal. Finally the G. Cal, which is more a marginal sea, presents waters which are mostly of tropical origin and are modified locally by strong exchanges with the atmosphere, with little influence found in the adjacent Pacific Ocean (Badan-Dangon et al., 1989).

The Northeastern Pacific (NE Pacific) margin is one of the Eastern boundary upwelling regions among those with the lowest pH (Feely et al., 2008). Seasonal upwelling typically begins in early spring resulting from a strengthening of the northwesterly winds (Hickey, 1998; Pennington and Chavez, 2000). The equatorward-flowing California Current (CC) and the poleward-flowing California Undercurrent (CU) are the main water currents controlling the NE Pacific waters (Fig. 5.1) during summer (Hickey, 1998). Both currents are part of the CCS which is part of the North Pacific Gyre. The CC is a weak surface current (less than 25 cm sec^{-1}) flowing southward carrying cold waters from the north, causing upwelling

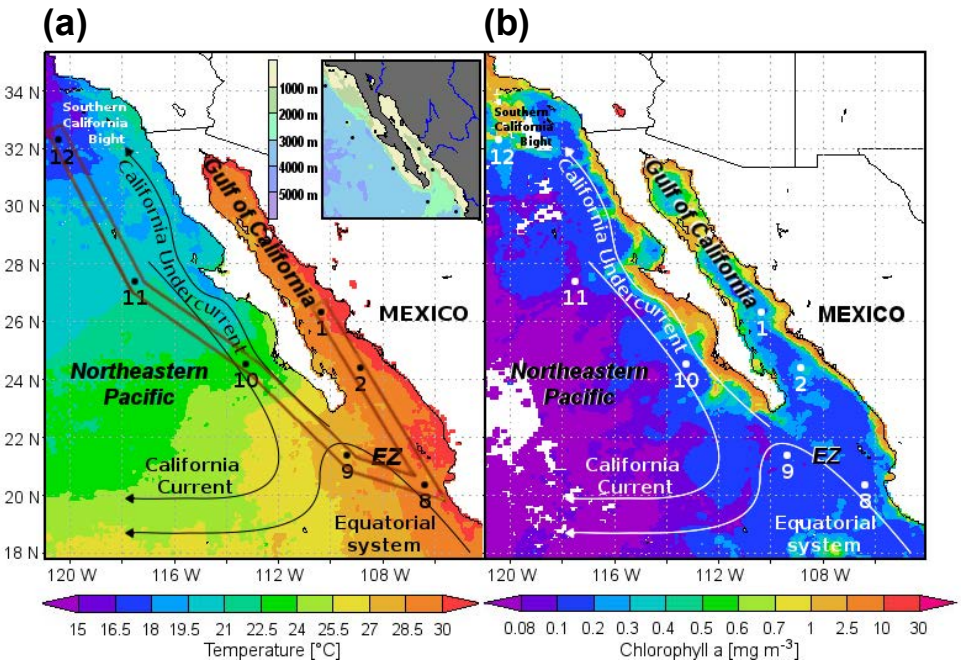

Figure 5.1: Mean temperatures (a) and chlorophyll-*a* concentrations (b) in surface waters in July 2008 Acker and Leptoukh (2007). The maps show the locations sampled in the Gulf of California (G. Cal), in the entrance zone (EZ) and in the northeastern Pacific margin (NE Pacific). The main water currents comprising the area are shown. A brown frame linking the locations sampled (a) shows the section used to plot vertical water profiles. Bathymetry and main rivers in the area are shown in the small map (a).

due to the Ekman Effect, bringing up nutrients increasing primary productivity. The CC has a width of up to 800 to 900 km and flows down to a depth of 300 m. The CU is a poleward weaker current (in average not higher than 8-10 cm sec^{-1}) which transports warm and salty equatorial waters along the continental slope. Maximum velocities in the CU are attained in the layer at 100 to 250 m depth where it transports up to 90 km^3 of water ever day (Pierce et al., 2000; Collins et al., 2003). The area is distinguished by wind forcing that is strongly influenced by the topography of the American continent (Kessler, 2006).

The G. Cal is a northward extension of the conditions that prevail in the eastern tropical Pacific. The G. Cal waters present a wide spectrum of motions as a result of different forcing functions, being the main ones: the heat exchange with the open Pacific Ocean, the tides, the fluxes of heat and moisture with the atmosphere, and the wind. These forcing functions are mainly related with the oceanography of the adjacent open ocean, the geometry of the gulf, the bathymetry, the land topography and the related large-scale pressure systems. The G. Cal is a region of strong evaporation which, however, gains heat through its surface during most of the year (Badan-Dangon, 1998).

The G. Cal and the NE Pacific are striking examples of the extreme alongshore scales at which they can maintain their own identity. Due to the oceanographic differences found in both regions and in their connection region, the study and comparison of these regions represent an invaluable source of information.

5.3.2 Water column survey and sampling

The sampling was conducted during the GoCAL4 oceanographic cruise aboard the R/V New Horizon, in summer of 2008 (July 10 - August 8). The sampling was conducted when maximum sea surface temperatures and minimum surface chlorophyll-*a* (Chl-*a*) concentrations were registered for that year in the area (according to monthly observations with data produced with the Giovanni online data system, developed and maintained by the NASA GES DISC). The sampling time do not correspond to the El Niño period. Based on a threshold of ± 0.5 °C for the Oceanic Niño Index (provided online by the NOAA Climate Prediction Centre), a cold episode occurred during the eleven previous months.

Samples were collected at selected depths in fine-scale water column sampling throughout the top 100 m, at seven locations labeled according to the original station number (Fig. 5.2). The upper 100 m of the vertical water profiles show a high stratification, with basically two main layers, an upper one characterized by nutrient depletion and a lower one by a sudden increase in nutrients. A coccolithophore-favorable 'mid-to-low nutrient' niche is absent as discussed by Wolhowe et al. (2014). With a Seabird SBE 9 CTD package equipped with additional sensors, temperature, salinity, dissolved oxygen concentration, chlorophyll fluorescence, water density, and photosynthetically active radiation (PAR) data were collected during the cruise. Nitrate, nitrite, phosphate, ammonium and silicate concentrations were determined shipboard by standard manual spectroscopic methods (Strickland and Parsons, 1972). Water samples were collected using a rosette of twenty-four 10 liter bottles attached to the CTD package. Several casts were made at each station in order to obtain sufficient material for all the chemical and biological analyses; for this study were used two casts per station (see Table C.1 in Appendix C.2).

Water column PAR profiles were measured in situ and used to calculate the depth of the base of the euphotic zone, represented by the 1% light level of the surface irradiance (SPAR). For each station, the SPAR and the two PAR measurements delimiting the layer with the base of the euphotic zone were used to calculate a light attenuation coefficient (k_{PAR}) for each station following (Letelier et al., 2004), assuming exponential PAR decrease with depth:

$$\mathrm{PAR} = a e^{-k_{\mathrm{PAR}} z}, \tag{5.1}$$

where a is SPAR and z is depth (see Popp et al., 2006). Giving specific fit for Eq. 5.1 to the PAR values, two k_{PAR} were calculated and averaged for each site which were then used to calculate an exact depth of the base of the euphotic zone with a clearance of the same equation.

Total alkalinity (TA) and dissolved inorganic carbon (DIC) were also measured from samples collected during the cruise. Carbonate system profiles were calculated from temperature, salinity, pressure and the concentrations of phosphate, silicate, TA and DIC, using the R package Seacarb Version 2.2 (Lavigne et al., 2009). For the calculation were used the dissociation constants of carbonic acid (K1 and K2) from Lueker et al. (2000), and the stability constant of hydrogen fluoride (Kf) from Dickson and Riley (1979). The total scale was chosen for pH. The variables selected from the carbonate system for the statistical analysis were pH, carbon dioxide (CO_2) and carbonate ion concentration [CO_3^{2-}]. Highly correlated variables of the carbonate system were removed from the analysis ($r > 0.95; r < -0.95$) (see Table C.13 in Appendix C.2).

Additional averaged data of July 2008, from online sources, was plotted for surface water profiles of temperature and chlorophyll-*a* (Chl-*a*) (Fig. 5.1). Both profiles were produced with the Giovanni online data system, developed and maintained by the NASA GES DISC (Acker and Leptoukh, 2007). The bathymetry was made with the program Ocean Data View (ODV).

5.3.3 Coccolithophore assemblages

In this study 68 water samples were analysed for coccolithophore study. From each water sample, two liters of seawater were filtered shipboard on cellulose nitrate and on polycarbonate filters (0.45 and 0.4 μm pore size, respectively, 47 mm diameter), with effective filtration areas of 881.676 mm^2. Samples were immediately oven dried at 50 °C for 2 hours and stored in Petri containers in a desiccator to avoid moisture exchange. By polarized light microscopy (LM; Leica DM4000 M) and by scanning electron microscopy (SEM; Jeol JSM-6300), the filters were used to determine abundances of each *E. huxleyi* morphotype and, for *E. huxleyi* type A, percentages of coccospheres with morphological variations in calcification.

By both microscopy methods, ~300 intact coccospheres and parts of them (when they corresponded to more than half of a broken coccosphere, considered as 6 or more coccoliths attached or grouped closely) were enumerated from a known portion of the filter for each sample. For cell quantification by SEM, a small portion of the polycarbonate filter of approximately 0.7 cm^2 was mounted on a SEM stub and coated with gold (E5000 Sputter Coater). Randomly selected transects were then counted from edge to edge of the filter mount at a magnification of 2000 x, with occasional magnifications up to 33000 x for detailed observations. By

SEM, counts were stopped until at least 50 cells of *E. huxleyi* were counted for each sample or until at least a total surface area of 1 mm^2 was analysed. For quantification by LM, a surface area of 112 mm^2 was scanned at 1000x along radial transects on a slice of cellulose nitrate filter previously mounted and made transparent with Canada balsam on a glass slide. Samples were scanned by LM until at least ∼300 cells were counted considering previous quantification by SEM. Cell counting and volume sampled were used to estimate cell densities (Eq. 5.2) for total coccolithophores as well as for the species *E. huxleyi*. Final cell densities were calculated adding both microscopy results.

Cell densities per liter of water were calculated as follows:

$$CD = \frac{N}{V_s}, \tag{5.2}$$

where CD = cell density [cell $\cdot$ L^{-1}], N = number of cells counted [cells] and V_s = Volume sampled [l].

Volume sampled was calculated as:

$$V_s = A_s \times V_f / A_f, \tag{5.3}$$

where A_s = Area sampled [mm^2], V_f = Volume filtered [l], and A_f = effective filtration area [mm^2].

A 95% confidence interval and a detection limit at a 95% probability level (Bollmann et al., 2002) were calculated for each species in each sample. Refitted from Bollmann et al. (2002), the 95% confidence interval was calculated as follows:

$$CD_{U,L} = C_{U,L} / V_s, \tag{5.4}$$

$$C_{U,L} = ((N + 0.982)^{\frac{1}{2}} \pm 0.98)^2, \tag{5.5}$$

where $CD_{U,L}$ = upper, lower confidence limit of the cell density based on the Poisson distribution and $C_{U,L}$ = upper, lower confidence limit for a Poisson distribution.

Refitted from Bollmann et al. (2002), calculated from a Poisson distribution, a detection limit at a 95% probability was obtained for each cell density if:

$$N > -\ln(0.05). \tag{5.6}$$

Hence, if 3 or more cells of certain species were counted in a sample, that species would have a detection limit at a 95% probability level in that sample. Similarly, at probabilities of 99% and 99.9%, the detection would be found with a minimum count of 5 and 7 cells respectively.

5.3.4 Variability in the morphology of *E. huxleyi*

Categories of the variability in the morphology of *E. huxleyi* type A (Table 5.1) were quantified by SEM. *Emiliania huxleyi* type A cells were classified as mono-layered or multi-layered coccospheres, as cells with normal or aberrant coccoliths (coccoliths with malformations or incompletions), and according to the amount of calcite covering the central area of their coccoliths (termed here under-calcified, normally calcified, and over-calcified). Regarding the malformed coccoliths, two different subcategories were observed and quantified independently, one of them corresponding to cells with the "collapsed" morphology described by Young (1994), and the other corresponding to cells with irregular coccoliths as described by Young and Westbroek (1991).

The morphological categories studied and the calculated cell densities were used to get an estimation of the concentration of calcite given by *E. huxleyi* coccospheres in each sample. Calcite per coccolith was estimated using the average length of the coccoliths of *E. huxleyi* cells found in this study and the formula and shape factors (k_s) given by Young and Ziveri (2000) for *E. huxleyi* type A under-calcified, normally calcified and over-calcified. For *E. huxleyi* type O was used the k_s given for the morphotype B. To calculate the calcite per coccosphere it was considered an estimated number of coccoliths for the mono-layered and the multi-layered coccospheres of the morphotypes A and O, estimated by quantifying the number of coccoliths in SEM images of different samples with cells of each morphotype.

The average length for *E. huxleyi* coccoliths was calculated through LM image analysis performed on frames (2403180 mm with a pixel area of 0.0225 mm^2) taken manually by a digital camera ("Spot insight") in transects per water sample slide until at least 300 cells were captured. Coccoliths were detected and classified by the SYRACO software (Beaufort and Dollfus, 2004; Dollfus and Beaufort, 1999), which performs pattern recognition using artificial neural networks (e.g. Beaufort et al., 2011; Grelaud et al., 2009). Thereafter, classified coccoliths were automatically measured by a birefringence method based on the coccoliths brightness when viewed in cross-polarized light (Beaufort, 2005).

A systematic manual correction was necessary in every set of results given by SYRACO. First, all images were carefully observed and those wrongly classified were removed. Thereafter, the outliers in each set of results from each sample were taken out. Finally the size calculated by SYRACO in pixel units was converted to micrometers according to measurements of 300 SEM images (using the program ImageJ on magnifications of 10000x to 20000x) of *E. huxleyi* type A coccoliths from 15 samples of different locations and depths where type A was dominant; the average given by SYRACO for the 15 samples was adjusted according to the average from the SEM images, hence a factor for all the results was calculated and applied for the final size of each water sample (832 pixels equaled 178.75 μm).

Table 5.1: Morphotypes and morphological categorization of coccospheres and coccoliths of *E. huxleyi* used in this study.

A

Emiliania huxleyi morphotype (genotypically controlled variation) (Hagino et al., 2011)	Size	Description
Type A (or var. huxleyi)	Medium-sized coccoliths (< 4 μm)	Moderate-heavily calcified elements distal shield elements and curved and rod-like central area elements that form a grill-like structure (Young and Westbroek, 1991; Young et al., 2003; Hagino et al., 2011). Comparable to the warm type from McIntyre and Bé (1967)
Type O	Varied in size	Characterized by coccoliths with an open central area and lightly calcified distal shield elements. Comparable to the subarctic type from Okada and Honjo (1973) and Type B from (Hagino et al., 2005) (Hagino et al., 2011).

B

Morphological category for coccospheres	Description
Mono-layered	Coccosphere composed of one layer of approximately 15 coccoliths.
Multi-layered	Coccosphere composed of more than one complete layer of coccoliths, usually 2–3 layers.

C

Coccolith calcification category in *E. huxleyi* type A (according to the width of the inner tube elements on the central area distal surface)	Description
Under-calcified	Very narrow inner and outer tube elements forming a narrow calcite ring barely attaching thinner distal shield elements.
Normally calcified	A clear calcite ring is formed in the border of the central area.
Over-calcified	Calcite entirely covering the central area or at least half of it.

D

Morphological category for other alterations in coccoliths	Description
Normal (non-aberrant)	Regular coccolith in shape, with robust distal shield elements and curved and rod-like central area elements seen together as a grill-like structure.
Malformed -irregular (aberrant coccolith)	Irregular coccolith, in shape or size of individual elements and a general reduction in the degree of radial symmetry shown; teratological malformation (Young and Westbroek, 1991).
Malformed -collapsed morphology (aberrant coccolith)	Very narrow or entirely missing inner and outer tube elements causing the collapse of the distal shield elements so that they rest wholly or in part on the proximal shield; weakening or loss of the "hammer-head" bifurcations of the distal shield elements; and loss of continuity between the constituent elements of single segments; according to Young (1994) possibly a secondary variation (occurring after the coccolith has been extruded outside the cell). In weakly affected specimens only a few distal shield elements have collapsed; severely affected specimens appear as a mass of isolated lath shaped elements. For more details look for "collapsed coccoliths" in Young (1994).
Incomplete (aberrant coccolith)	Coccolith with variations in its degree of completion according to its normal growing order; primary calcification variation (Young, 1994).

5.3.5 Data analysis and statistical treatment

Different multivariate statistical analyses were used to help determine the main environmental variables (abiotic data) related to changes in the cell density (cell $\cdot$ L^{-1}) of the different morphotypes and morphological categories (biotic data). The analyses were carried out using PRIMER-E v. 6.0, following the methods described by Clarke and Gorley (2006). A square root transformation was applied to the biotic data. A logarithmic transformation was applied to selected environmental variables (nutrients and PAR) when the scatter plots between pairs of environmental variables were markedly skewed on any of the variable axes (as described by Clarke and Ainsworth, 1993).

A BEST analysis –Spearman's rank correlation method– was used to obtain the variable or combination of environmental variables that better explain one biotic variable (the correlation gives only one correlation coefficient), it was limited from 1 to maximum 5 combined variables in order to find the main controlling or limiting single or combined variables.

The multivariate analyses included the following 14 environmental variables: pH, CO_2, CO_3^{2-}, pressure, temperature, salinity, Chl-*a*, Log(PAR), dissolved oxygen, Log(nitrate), Log(nitrite), Log(phosphate), Log(silicate), and Log(ammonium); Log: logarithmic transformation applied. As several variables can be highly correlated between them, the strongly correlated variables ($r > 0.95, r < -0.95$) in the multivariate analysis were picked out (Table C.13 in Appendix C.2). This last means that when one of the strongly correlated variables resulted significant in the statistical analysis, the other would also appear as an explaining variable.

Similarly to the water column profiles of the abiotic data, the biotic data was also plotted in ODV as vertical profiles (Figs. 5.3 and 5.5) following a continuous section from station 1 to station 12 (Fig. 5.1a). The data was similarly extrapolated to be correspondent with the isolines of the abiotic data and detect or show the relationships found between the biotic and the abiotic data, both by observing the plots and with the statistics. Further 3D scatter plots (shown in Appendix C.1) were plotted to analyse pair of abiotic variables mainly describing biotic variables according to the multivariate analyses.

5.4 Results

5.4.1 Water profiles of abiotic conditions

Surface and vertical profiles of the water conditions (Fig. 5.1 and Fig. 5.2), as well as the PCA of the water conditions (Fig. 6.1a), show differences among the different regions studied and among the water depths. The samples from the G. Cal (stations 1 and 2) and the EZ (stations 8 and 9) are distinguished from the NE Pacific samples (stations 10 to 12) mainly by their warmer and saltier waters (Fig. 5.2a-b), with higher total alkalinity concentrations (Fig. 6.1a), higher $[CO_3^{2-}]$ (Fig. 5.2c), and lower water densities (Fig. 6.1a) during the sampling time. Regarding the vertical profiles, from the surface to lower water depths, temperature decreased, nutrient concentrations increased, and pH and the $[CO_3^{2-}]$ decreased.

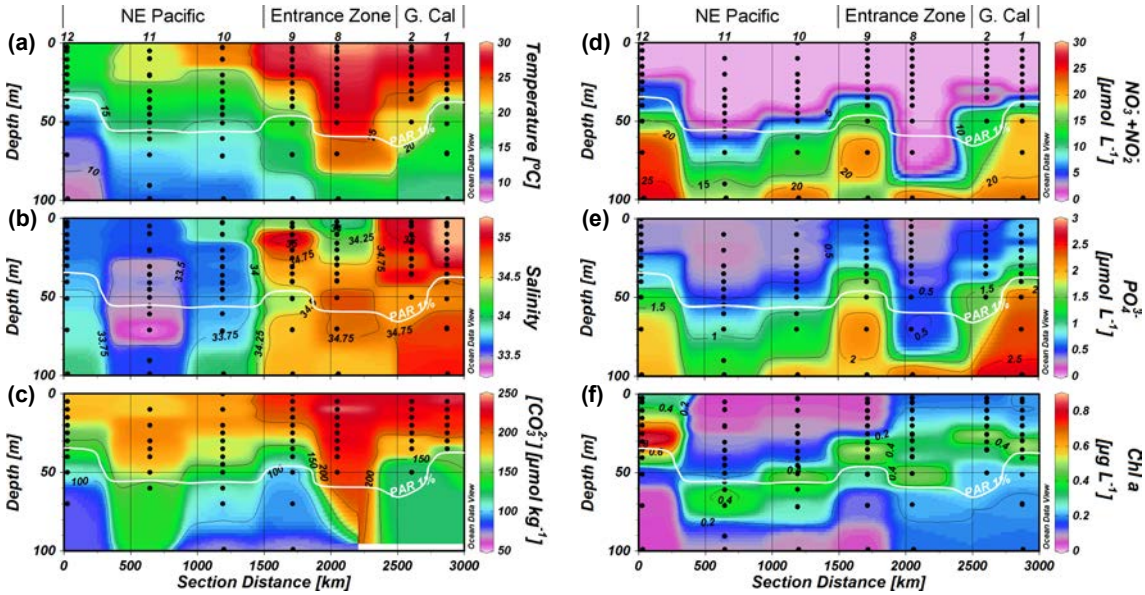

Figure 5.2: Vertical profiles of temperature (a), salinity (b), carbonate ion concentration (c), nitrate plus nitrite concentration (d), phosphate concentration (e), and chlorophyll-a concentration (f). Measured in situ throughout the upper 100 m of the water column along the transect followed by the GoCal4 cruise (see Fig. 5.1); colors and isolines represent an extrapolation of the selected variable measured at each sample (black dots) and the numbers on top represent their station number during the cruise. The base of the euphotic zone (white isoline, PAR 1%) is shown. G. Cal: Gulf of California.

Online data from NASA GES DISC (Acker and Leptoukh, 2007) for temperature and Chl-*a* surface averages for the month of July 2008 (Fig. 5.1), show a picture of the general conditions during the cruise. Stations in the G. Cal and in the EZ present warmer surface waters and higher surface [Chl-*a*] than those in the NE Pacific margin, where water temperature decreases northward. The mean temperatures of surface waters in July 2008 (Fig. 5.1a) show similar temperatures

along the G. Cal waters and in the waters south of the G. Cal along the west coast of Mexico. Warmest surface waters are found in station 8 (Fig. 5.2a) located in the EZ and at the lowest latitude studied (Fig. 5.1). NE Pacific surface waters show a temperature gradient with colder waters at higher latitudes. Surface waters in stations 1 to 9 (G. Cal and EZ) are above 28 °C and in stations 10 to 12 (NE Pacific) below 24 °C.

The vertical water profiles (Fig. 5.2) show the hydrographic conditions with the data collected in situ (for more information see Table C.1 to C.6 in the Appendix C.2), for the upper 100 m, along the transect followed by the GoCal4 cruise (brown frame in Fig. 5.1a). The colors and isolines in the vertical profiles represent an extrapolation of the selected variable measured at each sample (black dots) and the numbers on top represent their station number during the cruise. The base of the euphotic zone of each station is shown with a white isoline in every vertical profile as a reference line.

According to the vertical water profiles, the G. Cal and the EZ in comparison with the NE Pacific show warmer and saltier waters (Fig. 5.2a-b), with lower pH (Fig. C.1a in Appendix C.1) and higher carbonate ion concentrations (Fig. 5.2c). The vertical water profiles also show that the southernmost location (station 8) presents the warmest waters. Station 9, with the influence of warm and cold waters, presents the widest range of temperatures along its water column.

Chlorophyll-*a* is more distributed along the water column in stations 1 to 8 (Fig. 5.2f) than in stations 9 to 12. Station 12, the northernmost station in the NE Pacific, presents the highest [Chl-*a*] in the water column. Station 11 presents the deepest chlorophyll maximum, location that presents the lowest [Chl-*a*] in the mean surface concentration (Fig. 5.1b) and location farthest from the coast and with the maximum depth of the sea floor (Table C.1 in Appendix C.2).

5.4.2 *Emiliania huxleyi* morphotypes A and O

The two morphotypes found of *E. huxleyi* in this study (Table 5.1A), correspond to the morphotypes A and O from Hagino et al. (2011). Cells with more than one complete layer of coccoliths, termed here multi-layered coccosphere (Table 5.1B), were found and quantified. According to the width of the inner tube elements on the distal surface of the central area, *E. huxleyi* type A presented different levels of calcification (Table 5.1C), termed here under-calcified, normally-calcified and over-calcified. Other morphologies were observed and quantified (Table 5.1D), but did not present a clear distribution or relationship with the environmental variables. Morphotypes and morphological categories were distinguished by SEM image analysis.

Among the two morphotypes found, *E. huxleyi* type A (Fig. 5.3a-b) was the dominant morphotype. With respect to *E. huxleyi* type O (Fig. 5.3c-d), type A presented a higher dominance in the G. Cal and EZ (in average 97% of the species) than in the NE Pacific (in average 83% of the species). *Emiliania huxleyi* type A was more abundant (higher than ∼10 000 cell $\cdot$ L^{-1}) from 11 °C to 28 °C and *E. huxleyi* type O from 10 °C to 17 °C. Both morphotypes were mainly found at higher nutrient concentrations. Percentages of *E. huxleyi* type A versus *E. huxleyi* type O, in the NE Pacific, mainly increased at higher [CO_3^{2-}] (Fig. 5.4), lower [HCO_3^-], lower DIC and lower nitrate concentrations.

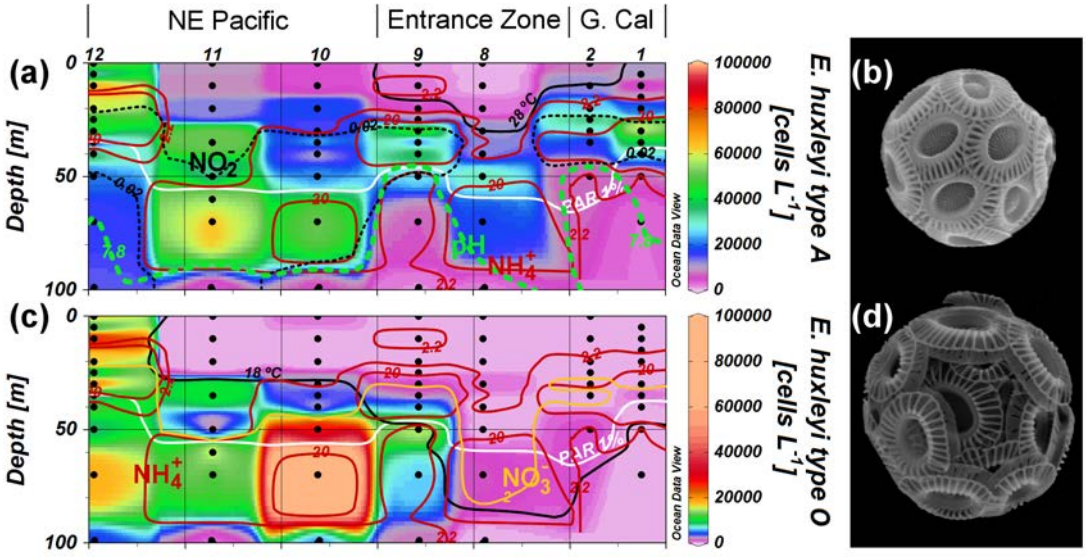

Figure 5.3: Cell density vertical profiles and coccosphere images of *E. huxleyi* type A (a, b) and *E. huxleyi* type O (c, d). The base of the euphotic zone (PAR 1%) is shown in each vertical profile with a white isoline. Isolines for different environmental variables related to the cell densities are shown in each profile: temperature (black isolines), pH (thicker green dotted isoline), nitrate concentration (yellow isoline), nitrite concentration (black dotted isoline), ammonium concentration (red isoline); nutrient concentrations are in μmol L^{-1}. The images show coccospheres with no aberrations and the minimum number of coccoliths typically found in a complete coccosphere. The cell density profiles include all the cells found regardless their morphology. G. Cal: Gulf of California.

In the NE Pacific, above and below the base of the euphotic zone, the species *E. huxleyi* accounted 62% of the total coccolithophore standing stocks, although the percentage of the morphotype O versus the morphotype A increased below the euphotic zone. In average, in the NE Pacific, *E. huxleyi* type A corresponded to the 44% of the total coccolithophore standing stocks and *E. huxleyi* type O corresponded to the 18%. Below the base of the euphotic zone in the NE Pacific, *E. huxleyi* type A corresponded to the 38% and *E. huxleyi* type O to the 24% of the total coccolithophore standing stocks.

In the euphotic zone of the G. Cal and EZ, higher cell densities of *E. huxleyi* type A were related with lower temperatures, higher DIC, higher [HCO_3^-] and

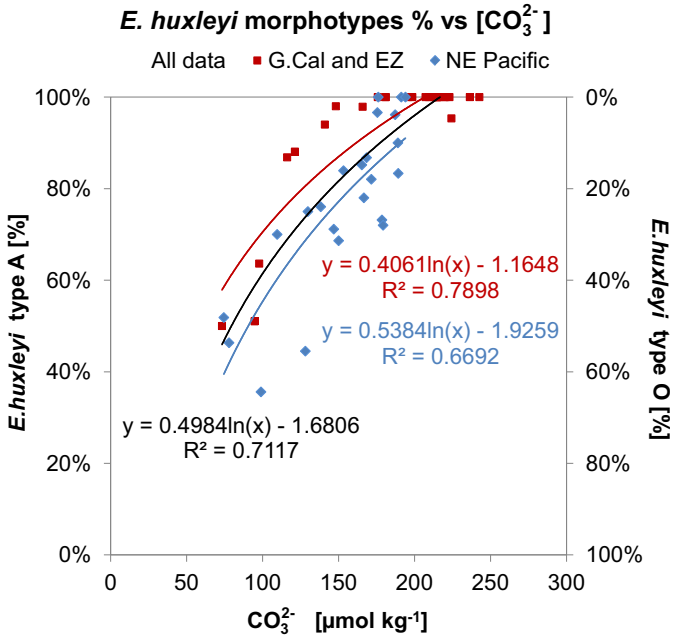

Figure 5.4: Scatter plot for *E. huxleyi* morphotypes in proportion to each other versus the main significantly linearly correlated environmental variable. Higher percentages of *E. huxleyi* type A, therefore lower of *E. huxleyi* type O, were found at higher $[CO_3^{2-}]$. Logarithmic fits are shown. G. Cal: Gulf of California; EZ: Entrance zone.

higher nutrient concentrations (see Table C.24 in Appendix C.2 for more information). In the euphotic zone of the NE Pacific, higher cell densities were related with higher ammonium concentrations and lower temperatures. In the NE Pacific, below the euphotic zone base, morphotype A was still abundant at higher nutrient concentrations and temperatures higher than 10 °C. A decrease in cell density was observed below a pH of 7.8 (Fig. 5.3b, below dotted green isoline).

Emiliania huxleyi type O (Fig. 5.3c-d) was mainly found at temperatures below 18 °C (in Fig. 5.3c, below black isoline) and below the nutricline at nitrate concentrations higher than 2 μmol L^{-1} or ammonium concentrations higher than 2.2 μmol L^{-1} (in Fig. 5.3c, below yellow isoline or inside red isolines). Hence it was mainly found in the NE Pacific. Higher cell densities in the NE Pacific, were related with lower $[CO_3^{2-}]$, higher $[HCO_3^-]$ and higher nitrate concentrations. Particularly below the euphotic zone in the NE Pacific, higher cell densities were observed at higher ammonium concentrations (see Table C.24 in Appendix C.2 for more detailed information).

5.4.3 *Emiliania huxleyi* morphological categories of calcification

Calcification of *E. huxleyi* was studied through the observation of SEM images of coccospheres and coccoliths (Fig. 5.5). It was observed if coccospheres presented more than one complete layer of coccoliths (termed multi-layered), the level of calcification of their coccoliths (Table 5.1C) and coccolith aberrations (Table 5.1D). The picture of *E. huxleyi* type A in Fig. 5.3b, shows normally calcified coccoliths and a mono-layered coccosphere.

Higher percentages (> 30%) of *E. huxleyi* type A cells with over-calcified coccoliths (Table 5.1C, Fig. 5.5a-b), were mainly found below the nutricline at nitrate concentrations higher than ∼2 μmol L^{-1} (in Fig. 5.5a, below yellow isoline), particularly from station 9 to 12. They were also found at temperatures lower than 22 °C (black isolines in Fig. 5.5a), at $[CO_3^{2-}]$ lower than 179 μmol kg^{-1} (below grey isoline in Fig. 5.5a) and between a pH of 7.76 and 8.05 (Fig. C.11 in the Appendix C.1); higher concentrations of ammonium were also related (in Fig. 5.5a, inside red isolines). Temperature was the main related environmental variable according to significant r Pearson correlation coefficients (alpha = 0.05, two-tailed test), the scatter plot is shown in Fig. 5.6a.

Higher percentages (> 20%) of *E. huxleyi* type A cells with under-calcified coccoliths (Fig. 5.5c) were mostly found at higher temperatures (above 15 °C), above the nutricline (at nitrate concentrations below 2 μmol L^{-1}, at ammonium concentrations lower than 20 μmol L^{-1}, and at observed punctual decreases in the phosphate concentration below ∼ 0.8 μmol L^{-1} in the water column profile), at higher $[CO_3^{2-}]$ (higher than 179 μmol kg^{-1}) and at a pH between 8 and 8.2.

Higher percentages (> 40%) of *E. huxleyi* type A with multi-layered cells (Fig. 5.5e-f) were found at higher temperatures (black thicker isoline in Fig. 5.5e), lower CO_2 (blue isolines in Fig. 5.5e) or higher $[CO_3^{2-}]$ (higher than 150 μmol kg^{-1}), and lower ammonium concentrations (red isolines in Fig. 5.5e). Hence, higher proportions were mainly observed above 50 m depth in the euphotic zone, especially above 17 °C and at lower nutrient concentrations. Temperature was the main related environmental variable according to significant r Pearson correlation coefficients (alpha = 0.05, two-tailed test), the scatter plot is shown in Fig. 5.6b.

Multi-layered coccospheres were also observed in *E. huxleyi* type O (not shown in the figures). In the NE Pacific, higher cell percentages of the multi-layered morphotype O were particularly observed between 15 and 20 °C. Both morphotypes of *E. huxleyi* increased their percentages of multi-layered coccospheres in the warmer euphotic zone and decreased it in the deeper colder layers of the water column.

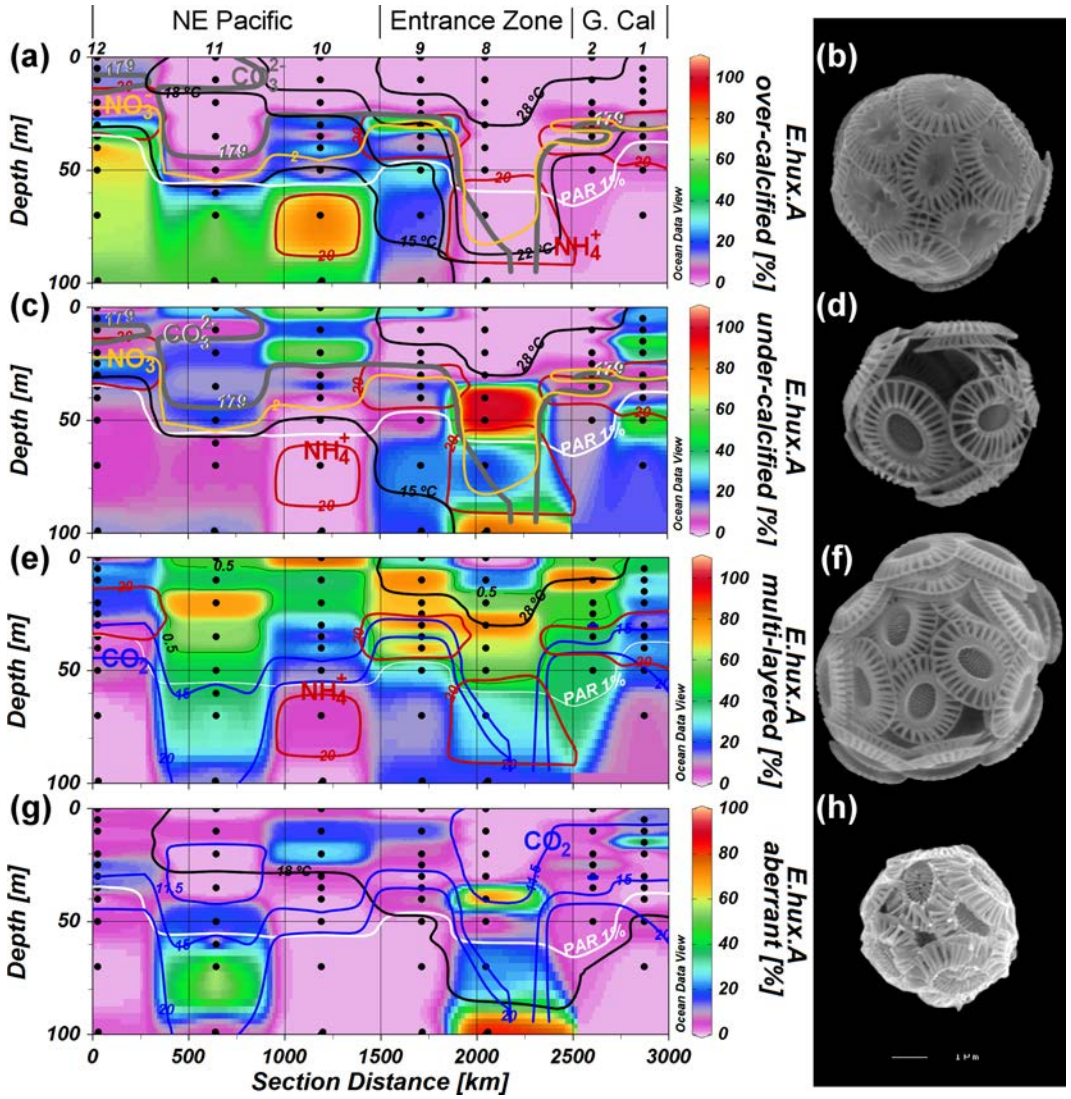

Figure 5.5: Vertical profiles and images of *E. huxleyi* type A cells with different morphological categories (profiles in percentage with respect to total *E. huxleyi* type A cell density). The base of the euphotic zone (PAR 1%) is shown in each vertical profile with a white isoline. Isolines for different environmental variables related to the cell densities are shown in each profile: temperature (black isolines), nitrate (yellow isoline), ammonium concentration (red isoline), carbonate ion concentration (gray isoline; μmol kg^{-1}); nutrient concentrations are in μmol L^{-1}. An over-calcified cell (b), an under-calcified cell (d), a multi-layered cell (f), and a cell with aberrant (collapsed morphology) coccoliths (h) are shown as a representative example of each morphological category. In (e), thinner black isolines delimit samples with at least 50% of *E. huxleyi* type A cells with the multi-layered category. After a thorough analysis of the plots, despite statistics, the aberrant category appears to be related to marked decreases in phosphate concentrations. G. Cal: Gulf of California.

The kind of aberration found in *E. huxleyi* type A cells was basically the collapsed morphology (Fig. 5.5g-h). This morphology, as percentage or as cell density, did not show a clear related variable. However it was possible to detect that most of the times their increase in the water column profile was related with a decrease

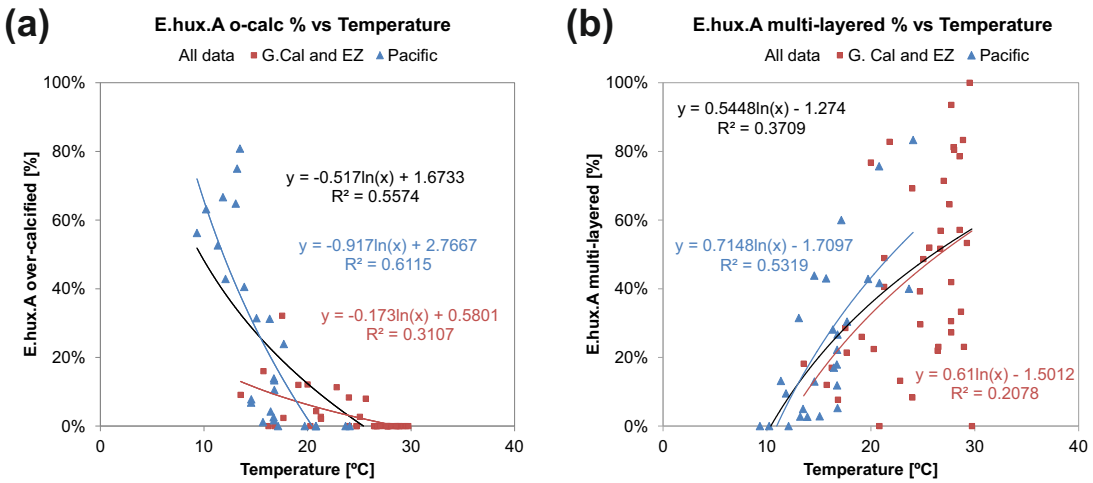

Figure 5.6: Scatter plots for the percentage of *E. huxleyi* type A coccospheres with different types of morphological calcification versus the main related environmental variable (according to significant r Pearson correlation coefficients, with an alpha = 0.05, two-tailed test). The plots show the logarithmic trend lines for all the data (black), for the NE Pacific (blue) and for the Gulf of California and the Entrance Zone(red).

in the phosphate concentration (observed above 18 °C in Fig. 5.5g, phosphate profile in Fig. 5.2e) at low nitrate and nitrite concentrations. Except for station 12, percentages higher than 14% in the euphotic zone were found at nitrate plus nitrite concentrations of less than 0.08 μmol L^{-1} and phosphate less than 0.63 μmol L^{-1}. Contrary to what would be intuitively expected, here we found a low percentage of coccospheres with collapsed coccoliths in shallow waters at extremely low phosphate concentrations (of ~0.3 μmol L^{-1}). Considering the maximum percentage in the euphotic zone (when PAR $\geq$ 1% of the SPAR) of each station (for station 12 considering depths 25 and 35), maximum percentages were found on average at a phosphate concentration of 0.55 μmol L^{-1}, in a range from 0.36 to 0.81 μmol L^{-1}. Below 18 °C, the increase observed in station 11 at depths 50–70 m coincided with the lowest salinity concentration found in this study (33.45 and 33.301 ‰, at 50 and 70 m respectively, from a studied range from 33.30 to 35.24‰). The increase observed in station 12 is not clearly explained with the studied variables, however it can be observed that in station 12 maximum percentages were found at the highest Chl-*a* concentrations of the study (maximum of 0.86 μg L^{-1} at 30 m). The increase observed at 100m in station 8 is not clearly explained with the studied variables and the carbonate chemistry data is missing for that sample. Percentages higher than 10% were found at phosphate concentrations from 0.36 to 1.01 μmol L^{-1}, except at 100 m in station 8 where the phosphate concentration was of 2.24 μmol L^{-1} (Table 5.2). Statistically they were mainly related with [CO_2] (r_s = 0.302; Table C.15G in the Appendix C.2), but the relationship is not as clear as the mentioned observations and moreover, from the scarce 5 samples that

presented more than 25% of cells with aberrations, two samples were not included in the multivariate analysis because the carbonate chemistry data was missing.

Observations posterior to the counting on samples with high percentage of coccospheres with the collapsed morphology, showed that many "non-aberrant" overcalcified coccospheres presented slight aberrations in the tube elements (Fig. C.6(b) in Appendix C.1), the same for the other levels of calcification, unfortunately this was not counted.

Table 5.2: Nutrient conditions in waters with an aberrant cell percentage higher than 10 %.

Station-Depth [number − m]	Phosphate 8 [μmol L^{-1}]	Nitrate+Nitrite [μmol L^{-1}]	Ammonium [μmol L^{-1}]	Silicate [μmol L^{-1}]	Aberrant cell density [cell L^{-1}]	Aberrant cell percentage [%]
1-5	0.74	0.03	0	1.68	1388	12.90
1-15	0.58	0.08	0	1.41	3500	38.89
2-25	0.58	0.61	9	1.5	4111	12.00
8-40	0.37	0.04	0	1.47	8280	70.83
8-70	0.47	0.17	61	2.06	3955	22.22
8-100	2.24	21.9	7	17.56	1961	83.33
9-10	0.63	0.04	3	1.59	270	14.30
10-10	0.36	0.05	0	2.43	724	16.00
10-20	0.36	0.01	0	2.21	4623	25.71
11-50	0.43	0.08	0	4.04	6001	18.60
11-70	1.01	9.77	7.7	8.93	42498	64.81
12-25	0.67	4.16	123	4.05	6605	14.89
12-30	0.75	5.5	115	5.32	5249	11.43
12-35	0.81	6.27	0	5.87	2474	16.22

5.5 Discussion

The results obtained in this study show a strong control of the seawater carbonate chemistry, the temperature and the nutrients on the distribution of *Emiliania huxleyi*, its morphotypes and morphogenesis. The stratification of the summertime analysed samples gave a large range of conditions allowing the distinction of different ecological niches. In general, the main specific controlling hydrographic parameters were the low pH limiting in the deeper waters, the temperature limiting in the shallower waters due to temperatures above the optimum, and the nutrients mainly enhancing the standing stocks to maximum values in the corresponding station when nutrient concentrations are high, and enhancing the aberrations when they are a bit above depletion. The values at which the different species or morphologies were controlled was specific to each one and are discussed in the following subsections.

5.5.1 Environmental conditions controlling *E. huxleyi* morphotypes A and O in the region

Here were identified the morphotypes A and O of the species *E. huxleyi*, both dominating specific niches of the studied areas. In general, the morphotype A was the dominant morphotype, confirming its wide tolerance to different conditions (Okada and McIntyre, 1979). However, at lower carbonate saturation states and lower temperatures the morphotype O equaled and even outnumbered the morphotype A. The morphotype O is known to be a subarctic (Okada and McIntyre, 1979; Hagino et al., 2005, 2011) and subantarctic (Findlay and Giraudeau, 2000; Malinverno et al., 2016) morphotype present at least in the Pacific and Atlantic Oceans. In the North Pacific, the morphotype O has been found in cold waters, specifically it has been found to be originated in the Oyashio current in the northern part of the Japan Sea from where it is distributed in the subarctic zone along the longitudinal flow of the Oyashio Current and its extension (Hagino et al., 2005). We found the morphotype O mostly restricted to the water mass below 18 °C of the NE Pacific and the EZ stations. These areas are influenced by the CCS, therefore the cold water mass in which the morphotype O was found presumably can be connected with the Japan Sea. Therefore, the proportion between the morphotype A and the morphotype O might be used as a proxy to distinguish two different water masses (similarly as in Fig. 6.1b), in our particular case to distinguish the cold waters coming from the north through the CCS, from the warm Equatorial waters coming from the south. In Fig. 6.1b can be observed two big clusters which delimited warm and cold waters – green clusters– and from the four main smaller clusters – blue clusters– the one in the left could be pointing out to the cold waters coming from the north through the CCS and the one in the right to the warm Equatorial waters.

Here we found that water temperature is one of the main parameters controlling the distribution of the two observed *E. huxleyi* morphotypes, controlling the minimum depth when shallower waters presented high temperatures. Specifically, the morphotype A was basically restricted to waters below 28 °C and the morphotype O to those below 18 °C. The morphotype A, seemed to be limited by high temperature but also by PAR higher than 750 μmol m^{-2} s^{-1}. Here we found that the changes in the proportion of the two morphotypes was mainly linked with the CO_3^{2-} ion concentration; however it is a parameter highly correlated with temperature and temperature is known to be a dominant factor (Watabe and Wilbur, 1966; Balch et al., 1992).

We found that the maximum depth at which both morphotypes were mostly found was mainly determined by pH. Minimum light at which they were found in relatively high concentrations (∼20 000 cells L^{-1}) was 0.1% of the surface PAR. Despite such low PAR, it was a pH lower than ∼7.8 what seemed critical to both morphotypes, but it was even more critical to the morphotype A. Therefore, ocean

acidification might be more critical to the dominant morphotype A. Morphotype A however seems to present a morphological variation, the over-calcification of its coccoliths, enhanced by lower temperature and lower pH. Therefore, ocean acidification might enhance the presence and abundance of individuals with this morphology. We will discuss this morphology in more detail later.

Therefore, temperature and pH were the main controlling factors of both morphotypes, the first restricting them from the upper warmer water layers, and the second restricting them from lower waters. Once the morphotypes were in a proper temperature and pH, nutrients were the main controlling parameters of their standing stocks, as it has been previously mentioned (Gravalosa et al., 2008). Both morphotypes were fueled by nitrate, nitrite and ammonium, but the morphotype O presented a particular preference to high concentrations of ammonium. Previous studies have shown that high concentrations of ammonium can lead the cells to reach faster the cell division phase by its use in the G1 phase (Müller et al., 2008; Page et al., 1999). The reason of the preference of ammonium by the morphotype O with respect to the morphotype A is not clear here but could be directly related with a better incorporation/assimilation of this nutrient by the cell or indirectly due to a less inhibition of its use by lower temperatures or lower light. In any case, our results clearly show the increase in abundance at the nitrogen nutricline in both morphotypes, even below the 1% of surface PAR (as it can also be observed in Figs. C.4 and C.5 in Appendix C.1). Here we call 'base of the euphotic zone' the water layer where PAR was equivalent to 1% the surface PAR; however from our results, *E. huxleyi* light limitation could be around the 0.1% of the surface PAR.

5.5.2 *Emiliania huxleyi* type A over-calcified

As an interesting finding, here we found a high correlation between *E. huxleyi* type O and *E. huxleyi* type A over-calcified. In agreement with this, the study of Schiebel et al. (2011) mentions a cold region in the Atlantic Ocean where the type A, the over-calcified type, and the type O (which they called type B) cohabited, and they also mention another less cold region where only type A was found. According to previous studies it is still not entirely clear if the over-calcified morphology corresponds to another genotype (as discussed by Smith et al., 2012), which could help explain the higher correlation observed here with the type O than with the total type A. However, although we presented the over-calcified morphology as nominative, a progressive increase in the coccolith calcification as also Young et al. (2014) showed, was observed along the water vertical profiles, in which in moderately calcified specimens was still observed a grill-like central area typical of the morphotype A. In agreement with this, in SW Pacific waters around New Zealand, *E. huxleyi* has been found with coccoliths progressively more calcified from tropical to subantarctic waters (Burns, 1977). Moreover, we even found

some cells with combined over-calcified and normally-calcified type A coccoliths (Fig. C.6(a)). These last observations support more that it is a variation in *E. huxleyi* type A depending on the environmental growing conditions.

The over-calcified type has been widely found, in the northern and southern hemispheres and in different oceans and seas, for example in the Patagonian-shelf and Eastern South Pacific upwelling waters (Beaufort et al., 2011; von Dassow et al., 2017), in the SW Pacific around New Zealand (Burns, 1977), in the Gulf of Biscay (Smith et al., 2012), in the UK North Atlantic (Young and Ziveri, 2000), and in the Mediterranean Sea (Cros i Miguel, 2001). According to the present study and previous ones, the over-calcified *E. huxleyi* is commonly found in winter conditions, at greater depths, and at higher latitudes, and is mainly associated with lower temperatures, lower pH, and higher nutrient concentrations. In relation to the pH, von Dassow et al. (2017) found through an experiment that some over-calcified forms of this species are not pre-adapted to ocean acidification, contrary to the results by Müller et al. (2015). To test OA future conditions von Dassow et al. (2017) used a pCO_2 of ∼1200 μatm, a level higher than that found in our field study. Therefore it cannot yet be ruled out a possible higher adaptation of the over-calcified morphology versus other morphologies to lower pH values, though above a limit as it is very likely that extremely low pH values or very high pCO_2 might be critical or cause different responses such as calcite dissolution. It would be interesting an experiment comparing different over-calcified strains grown in a broad pCO_2 range using intermediate values.

One of the open questions is if the correlation with low pH observed in this study and previous ones is due to ecologically correlated factors (von Dassow et al., 2017). In this sense, our Spearmans rank correlation (r_S)results with a BEST analysis limited to a combination of maximum 5 variables from 14 possible variables (Table C.14), showed that the over-calcified morphology distribution is mostly controlled by temperature and nutrients. In the context of global warming, the nutricline deepening due to the stratification (Cermeño et al., 2008) might enhance the cold-related morphologies such as the over-calcified one.

The fully over-calcified coccolith morphology (central area mostly calcified) has not been obtained from normally-calcified strains in laboratory experiments, however several factors have been found to stimulate coccolith calcite quotas in laboratory experiments. In agreement with the present study, in Bach et al. (2011) laboratory experiment, it seems that at constant pH (of approximately pH=8), higher [CO_2] produces more heavily calcified or larger coccoliths. This pH of ∼8 corresponds to that where higher percentages were found here (between a pH of 7.76 and 8.05; Fig. C.11b-c), and [CO_2] here were higher than those of the experiment. Another experiment (Iglesias-Rodriguez et al., 2008) also showed an increase in the coccolith calcite quota at higher pCO_2, particularly observed at 595 ppmv at a pH of 7.82, again similar to the observations in the present field study

where higher percentages of cells with over-calcified coccoliths were found between a pCO_2 of ~450 and ~850 ppmv. The relationships obtained in the present study with the pH also apply for the pCO_2 as both variables are highly correlated among them (r = -0.99; Table C.13 in the Appendix C.2).

Regarding the relationship between temperature and the over-calcified morphology, culture experiments show an increase in the coccolith tube width from sub-optimal to optimal temperatures at non-limiting nutrient conditions (Rosas-Navarro et al., 2016). In the present field study from 0 to 100 m depth, temperature decreased to sub-optimal temperatures while nutrient concentrations increased starting from nutrient depleted waters in the surface. In the field study, *E. huxleyi* increased its coccolith tube width with depth, that is at lower temperatures but higher nutrient concentrations. Our field samples highlight an inverse relationship of temperature with the percentage of over-calcified coccospheres (Fig. C.11a in Appendix C.1).

In the context of global warming and related deepening of the nutricline depth (Cermeño et al., 2008), *E. huxleyi* is more likely to have to cope with similar non-optimal conditions like the ones found here, i.e. finding higher nutrient concentrations at their sub-optimal temperature ranges. Therefore we expect an increase in the abundance of the over-calcified morphology of *E. huxleyi* at subsurface water layers in the near future. Scientists are already finding evidence of ecological changes in *E. huxleyi* distribution due to climate change (Winter et al., 2014).

Another rising question from this morphological variation is if it could be useful for the cell to increase its individual density through an increase in coccolith calcite mass (Baumann et al., 1978; Paasche, 2001; Hoffmann et al., 2015), which from our data does not seem clearly useful due to the fact that it was mainly found below the nutricline, and that going to deeper water layers would represent going to darker and colder waters with lower calcite saturation states.

5.5.3 Collapsed morphology in *Emiliania huxleyi* type A coccoliths

The type of aberration found in this study, in *E. huxleyi* type A coccospheres, is the one called "collapsed" (Fig. 5.5h, Table 5.1D), a morphology originally described and discussed by Young (1994). Some authors have referred to this morphology as a malformation (Okada and Honjo, 1975; Verbeek, 1989; Kleijne, 1990). However according to Young (1994) it is a dissolution effect primarily affecting the tube elements, occurring after the coccolith has been formed, which causes the breakage and loss of continuity of elements of a single segment of the coccolith. We agree with Young (1994) because the distal elements need the tube elements to be formed first. Nevertheless, as the effect is primarily tied to the tube elements, it probably

starts as a kind of malformation weakening the tube elements. Such weakening could be primarily caused by detrimental environmental growing conditions. The final collapsed morphology in those coccoliths could be related to dissolution once the coccoliths are outside the cell.

Here the collapsed morphology was mainly related to low nutrient concentrations (though not the lowest where calcification was probably restricted), also to low salinity (of $\sim$ 33.45 ‰ from a studied range from 33.30 to 35.24‰) and to high Chl-*a* concentration. The relationships found here with nutrients and salinity could be the primary cause of the collapse morphology. Other studies point to a relationship with either low nutrients (Okada and Honjo, 1975; Kleijne, 1990), low salinity (Kleijne, 1990), or low temperature (Verbeek, 1989). Besides nutrients and as suggested by Young and Westbroek (1991), it could also be related to a shortage of a trace nutrient; unfortunately we do not have this information for our study.

Supporting the dissolution as a cause of the collapsed morphology, Ziveri et al. (2014) found them at low ph and low calcite saturation state (pH of 6.84, calcite saturation state of 0.37). The authors reported the presence of corroded coccospheres in waters with low calcite saturation (lower than 1.13). Here we found the collapsed morphology in calcite saturated conditions, therefore if there was dissolution it could have happened in a microenvironment such as the copepod gut or aggregates. Similarly to our observation with the highest Chl-*a* concentration, Okada and Honjo (1975) related their increase with the blooms when extremely high phytoplankton population densities are achieved.

In a laboratory experiment phosphorus limitation did not lead to malformations in different *E. huxleyi* Mediterranean strains Oviedo et al. (2014). We found a main association with low phosphate, but low nitrogen concentration conditions (specially of nitrate and nitrite) were also present in such samples. Therefore, our results suggest that other limiting conditions such as that of nitrogen might be necessary to trigger this kind of aberration.

Consistently with the relationship between the collapsed morphology, the under-calcified morphology, and the growing water conditions, it was observed that cells of *G. oceanica* presented very similar aberrations in the same samples (Fig. 6.3), showing aberrations in the tube elements, a thinner bridge and sometimes an open bridge which could be a sign for an under-calcified coccolith. Young (1994) mentioned the occurrence of the collapsed morphology in the species *E. huxleyi*, *G. oceanica* and *Calcidiscus leptoporus*, in the same sample. He noted that Okada and Honjo (1975) also found the collapsed morphology occurring together in *E. huxleyi* and in other species such as *G. oceanica*, *Florisphaera profunda* and *Umbilicosphaera sibogae*. Young (1994) also noted that Giraudeau et al. (1993) found similar abnormal coccoliths in *Coccolithus pelagicus* and in *G. oceanica* in the NE Atlantic off SW Africa. The study of Okada and Honjo (1975), made in the

marginal meas along the Western Pacific Ocean and in the Red Sea, show that almost all neritic areas presented malformed coccoliths, and pointed out that *G. oceanica* dominated the studied areas. In our study we can also observe that waters dominated by *G. oceanica* or by *G. muellerae* presented high percentages of aberrant *E. huxleyi* type A. These results show (1) that the environmental conditions causing this kind of aberration affects different coccolithophore species, (2) that coccolithophore species akin to limited water conditions could be a reference for areas where aberrant coccolithophores may be found, and (3) that they can be similarly affected despite their difference in coccosphere calcite weight.

Giraudeau et al. (1993) discussed that the characteristic low standing crops of the malformed populations, combined with their apparent higher coccolith fragility, may act against a geological record of these malformations. Following the same reasoning, the effect of these populations in the biogeochemical cycles point to possible increase in the recycling of calcite before sedimentation. The high percentage found in station 8 at 100 m could represent a glimpse of that recycling. What we observe in the mentioned sample is probably an accumulation of cells coming from upper layers in a highly stratified water column; the upper layers presented very high percentages of coccospheres with the collapsed morphology (up to 70%), and assuming it is a dissolution effect on "weakened" tube elements, it is possible that the collapsed morphology could have been accentuated in the cells through more dissolution while continuing to sink.

5.5.4 *Emiliania huxleyi* type A multi-layered

About the multi-layered morphology, it was the high temperature (especially above 20 °C but below 29 °C) the main related variable. Approximately at 25 °C an average of 50% of the cells of *E. huxleyi* were multi-layered, assuming a double number of coccoliths in the multi-layered cells (Paasche, 2001; Hoffmann et al., 2015), the group of type A cells would present an increase of one third in their calcium carbonate quota contribution. Similarly, in the culture experiment in Chapter 3, at optimal temperatures compared to sub-optimal temperatures, the three different studied strains increased their number of attached coccoliths giving place to multi-layered cells. From the same experiment, Rosas-Navarro et al. (2016) found at optimum temperature conditions compared with the sub-optimal temperatures, higher coccolith production despite that the quota of the total number of coccoliths per cell was lower at higher production rates. This last means that the coccolith production is not strictly correlated to the number of coccoliths produced by the cell but to the cell production rates. In the present field study, the primary production of *E. huxleyi* was reduced at those high temperatures (Wolhowe et al., 2014) due to the nutrient limitation, therefore the enhancement of calcium carbonate production by the increase in the individual calcium carbonate quota from the extra coccoliths is lower than it would be at nutrient-replete con-

ditions (Rosas-Navarro et al., 2016). Hence, in the context of global warming and the related deepening of the nutricline (Cermeño et al., 2008), we expect to find a lower contribution of *E. huxleyi* type A to the calcium carbonate production in the upper warmer nutrient-depleted water layers despite the increase of the multi-layer morphology in those layers.

Related to the sinking of individual living cells, our results show that the increase in weight of individual cells due to more attached coccoliths would give an advantage because they can sink faster (Chapter 3, Rosas-Navarro et al., 2018) and can reach deeper water layers with more nutrient concentrations, especially in sharply stratified waters just as the ones of the present study. These findings highlight once again the potential for adaptation of the species *E. huxleyi* because if the conditions are not optimal at the surface layers in stratified waters, it may sink faster pulled by a higher number of attached coccoliths.

5.6 Conclusions

In conclusion, the over-calcified *E. huxleyi* type A shares niche with the morphotype O. The collapsed morphology seems to have a two step cause linked to both malformation and dissolution, the first due to unfavorable conditions for the cell such as the simultaneous low concentration (though not minimum) of different nutrients or the low salinity. The under-calcified morphology was mainly associated with low nutrient concentrations, specially of phosphate. The morphotypes and morphological variations of *E. huxleyi* can be used as proxies to delimit different hydrographic zones and to associate the corresponding hydrographic conditions to each zone.

Climate changes such as ocean acidification (Doney et al., 2009), global warming and a resulted deepening of the nutricline due to an enhanced stratification (Cermeño et al., 2008), might decrease the relative abundance of the morphotype A of the species *E. huxleyi* versus its less calcified morphotype O, while the relative abundance of the over-calcified morphotype A might increase versus the normally-calcified morphotype A.

Chapter 6

Environmental conditions controlling *Emiliania huxleyi* and *Gephyrocapsa* spp. distribution

6.1 Abstract

Coccolithophores are unicellular calcifying phytoplankton sensitive to the marine environmental changes and are involved in the carbon and carbonate cycles. Given that warming, acidification, and lowered nutrient availability might occur simultaneously under climate change scenarios, there is the question about what the net effect of different influential factors will be. Therefore, we analysed 68 summertime samples along a transect covering the Gulf of California and NE Pacific margin waters at different stations and depths, giving a large range of conditions. We focused the study on the coccosphere standing stock variations of the different species of *Gephyrocapsa*. We also estimated calcite concentration and production for the *Gephyrocapsa* spp. and for *Emiliania huxleyi*. Considering all the studied samples, we found that the PIC contribution per liter of *G. oceanica* was higher than that of *E. huxleyi*, in third place was that of *G. muellerae*. *Gephyrocapsa oceanica* presented the highest affinity to warmer waters with lower nutrient concentrations, and *G. muellerae* the highest tolerance to lower pH. In the context of climate change, *G. oceanica* and *G. muellerae* might increase their relative abundance with subsequent changes in the coccolithophore PIC production.

6.2 Introduction

Climate change carries ecological changes because different groups of organisms might be differently affected and therefore ecological succession patterns might change. This last also means that their feedback on the biogeochemical cycles might also change. Understanding the ecology of coccolithophores, a calcifying unicellular phytoplankton, will allow better predictions on the effects of global change on their distribution and feedbacks. Coccolithophores are important marine calcifiers which have a direct effect on the global carbon cycle (Zondervan, 2007). They are sensitive to the marine environmental changes (Paasche, 2001; Zondervan, 2007; Ziveri et al., 2014). Coccolithophores produce calcite plates called coccoliths. Through photosynthesis they capture CO_2 and through calcification they release it. The carbon contained in coccolithophores is differentiated as particulate organic carbon (contained in the organic matter) and particular inorganic carbon (contained in the calcite). They are organisms which may sink filling the repositories of carbon and calcite in the sediments of the seafloor. The amount of carbon and calcite they collect depends on the PIC and POC production which vary on space and time. Therefore understanding their spatial and temporal distribution is necessary. Here we make a study which mainly helps to understand their spatial distribution. We selected water samples along the upper 100 meters from the Gulf of California (G. Cal) and the NE Pacific margin waters, giving a wide range of water conditions. Here we also provide data related on the PIC production of the dominant species *Emiliania huxleyi* and the different species of *Gephyrocapsa* found in the area.

Coccolithophores are important marine calcifying organisms in both the NE Pacific margin (Matsueda et al., 1986; Ziveri et al., 1995; Hernández-Becerril et al., 2007) and the G. Cal (Zeitzschel, 1969; Hernández-Becerril, 1987). The species *E. huxleyi* and species within the genus *Gephyrocapsa*, all belonging to the Noelaerhabdaceae family, dominate the waters of the NE Pacific margin and the G. Cal on a seasonal fashion due to hydrographic-climatic forcing that occurs there. Coccolithophores alternate mainly with diatom species (Thunell et al., 1996; Bollmann, 1997; Ziveri et al., 1995; Hernández-Becerril et al., 2007; Álvarez et al., 2010a). Coccolithophores and silicoflagellates typically bloom in later stages of a phytoplankton succession (sequence typically starting with the opportunistic diatoms) (Young, 1994), reflecting their tolerance for a more stratified water column and lower nutrient conditions. Species such as *Emiliania huxleyi* and from the genus *Gephyrocapsa* are cosmopolitan and common/dominant in both plankton populations and fossil assemblages (Bollmann, 1997; Ziveri et al., 1995; Hernández-Becerril et al., 2007; Álvarez et al., 2010a), therefore correlations of their coccolith response and the environmental growing conditions might become good proxies (e.g. Beaufort et al., 2011).

Water samples were collected during summertime hydrographic conditions when coccolithophore species are mostly found vertically distributed along the stratified waters of the region (Malinverno et al., 2008). The summertime conditions together with the large environmental ranges between and within the selected sampling locations allow the characterization and understanding of the main environmental factors guiding the distribution of the studied coccolithophore species in the region. Species of the genus *Gephyrocapsa* as well as *E. huxleyi* morphotypes and variations in their morphology were analysed to illustrate their ecological response to different environmental variables including those of the carbonate system such as pH and calcite saturation state. A previous study performed on the same sampling locations during the same cruise (Wolhowe et al., 2014) analysed the primary productivity of the species *E. huxleyi* and the *Gephyrocapsa* species.

In summary, the main scientific questions addressed in this work are: (1) Which are the main environmental conditions in which maximum standing stocks of the different *Gephyrocapsa* species are found, and (2) which are the future perspectives for the particulate inorganic carbon (PIC) quotas and PIC production of *E. huxleyi* and the *Gephyrocapsa* species at stratified warm conditions.

6.3 Materials and methods

The water samples and hydrographic measurements for this study are the same as those used in Chapter 5, described in section 5.3 (subsections 5.3.1 and 5.3.2). Coccolithophore assemblages were studied as in Chapter 5 (section 5.3.3) but focusing in the different species of *Gephyrocapsa*.

6.3.1 Variability in the morphology of *Gephyrocapsa spp.*

Calcite per coccolith was estimated for *G. oceanica* according to the shape factor (k_s) given by Young and Ziveri (2000) for this species. Calcite per liter was estimated in each sample, using a calculated averaged length (calculated on 60 coccoliths on SEM images from various samples), using the mono-layered or multi-layered proportions in the species coccospheres at each sample, together with an average of the number of coccoliths on each category (calculated from 30 coccospheres) and cell abundance.

For the different species of *Gephyrocapsa* found in this study, calcite per coccolith was estimated using the shape factor (k_s) given by Young and Ziveri (2000) for *G. oceanica*, as they did with *G. muellerae* and *G. ericsonii*. Calcite per liter was estimated for each species in each sample, similarly as for *G. oceanica*, but without considering if it was a multi-layered coccosphere or not.

6.3.2 Data analysis and statistical treatment

A principal component analysis (PCA) was applied to the abiotic data in order to have a complete view of the hydrographic conditions associated with each location, depth and region (Fig. 6.1a). The PCA was performed using the statistics software XLSTAT 7.5.2.

Different multivariate statistical analyses were used to help determine the main environmental variables (abiotic data) related to changes in the cell density (cell $\cdot$ L^{-1}) of the different studied coccolithophore species and morphotypes (biotic data). The analyses were carried out using PRIMER-E v. 6.0, following the methods described by Clarke and Gorley (2006). A square root transformation was applied to the biotic data. A logarithmic transformation was applied to selected environmental variables (nutrients and PAR) when the scatter plots between pairs of environmental variables were markedly skewed on any of the variable axes (as described by Clarke and Ainsworth, 1993).

The cell densities, standardized and square-root-transformed, of all the analysed morphological categories of *E. huxleyi* used in this study (Table 5.1B–D) and of the different species of *Gephyrocapsa* were analysed with a cluster analysis and non-metric multidimensional scaling (NMDS) ordination of samples based on Bray-Curtis similarity. These analyses can group the studied sites using the variation in the cell densities, and therefore can detect different ecological regions and can demonstrate spatial changes in the cell densities of the morphological categories, morphotypes, and species. The abiotic data was then standardized and analysed by a SIMPER analysis according to the samples grouped by the previous analyses. The SIMPER analysis was used to detect the abiotic variables responsible for the differences between the groups of samples clustered with the biotic data. The analysis gives the contribution of each variable.

A BEST analysis –Spearman's rank correlation method– was used to obtain the variable or combination of environmental variables that better explain one biotic variable (the correlation gives only one correlation coefficient), it was limited from 1 to maximum 5 combined variables in order to find the main controlling or limiting single or combined variables.

The multivariate analyses included the following 14 environmental variables: pH, CO_2, CO_3^{2-}, pressure, temperature, salinity, Chl-*a*, Log(PAR), dissolved oxygen, Log(nitrate), Log(nitrite), Log(phosphate), Log(silicate), and Log(ammonium); Log: logarithmic transformation applied. As several variables can be highly correlated between them, the strongly correlated variables ($r > 0.95, r < -0.95$) in the multivariate analysis were picked out (Table C.13 in Appendix C.2). This last means that when one of the strongly correlated variables resulted significant in the statistical analysis, the other would also appear as an explaining variable.

Similarly to the water column profiles of the abiotic data, the biotic data was also plotted in ODV as vertical profiles (Fig. 6.2) following a continuous section from station 1 to station 12 (Fig. 5.1a). The data was similarly extrapolated to be correspondent with the isolines of the abiotic data and detect or show the relationships found between the biotic and the abiotic data, both by observing the plots and with the statistics. Further 3D scatter plots (shown in Appendix C.1) were plotted to analyse pair of abiotic variables mainly describing biotic variables according to the multivariate analyses.

6.4 Results

6.4.1 Water profiles of abiotic conditions

Surface and vertical profiles of the water conditions are found in Figs. 5.1 and 5.2 in Chapter 5. Extra profiles are found in Appendix C.1. The PCA of the water conditions is shown in this chapter in Fig. 6.1a.

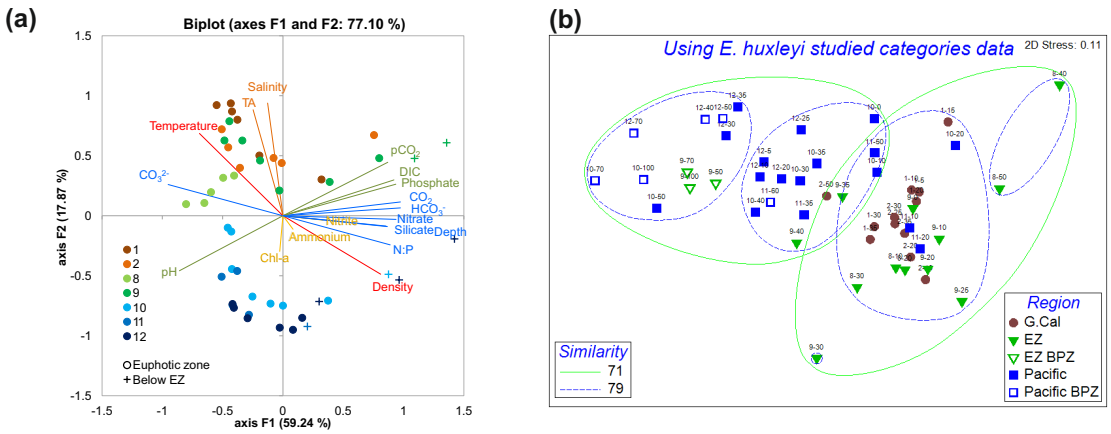

Figure 6.1: Ordination plots of samples using the data from all the studied environmental variables (a) and, independently, using the data from all the morphological variability studied in *E. huxleyi* (b). In (a) highly correlated and anticorrelated hydrographical variables are marked with the same color; the position of the plotted symbols in the correlation circle (color for the station number, symbol for the location in the water column) show the main hydrographic conditions associated and show near the most similar samples. In a PCA, an anticorrelated variable will be placed in the opposite side of the center and those not correlated will be orthogonal. In (b) standardized and square-root-transformed cell densities of all the analysed morphological categories of *E. huxleyi* used in this study (Table 5.1B–D) were analysed with a non-metric multidimensional scaling (NMDS) ordination of samples (symbols) based on Bray-Curtis similarity. This ordination demonstrates spatial changes in *E. huxleyi* morphological categories and morphotypes; solid and dashed lines represent the superimposed sample clusters at the similarity levels of 71 and 79, respectively. G.Cal: Gulf of California; EZ: entrance zone; BPZ: below euphotic zone.

6.4.2 Cell densities and distribution of coccolithophores

Considering the 68 samples analysed, the coccolithophore cell density was in average of 5.1×10^4 cells per liter, being lower in the G. Cal and EZ (4.1×10^4 cell $\cdot$ L^{-1}) than in the NE Pacific (6.5×10^4 cell $\cdot$ L^{-1}), above and below the euphotic zone base. If dividing the data in four subsets, maximum coccolithophore standing stock averages were found in the following order: below the euphotic zone in the NE Pacific (7.9×10^4 cell $\cdot$ L^{-1}), in the euphotic zone of the NE Pacific (5.8×10^4 cell $\cdot$ L^{-1}), in the euphotic zone of the G. Cal and EZ (4.7×10^4 cell $\cdot$ L^{-1}) and, finally, below the base of the euphotic zone in the G. Cal and EZ (2.0×10^4 cell $\cdot$ L^{-1}). Samples with maximum abundances of coccolithophores in the upper 100 m of the water column, reaching 18.5 $\times 10^4$ cell $\cdot$ L^{-1}, were found in the NE Pacific. The lowest coccolithophore cell densities (8×10^3 cell $\cdot$ L^{-1}) in the euphotic zone were found at the northernmost location of the G. Cal (station 1), which presented the maximum salinity concentrations (maximum salinity = 35.24‰). In the euphotic zone of the NE Pacific waters, higher cell densities were found at lower temperature and lower salinity. Below the euphotic zone base, maximum cell densities were found at higher ammonium concentrations.

At a 95% confidence interval, total coccolithophore cell counts between 300 and 200 cells per sample have an average error of 12%, with minimum average errors of ±7% and maximum average errors of ±15%. Cell counts were in average 300 coccospheres per sample, with minimum counts of ∼200 coccospheres per sample. A detection limit higher than a 99.9% probability was obtained for each cell density.

Emiliania huxleyi was the main species found in the study, comprising on average 50% of the total number of coccolithophores, and presented a r^2 of 75% with the total number of coccolithophores. *Emiliania huxleyi* was the main species found in the colder NE Pacific, comprising 60% of the total number of coccolithophores, and there it presented a r^2 of 80%. Samples with maximum abundances of the species *E. huxleyi* (reaching 14.2 $\times 10^4$ cell $\cdot$ L^{-1}) were found in the NE Pacific. *Gephyrocapsa oceanica* was present and sometimes a dominant species in the G. Cal and EZ. *Gephyrocapsa muellerae*, contrary to *G. oceanica*, was almost only found in the colder NE Pacific. *Gephyrocapsa ericsonii* and *G. ornata* were the other two species of the genus found and analysed in this study.

6.4.3 Cell densities and distribution of species of Gephyrocapsa

Gephyrocapsa oceanica (Fig. 6.2a-b) was the most abundant species of the genus; it was restricted to the G. Cal and the EZ (stations 1 to 9) where it was the second

most abundant species of coccolithophore. Maximum abundances of *G. oceanica* (higher than ∼10 000 cell · L^{-1}) were found above 25 °C, including the maximum temperature sampled (∼25 000 cell · L^{-1} at 29 °C), except where salinity was higher than 35.15‰or silicate was higher than 4.5 μmol L^{-1}. Cells densities were very low (< 4000 cell · L^{-1}) below 24 °C and were not found at temperatures below 15 °C nor at salinities below 33.9‰. At lower DIC concentrations (< 2050 μmol kg^{-1}) or lower phosphate concentrations (< 0.5 μmol L^{-1}), *G. oceanica* presented a predominant contribution and even outnumbered *E. huxleyi*. *Gephyrocapsa oceanica* mainly dominated above 24 °C, with higher cell densities (up to 37×10^3 cell · L^{-1}) in the warmest and southernmost location (station 8). On average, *G. oceanica* corresponded to 25% of the total number of coccolithophores in the G. Cal and EZ. Lower [HCO_3^-], which is highly correlated with DIC, was also associated to higher abundances. However, both DIC and [HCO_3^-] concentrations were high (from 1944 to 2230 μmol kg^{-1} and from 1692 to 2118 μmol kg^{-1}, respectively). Cell densities lower than 10 000 cell · L^{-1} were found below a pH of 7.99 and cell densities lower than 2500 cell · L^{-1} below a pH of 7.9.

The proportion of *G. oceanica* versus *E. huxleyi* was included in a matrix correlation and presented several significant correlations (Table C.23 in Appendix C.2); the main ones were with DIC concentration, [HCO_3^-], density, phosphate concentration, temperature and [CO_3^{2-}]. Above 22 °C and particularly in low nutrient conditions, the proportion of *G. oceanica* was better correlated with temperature. The region in which the two species had the same proportion marked the border of nitrite depletion in the euphotic zone. The negative correlation with DIC was the highest significant correlation ($r^2 = 0.58$), particularly above the euphotic zone base at a DIC concentration lower than ∼2140 μmol kg^{-1} ($r^2 = 0.77$).

Gephyrocapsa muellerae (Fig. 6.2c-d) was almost restricted to the NE Pacific, as it was found from station 9 to 12. It was the second more abundant species in the NE Pacific, comprising approximately 7% of the total number of coccolithophores there. It was found mainly below 18 °C and almost not found above 21 °C. Cell densities were usually lower than 500 cell · L^{-1} in samples with a pH lower than 7.8. Maximum abundances (up to 13 000 cell · L^{-1}) were found in stations 11 and 12, the two northernmost locations in the NE Pacific.

Gephyrocapsa ericsonii (Fig. 6.2e-f) was the second most abundant species of the genus Gephyrocapsa, comprising 4% of the total number of coccolithophores. It presented a slightly higher relative abundance in the G. Cal and EZ (5%) than in the NE Pacific (3%). It was found below temperatures of 28 °C, and presented its higher abundances at nitrite concentrations higher than 0.02 μmol L^{-1}, or ammonium concentrations higher than 2.2 μmol L^{-1}. It presented cell densities below 1000 cell · L^{-1} at temperatures lower than 13 °C.

Gephyrocapsa ornata (Fig. 6.2g-h) was mainly present in the NE Pacific, where it comprised 2% of the total number of coccolithophores. It was particularly

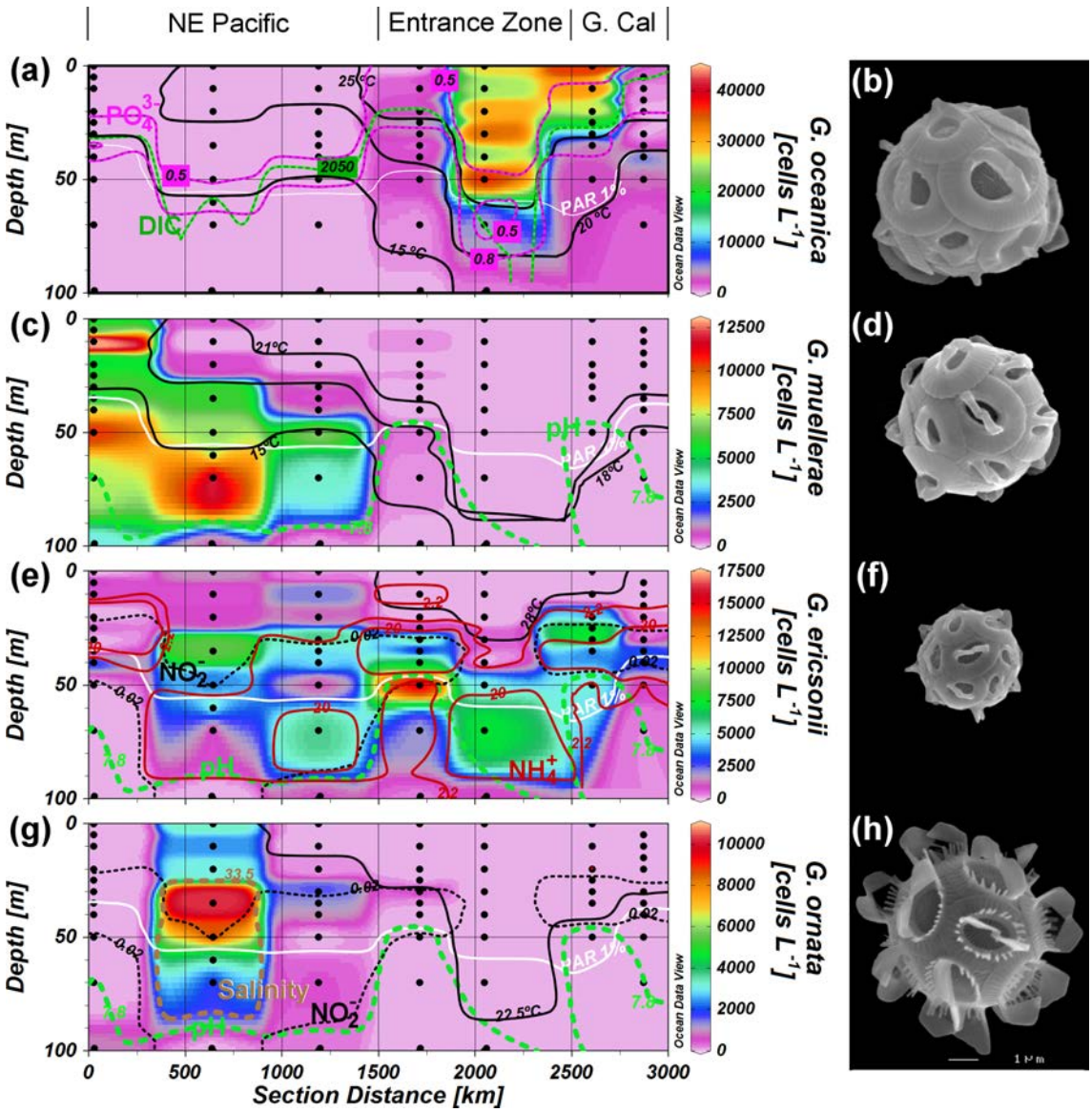

Figure 6.2: Cell density vertical profiles and coccosphere images of *G. oceanica* (a, b), *G. muellerae* (c, d), *G. ericsonii* (e, f), and *G. ornata* (g, h). The base of the euphotic zone (PAR 1%) is shown in each vertical profile with a white isoline. Isolines for different environmental variables related to the cell densities are shown in each profile: temperature (black isolines), phosphate concentration (pink dotted isoline), dissolved inorganic carbon concentration (thin green dotted isoline, μmol kg^{-1}), pH (green dotted isoline), nitrite concentration (black dotted isoline), ammonium concentration (red isoline), and salinity (golden dotted line). Nutrient concentrations are in μmol L^{-1}. G. Cal: Gulf of California.

abundant in station 11, where it was the fourth most abundant species, with a relative abundance of 6%. It was found below a temperature of 22.5 °C and above a pH of 7.8. Station 11 presented the lowest salinity concentrations (down to 33.3 ‰), and as mentioned previously, it presented the deepest chlorophyll maximum,

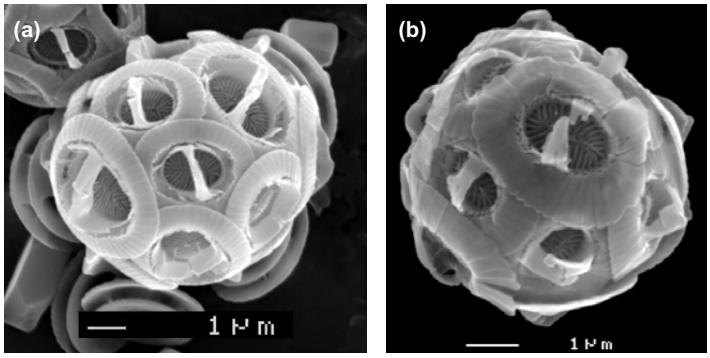

Figure 6.3: *Gephyrocapsa oceanica* malformed coccospheres, from station 8 at 40m (a) and station 9 at 40m (b), with aberrations in the tube elements or in the bridge.

the maximum depth of the sea floor and was the station located farthest from the coast.

A hierarchical cluster analysis (Fig. 6.4a), based on the Bray-Curtis similarity using the group average method on square-root-transformed cell densities, associated species and *E. huxleyi* morphologies with similar distributions. The analysis used the cell densities of the different species of *Gephyrocapsa*, of the different calcification morphologies of *E. huxleyi* and of its morphotypes, and included the rest of species as one group. Specifically, at the similarity level of 50, five clusters were found: the under-calcified *E. huxleyi* type A was associated with the species *G. ericsonii*, the normally-calcified *E. huxleyi* type A was associated with the rest of species, *E. huxleyi* over-calcified was associated with *E. huxleyi* type O and with *G. muellerae*, and *G. ornata* and *G. oceanica* were not associated with others. The studied sites were grouped in an ordination plot of samples (Fig. 6.4b) using the same biotic variables (samples standardized and square-root-transformed) of the cluster analysis for the genera *Emiliania* and *Gephyrocapsa*. The identified samples were clustered and analysed in four main groups (Table C.2 in Appendix C.2) which were then analysed by a SIMPER analysis to detect the abiotic variables responsible for the differences between the groups of samples clustered with the biotic data. The results of the SIMPER analysis are shown in Table 6.1, there are also shown the species or morphologies characterizing each group.

Thus, the results and the SIMPER analysis show that:

1. Temperature mainly explains the higher abundance of *G. oceanica* in station 8 versus that in stations 9-12; however the lower nutrients in station 8 explain its higher abundance there than in the euphotic zone of stations 1,2 and 9, stations characterized by *E. huxleyi* type A under-calcified and *G. ericsonii*. Related to the previous sentence, although not shown in Table 6.1, the two small clusters of the euphotic zone of station 8 obtained by the biotic data, according to the SIMPER analysis, were distinguished from

each other mainly by ammonium (20%) and nitrate (17%), the lower layers with higher nutrient concentrations were characterized by an increase of the cell densities of *E. huxleyi* type A under-calcified and *G. ericsonii*.

2. Salinity mainly explains the characteristic presence of *G. ornata* in stations 10 and 11 at the euphotic zone and its low or absent cell densities in the euphotic zone of the Gulf of California and station 9 of the EZ, pointing to a preference of the species to less saline waters.

3. Temperature explains the higher cell densities of *E. huxleyi* type A over-calcified, *E. huxleyi* type O and *G. muellerae* in station 12 and below the euphotic zone of stations 9 to 12, and the lower cell densities in the Gulf of California and EZ.

4. The dissolved oxygen concentration and pH were the main variables distinguishing the euphotic zone of stations 10 and 11 from the euphotic zone of station 12 and below the euphotic zone of stations 9-12; the samples with higher pH and higher dissolved oxygen concentrations (Fig. C.1a,h in Appendix C.1) were mainly characterized by *G. ornata*, *E. huxleyi* type A under-calcified and *G. ericsonii* (less abundant but also present were *E. huxleyi* type A over-calcified, *E. huxleyi* type A normally-calcified ,and *G. muellerae*; and the samples with lower pH and lower dissolved oxygen concentrations were characterized by *E. huxleyi* type A over-calcified, *E. huxleyi* type O and *G. muellerae*.

A very similar ordination plot of samples to the one derived from the biotic data was also obtained only using the morphological variability and the morphotypes of the species *E. huxleyi* (Fig. 6.1b), its visual comparison with the PCA derived from the abiotic data (Fig. 6.1a) gives a general view of the results extracted from the SIMPER analysis. In both ordinations the G. Cal and the Pacific regions are distinguished from each other, while the EZ clearly presents a large variability as observed by its stations grouped in different clusters. Samples below the euphotic zone are also distinguished in both ordinations derived from biotic data.

6.4.4 *Emiliania huxleyi* and *Gephyrocapsa spp.* estimated calcite

Calcite per liter was estimated for the different species of *Gephyrocapsa* and the different morphotypes of *E. huxleyi*. *Gephyrocapsa oceanica* presented the highest calcite concentrations per liter (Fig. 6.5), its calcite per liter reached maximum values of up to three times higher than the maximum from *E. huxleyi*. Although *G. oceanica* was not the most abundant species of the study (Table 6.2), it presented the maximum total calcite quota of the whole study (Table 6.3), accounting for

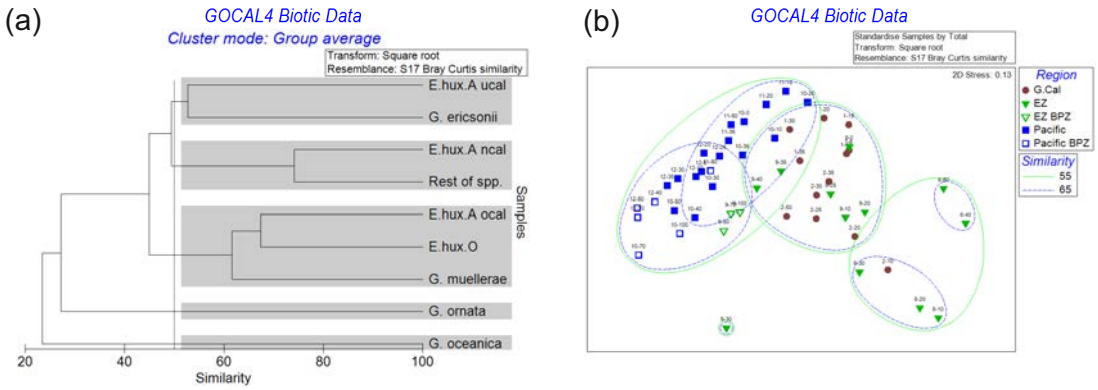

Figure 6.4: Hierarchical cluster analysis and ordination plot of samples using the cell densities. In (a), hierarchical cluster analysis (group average method) of the different species of *Gephyrocapsa* and morphologies of *E. huxleyi* (biotic variables), based on Bray-Curtis similarity, using the square-root-transformed cell densities; and in (b), ordination plot of samples using the biotic variables standardized and square-root-transformed. In (a), at the similarity level of 50 (dashed line) five clusters are highlighted in gray. In (b), the cell density correspondent to the rest of species (others than the genera *Emiliania* or *Gephyrocapsa*) was not included in the analysis. E.hux.A: *E. huxleyi* type A; E.hux.O: *E. huxleyi* type O; ucal: under-calcified; ncal: normally-calcified; ocal: over-calcified; G.Cal: Gulf of California; EZ: entrance zone; BPZ: below euphotic zone.

the 55%. The calcite quota derived from *E. huxleyi* was the second highest and that from *G. muellerae* the third one.

Calcite per liter from *E. huxleyi* (Fig. 6.5a–c) was estimated for each sample (see Methods). Calcite was calculated using the averaged length of 2.94 μm for both morphotypes. For *E. huxleyi* type A, together with the morphological level of calcification, calcite was calculated considering 15 coccoliths per cell for the mono-layered coccospheres, and 30 coccoliths per cell for the multi-layered coccospheres. For *E. huxleyi* type O, calcite was calculated considering 15 coccoliths per cell for the mono-layered and 35 coccoliths per cell for the multi-layered coccospheres. *Emiliania huxleyi* type A was the morphotype dominating the species; hence the species calcite concentration presented an almost equal distribution to the cell density of *E. huxleyi* type A and therefore the same relationships with the environmental variables.

For the estimation of calcite per liter given by *G. oceanica* in each sample (Fig. 6.5d), it was used the calculated cell abundances, the estimated number of coccoliths for the mono-layered (average = 21 coccoliths cell^{-1}, SD = 6.87, N = 30) and multi-layered (42 coccoliths cell^{-1}) cells, and a coccolith average length of 3.64 μm (SD = 0.68 μm, N = 60).

For the estimated calcite on *G. muellerae, G. ericsonii,* and *G. ornata* (Fig. 6.5f–h), SEM images of 30 coccospheres of each species were analysed. For each species and sample, the estimated calcite per liter was calculated with the cell abundance

Table 6.1: SIMPER results of variables responsible for 50% of differences between the groups of samples clustered with the biotic data at a similarity level of 65% (Fig. 6.4b). Contribution of each variable to Euclidean distance between groups is given in brackets. Species or morphotypes associated to the groups analyzed are in brackets (supported by cluster analysis in Fig. 6.4a and by Figs. 5.3, 5.5 and 6.2). G. Cal: Gulf of California; EPZ: euphotic zone; E. hux. A: *E. huxleyi* type A; E. hux. O: *E. huxleyi* type O; u-calc: under-calcified; o-calc: over-calcified.

	Stations 10-11 EPZ (*)	G. Cal and Station 9 –EPZ–	Station 8
G. Cal and Station 9 –EPZ– (*E. hux.* A u-calc, *G. ericsonii*, some *G. oceanica*)	Salinity (21.14%) Ammonium (9.4%) Temperature (8.51%) Phosphate (8.43%) pH (7.75%)		
Station 8 (*G. oceanica*)	Temperature (16.43%) Salinity (15.67%) Nitrate (10.13%) Silicate (8.96%)	Nitrate (15.13%) Ammonium (15.06%) Phosphate (11.69%) Nitrite (9.32%)	
Station 12 and below euphotic zone of stations 9-12 (*E. hux.* A o-calc, *E. hux.* O, *G. muellerae*)	Dissolved Oxygen (11.1%) pH (10.89%) CO_2 (10.03%) Phosphate (9.96%) PAR (9.55%)	Temperature (9.83%) PAR (8.45%) CO_3^{2-} (8.39%) Pressure (8.19%) Salinity (8.12%) CO_2 (8.04%)	Temperature (12.34%) CO_3^{2-} (11.83%) CO_2 (9.08%) Silicate (9.04%) Nitrate (8.63%)

**G. ornata*, *E. huxleyi* type A under-calcified, *G. ericsonii*, some *E. huxleyi* type A over-calcified, some *E. huxleyi* type A normally-calcified and some *G. muellerae*.

(Fig. 6.2), the estimated number of coccoliths per cell (21 coccoliths cell^{-1}, 24 coccoliths cell^{-1}, and 22 coccoliths cell^{-1}, respectively), and the coccolith average length (3 μm, 1.9 μm, and 2.8 μm, respectively).

In terms of calcite per cell, *G. oceanica* was the most heavily calcified of the species studied and *G. muellerae* the second one. The estimations in the present study for individual coccospheres gave an average of 76 pg of calcite per cell for *G. muellerae* versus 142 pg of calcite per cell for *G. oceanica*, i.e. the coccosphere calcite weight of *G. oceanica* is $\sim$ 2 times the coccosphere calcite weight of *G. muellerae*.

Calcite per liter given by different species together (*E. huxleyi* and *Gephyrocapsa spp.*) was also calculated. Only considering the standard deviations for the number of coccoliths per cell and for the coccolith length, total estimations of calcite per liter had a maximum deviation interval of $\pm$0.18%. Estimated calcite per liter was mostly dependent on cell abundance; hence, they had almost the same errors as the calculated cell abundances and at the same time the same relationships with the environmental variables. Considering *E. huxleyi* and *Gephyrocapsa spp.* together, higher calcite concentrations per liter were given by *G. oceanica*, so higher concentrations were found in stations 2 and 8, at the G. Cal and the

Table 6.2: Percentage of the total cell density contribution of each species or morphotype in the whole study and by regions. Contributions are only calculated for *E. huxleyi* and the *Gephyrocapsa* species.

Species or morphotype	All stations	G.Cal	EZ	Pacific	Station 8	Station 9	Stations 10-11	Station 12
G. oceanica (cell density)	16.73%	34.66%	38.71%	0.00%	66.56%	7.21%	0.00%	0.00%
E. huxleyi type A (cell density)	56.12%	57.77%	45.69%	59.48%	27.94%	65.76%	55.98%	63.32%
G. muellerae (cell density)	5.13%	0.00%	0.18%	9.40%	0.00%	0.38%	6.84%	12.20%
G. ericsonii (cell density)	5.77%	6.88%	9.00%	3.99%	4.82%	13.74%	6.89%	0.82%
G. ornata (cell density)	1.62%	0.00%	0.16%	2.92%	0.00%	0.34%	5.45%	0.14%
E. huxleyi type O (cell density)	14.63%	0.69%	6.26%	24.21%	0.68%	12.57%	24.84%	23.52%

Table 6.3: Percentage of the total calcite quota contribution of each species or morphotype in the whole study and by regions. Contributions are only calculated for *E. huxleyi* and the *Gephyrocapsa* species.

Species or morphotype	All stations	G.Cal	EZ	Pacific	Station 8	Station 9	Stations 10-11	Station 12
G. oceanica (calcite)	54.78%	73.00%	82.42%	0.00%	94.99%	27.20%	0.00%	0.00%
E. huxleyi type A (calcite)	32.43%	24.63%	15.04%	63.07%	4.24%	62.47%	62.79%	63.39%
G. muellerae (calcite)	7.77%	0.00%	0.15%	25.76%	0.00%	0.81%	18.28%	34.41%
G. ericsonii (calcite)	2.54%	2.36%	2.18%	3.18%	0.76%	8.43%	5.34%	0.67%
G. ornata (calcite)	2.08%	0.00%	0.11%	6.81%	0.00%	0.61%	12.40%	0.33%
E. huxleyi type O (calcite)	0.40%	0.01%	0.09%	1.19%	0.01%	0.48%	1.19%	1.19%

EZ, respectively, even though total coccolithophore cell numbers were higher in the NE Pacific.

6.5 Discussion

6.5.1 Environmental conditions controlling the *Gephyrocapsa spp.* distribution

The results obtained in this study show a strong control of the seawater carbonate chemistry, the temperature and the nutrients on the distribution of *Emiliania huxleyi*, its morphotypes and morphogenesis, and on the distribution of the *Gephyrocapsa* species. The stratification of the summertime analysed samples gave a large range of conditions allowing the distinction of different ecological niches.

Likewise to the morphotypes A and O of *E. huxleyi*, the boundaries of the vertical and horizontal distribution of the *Gephyrocapsa* species are mainly controlled by temperature, pH and nutrients, but also by salinity. *Gephyrocapsa oceanica*, the most heavily calcified of the species studied (in terms of calcite per cell), is the warmest species and the most tolerant and even akin to nutrient depleted waters. *Gephyrocapsa ornata* and *G. ericsonii* are less warmer species than *G. oceanica*, *G. ornata* additionally prefers less saline waters than the rest of the *Gephyrocapsa*

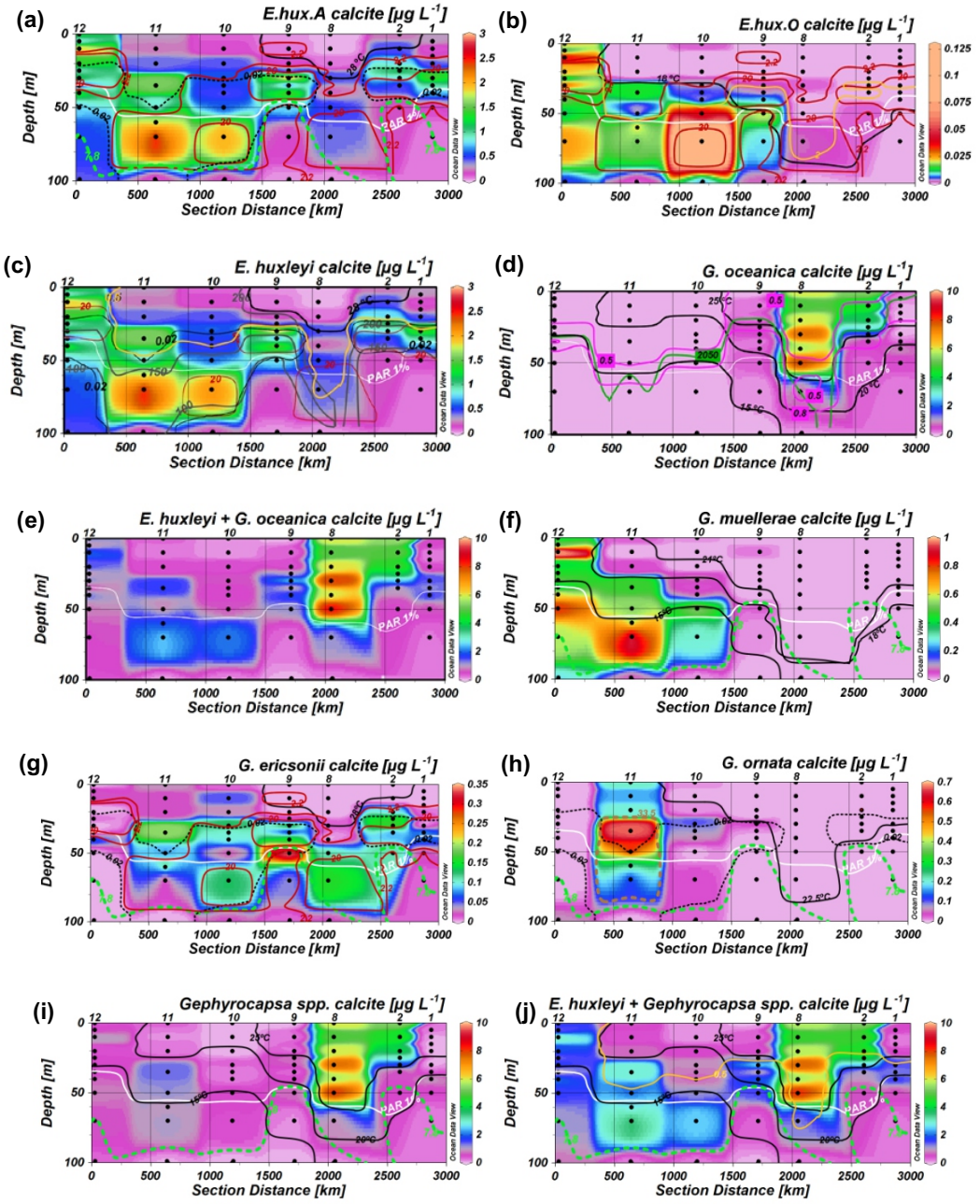

Figure 6.5: Estimated total amount of calcite per liter of the different morphotypes *E. huxleyi* and of the different species of *Gephyrocapsa*. Temperature (thicker black isolines), CO_3^{2-} (grey isolines, μmol kg^{-1}, nitrite (black thinner isolines, μmol L^{-1}), ammonium (red isolines, μmol L^{-1}), (Nitrate + Nitrite):Phosphate ratio (yellow isoline), euphotic zone (above white isoline), dissolved inorganic carbon (green isoline, μmol kg^{-1}), phosphate (pink isolines, μmol L^{-1}), pH (green dotted isoline), salinity (golden dotted isoline).

species. *Gephyrocapsa muellerae*, the second most calcified of the studied species

(in terms of calcite per cell), was the coldest *Gephyrocapsa* species and the most tolerant to lower pH.

6.5.2 Future perspectives

Climate changes such as ocean acidification (Doney et al., 2009), global warming and a resulted deepening of the nutricline due to an enhanced stratification (Cermeño et al., 2008), might decrease the relative abundance of the morphotype A of the species *E. huxleyi* versus its less calcified morphotype O, while the relative abundance of the over-calcified morphotype A might increase versus the normally-calcified morphotype A. In such conditions, *G. oceanica* and *G. muellerae* might increase their relative abundances versus the rest of species of coccolithophores. Then one of the remaining questions is if the particulate inorganic carbon (PIC) production might also increase due to climate change.

From the results presented here and using the available data on the same samples reported by Wolhowe et al. (2014), we observe that the PIC per liter and the PIC production were positively related and that, contrary to what could be intuitively expected, maximum PIC values were found at low cell densities and low cell production rates (Fig. 6.6) (all estimated for *E. huxleyi* together with the *Gephyrocapsa* species). Maximum PIC values were found at station 8, the station where the species *G. oceanica* was highly dominant (Table 6.2). We found that the highest PIC values obtained in this study are given by *G. oceanica* (Table 6.3) (calcite per liter is concomitant to PIC per liter and is plotted in Fig. 6.5). If heavy species such as *G. oceanica* and *G. muellerae* are favored by climate change conditions then an increase in the PIC production might occur.

The detached coccoliths were not considered in the PIC estimations. The species *E. huxleyi* has been found to present high number of detached coccoliths, however especially at non-optimal conditions presenting lower coccolith production and lower production rates (Rosas-Navarro et al., 2016). Even so, extra estimations were calculated here using different possible number of total coccoliths per cell for *E. huxleyi*; 40, 45, and 50 coccoliths per cell were used and the results can be observed in Fig. C.14 and Table C.28. As can be expected, the stations where *E. huxleyi* was more dominant the increase in the number of coccoliths per cell gave more weight to the PIC estimations. Still, station 8 with the dominance of the heavier *G. oceanica* presented the highest estimations of PIC per liter and PIC production rate. One sample from station 12 presented a high PIC production rate estimation (Fig. 6.6b), station 12 presented the shallowest nitracline (Fig. 5.2d). These findings show that at stratified warm conditions heavy species such as *G. oceanica* can increase the PIC quotas and production. Warming at no so stratified conditions can also increase the PIC production by approaching species such as the dominant *E. huxleyi* to their optimum growing conditions of temperature,

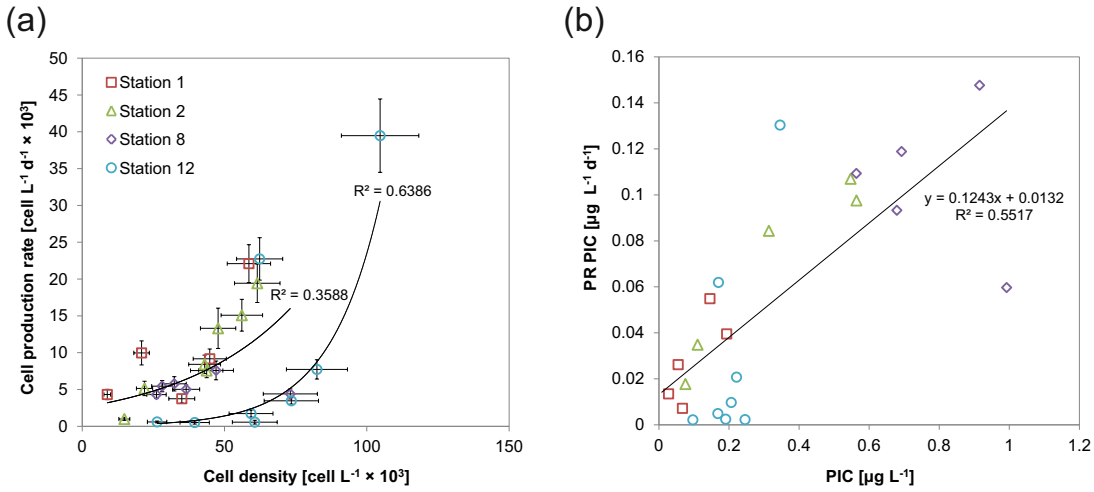

Figure 6.6: Cell density and estimated particulate inorganic carbon (PIC) relationship with productivity. In (a), cell density of the alkenone-producing coccolithophores (*E. huxleyi* and the *Gephyrocapsa* species) versus their cell production rate estimates (data from Wolhowe et al., 2014). And in (b), from the two previous variables together with the estimated PIC per liter (from the estimated calcite per liter) was calculated a PIC production rate (PR PIC). Results were obtained for stations 1, 2, 8, and 12. In (a), the upper 95% confidence interval using the Poisson cell counting statistics (Bollmann et al., 2002) is shown for the cell densities; the standard deviations calculated by Wolhowe et al. (2014) are shown for the cell production rate. In (a) two exponential fits are shown, one for the data from stations 1, 2, and 8, and the other one for station 12 data. In (b) a linear fit is shown for all the data together.

light, and nutrients. All of the above suggests that at least for the species studied here, which were dominant in the region and accounted for the 72% of the total coccolithophore cell density, their particulate inorganic carbon (PIC) production might increase due to the combined effect of global warming, ocean acidification, and deepening of the nutricline, especially in regions prone to sharp stratification such as the one studied here. Hence, as eastern boundary upwelling regions are areas particularly affected by climate change (Feely et al., 2008), they might present higher PIC production in future scenarios. However, it is still important to study the effect in the rest of species of coccolithophores, especially the heavy ones. From rough estimates (not shown) based on the coccolith mass (Young and Ziveri, 2000) and abundance of the rest of species, the calcite contribution from *E. huxleyi* and the species of *Gephyrocapsa* may only have accounted for approximately 30% of the total coccolithophore calcite per liter.

An impact in the global PIC production due to global warming is still highly likely because temperature can strongly influence the distribution of the coccolithophore species, rapidly changing their biogeography through water mass circulation (Winter et al., 2014; Dimiza et al., 2015; Kang et al., 2016). Hence, the tropical-subtropical species *G. oceanica* might occupy higher latitudes and, in contrast, *E. huxleyi* type O might reduce its latitudinal distribution being more

restricted to polar regions since it seems limited by temperatures warmer than 18 °C.

Due to climate change, in highly stratified temperate waters we might find in the upper water layers a relative increase in the species/morphologies tolerant to higher temperatures and lower nutrient concentrations such as the species *G. oceanica*, while in the subsurface waters we might find a relative increase in the species/morphologies tolerant to lower temperatures and lower pH such as the species *G. muellerae*, the over-calcified morphology of *E. huxleyi* type A, and *E. huxleyi* type O. Likewise, the warm species/morphologies might expand poleward while the cold ones might be more restricted to poleward regions. The changes in species richness and abundance of each region should depend on the regional ecological and physical oceanographical changes, but from what we observe in our results, the coccolithophore community composition and the water masses will be key players. Of course the species adaptation rates might also play a role in enhancing their relative and absolute abundances (Jin et al., 2013) and depending on the location the same species might present different optimal growing conditions.

The PIC to particulate organic (POC) ratio might also increase under climate change conditions. From the PIC estimates from the calcite estimates obtained in this study, and compared with the total POC measurements made by Wolhowe et al. (2014) for the same samples, we calculated a PIC : POC ratio (Table C.26 and Table C.27). The samples analysed in this study presented on average for each PIC unit (estimated for the studied species) 250 POC units. Here we are missing to include PIC estimates for the rest of the species of coccolithophores, however even if an increase in PIC production might occur it does not imply a positive PIC : POC ratio, that is a release of CO_2, although a climate change effect on the carbon and carbonate biochemical cycles is expected if the PIC : POC ratio increases.

6.6 Conclusions

In conclusion, the four species of *Gephyrocapsa* found in the study can also be used together with *E. huxleyi* as proxies. *Gephyrocapsa oceanica* is the species with the highest coccosphere calcite mass of the species studied and the warmest and most tolerant species and even akin to nutrient depleted waters; in the context of climate change its cell density and PIC contribution might be particularly relevant. *Gephyrocapsa muellerae*, the second species with high coccosphere calcite mass, was the coldest *Gephyrocapsa* species and the most tolerant to lower pH; therefore it might be relevant in the context of ocean acidification. Hence, in the context climate change, highly stratified temperate waters might present changes in the

vertical and horizontal distributions of the species, morphotypes and morphologies, with subsequent changes in the coccolithophore PIC production.

Chapter 7

Conclusions

The temperature experiment results in Chapters 2 and 3, from different *E. huxleyi* strains from the North Pacific grown under non-limiting conditions of light and nutrients, showed that over the sub-optimum to optimum temperature range (10–25 °C):

- Elemental production (PIC, POC, TPN), coccolith mass, coccolith size, width of the tube element cycle, number of attached coccoliths per coccosphere, coccosphere mass, individual sinking velocity, and coccolith production rate, are positively correlated with temperature.
- Incompleteness of coccoliths is not due to time shortage at high PIC production.
- Sub-optimal growth temperatures lead to an increase in the percentage of malformed coccoliths in a strain-specific fashion.
- The correlation between PIC production and coccolith mass/size supports the notion that coccolith mass can be used as a proxy for PIC production in sediment samples.
- Coccolith mass, and to a lesser extent also the number of attached coccoliths per coccosphere, significantly determine the individual sinking velocity increasing it linearly from sub-optimal to optimal temperatures, effect that could benefit the species and even be essential for its survival. These results support the coccolith ballasting function hypothesis.
- Although the total number of coccoliths per cell and the number of loose coccoliths per cell are higher at sub-optimal temperatures, the increase in temperature (from sub-optimum to optimum) increases *E. huxleyi* coccolith production.

- The PIC : POC ratio shows a minimum at optimum growth temperature in all investigated strains.
- While the bulk PIC : POC decreases with increasing temperature, the individual cell PIC : POC increases, supporting the need of considering individual cell PIC : POC, not bulk PIC : POC, as an indicator of sinking velocity in *E. huxleyi* (Milner et al., 2016).
- It is possible to determine the PIC : POC vs sinking velocity relationship based on geometrically derived PIC and POC quotas.
- Global warming might cause a decline in coccolithophore's PIC contribution to the rain ratio.
- Global warming might cause a an improved fitness in some genotypes due to fewer coccolith malformations.
- Global warming will exert the foremost influence on coccolithophore sinking behaviour as opposed to ocean acidification and nutrient limitation.

The set of results in Chapters 5 and 6, obtained from the detailed study of summertime water samples along a transect covering Gulf of California and NE Pacific margin waters, showed a strong control of seawater carbonate chemistry, temperature and nutrients on the distribution of *Emiliania huxleyi*, its morphotypes and morphogenesis, and on the distribution of the *Gephyrocapsa* species. In particular, it was found that:

- The morphotype O is a colder morphotype more akin with higher ammonium concentrations and more tolerant to lower pH values than the morphotype A.
- The over-calcified *E. huxleyi* type A shares niche with the morphotype O. They are found at lower calcite saturation states than the normally-calcified morphotype A.
- The "collapsed" morphology is probably the result of a two-step effect, a malformation followed by dissolution. The first step (the malformation affecting primarily the tube elements) seems to be due to unfavorable conditions for the cell such as the simultaneous low concentration (though not minimum) of different nutrients, enhanced by low salinity and by high coccolithophore/phytoplankton densities. The second step (dissolution) is probably due to microenvironments in the calcite saturated waters.
- The under-calcified morphology is mainly associated with low nutrient concentrations, specially of phosphate.

- In the context of climate change, elevated temperatures as well as a nutricline deepening on highly stratified temperate waters might restrict *E. huxleyi* morphotypes A and O to lower depths in the euphotic zone, while the lowering of pH due to upward migrations of the calcite saturation horizons might restrict them from lower water layers.

- *Gephyrocapsa oceanica* has the highest affinity to warmer waters with lower nutrient concentrations, and *G. muellerae* the highest tolerance to lower pH.

- Such as was observed in the studied summertime water samples, the PIC contribution per liter of *G. oceanica* can be higher than that of *E. huxleyi*, and the PIC *G. muellerae* can also be relevant.

- In the context of climate change, *G. oceanica* and *G. muellerae* might increase their relative abundance with subsequent changes in the coccolithophore PIC production.

- Temperature can strongly influence the distribution of these species, therefore the biogeography of coccolithophores might drastically change in the near future. In the context of global warming, the tropical-subtropical species *Gephyrocapsa oceanica* might occupy higher latitudes and, in contrast, *Emiliania huxleyi* type O could drastically constrain its distribution to the higher latitudes, being limited to live at temperatures below 18 °C.

- In contrast to the possible global warming effects, ocean acidification might decrease the relative abundance of the relatively highly calcified species *G. oceanica* against the less calcified *E. huxleyi* and might decrease the relative abundance of *E. huxleyi* morphotype A versus the less calcified type O.

Coccolithophores are important as primary producers and as calcifiers. In order to understand the impact of the current climate changes, furthermore work is necessary studying the environmental effects on the morphology, calcification, production and distribution of different coccolithophore species and strains. Their study will also help in stratigraphic and paleoceanographic studies. The more we understand, the more we will be able to predict/reconstruct.

Appendix A

Supplementary material for Chapter 2

A.1 Supplementary figures for Chapter 2

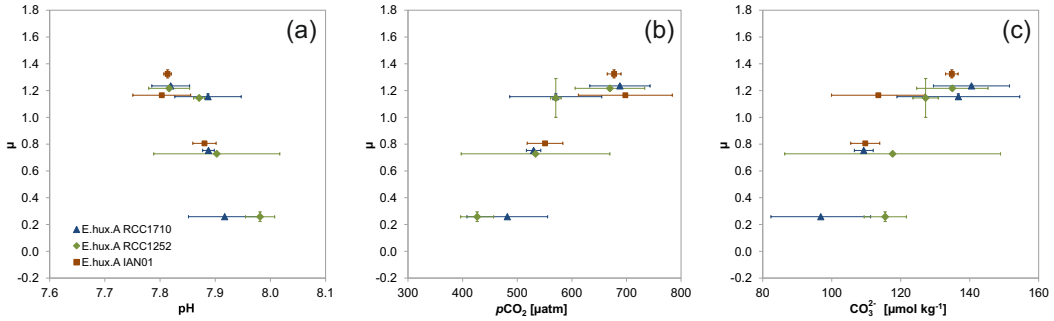

Figure A.1: Growth rate in relation to the values of pH (a), pCO_2 (b) and CO_3^{2-} concentration (c) at the end of the temperature experiment. Standard deviations of the triplicate experiment results are shown. Three different strains of *E. huxleyi* were used.

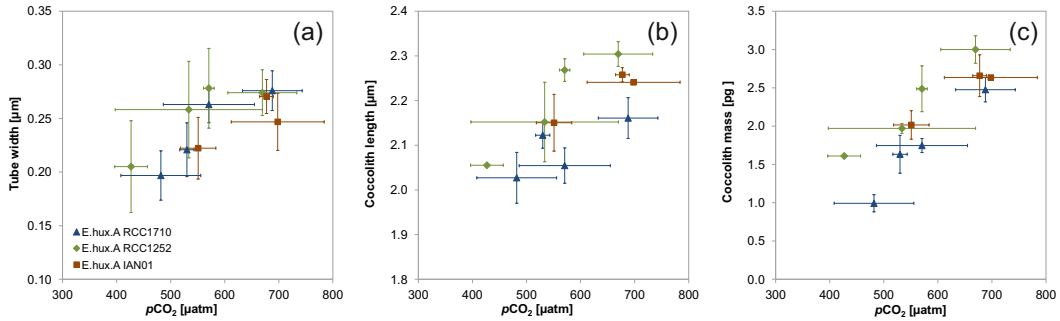

Figure A.2: Coccolith morphometry (a and b) and mass (c), in three *E. huxleyi* strains grown at different temperatures, in relation to the final values of pCO_2. Standard deviations of the triplicate experiment results are shown.

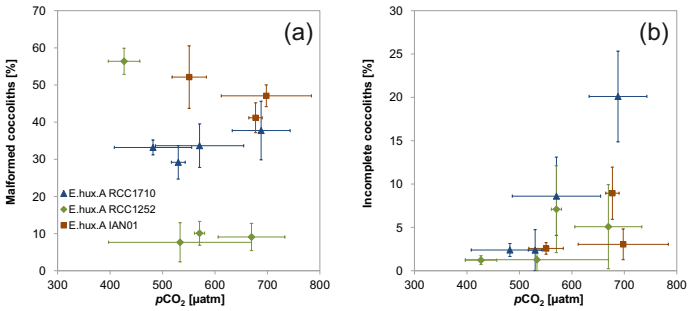

Figure A.3: Percentage of malformed (a) and incomplete (b) coccoliths, in three *E. huxleyi* strains grown at different temperatures, in relation to the final values of pCO_2. Standard deviations of the triplicate experiment results are shown.

A.2 Supplementary tables for Chapter 2

Table A.1: Cellular calcite and total particulate carbon (TPC) content and production, and PIC : POC and POC : TPN ratios of the three strains of *E. huxleyi* at different temperatures. Standard deviation of the triplicates in parentheses. P_{Calcite}: calcite production; P_{TPC}: TPC production.

Strain	T [°C]	Calcite [pg cell^{-1}]	TPC [pg cell^{-1}]	PIC : POC	POC : TPN	P_{Calcite} [pg cell^{-1} day^{-1}]	P_{TPC} [pg cell^{-1} day^{-1}]
RCC1710	10	127.54 (1.24)	24.92 (1.23)	1.72 (0.07)	5.92 (0.11)	32.97 (0.32)	6.44 (0.32)
RCC1710	15	117.24 (3.32)	24.06 (0.39)	1.42 (0.02)	6.74 (0.10)	88.29 (2.50)	18.12 (0.29)
RCC1710	20	95.55 (0.77)	23.52 (0.88)	0.95 (0.05)	6.92 (0.32)	110.34 (0.89)	27.15 (1.01)
RCC1710	25	90.00 (1.98)	20.10 (0.59)	1.17 (0.13)	6.73 (0.48)	111.16 (2.45)	24.82 (0.73)
RCC1252	10	69.09 (4.06)	14.64 (0.58)	1.31 (0.06)	5.48 (0.07)	17.83 (1.05)	3.78 (0.15)
RCC1252	15	82.70 (2.69)	18.57 (0.04)	1.15 (0.07)	6.47 (0.19)	60.20 (1.96)	13.52 (0.03)
RCC1252	20	82.39 (2.31)	17.96 (1.53)	1.13 (0.1)	6.47 (0.57)	94.35 (2.64)	20.57 (1.76)
RCC1252	25	101.65 (1.73)	22.38 (0.54)	1.20 (0.1)	7.21 (0.45)	123.69 (2.10)	27.24 (0.66)
IAN01	15	84.80 (2.47)	20.06 (0.72)	1.03 (0.02)	6.74 (0.08)	68.36 (1.99)	16.17 (0.58)
IAN01	20	67.66 (1.72)	17.07 (0.63)	0.91 (0.02)	5.11 (0.09)	78.86 (2.00)	19.89 (0.73)
IAN01	25	93.40 (3.03)	21.15 (0.33)	1.13 (0.04)	6.79 (0.08)	123.70 (4.01)	28.02 (0.44)

Table A.2: The carbonate system final values of each replicate.

ID	Strain	T [°C]	Bottle	TA [μmol kg^{-1}]	DIC [μmol kg^{-1}]	pH (total scale)	CO_2 [μmol kg^{-1}]	pCO_2 [μatm]	HCO_3^- [μmol kg^{-1}]	CO_3^{2-} [μmol kg^{-1}]	Omega calcite
1710 10-1	RCC1710	10	1	2121.00	2012.00	7.91	23.69	532.61	1900.33	87.09	2.13
1710 10-2	RCC1710	10	2	2129.00	2015.00	7.92	22.94	515.80	1901.13	89.96	2.20
1710 10-3	RCC1710	10	3	2163.50	2009.00	8.03	17.66	397.14	1876.30	113.42	2.79
1710 15-1	RCC1710	15	1	2174.50	2026.00	7.94	19.56	515.25	1892.66	112.34	2.77
1710 15-2	RCC1710	15	2	2150.50	2010.00	7.92	20.27	534.12	1881.28	107.11	2.64
1710 15-3	RCC1710	15	3	2175.50	2034.00	7.92	20.52	540.67	1903.77	108.38	2.67
1710 20-1	RCC1710	20	1	2318.50	2108.00	7.99	15.90	484.50	1934.17	155.68	3.86
1710 20-2	RCC1710	20	2	2284.50	2107.75	7.92	18.85	574.34	1953.06	134.10	3.32
1710 20-3	RCC1711	20	3	2269.00	2114.75	7.87	21.43	652.94	1971.55	120.37	2.98
1710 25-1	RCC1710	25	1	2333.00	2131.00	7.89	18.04	627.52	1958.11	152.83	3.82
1710 25-2	RCC1710	25	2	2289.00	2120.00	7.83	21.15	735.70	1965.74	131.57	3.28
1710 25-3	RCC1710	25	3	2296.00	2118.00	7.85	20.14	700.68	1959.05	137.14	3.42
1252 10-1	RCC1252	10	1	2241.00	2083.50	8.03	18.38	413.33	1946.20	117.31	2.88
1252 10-2	RCC1252	10	2	2250.00	2108.00	7.99	20.52	461.35	1977.49	108.65	2.67
1252 10-3	RCC1252	10	3	2256.50	2094.25	8.04	18.03	405.52	1954.03	120.51	2.96
1252 15-1	RCC1252	15	1	2284.00	2072.00	8.07	14.42	379.84	1901.75	153.44	3.79
1252 15-2	RCC1252	15	2	2180.00	2062.00	7.85	24.29	639.83	1941.32	95.45	2.34
1252 15-3	RCC1252	15	3	2193.00	2060.00	7.89	22.04	580.79	1932.70	104.08	2.56
1252 20-1	RCC1252	20	1	2235.00	2060.25	7.92	18.37	559.48	1908.70	131.44	3.26
1252 20-2	RCC1252	20	2	2201.50	2035.25	7.90	18.86	574.63	1889.33	125.42	3.11
1252 20-3	RCC1252	20	3	2200.00	2034.75	7.90	18.96	577.60	1889.38	124.79	3.09
1252 25-1	RCC1252	25	1	2224.50	2062.00	7.82	20.96	729.12	1913.74	125.81	3.14
1252 25-2	RCC1252	25	2	2238.00	2042.00	7.89	17.31	602.17	1876.50	146.18	3.65
1252 25-3	RCC1252	25	3	2225.50	2051.00	7.85	19.48	677.60	1896.94	132.90	3.32
IAN01 15-1	IAN01	15	1	2201.50	2058.00	7.92	20.65	543.94	1925.77	110.24	2.71
IAN01 15-2	IAN01	15	2	2200.50	2051.00	7.94	19.82	522.10	1916.10	113.65	2.80
IAN01 15-3	IAN01	15	3	2216.00	2082.00	7.89	22.26	586.59	1953.29	105.27	2.59
IAN01 20-1	IAN01	20	1	2244.33	2105.25	7.83	23.24	707.88	1969.89	110.95	2.74
IAN01 20-2	IAN01	20	2	2279.50	2112.50	7.90	19.94	607.37	1962.82	128.15	3.17
IAN01 20-3	IAN01	20	3	2224.50	2101.50	7.79	25.56	778.51	1973.61	101.40	2.50
IAN01 25-1	IAN01	25	1	2244.50	2067.00	7.85	19.41	675.37	1910.61	135.27	3.38
IAN01 25-2	IAN01	25	2	2242.50	2069.00	7.84	19.86	690.85	1914.66	132.83	3.32
IAN01 25-3	IAN01	25	3	2241.50	2062.00	7.86	19.14	665.72	1904.75	136.37	3.41

Table A.3: Cellular TPC, PIC, POC, calcite, and TPN content and production, and PIC : POC and POC : TPN ratios, of each replicate.

ID	TPC [pg cell^{-1}]	PIC [pg cell^{-1}]	POC [pg cell^{-1}]	Calcite [pg cell^{-1}]	TPN [pg cell^{-1}]	PIC : POC	POC : TPN	P_{TPC} [pg cell^{-1} day^{-1}]	P_{PIC} [pg cell^{-1} day^{-1}]	P_{POC} [pg cell^{-1} day^{-1}]	$P_{Calcite}$ [pg cell^{-1} day^{-1}]	P_{TPN} [pg cell^{-1} day^{-1}]
1710 10-1	26.338				1.624			6.734				0.415
1710 10-2	24.319	15.201	9.118	126.669	1.520	1.667	6.000	6.335	3.960	2.375	32.997	0.396
1710 10-3	24.116	15.410	8.706	128.417	1.490	1.770	5.841	6.256	3.998	2.258	33.315	0.387
1710 15-1	23.607	13.787	9.820	114.890	1.472	1.404	6.672	17.564	10.258	7.306	85.478	1.095
1710 15-2	24.238				1.462			18.411				1.110
1710 15-3	24.322	14.351	9.971	119.587	1.463	1.439	6.815	18.379	10.844	7.535	90.366	1.106
1710 20-1					1.653							1.933
1710 20-2	22.894	11.401	11.493	95.009	1.717	0.992	6.695	26.636	13.265	13.372	110.537	1.997
1710 20-3	24.136	11.532	12.604	96.101	1.765	0.915	7.142	27.306	13.047	14.259	108.724	1.996
1710 25-1	19.440	10.992	8.448	91.595	1.338	1.301	6.314	23.949	13.541	10.408	112.842	1.648
1710 25-2	20.278	10.874	9.404	90.617	1.418	1.156	6.631	25.220	13.524	11.696	112.700	1.764
1710 25-3	20.573	10.534	10.039	87.778	1.384	1.049	7.256	25.299	12.953	12.346	107.941	1.701
1252 10-1	14.431	8.181	6.249	68.176	1.125	1.309	5.557	4.045	2.293	1.752	19.111	0.315
1252 10-2	14.194	7.869	6.325	65.571	1.163	1.244	5.440	3.076	1.705	1.371	14.211	0.252
1252 10-3	15.295	8.824	6.470	73.535	1.191	1.364	5.433	4.236	2.444	1.792	20.366	0.330
1252 15-1	18.581	10.191	8.390	84.920	1.341	1.215	6.257	13.445	7.374	6.071	61.447	0.970
1252 15-2	18.522	9.565	8.957	79.709	1.358	1.068	6.596	13.475	6.959	6.516	57.991	0.988
1252 15-3	18.595	10.017	8.578	83.474	1.306	1.168	6.566	13.625	7.340	6.285	61.164	0.957
1252 20-1	16.529		8.669		1.277		6.787	16.584		8.698		1.282
1252 20-2	17.779	9.692	8.088	80.761	1.392	1.198	5.811	22.985	12.529	10.456	104.408	1.799
1252 20-3	19.579	10.083	9.497	84.021	1.395	1.062	6.810	22.305	11.486	10.818	95.716	1.589
1252 25-1	22.134	12.277	9.857	102.307	1.412	1.246	6.980	26.635	14.774	11.861	123.110	1.699
1252 25-2	22.013	12.354	9.659	102.945	1.396	1.279	6.922	27.191	15.259	11.931	127.158	1.724
1252 25-3	23.006	11.963	11.043	99.689	1.428	1.083	7.736	27.886	14.500	13.385	120.834	1.730
IAN01 15-1	20.494	10.364	10.130	86.365	1.512	1.023	6.701	16.501	8.344	8.156	69.536	1.217
IAN01 15-2	20.471	10.330	10.141	86.085	1.515	1.019	6.693	16.399	8.275	8.124	68.961	1.214
IAN01 15-3	19.228	9.835	9.393	81.957	1.376	1.047	6.827	15.615	7.987	7.628	66.557	1.117
IAN01 20-1	17.220	8.124	9.096	67.699	1.749	0.893	5.201	20.109	9.487	10.622	79.054	2.042
IAN01 20-2	16.375	7.911	8.463	65.927	1.660	0.935	5.099	19.057	9.207	9.850	76.725	1.932
IAN01 20-3	17.602	8.324	9.279	69.363	1.846	0.897	5.025	20.504	9.696	10.808	80.795	2.151
IAN01 25-1	21.009	10.945	10.065	91.202	1.465	1.087	6.872	27.416	14.282	13.134	119.015	1.911
IAN01 25-2	20.921	11.057	9.863	92.143	1.454	1.121	6.783	28.434	15.029	13.406	125.237	1.976
IAN01 25-3	21.533	11.622	9.911	96.850	1.475	1.173	6.717	28.193	15.217	12.976	126.805	1.932

Table A.4: Coccoliths morphology and mass of each replicate.

ID	Growth rate (μ)	Tube width [μm]	Coccolith length [μm]	Coccolith mass [pg]	Malformed [%]	Incomplete [%]
1710 10-1	0.256	0.18	2.03	0.86	30.89	3.25
1710 10-2	0.260	0.18	2.08	1.04	33.96	1.89
1710 10-3	0.259	0.22	1.97	1.07	34.69	2.04
1710 15-1	0.744	0.23	2.09	1.38	33.23	2.42
1710 15-2	0.760	0.19	2.13	1.65	30.00	0.00
1710 15-3	0.756	0.24	2.15	1.87	24.35	4.72
1710 20-1	1.169	0.24	2.01	1.64	39.56	7.26
1710 20-2	1.163	0.28	2.06	1.78	33.55	4.92
1710 20-3	1.131	0.27	2.09	1.81	27.87	13.64
1710 25-1	1.232	0.26			46.13	15.67
1710 25-2	1.244	0.27	2.19	2.59	36.67	25.89
1710 25-3	1.230	0.30	2.13	2.36	30.44	18.75
1252 10-1	0.280	0.16	2.05	1.60	55.33	1.33
1252 10-2	0.217	0.24	2.06	1.61	53.49	1.66
1252 10-3	0.277	0.22	2.06	1.61	60.33	0.67
1252 15-1	0.724	0.28	2.17	2.05	2.43	2.49
1252 15-2	0.728	0.29	2.06	1.93	7.52	0.00
1252 15-3	0.733	0.21	2.23	1.93	13.00	1.33
1252 20-1	1.003	0.31	2.29	2.65	6.38	12.77
1252 20-2	1.293	0.28	2.28	2.67	12.00	5.21
1252 20-3	1.139	0.24	2.24	2.14	11.88	3.30
1252 25-1	1.203	0.27	2.27	2.91	4.85	10.68
1252 25-2	1.235	0.30	2.33	2.88	11.21	2.33
1252 25-3	1.212	0.25	2.31	3.21	11.21	2.24
IAN01 15-1	0.805	0.22	2.22	2.17	48.68	2.43
IAN01 15-2	0.801	0.25	2.09	2.07	46.00	2.00
IAN01 15-3	0.812	0.20	2.14	1.81	61.72	3.30
IAN01 20-1	1.168	0.22	2.24	2.63	47.68	3.97
IAN01 20-2	1.164	0.28	2.24	2.63	49.67	1.00
IAN01 20-3	1.165	0.24	2.25	2.64	43.91	4.17
IAN01 25-1	1.305	0.26	2.28	2.93	42.52	9.97
IAN01 25-2	1.359	0.29	2.25	2.66	44.34	11.32
IAN01 25-3	1.309	0.26	2.24	2.39	36.67	5.56

Table A.5: Coccolith production time of each replicate. Lith: coccolith, d: day, h: hour, min: minutes.

ID	pgPIC · lith^{-1}	Lith · cell^{-1}	Lith · cell^{-1} · d^{-1}	Lith · cell^{-1} · h^{-1}	Min · lith^{-1}	pgPIC · h^{-1}
1710 10-1	0.104					
1710 10-2	0.125	121.86	31.74	1.98	30.24	0.25
1710 10-3	0.129	119.65	31.04	1.94	30.93	0.25
1710 15-1	0.165	83.41	62.06	3.88	15.47	0.64
1710 15-2	0.198					
1710 15-3	0.225	63.88	48.27	3.02	19.89	0.68
1710 20-1	0.197					
1710 20-2	0.214	53.31	62.03	3.88	15.48	0.83
1710 20-3	0.218	52.97	59.92	3.75	16.02	0.82
1710 25-1						
1710 25-2	0.311	35.00	43.53	2.72	22.06	0.85
1710 25-3	0.283	37.16	45.69	2.86	21.01	0.81
1252 10-1	0.192	42.50	11.91	0.74	80.58	0.14
1252 10-2	0.193	40.69	8.82	0.55	108.87	0.11
1252 10-3	0.194	45.58	12.62	0.79	76.05	0.15
1252 15-1	0.245	41.51	30.04	1.88	31.96	0.46
1252 15-2	0.232	41.20	29.98	1.87	32.02	0.43
1252 15-3	0.232	43.24	31.68	1.98	30.30	0.46
1252 20-1	0.318					
1252 20-2	0.320	30.28	39.14	2.45	24.53	0.78
1252 20-3	0.257	39.23	44.70	2.79	21.48	0.72
1252 25-1	0.350	35.10	42.24	2.64	22.73	0.92
1252 25-2	0.346	35.73	44.14	2.76	21.75	0.95
1252 25-3	0.385	31.10	37.70	2.36	25.46	0.91
IAN01 15-1	0.260	39.82	32.06	2.00	29.94	0.52
IAN01 15-2	0.248	41.62	33.34	2.08	28.79	0.52
IAN01 15-3	0.217	45.30	36.79	2.30	26.09	0.50
IAN01 20-1	0.316	25.74	30.05	1.88	31.94	0.59
IAN01 20-2	0.316	25.02	29.12	1.82	32.97	0.58
IAN01 20-3	0.316	26.30	30.63	1.91	31.34	0.61
IAN01 25-1	0.352	31.11	40.60	2.54	23.65	0.89
IAN01 25-2	0.319	34.68	47.13	2.95	20.37	0.94
IAN01 25-3	0.286	40.59	53.14	3.32	18.07	0.95

Appendix B

Supplementary material for Chapter 3

B.1 Supplementary tables for Chapter 3

Table B.1: Correlation matrix including all the biotic variables analysed in this chapter and in Chapter 2 (published by Rosas-Navarro et al. (2016)). Note that even the variables without significant differences between the temperature treatments were included. Ind: individual; vel: velocity; Sph: coccosphere; th: theoretical; P: production; lith: coccolith.

	μ	TPC	PIC	POC	PIC : POC	TPN	POC:TPN	P_TPC	P_PIC
μ									
TPC	0.058								
PIC	-0.210	0.925							
POC	0.586	0.719	0.409						
PIC : POC	-0.698	0.411	0.718	-0.333					
TPN	0.358	0.441	0.183	0.670	-0.320				
POC:TPN	0.459	0.567	0.421	0.679	-0.091	-0.076			
P_TPC	0.956	0.299	0.016	0.752	-0.579	0.394	0.634		
P_PIC	0.932	0.345	0.101	0.724	-0.478	0.310	0.691	0.989	
P_POC	0.967	0.219	-0.091	0.747	-0.680	0.452	0.558	0.988	0.955
P_TPN	0.968	0.094	-0.214	0.655	-0.744	0.556	0.341	0.933	0.882
Malformed	-0.242	-0.254	-0.280	-0.202	-0.097	0.136	-0.467	-0.268	-0.336
Incomplete	0.625	0.108	-0.019	0.328	-0.263	0.043	0.396	0.623	0.627
Tube_width	0.897	-0.057	-0.255	0.414	-0.605	0.073	0.501	0.839	0.834
Attached_liths	0.807	0.149	0.009	0.421	-0.333	-0.015	0.600	0.834	0.867
Cell_diameter	-0.109	0.674	0.653	0.432	0.349	0.126	0.445	0.119	0.173
Coccolith_length	0.730	-0.220	-0.294	0.092	-0.444	-0.019	0.223	0.603	0.626
Coccolith_mass	0.845	-0.283	-0.435	0.174	-0.633	0.017	0.266	0.728	0.722
Cell_mass	-0.111	0.668	0.649	0.429	0.345	0.129	0.437	0.116	0.171
Cell_volume	-0.111	0.668	0.649	0.429	0.345	0.129	0.437	0.115	0.171
Sph_mass	0.860	-0.132	-0.274	0.251	-0.519	-0.018	0.403	0.789	0.802
Sph_volume	0.860	-0.132	-0.274	0.251	-0.519	-0.018	0.404	0.789	0.802
Ind's_density	0.703	-0.490	-0.649	0.011	-0.728	0.221	-0.160	0.504	0.449
Sph_diameter	0.142	0.624	0.577	0.507	0.242	0.020	0.624	0.342	0.394
Ind's_sinking_vel	0.886	-0.130	-0.289	0.265	-0.543	0.083	0.324	0.804	0.804
Ind's_mass	0.551	0.358	0.283	0.437	-0.057	-0.137	0.741	0.665	0.731
Total_liths_th	-0.656	0.646	0.813	0.029	0.843	0.139	-0.079	-0.497	-0.449
Detached_liths_th	-0.691	0.609	0.780	-0.004	0.835	0.134	-0.121	-0.540	-0.497
Loose_PICcell	-0.626	0.709	0.843	0.138	0.788	0.124	0.073	-0.432	-0.379
PICgeom	0.858	-0.146	-0.287	0.241	-0.525	-0.014	0.386	0.784	0.795
POCgeom	-0.111	0.669	0.651	0.429	0.346	0.129	0.438	0.116	0.171
PICgeom:POC geom	0.819	-0.343	-0.464	0.089	-0.592	-0.013	0.179	0.672	0.664
PICgeom:POCchem	0.674	-0.453	-0.492	-0.123	-0.461	-0.241	0.114	0.527	0.542
P_lith_cell	0.611	0.695	0.473	0.882	-0.193	0.476	0.712	0.768	0.786

	P_POC	P_TPN	Malformed	Incomplete	Tube_width	Attached_liths	Cell_diameter	Coccolith_length	Coccolith_mass
μ									
TPC									
PIC									
POC									
PIC : POC									
TPN									
POC:TPN									
P_TPC									
P_PIC									
P_POC									
P_TPN	0.966								
Malformed	-0.212	-0.130							
Incomplete	0.607	0.546	0.024						
Tube_width	0.844	0.805	-0.513	0.629					
Attached_liths	0.786	0.699	-0.495	0.692	0.889				
Cell_diameter	0.033	-0.086	-0.334	-0.028	-0.088	0.188			
Coccolith_length	0.587	0.627	-0.382	0.184	0.694	0.603	-0.373		
Coccolith_mass	0.730	0.759	-0.243	0.406	0.805	0.742	-0.343	0.927	
Cell_mass	0.030	-0.086	-0.317	-0.046	-0.105	0.168	0.998	-0.368	-0.348
Cell_volume	0.030	-0.086	-0.317	-0.046	-0.105	0.168	0.998	-0.368	-0.348
Sph_mass	0.768	0.753	-0.355	0.517	0.862	0.872	-0.191	0.882	0.971
Sph_volume	0.768	0.753	-0.355	0.518	0.862	0.872	-0.192	0.882	0.971
Ind's_density	0.558	0.700	0.161	0.285	0.540	0.365	-0.592	0.770	0.846
Sph_diameter	0.277	0.101	-0.315	0.513	0.219	0.471	0.674	-0.289	-0.173
Ind's_sinking_vel	0.792	0.803	-0.233	0.562	0.838	0.834	-0.261	0.870	0.969
Ind's_mass	0.584	0.430	-0.689	0.428	0.693	0.891	0.449	0.449	0.513
Total_liths_th	-0.551	-0.597	0.000	-0.290	-0.663	-0.492	0.432	-0.667	-0.826
Detached_liths_th	-0.589	-0.626	0.036	-0.331	-0.703	-0.548	0.399	-0.687	-0.850
Loose_PICcell	-0.495	-0.573	-0.009	-0.308	-0.653	-0.482	0.551	-0.688	-0.842
PICgeom	0.765	0.754	-0.344	0.512	0.858	0.866	-0.201	0.884	0.974
POCgeom	0.030	-0.086	-0.318	-0.044	-0.104	0.169	0.998	-0.369	-0.349
PICgeom:POC geom	0.685	0.726	-0.207	0.451	0.799	0.695	-0.503	0.922	0.972
PICgeom:POCchem	0.519	0.552	-0.286	0.381	0.741	0.722	-0.384	0.874	0.935
P_lith_cell	0.728	0.623	-0.311	0.467	0.491	0.543	0.542	0.122	0.165

	Cell_mass	Cell_volume	Sph_mass	Sph_volume	Ind's_density	Sph_diameter	Ind's_sinking_vel	Ind's_mass	Total_liths_th
μ									
TPC									
PIC									
POC									
PIC : POC									
TPN									
POC:TPN									
P_TPC									
P_PIC									
P_POC									
P_TPN									
Malformed									
Incomplete									
Tube_width									
Attached_liths									
Cell_diameter									
Coccolith_length									
Coccolith_mass									
Cell_mass									
Cell_volume	1.000								
Sph_mass	-0.204	-0.204							
Sph_volume	-0.204	-0.204	1.000						
Ind's_density	-0.585	-0.586	0.716	0.716					
Sph_diameter	0.662	0.662	0.037	0.037	-0.519				
Ind's_sinking_vel	-0.273	-0.273	0.984	0.984	0.787	-0.024			
Ind's_mass	0.428	0.428	0.686	0.686	0.002	0.631	0.589		
Total_liths_th	0.429	0.429	-0.731	-0.731	-0.805	0.311	-0.718	-0.230	
Detached_liths_th	0.398	0.398	-0.768	-0.768	-0.801	0.264	-0.753	-0.287	0.998
Loose_PICcell	0.556	0.556	-0.747	-0.747	-0.852	0.377	-0.751	-0.185	0.969
PICgeom	-0.213	-0.213	1.000	1.000	0.727	0.024	0.985	0.676	-0.738
POCgeom	1.000	1.000	-0.203	-0.203	-0.587	0.664	-0.272	0.430	0.430
PICgeom:POC geom	-0.508	-0.508	0.938	0.938	0.853	-0.214	0.952	0.430	-0.791
PICgeom:POCchem	-0.393	-0.393	0.924	0.924	0.752	-0.173	0.902	0.516	-0.795
P_lith_cell	0.552	0.552	0.278	0.278	-0.056	0.664	0.276	0.549	0.044

	Detached_liths_th	Loose_PICcell	PICgeom	POCgeom	PICgeom:POCgeom	PICgeom:POCchem
μ						
TPC						
PIC						
POC						
PIC : POC						
TPN						
POC:TPN						
P_TPC						
P_PIC						
P_POC						
P_TPN						
Malformed						
Incomplete						
Tube_width						
Attached_liths						
Cell_diameter						
Coccolith_length						
Coccolith_mass						
Cell_mass						
Cell_volume						
Sph_mass						
Sph_volume						
Ind's_density						
Sph_diameter						
Ind's_sinking_vel						
Ind's_mass						
Total_liths_th						
Detached_liths_th						
Loose_PICcell	0.967					
PICgeom	-0.774	-0.756				
POCgeom	0.399	0.557	-0.213			
PICgeom:POCgeom	-0.812	-0.841	0.941	-0.508		
PICgeom:POCchem	-0.818	-0.853	0.929	-0.393	0.937	
P_lith_cell	0.001	0.172	0.267	0.551	0.101	-0.048

Table B.2: Protoplast and coccosphere diameter, number of attached and detached coccoliths per cell, PIC per coccolith, and loose PIC per cell, of each replicate. Sph: coccosphere.

Strain	T [°C]	Protoplast diameter [μm]	Sph diameter [μm]	Attached coccoliths sph^{-1}	Detached coccoliths cell^{-1}	PIC/coccolith [pg]	Loose PIC/cell [pg]
RCC1710	10	4.81	6.50	16.11		0.10	
RCC1710	10	4.80	6.26	15.98	105.88	0.12	13.21
RCC1710	10	4.79	6.55	17.78	101.87	0.13	13.12
RCC1710	15	5.08	7.08	18.83	64.59	0.17	10.68
RCC1710	15	5.42	6.66	17.82		0.20	
RCC1710	15	5.24	6.98	19.78	44.11	0.22	9.91
RCC1710	20	4.98	6.69	20.21		0.20	
RCC1710	20	4.99	7.02	19.92	33.39	0.21	7.14
RCC1711	20	5.00	7.22	20.39	32.58	0.22	7.09
RCC1710	25	4.72	6.96	21.84			
RCC1710	25	4.76	6.87	22.10	12.90	0.31	4.01
RCC1710	25	4.85	7.02	22.48	14.68	0.28	4.16
RCC1252	10	4.61	6.67	18.18	24.33	0.19	4.68
RCC1252	10	4.56	5.89	16.48	24.21	0.19	4.68
RCC1252	10	4.65	6.25	16.74	28.84	0.19	5.58
RCC1252	15	4.89	6.77	18.61	22.90	0.25	5.62
RCC1252	15	4.84	6.87	18.90	22.31	0.23	5.18
RCC1252	15	4.84	6.59	19.54	23.70	0.23	5.49
RCC1252	20	4.45	7.03	20.37		0.32	
RCC1252	20	4.47	6.80	20.85	9.43	0.32	3.02
RCC1252	20	4.49	6.64	19.39	19.84	0.26	5.10
RCC1252	25	4.88	7.46	22.93	12.17	0.35	4.26
RCC1252	25	4.89	7.60	21.82	13.91	0.35	4.81
RCC1252	25	4.89	7.49	23.04	8.06	0.38	3.10
IAN01	15	4.54	6.29	17.01	22.81	0.26	5.94
IAN01	15	4.58	5.94	16.97	24.65	0.25	6.12
IAN01	15	4.48	5.97	16.44	28.87	0.22	6.27
IAN01	20	4.51	6.04	18.21	7.52	0.32	2.37
IAN01	20	4.50	5.91	18.61	6.41	0.32	2.03
IAN01	20	4.51	5.82	18.83	7.47	0.32	2.36
IAN01	25	4.52	7.10	20.64	10.47	0.35	3.68
IAN01	25	4.59	6.51	20.69	13.98	0.32	4.46
IAN01	25	4.63	6.37	20.81	19.78	0.29	5.66

Table B.3: *Emiliania huxleyi* estimated individual density and estimated individual sinking velocity. Calculated masses and volumes involved in the estimations are shown. Standard deviation of the triplicates are shown in parentheses. Cell: protoplast; Sph: coccosphere; SW: extracellular matrix seawater.

Strain	T [°C]	Cell mass [pg]	Cell volume [μm^3]	Sph. calcite mass [pg]	Sph. calcite volume [μm^3]	SW mass [pg]	SW volume [μm^3]	Individual mass [pg]	Individual volume [μm^3]	Individual density [$g \cdot cm^{-3}$]	Individual sinking velocity [$m \cdot d^{-1}$]
RCC1710	10	61.07	58.16	13.90	5.15	82.25	80.27	157.22	143.58	1.09	0.10
RCC1710	10	60.69	57.80	16.61	6.15	66.01	64.42	143.30	128.37	1.12	0.12
RCC1710	10	60.50	57.62	19.08	7.07	84.68	82.65	164.26	147.33	1.11	0.13
RCC1710	15	71.95	68.52	25.93	9.60	110.47	107.92	208.35	186.04	1.12	0.19
RCC1710	15	87.34	83.18	29.34	10.87	62.26	60.82	178.94	154.87	1.16	0.23
RCC1710	15	79.15	75.38	37.02	13.71	90.84	88.74	207.01	177.83	1.16	0.27
RCC1710	20	67.90	64.67	33.20	12.29	81.84	80.04	182.93	157.00	1.17	0.28
RCC1710	20	68.35	65.10	35.50	13.15	105.11	102.80	208.96	181.04	1.15	0.29
RCC1711	20	68.89	65.61	36.99	13.70	120.15	117.51	226.03	196.82	1.15	0.29
RCC1710	25	57.81	55.06						176.22		
RCC1710	25	59.29	56.47	57.21	21.19	94.26	92.31	210.76	169.97	1.24	0.51
RCC1710	25	62.57	59.59	53.09	19.66	104.00	101.85	219.66	181.10	1.21	0.47
RCC1252	10	53.69	51.13	29.15	10.80	95.98	93.67	178.82	155.60	1.15	0.19
RCC1252	10	52.06	49.58	26.56	9.84	48.61	47.44	127.23	106.86	1.19	0.20
RCC1252	10	55.21	52.58	27.01	10.00	66.96	65.35	149.17	127.93	1.17	0.19
RCC1252	15	64.36	61.30	38.07	14.10	89.13	87.07	191.57	162.47	1.18	0.28
RCC1252	15	62.41	59.44	36.56	13.54	99.33	97.04	198.30	170.01	1.17	0.26
RCC1252	15	62.18	59.22	37.72	13.97	78.75	76.93	178.65	150.12	1.19	0.28
RCC1252	20	48.35	46.05	54.01	20.00	118.08	115.48	220.43	181.53	1.21	0.42
RCC1252	20	49.04	46.70	55.61	20.60	99.29	97.11	203.94	164.41	1.24	0.44
RCC1252	20	49.70	47.33	41.53	15.38	92.92	90.88	184.16	153.60	1.20	0.34
RCC1252	25	63.97	60.92	66.82	24.75	134.45	131.67	265.24	217.35	1.22	0.55
RCC1252	25	64.25	61.19	62.87	23.29	148.24	145.18	275.36	229.65	1.20	0.51
RCC1252	25	64.09	61.04	73.85	27.35	133.98	131.21	271.92	219.60	1.24	0.60
IAN01	15	51.34	48.90	36.89	13.66	69.16	67.56	157.39	130.12	1.21	0.29
IAN01	15	52.65	50.14	35.10	13.00	47.46	46.36	135.20	109.50	1.23	0.29
IAN01	15	49.57	47.21	29.74	11.01	54.68	53.42	133.98	111.64	1.20	0.24
IAN01	20	50.50	48.10	47.91	17.74	50.88	49.76	149.29	115.60	1.29	0.43
IAN01	20	49.97	47.59	49.05	18.17	43.52	42.57	142.54	108.32	1.32	0.45
IAN01	20	50.43	48.03	49.66	18.39	37.40	36.58	137.49	103.00	1.33	0.46
IAN01	25	50.87	48.45	60.50	22.41	118.71	116.26	230.08	187.11	1.23	0.52
IAN01	25	53.27	50.73	54.99	20.37	75.16	73.61	183.42	144.71	1.27	0.52
IAN01	25	54.60	52.00	49.66	18.39	66.25	64.89	170.51	135.28	1.26	0.48

Table B.4: Chemically (chem) and geometrically (geom) derived PIC and POC. The chemical PIC corresponds to the bulk PIC, that is the PIC in the attached and in the detached coccoliths, while the geometrical PIC corresponds to the individual cell PIC. Standard deviation of the triplicates is shown in parentheses. Sph: coccosphere.

Strain	T [°C]	PIC (chem) [pg cell^{-1}]	PIC (geom) [pg sph^{-1}]	POC (chem) [pg cell^{-1}]	POC (geom) [pg cell^{-1}]	PIC : POC ratio (chem : chem)	PIC : POC ratio (geom : geom)	PIC : POC ratio (geom : chem)	POC ratio (chem : geom)
RCC1710	10		1.67		9.80		0.17		
RCC1710	10	15.20	1.99	9.12	9.75	1.67	0.20	0.22	0.94
RCC1710	10	15.41	2.29	8.71	9.72	1.77	0.24	0.26	0.90
RCC1710	15	13.79	3.11	9.82	11.44	1.40	0.27	0.32	0.86
RCC1710	15		3.52		13.72		0.26		
RCC1710	15	14.35	4.44	9.97	12.51	1.44	0.36	0.45	0.80
RCC1710	20		3.98		10.83		0.37		
RCC1710	20	11.40	4.26	11.49	10.90	0.99	0.39	0.37	1.05
RCC1711	20	11.53	4.44	12.60	10.98	0.92	0.40	0.35	1.15
RCC1710	25	10.99		8.45	9.31	1.30			0.91
RCC1710	25	10.87	6.87	9.40	9.54	1.16	0.72	0.73	0.99
RCC1710	25	10.53	6.37	10.04	10.03	1.05	0.64	0.63	1.00
RCC1252	10	8.18	3.50	6.25	8.69	1.31	0.40	0.56	0.72
RCC1252	10	7.87	3.19	6.33	8.44	1.24	0.38	0.50	0.75
RCC1252	10	8.82	3.24	6.47	8.92	1.36	0.36	0.50	0.73
RCC1252	15	10.19	4.57	8.39	10.30	1.21	0.44	0.54	0.81
RCC1252	15	9.57	4.39	8.96	10.01	1.07	0.44	0.49	0.90
RCC1252	15	10.02	4.53	8.58	9.97	1.17	0.45	0.53	0.86
RCC1252	20		6.48	8.67	7.87		0.82	0.75	1.10
RCC1252	20	9.69	6.67	8.09	7.98	1.20	0.84	0.83	1.01
RCC1252	20	10.08	4.98	9.50	8.08	1.06	0.62	0.52	1.18
RCC1252	25	12.28	8.02	9.86	10.24	1.25	0.78	0.81	0.96
RCC1252	25	12.35	7.54	9.66	10.28	1.28	0.73	0.78	0.94
RCC1252	25	11.96	8.86	11.04	10.26	1.08	0.86	0.80	1.08
IAN01	15	10.36	4.43	10.13	8.33	1.02	0.53	0.44	1.22
IAN01	15	10.33	4.21	10.14	8.53	1.02	0.49	0.42	1.19
IAN01	15	9.84	3.57	9.39	8.06	1.05	0.44	0.38	1.17
IAN01	20	8.12	5.75	9.10	8.20	0.89	0.70	0.63	1.11
IAN01	20	7.91	5.89	8.46	8.12	0.93	0.72	0.70	1.04
IAN01	20	8.32	5.96	9.28	8.19	0.90	0.73	0.64	1.13
IAN01	25	10.94	7.26	10.06	8.26	1.09	0.88	0.72	1.22
IAN01	25	11.06	6.60	9.86	8.62	1.12	0.77	0.67	1.14
IAN01	25	11.62	5.96	9.91	8.83	1.17	0.68	0.60	1.12

B.2 Supplementary calculations for Chapter 3

Individual Sinking Velocity and Error Propagation Calculation

Here we put the formulas used to calculate the individual sinking velocity of the coccospheres and the error propagation. The units and code names used for each variable are defined in Table B.5. From seven variables in the formula, the following four correspond to laboratory measurements: number of observed attached coccoliths, protoplast diameter, coccolith calcite mass and coccosphere diameter. The experiment was performed by triplicate, each variable of each replicate presented an standard error (standard deviation divided by the square root of the sample size) which was used in the error propagation formula. The errors used for water density and dynamic viscosity (both dependent on temperature, salinity and pressure) were based on the maximum errors found for temperature and salinity during the experiment (0.5 °C and 0.5‰ respectively). The error used for the gravitational acceleration constant represents the maximum and minimum values that can be found on Earth.

Table B.5: Variables, units, and code names used in the formulas to calculate the individual sinking velocity of the coccospheres and the error propagation.

Variable	Unit	Symbol	Excel cell with variable value	Excel cell with standard error
Water density	[kg m^{-3}]	ρ	W3	X3
Dynamic viscosity	[kg m^{-1} s^{-1}]	ν	Y3	Z3
Gravitational acceleration	[m s^{-2}]	g	AA3	AB3
Observed attached coccoliths	[number]	N_c	I3	L3
Protoplast diameter	[micrometers]	d_p	F3	H3
Coccolith calcite mass	[picograms]	m_c	S3	V3
Coccosphere diameter	[micrometers]	d_c	O3	R3

Formula (F) for calculating the individual sinking velocity of coccospheres based on Stoke's law (Excel format):

```
F=(2*((PI()*4/3*(F3/2)^3*1.05+S3*I3/0.75+(PI()*4/3*(O3/2)^3
-S3*I3/0.75/2.7-PI()*4/3*(F3/2)^3)*W3/1000)/(PI()*4/3*(O3/2)^3)
-W3/1000)*$AA$3*100*((O3/(10000*2))^2))/(9*Y3*10)/100*86400
```

Simplified formula for calculating the individual sinking velocity of coccospheres (EXCEL format):

```
F=(((PI()*0.175*F3^3+S3*I3/0.75+(PI()/6*O3^3-S3*I3/0.75/2.7
-PI()*F3^3/6)*W3/1000)/PI()*6/O3^3-W3/1000)*$AA$3*100*O3^2
/200000000)*9.6/Y3
```

We can calculate the error of the F according to Courant (Courant, R.: Differential and integral calculus, vol. 2, John Wiley and Sons, 2011, page 66), as:

$$\Delta F = |\partial m_c F|\Delta m_c + |\partial d_c F|\Delta d_c + |\partial d_p F|\Delta d_p + |\partial N_c F|\Delta N_c + |\partial g F|\Delta g + |\partial \nu F|\Delta \nu + |\partial \rho F|\Delta \rho \quad \text{(B.1)}$$

This is valid since F and its first partial derivatives are continuous. The symbols in Eq. (B.1) are defined in Table B.5.

Error propagation formula for each replicate (Excel Format):

```
=Z3*ABS(($AA$3*(F3^3*(0.00000504 -0.0000000048*W3)+I3*S3*
(0.0000122230996294575 - 4.52707393683613E-09*W3)))/ (O3*Y3^2))

+X3*ABS(((-0.0000000048*F3^3 - 4.52707393683613E-09*I3*S3)
*$AA$3)/(O3*Y3))

+$AB$3*ABS((F3^3*(0.00000504 -0.0000000048*W3) +I3*S3*
(0.0000122230996294575 - 4.52707393683613E-09*W3))/(O3*Y3))

+R3*ABS(($AA$3*(F3^3*(0.00000504 - 0.0000000048*W3) + I3*S3*
(0.0000122230996294575 - 4.52707393683613E-09*W3)))/(O3^2*Y3))

+3*H3*ABS((F3^2*$AA$3*(0.00000504 - 0.0000000048*W3))/(O3*Y3))

+V3*ABS((I3*$AA$3*(0.0000122230996294575 - 4.52707393683613E-09*W3))
/(O3*Y3))

+L3*ABS((S3*$AA$3*(0.0000122230996294575 - 4.52707393683613E-09*W3))
/(O3*Y3))
```

The average error propagation was of 0.038 $\pm$0.003 m d^{-1}, which resulted from the different variables in the percentages shown in Table B.6.

The individual sinking velocity calculations for each replicate of the strains RCC1710, RCC1252 and IAN01, with their corresponding error propagation, are shown in Fig. B.1.

The calculated velocities and their error propagation observed in Fig. B.1 show a positive trend with temperature in the three strains.

In the following tables we give the values of each measurement used in the formulas for individual sinking velocity and error propagation. The value used for

Table B.6: Average of the individual sinking velocity error propagation (prop) calculations in percentage resulted from each variable.

Variable	Expression	Average (SD) [%]
Error prop from water density	$\lvert\partial\rho F\rvert\Delta\rho$	1.40 (0.66)
Error prop from dynamic viscosity	$\lvert\partial\nu F\rvert\Delta\nu$	12.68 (2.50)
Error prop from gravitational acceleration	$\lvert\partial g F\rvert\Delta g$	3.33(0.56)
Error prop from observed attached coccoliths	$\lvert\partial N_c F\rvert\Delta N_c$	33.59(4.54)
Error prop from protoplast diameter	$\lvert\partial d_p F\rvert\Delta d_p$	0.20(0.11)
Error prop from coccolith mass	$\lvert\partial m_c F\rvert\Delta m_c$	30.39(7.19)
Error prop from coccosphere diameter	$\lvert\partial d_c F\rvert\Delta d_c$	18.41(2.81)
Total error propagation	ΔF	100

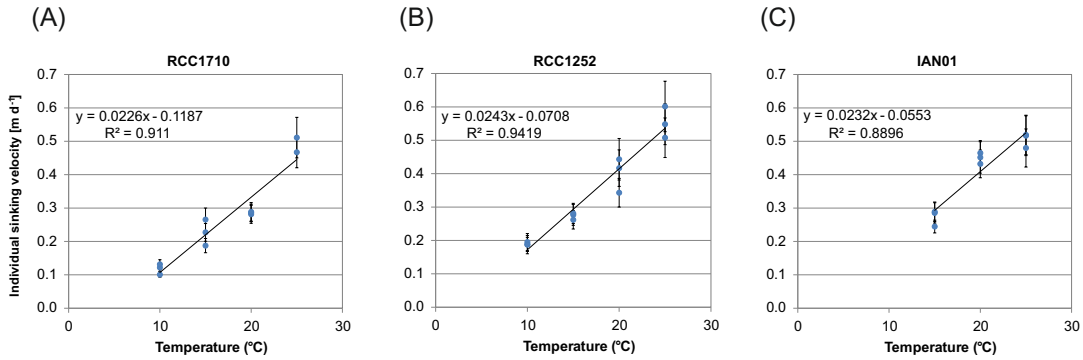

Figure B.1: Individual sinking velocity calculation with the corresponding error propagation, for each replicate of the experiment with different *E. huxleyi* strains. Results are shown for strain RCC1710 (A), strain RCC1252 (B), and strain IAN01 (C), grown at different temperatures. Linear trend lines and r-squared values are shown for the calculated changes in velocity with temperature of each strain.

the gravitational acceleration constant is 9.80665 $\pm$0.035 $\mathrm{m\,s^{-2}}$. In Table B.9 we also give the results of the calculations for individual sinking velocity and error propagation. Table B.10 gives the results of the error propagation from each of the variables, and Table B.11 gives these same results but it percentage.

Table B.7: Constants or values as a function of temperature used for the calculation of sinking velocity and error propagation. Temperature (T).

T [°C]	Water density [$\mathrm{kg\,m^{-3}}$]	Water density error [$\mathrm{kg\,m^{-3}}$]	Dynamic viscosity [$\mathrm{kg\,m^{-1}\,s^{-1}}$]	Dynamic viscosity error [$\mathrm{kg\,m^{-1}\,s^{-1}}$]
10	1024.611	0.472	0.0013881	0.00002110
15	1023.661	0.492	0.0012120	0.00001705
20	1022.476	0.5105	0.0010696	0.0000140
25	1021.078	0.527	0.0009524	0.00001170

Table B.8: Part of the data used for the calculation of sinking velocity and error propagation. The column "Code" gives the strain name, the temperature and the bottle number. Protoplast diameter (prot diam); standard deviation (SD); standard error (SE); observed (obs); attached (att); coccolith (lith); coccosphere (sph); sample size (N).

Code	Prot diam [μm]	SD	SE	Obs att lith sph^{-1}	SD	N	SE	Att lith sph^{-1}
RCC1710 10-1	4.81	1.17	0.01	12.08	3.16	100	0.32	16.11
RCC1710 10-2	4.80	1.17	0.01	11.98	2.89	60	0.37	15.98
RCC1710 10-3	4.79	1.16	0.01	13.33	4.06	60	0.52	17.78
RCC1710 15-1	5.08	1.15	0.01	14.12	4.24	34	0.72	18.83
RCC1710 15-2	5.42	1.17	0.01	13.36	3.74	54	0.51	17.82
RCC1710 15-3	5.24	1.16	0.01	14.83	5.78	54	0.79	19.78
RCC1710 20-1	4.98	1.16	0.01	15.16	4.32	46	0.63	20.21
RCC1710 20-2	4.99	1.15	0.01	14.94	4.07	51	0.57	19.92
RCC1710 20-3	5.00	1.15	0.01	15.29	4.47	48	0.65	20.39
RCC1710 25-1	4.72	1.18	0.01	16.38	4.76	39	0.77	21.84
RCC1710 25-2	4.76	1.16	0.01	16.57	4.00	49	0.57	22.10
RCC1710 25-3	4.85	1.16	0.01	16.86	5.29	49	0.76	22.48
RCC1252 10-1	4.61	1.18	0.01	13.63	3.56	57	0.47	18.18
RCC1252 10-2	4.56	1.19	0.01	12.36	4.03	61	0.52	16.48
RCC1252 10-3	4.65	1.19	0.01	12.56	5.04	61	0.65	16.74
RCC1252 15-1	4.89	1.15	0.01	13.96	4.62	47	0.67	18.61
RCC1252 15-2	4.84	1.15	0.01	14.17	3.33	52	0.46	18.90
RCC1252 15-3	4.84	1.16	0.01	14.65	3.93	52	0.54	19.54
RCC1252 20-1	4.45	1.21	0.01	15.28	5.11	47	0.75	20.37
RCC1252 20-2	4.47	1.18	0.01	15.63	6.22	52	0.86	20.85
RCC1252 20-3	4.49	1.18	0.01	14.55	4.52	55	0.61	19.39
RCC1252 25-1	4.88	1.19	0.01	17.20	5.08	51	0.71	22.93
RCC1252 25-2	4.89	1.19	0.01	16.37	4.39	49	0.63	21.82
RCC1252 25-3	4.89	1.19	0.01	17.28	5.30	49	0.76	23.04
IAN01 15-1	4.54	1.15	0.01	12.76	2.74	62	0.35	17.01
IAN01 15-2	4.58	1.15	0.01	12.73	3.31	55	0.45	16.97
IAN01 15-3	4.48	1.16	0.01	12.33	2.52	55	0.34	16.44
IAN01 20-1	4.51	1.16	0.01	13.66	3.32	53	0.46	18.21
IAN01 20-2	4.50	1.16	0.01	13.96	3.51	51	0.49	18.61
IAN01 20-3	4.51	1.16	0.01	14.12	3.39	58	0.44	18.83
IAN01 25-1	4.52	1.16	0.01	15.48	4.18	48	0.60	20.64
IAN01 25-2	4.59	1.16	0.01	15.52	3.81	50	0.54	20.69
IAN01 25-3	4.63	1.17	0.01	15.61	4.35	51	0.61	20.81

Table B.9: Part of the data used for the calculation of sinking velocity and error propagation and the resulted calculations. The coccolith mass refers to the coccolith calcite mass. The column "Code" gives the strain name, the temperature and the bottle number. Coccosphere (sph); diameter (diam); standard deviation (SD); standard error (SE); coccolith (lith); sample size (N); individual sinking velocity (ind sink vel); propagation (prop).

Code	Sph diam [μm]	SD	N	SE	Lith mass [pg]	SD	N	SE	Ind sink vel [m d^{-1}]	Error prop [m d^{-1}]
RCC1710 10-1	6.50	0.85	90	0.09	0.86	0.37	463	0.02	0.101	0.008
RCC1710 10-2	6.26	1.05	46	0.15	1.04	0.56	661	0.02	0.122	0.011
RCC1710 10-3	6.55	1.10	49	0.16	1.07	0.68	517	0.03	0.131	0.014
RCC1710 15-1	7.08	0.97	77	0.11	1.38	1.02	451	0.05	0.188	0.021
RCC1710 15-2	6.66	1.04	45	0.16	1.65	1.50	435	0.07	0.227	0.026
RCC1710 15-3	6.98	1.12	49	0.16	1.87	1.62	421	0.08	0.265	0.035
RCC1710 20-1	6.69	0.92	62	0.12	1.64	1.05	788	0.04	0.281	0.027
RCC1710 20-2	7.02	0.89	44	0.13	1.78	1.00	827	0.03	0.286	0.026
RCC1710 20-3	7.22	0.92	44	0.14	1.81	1.15	929	0.04	0.289	0.028
RCC1710 25-1	6.96	0.96	45	0.14	N/A	N/A	N/A	N/A	N/A	N/A
RCC1710 25-2	6.87	1.04	48	0.15	2.59	2.29	324	0.13	0.511	0.061
RCC1710 25-3	7.02	1.06	47	0.15	2.36	1.49	1160	0.04	0.467	0.046
RCC1252 10-1	6.67	0.73	38	0.12	1.60	1.35	350	0.07	0.188	0.021
RCC1252 10-2	5.89	0.84	79	0.09	1.61	1.82	358	0.10	0.195	0.026
RCC1252 10-3	6.25	1.11	61	0.14	1.61	1.73	325	0.10	0.187	0.027
RCC1252 15-1	6.77	0.99	39	0.16	2.05	1.01	325	0.06	0.277	0.031
RCC1252 15-2	6.87	0.75	52	0.10	1.93	1.50	322	0.08	0.262	0.028
RCC1252 15-3	6.59	0.84	52	0.12	1.93	1.33	327	0.07	0.281	0.030
RCC1252 20-1	7.03	1.24	48	0.18	2.65	2.20	379	0.11	0.417	0.055
RCC1252 20-2	6.80	1.20	53	0.16	2.67	2.54	406	0.13	0.443	0.062
RCC1252 20-3	6.64	0.96	55	0.13	2.14	2.10	376	0.11	0.343	0.043
RCC1252 25-1	7.46	1.02	48	0.15	2.91	1.94	330	0.11	0.548	0.061
RCC1252 25-2	7.60	1.16	50	0.16	2.88	2.59	430	0.13	0.508	0.059
RCC1252 25-3	7.49	1.19	43	0.18	3.21	2.69	365	0.14	0.601	0.076
IAN01 15-1	6.29	0.90	48	0.13	2.17	1.77	350	0.09	0.285	0.031
IAN01 15-2	5.94	0.78	54	0.11	2.07	1.27	337	0.07	0.289	0.029
IAN01 15-3	5.97	0.64	55	0.09	1.81	0.65	323	0.04	0.245	0.019
IAN01 20-1	6.04	0.72	54	0.10	2.63	1.69	418	0.08	0.432	0.042
IAN01 20-2	5.91	0.86	45	0.13	2.63	1.61	360	0.08	0.452	0.047
IAN01 20-3	5.82	0.71	57	0.09	2.64	0.79	352	0.04	0.465	0.037
IAN01 25-1	7.10	1.02	47	0.15	2.93	2.19	355	0.12	0.519	0.059
IAN01 25-2	6.51	0.99	49	0.14	2.66	2.35	386	0.12	0.517	0.060
IAN01 25-3	6.37	0.90	51	0.13	2.39	2.14	366	0.11	0.480	0.057

Table B.10: Error propagation from each variable. The column "Code" gives the strain name, the temperature and the bottle number.

Code	$\lvert\partial\rho F\rvert\Delta\rho$ $[\mathrm{m\,d^{-1}}]$	$\lvert\partial\nu F\rvert\Delta\nu$ $[\mathrm{m\,d^{-1}}]$	$\lvert\partial g F\rvert\Delta g$ $[\mathrm{m\,d^{-1}}]$	$\lvert\partial N_c F\rvert\Delta N_c$ $[\mathrm{m\,d^{-1}}]$	$\lvert\partial d_p F\rvert\Delta d_p$ $[\mathrm{m\,d^{-1}}]$	$\lvert\partial m_c F\rvert\Delta m_c$ $[\mathrm{m\,d^{-1}}]$	$\lvert\partial d_c F\rvert\Delta d_c$ $[\mathrm{m\,d^{-1}}]$
RCC1710 10-1	0.000	0.002	0.000	0.002	0.000	0.002	0.001
RCC1710 10-2	0.000	0.002	0.000	0.003	0.000	0.002	0.003
RCC1710 10-3	0.000	0.002	0.000	0.005	0.000	0.003	0.003
RCC1710 15-1	0.000	0.003	0.001	0.009	0.000	0.006	0.003
RCC1710 15-2	0.001	0.003	0.001	0.008	0.000	0.009	0.005
RCC1710 15-3	0.000	0.004	0.001	0.013	0.000	0.010	0.006
RCC1710 20-1	0.000	0.004	0.001	0.011	0.000	0.006	0.005
RCC1710 20-2	0.000	0.004	0.001	0.010	0.000	0.005	0.005
RCC1710 20-3	0.000	0.004	0.001	0.011	0.000	0.006	0.006
RCC1710 25-2	0.001	0.006	0.002	0.017	0.000	0.024	0.011
RCC1710 25-3	0.001	0.006	0.002	0.020	0.000	0.008	0.010
RCC1252 10-1	0.000	0.003	0.001	0.006	0.000	0.008	0.003
RCC1252 10-2	0.000	0.003	0.001	0.008	0.000	0.011	0.003
RCC1252 10-3	0.000	0.003	0.001	0.009	0.000	0.010	0.004
RCC1252 15-1	0.000	0.004	0.001	0.013	0.000	0.007	0.006
RCC1252 15-2	0.000	0.004	0.001	0.008	0.000	0.011	0.004
RCC1252 15-3	0.000	0.004	0.001	0.010	0.000	0.010	0.005
RCC1252 20-1	0.000	0.005	0.001	0.020	0.000	0.017	0.011
RCC1252 20-2	0.000	0.006	0.002	0.024	0.000	0.020	0.011
RCC1252 20-3	0.000	0.004	0.001	0.014	0.000	0.016	0.007
RCC1252 25-1	0.001	0.007	0.002	0.022	0.000	0.019	0.011
RCC1252 25-2	0.001	0.006	0.002	0.019	0.000	0.021	0.011
RCC1252 25-3	0.001	0.007	0.002	0.025	0.000	0.025	0.015
IAN01 15-1	0.000	0.004	0.001	0.007	0.000	0.012	0.006
IAN01 15-2	0.000	0.004	0.001	0.010	0.000	0.009	0.005
IAN01 15-3	0.000	0.003	0.001	0.006	0.000	0.005	0.004
IAN01 20-1	0.000	0.006	0.002	0.014	0.000	0.013	0.007
IAN01 20-2	0.000	0.006	0.002	0.015	0.000	0.014	0.010
IAN01 20-3	0.000	0.006	0.002	0.014	0.000	0.007	0.008
IAN01 25-1	0.000	0.006	0.002	0.020	0.000	0.020	0.011
IAN01 25-2	0.001	0.006	0.002	0.017	0.000	0.022	0.011
IAN01 25-3	0.001	0.006	0.002	0.018	0.000	0.021	0.009

Table B.11: Propagation of the error in percentage from each variable. The column "Code" gives the strain name, the temperature and the bottle number.

Code	$\lvert\partial\rho F\rvert\Delta\rho$ [%]	$\lvert\partial\nu F\rvert\Delta\nu$ [%]	$\lvert\partial g F\rvert\Delta g$ [%]	$\lvert\partial N_c F\rvert\Delta N_c$ [%]	$\lvert\partial d_p F\rvert\Delta d_p$ [%]	$\lvert\partial m_c F\rvert\Delta m_c$ [%]	$\lvert\partial d_c F\rvert\Delta d_c$ [%]	Total [%]
RCC1710 10-1	3.92	20.14	4.73	29.57	0.63	22.70	18.32	100
RCC1710 10-2	2.79	16.54	3.88	29.66	0.44	19.89	26.80	100
RCC1710 10-3	2.18	14.46	3.39	33.29	0.34	23.44	22.90	100
RCC1710 15-1	1.89	12.41	3.15	40.71	0.27	27.80	13.77	100
RCC1710 15-2	1.95	12.07	3.06	29.20	0.27	33.40	20.05	100
RCC1710 15-3	1.35	10.80	2.74	37.50	0.18	29.76	17.67	100
RCC1710 20-1	1.83	13.68	3.73	40.29	0.26	21.87	18.33	100
RCC1710 20-2	1.84	14.40	3.93	38.81	0.26	19.82	20.95	100
RCC1710 20-3	1.70	13.62	3.71	40.73	0.23	20.10	19.90	100
RCC1710 25-2	0.93	10.34	3.01	27.76	0.12	39.53	18.31	100
RCC1710 25-3	1.21	12.36	3.59	42.89	0.16	17.67	22.11	100
RCC1252 10-1	1.34	13.52	3.17	28.73	0.21	37.20	15.82	100
RCC1252 10-2	1.21	11.62	2.73	29.62	0.19	42.34	12.28	100
RCC1252 10-3	1.12	10.41	2.44	32.61	0.17	37.73	15.51	100
RCC1252 15-1	1.30	12.41	3.15	39.90	0.18	22.51	20.56	100
RCC1252 15-2	1.40	13.34	3.38	28.90	0.19	38.43	14.36	100
RCC1252 15-3	1.34	13.10	3.32	32.43	0.19	33.18	16.44	100
RCC1252 20-1	0.74	9.96	2.72	35.78	0.10	31.27	19.44	100
RCC1252 20-2	0.68	9.31	2.54	37.80	0.09	32.37	17.21	100
RCC1252 20-3	0.94	10.45	2.85	31.81	0.14	38.34	15.48	100
RCC1252 25-1	0.93	11.01	3.20	35.56	0.12	31.48	17.70	100
RCC1252 25-2	0.93	10.52	3.06	31.36	0.12	35.57	18.43	100
RCC1252 25-3	0.78	9.77	2.84	33.53	0.10	33.65	19.33	100
IAN01 15-1	1.19	13.15	3.34	24.13	0.17	38.61	19.42	100
IAN01 15-2	1.32	13.86	3.52	32.55	0.19	31.00	17.56	100
IAN01 15-3	1.86	17.98	4.56	32.97	0.28	23.98	18.37	100
IAN01 20-1	1.12	13.61	3.71	33.19	0.15	31.35	16.87	100
IAN01 20-2	1.01	12.56	3.43	32.40	0.14	29.60	20.86	100
IAN01 20-3	1.32	16.44	4.48	37.95	0.18	19.23	20.39	100
IAN01 25-1	0.84	10.80	3.14	33.06	0.11	33.63	18.42	100
IAN01 25-2	0.91	10.65	3.09	28.87	0.12	37.47	18.89	100
IAN01 25-3	0.96	10.33	3.00	31.32	0.13	37.64	16.61	100

Appendix C

Supplementary material for Chapters 5 and 6

C.1 Supplementary figures for Chapters 5 and 6

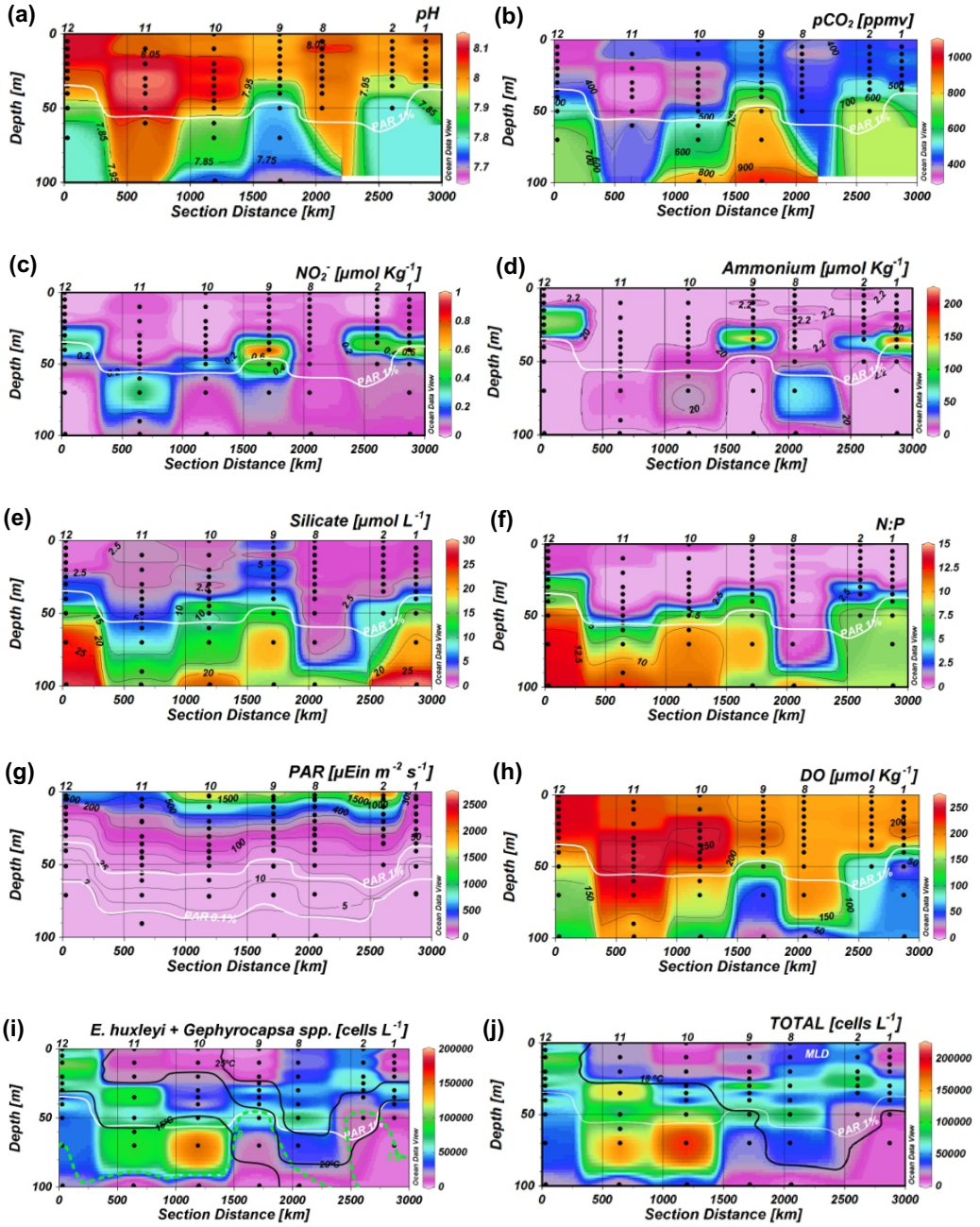

Figure C.1: Vertical profile of different abiotic and biotic variables. pH in total scale (a), pCO_2 (b), nitrite concentration (c), ammonium concentration (d), silicate concentration (e), N:P ratio (N: nitrate plus nitrite; P: phosphate) (f), photosynthetic active radiation (g), dissolved oxygen (h), *E. huxleyi* together with *Gephyrocapsa spp.* cell density (i), and total number of coccolithophores per liter (j).

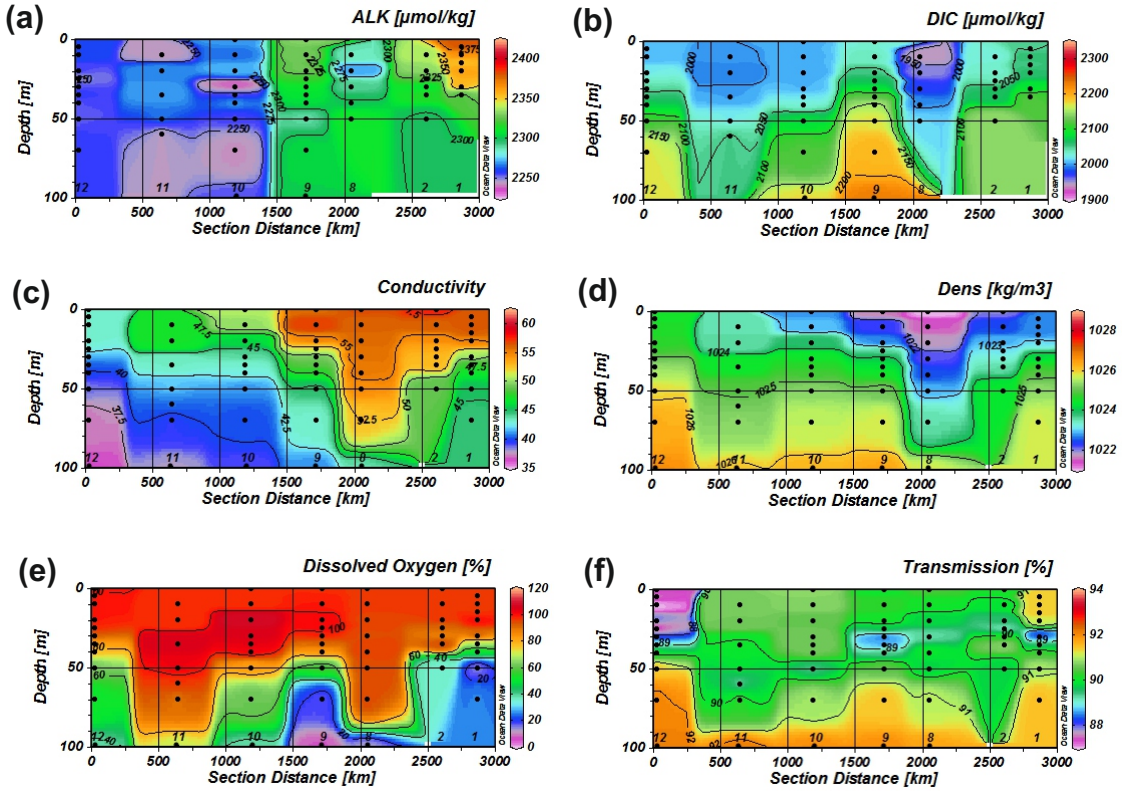

Figure C.2: Vertical profile of different abiotic and biotic variables. total alkalinity (a), dissolved inorganic carbon (b), conductivity (c), water density (d), dissolved oxygen percentage (e), and transmission percentage.

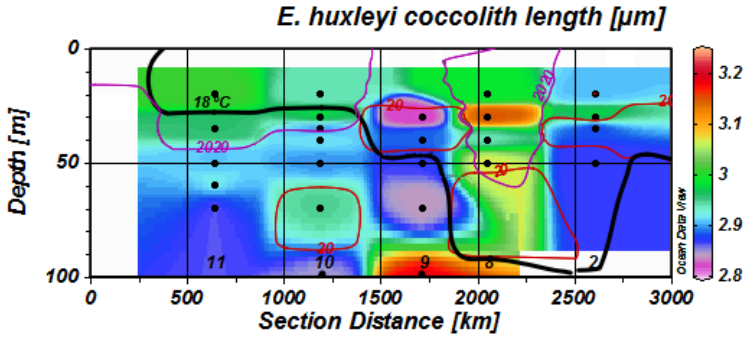

Figure C.3: Vertical profile of the coccolith length of *Emiliania huxleyi*. Measured with the program SYRACO on light microscopy images. Isolines for different environmental variables are shown: temperature (black isoline), ammonium concentration (red isoline, μmol L^{-1}), DIC (purple isoline, μmol kg^{-1}).

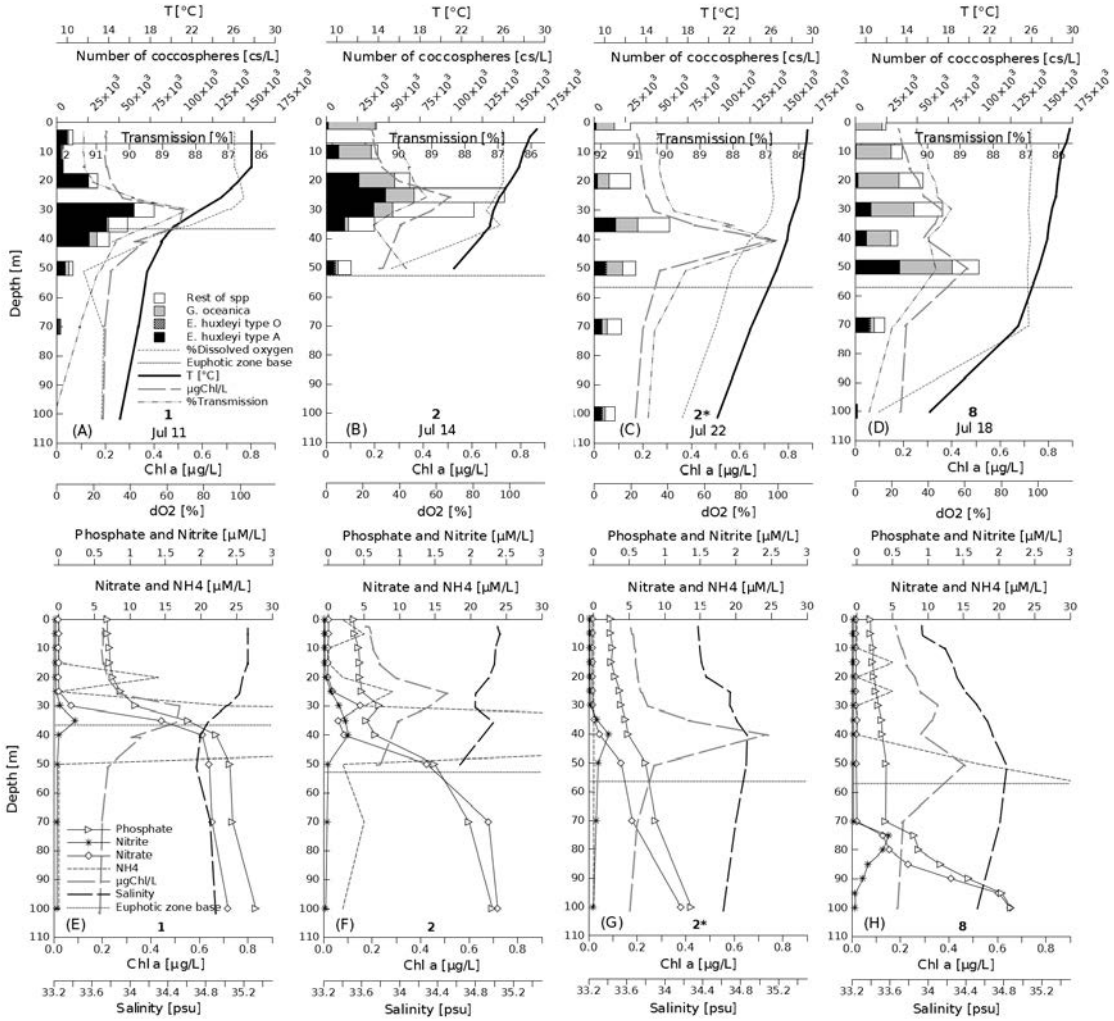

Figure C.4: Profiles of biological and chemical measurements made in the upper 100 m at two stations located in the Gulf of California (stations 1 and 2) and one in the entrance zone (station 8), in summer 2008. Station 2 was sampled twice on different dates, on July 14 (B, F) and July 22 (C, G). Each station is shown in two figures, both show the externally calibrated chlorophyll-*a* fluorescence (long-dash gray line) and the base of the euphotic zone (horizontal dotted line) representing 1% of the surface PAR value, which was calculated using equation 1 with the k_{PAR} coefficient and the surface PAR value for each station (Station 1: 0.108 m^{-1}, 2425 $\mu\mathrm{Ein\,m^{-2}\,s^{-1}}$; Station 2: 0.087 m^{-1}, 2418 $\mu\mathrm{Ein\,m^{-2}\,s^{-1}}$; Station 2*: 0.082 m^{-1}, 2445 $\mu\mathrm{Ein\,m^{-2}\,s^{-1}}$; Station 8: 0.081 m^{-1}, 1674 $\mu\mathrm{Ein\,m^{-2}\,s^{-1}}$). The vertical profiles for each location, in figures E-H, include percentage of dissolved oxygen (dotted line), water temperature (solid black line), transmission percentage (dash-dot line) and the coccolithophores abundance (bars). The coccolithophores bars include the species *E. huxleyi* type A (black bars), *E. huxleyi* type O (left-inclined-dash bars), *G. oceanica* (light-gray bars) and the rest of coccolithophores (white bars). Nutrient measurements (E-H) include phosphate (triangles), nitrite (asterisks), nitrate (diamonds), and ammonium (short-dash line) concentrations. Salinity (long-dash line) is shown in this last group of figures. The figure shows the importance of *E. huxleyi* type A and the species *G. oceanica* in the coccolithophore assemblage of these locations. *G. oceanica* increases its absolute and relative numbers in the stations located in the warmer and lower latitudes.

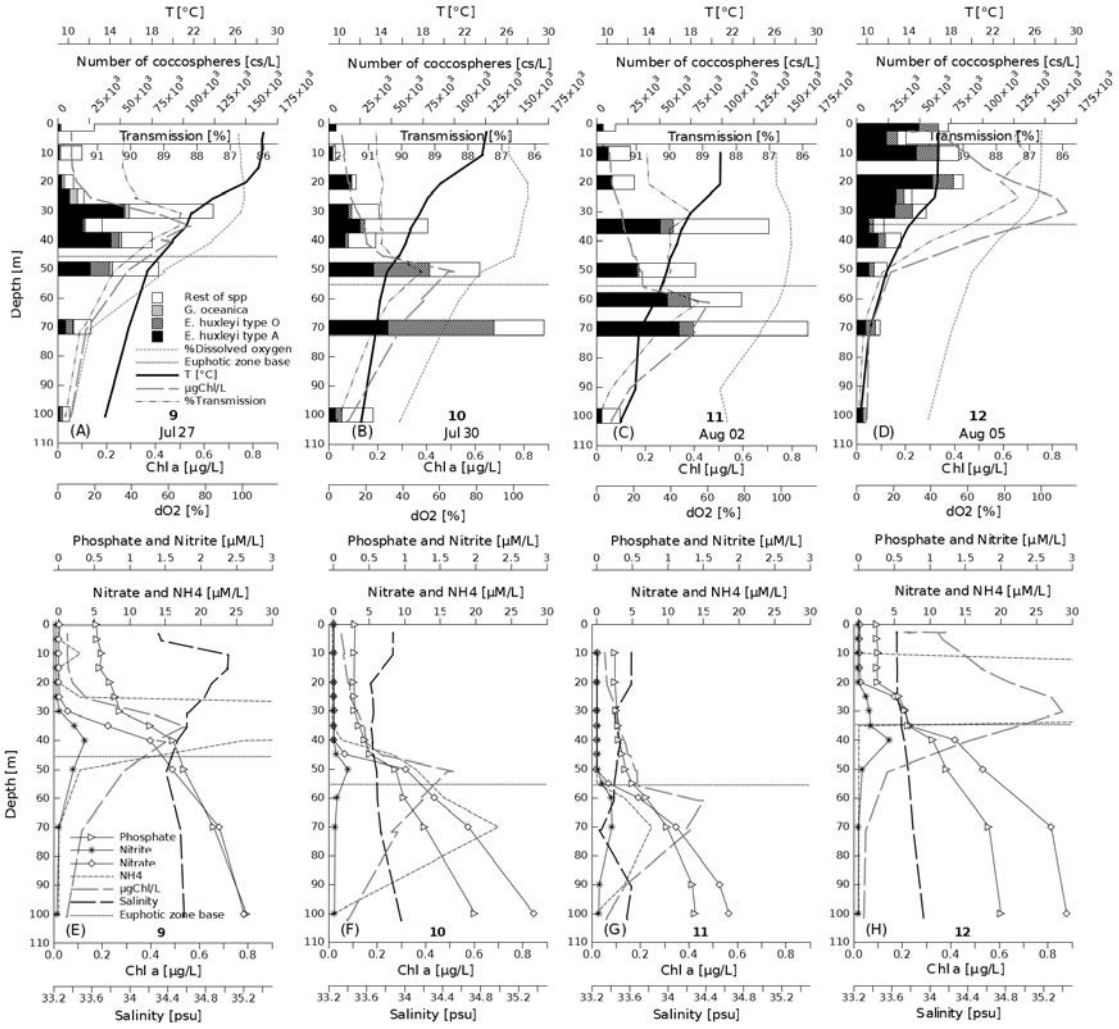

Figure C.5: As in the previous figure, profiles of biological and chemical measurements made in the upper 100m, here at four different locations, one in the entrance zone (station 9) and three in the NE Pacific (stations 10 to 12), in summer 2008. The depth of the euphotic zone base (1% surface PAR) was also calculated with the k_{PAR} coefficient and the surface PAR value for each location (Station 9, 0.101 m^{-1}, 2393 $\mu\mathrm{Ein\,m^{-2}\,s^{-1}}$; Station 10, 0.083 m^{-1}, 2415 $\mu\mathrm{Ein\,m^{-2}\,s^{-1}}$; Station 11, 0.083 m^{-1}, 2189 $\mu\mathrm{Ein\,m^{-2}\,s^{-1}}$; Station 12, 0.133 m^{-1}, 1467 $\mu\mathrm{Ein\,m^{-2}\,s^{-1}}$). The figure shows the dominance, both in proportion and absolute numbers, of *E. huxleyi* type A and type O in the coccolithophore assemblage of these locations.

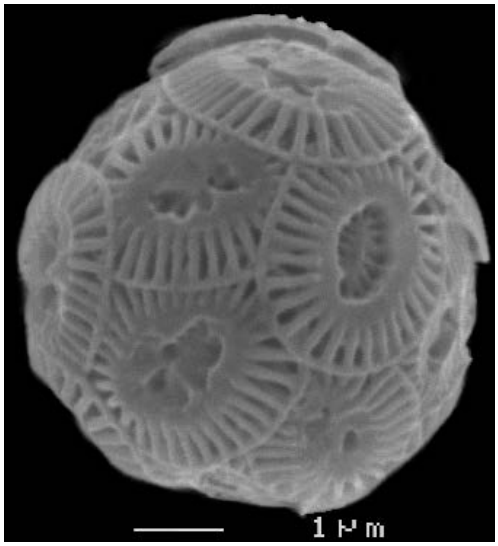

(a) SEM image of an over-calcified *E. huxleyi* with a normally-calcified coccolith.

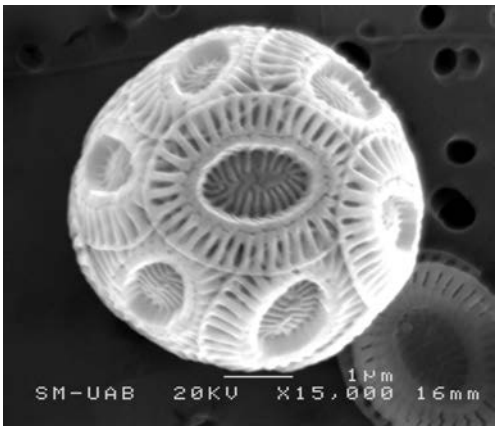

(b) SEM image of an *Emiliania huxleyi* over-calcified with slight aberrations on the tube elements, possible initial features of the collapsed kind of malformation. From station 10 at 20m.

Figure C.6: SEM images of *Emiliania huxleyi*.

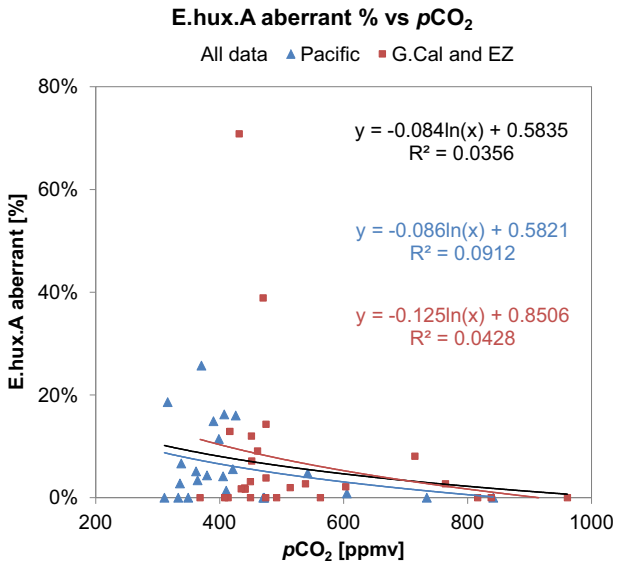

Figure C.7: Scatter plots for the percentage of *E. huxleyi* type A coccospheres with aberrant coccoliths versus pCO_2 (the main related environmental variable according to significant r Pearson correlation coefficients, with an alpha = 0.05, two-tailed test). Logarithmic trend lines are shown for all the data (black), for the data from the NE Pacific (blue) and for the Gulf of California and the Entrance Zone (red).

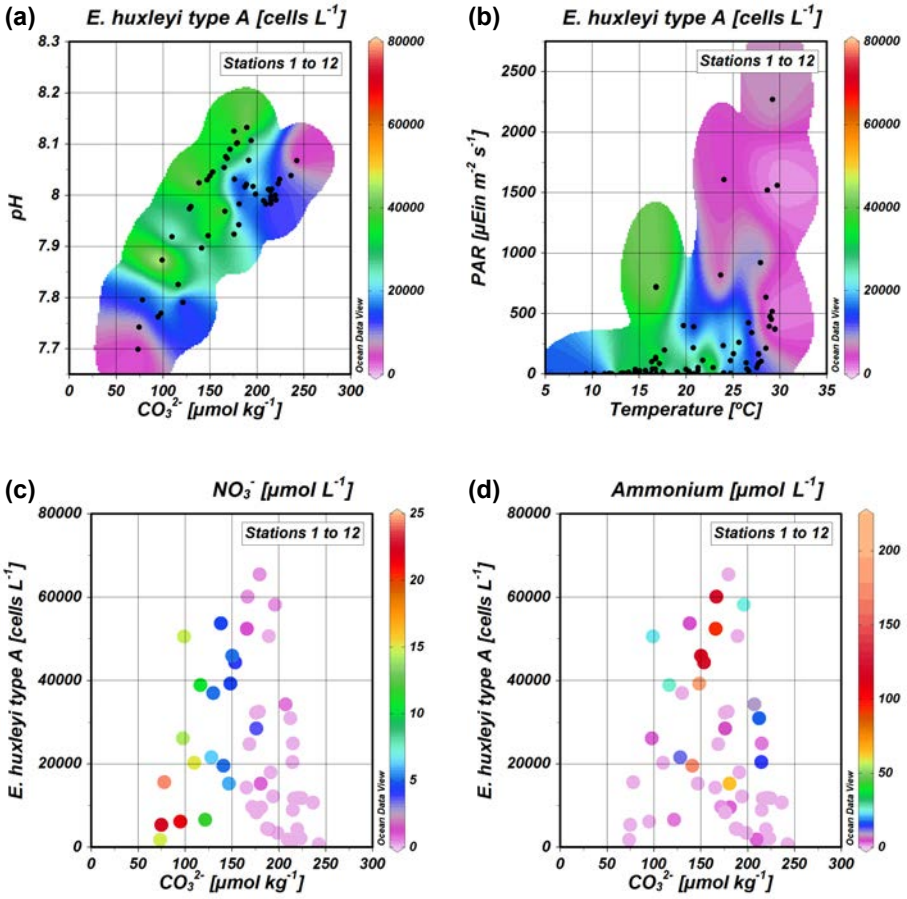

Figure C.8: Main explaining environmental variables of the cell densities of the morphotype A of *E. huxleyi* (a-d). In a and b, colors represent the cell densities at each sample (black dots), extrapolated for an enhanced view.

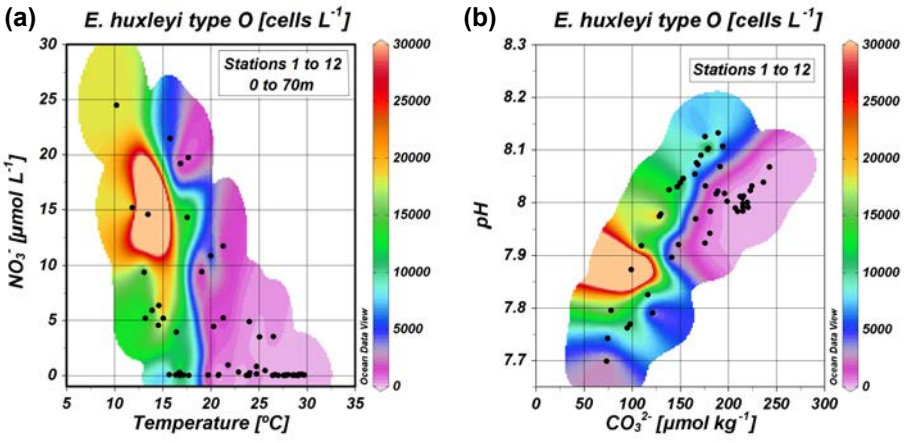

Figure C.9: Main explaining environmental variables of the cell densities of the morphotype O of *E. huxleyi* (a-b). Colors represent the cell densities at each sample (black dots), extrapolated for an enhanced view.

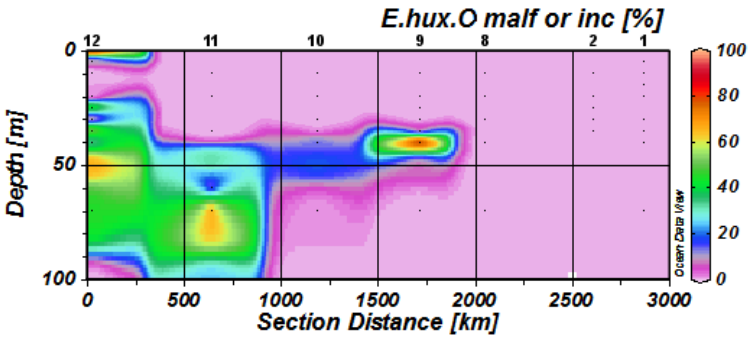

Figure C.10: Vertical profile of *Emiliania huxleyi* type O with malformed or incomplete coccoliths.

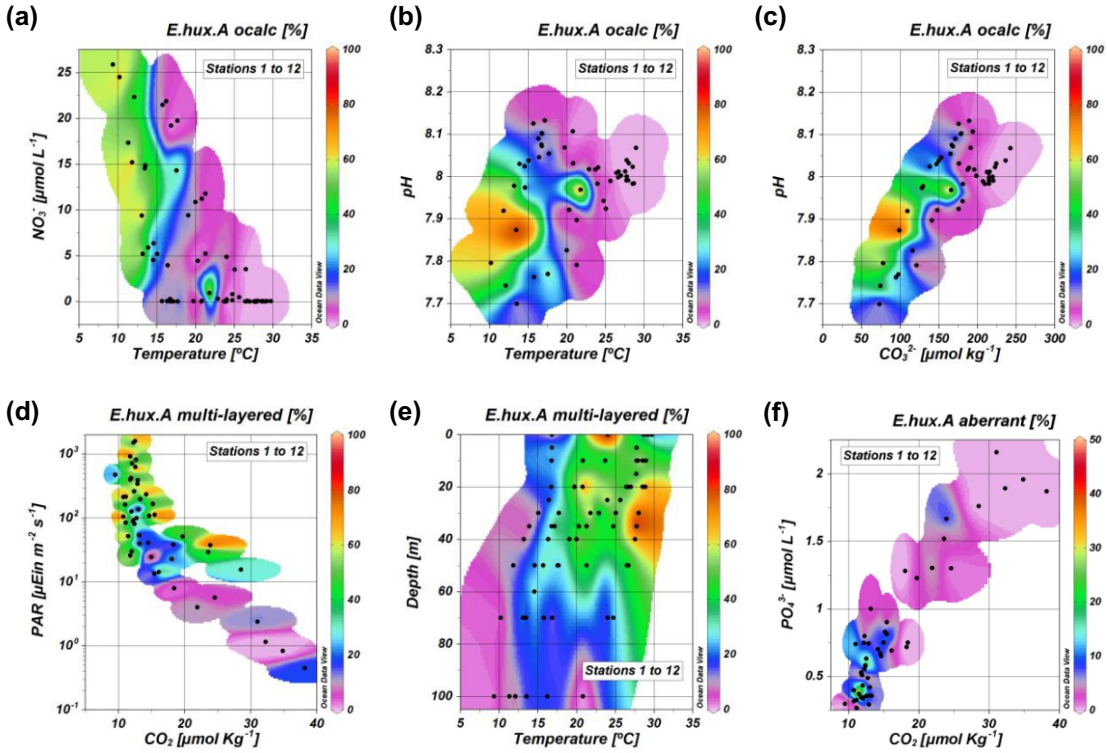

Figure C.11: Main environmental variables (axes x and y) explaining the cell density or proportion of different morphological categories observed in *E. huxleyi* type A (in colors, extrapolated for an enhanced view). ocalc: over-calcified.

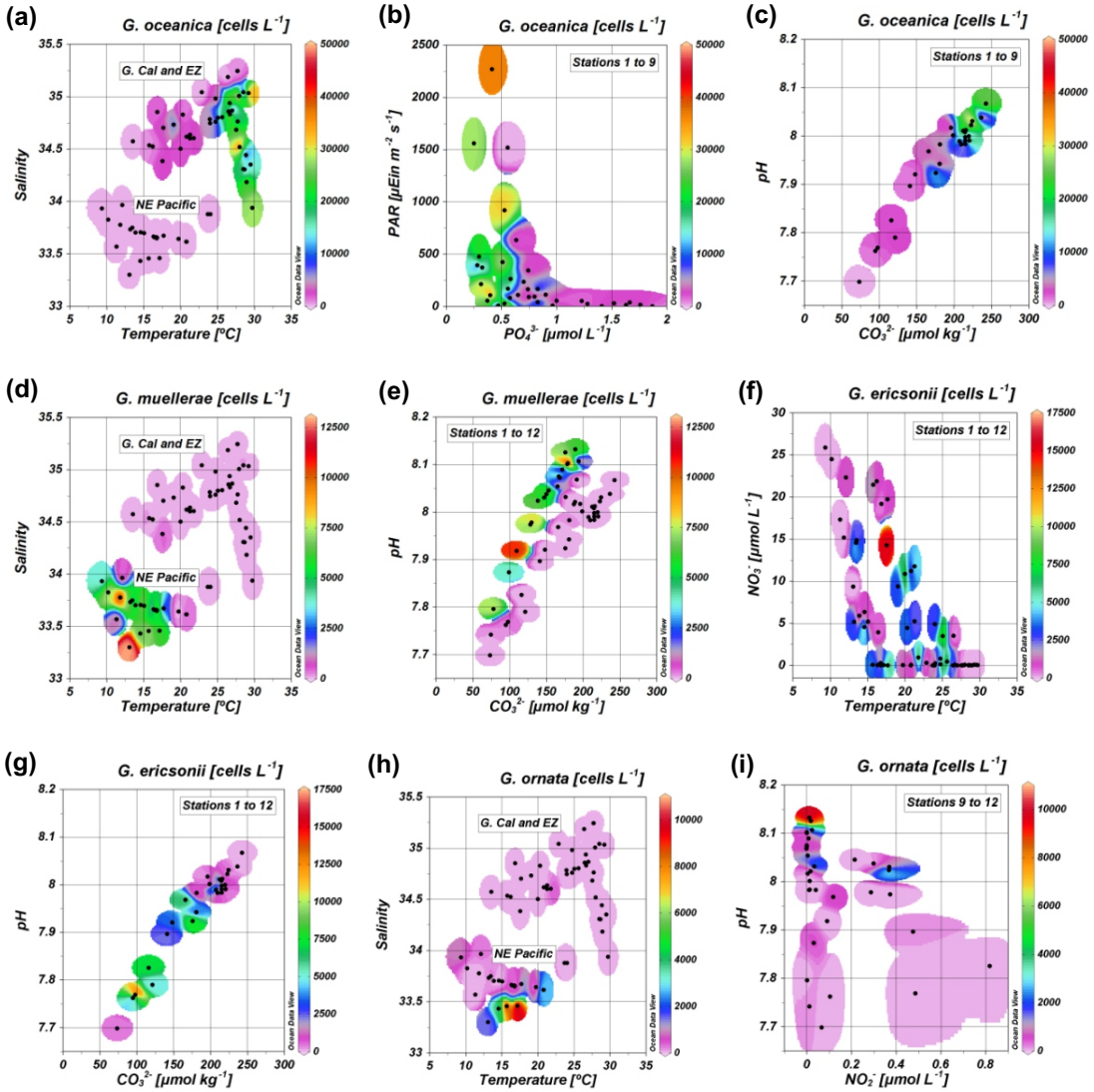

Figure C.12: Main explaining environmental variables of the cell densities of *G. oceanica* (a-c), *G. muellerae* (d-e), *G. ericsonii* (f-g), and *G. ornata* (h-i). Colors represent the cell densities at each sample (black dots), extrapolated for an enhanced view.

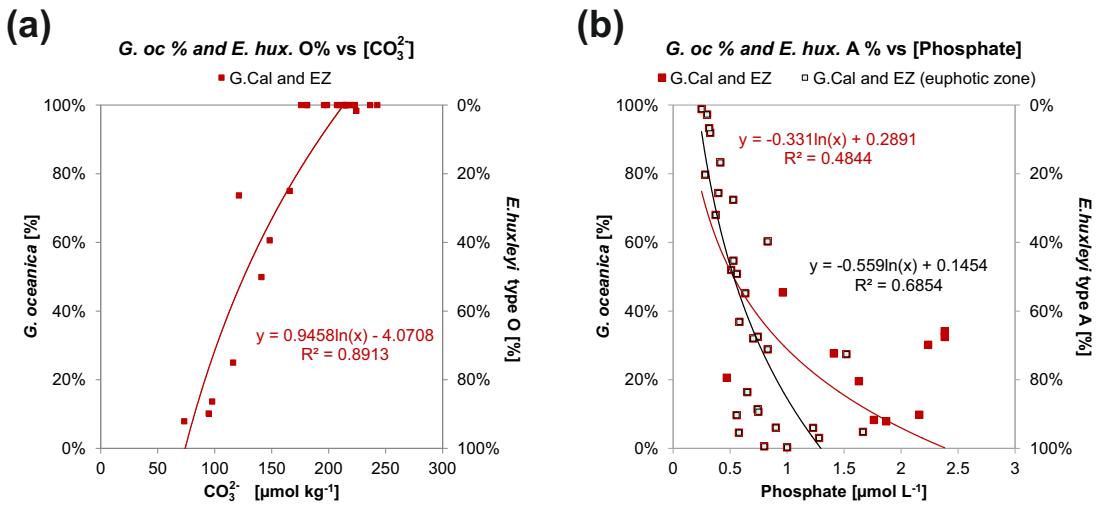

Figure C.13: Scatter plot for *G. oceanica* proportion relative to *E. huxleyi* type O (a) and for *G. oceanica* proportion relative to *E. huxleyi* type A (b), versus one of the main significantly linearly correlated environmental variables. In (a), higher percentages of *G. oceanica*, therefore lower of *E. huxleyi* type O, were found at higher $[CO_3^{2-}]$. In (b), higher percentages of *G. oceanica*, therefore lower of *E. huxleyi* type A, were found at higher phosphate concentrations. Logarithmic fits show the trend of the correlations. G. Cal: Gulf of California; EZ: Entrance zone.

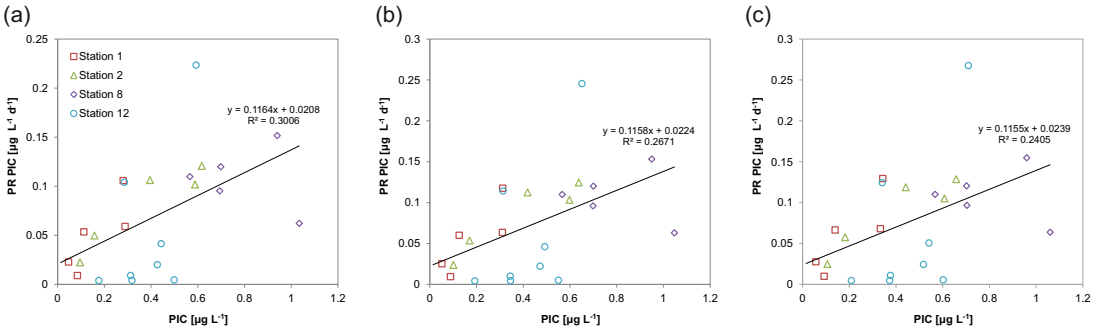

Figure C.14: Estimation of particulate inorganic carbon (PIC) per liter and PIC production rate (PR PIC), using three different possible number of total coccoliths (attached plus detached) per cell for *E. huxleyi*; 40 (a), 45 (b) and 50 (c) coccoliths. The growth rates for the PR PIC were calculated from the cell production rate (data from Wolhowe et al. (2014)) and the cell density of the alkenone-producing coccolithophores (*E. huxleyi* and the *Gephyrocapsa* species). Results were obtained for stations 1, 2, 8, and 12. Linear fits are shown for all the data together.

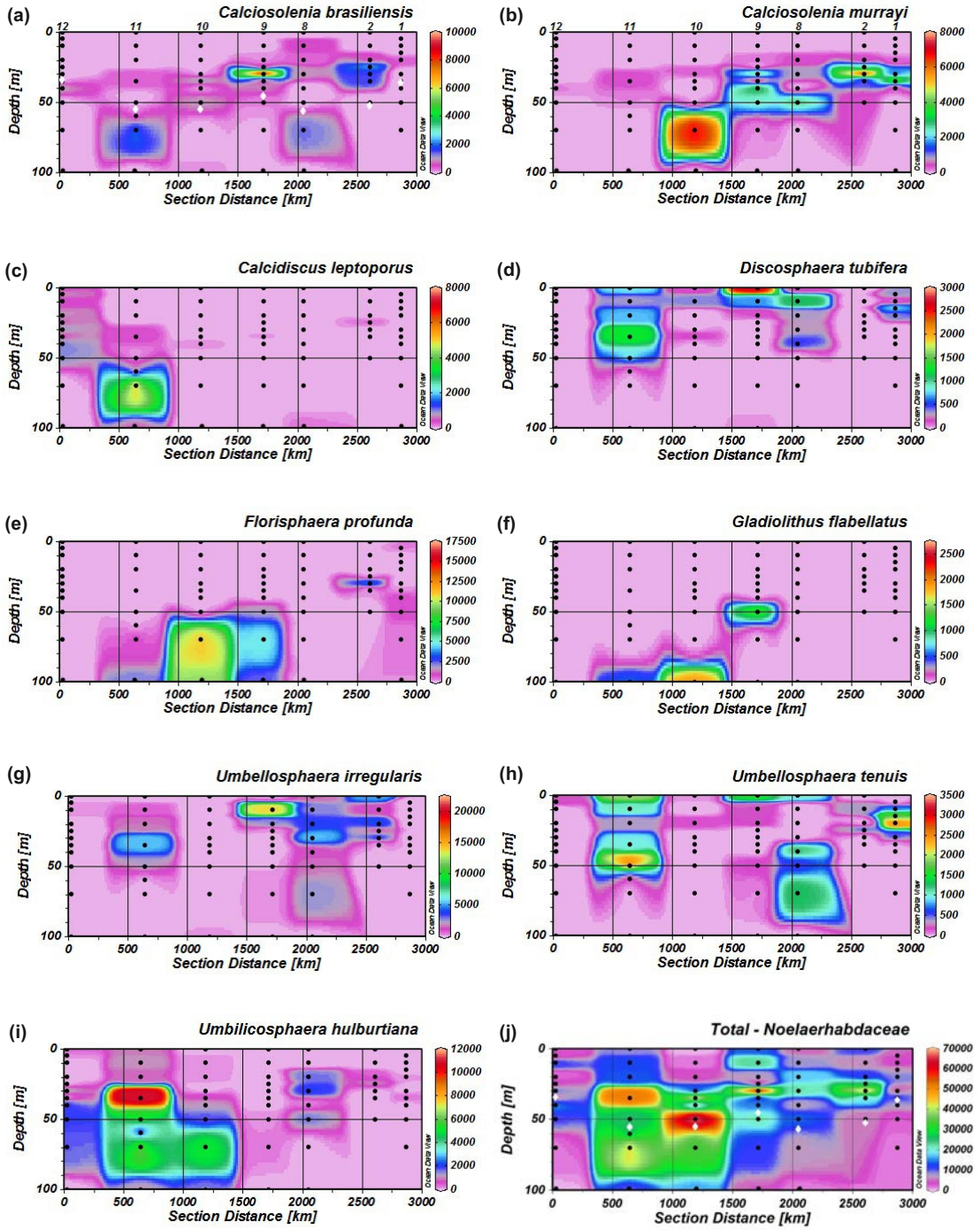

Figure C.15: Vertical profiles of the cell standing stocks [cells L^{-1}] of different coccolithophore species. *Calciosolenia brasiliensis* (a), *Calciosolenia murrayi* (b), *Calcidiscus leptoporus* (c), *Discosphaera tubifera* (d), *Florisphaera profunda* (e), *Gladiolithus flabellatus* (f), *Umbellosphaera irregularis* (g), *Umbellosphaera tenuis* (h), *Umbilicosphaera hulburtiana* (i), and all the species together without the Noelaerhabdaceae family (j). The numbers on top in Figs. (a) and (b), represent the station number of each vertical profile. White diamonds in (a) and (j) represent the base of the euphotic zone (1% light level of the surface irradiance); it is the same in all the profiles (a-j).

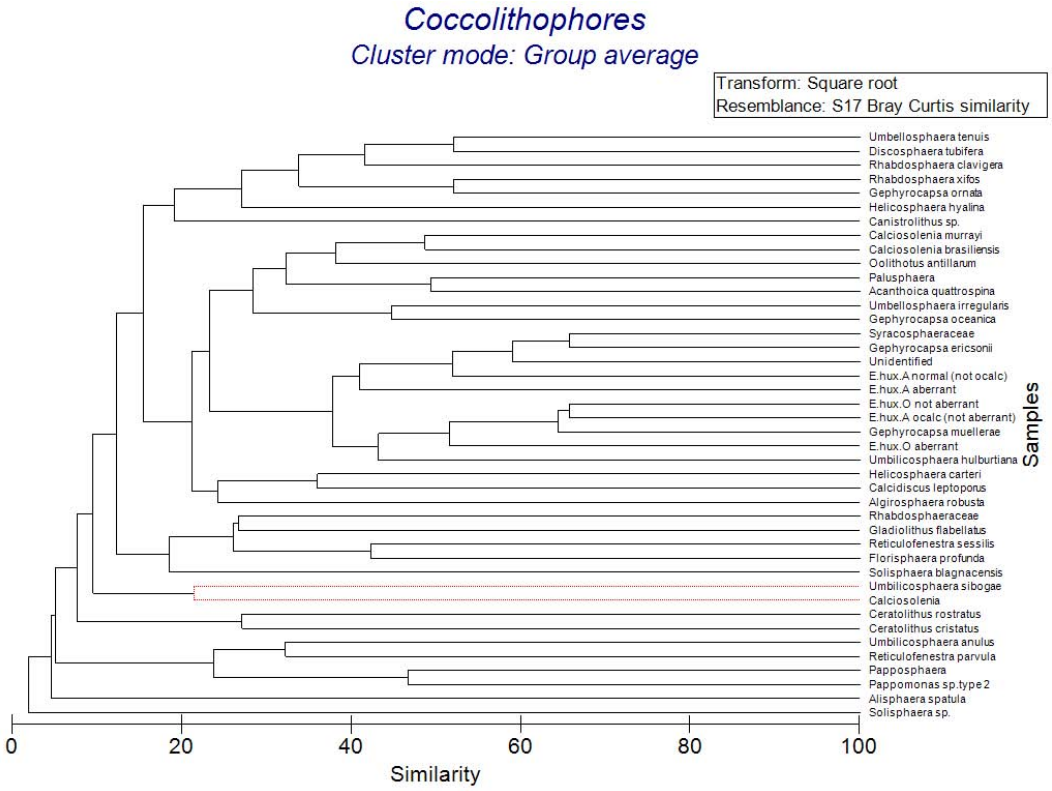

Figure C.16: Hierarchical cluster analysis on coccolithophore cell densities. Coccolithophore species and *E. huxleyi* morphologies with similar distributions are associated. The analysis is based on the Bray-Curtis similarity using the group average method on square-root-transformed cell densities. Not significant Simprof test results with a significance level higher than 5% are shown with red dotted lines. Figure C.17 shows a simplified cluster.

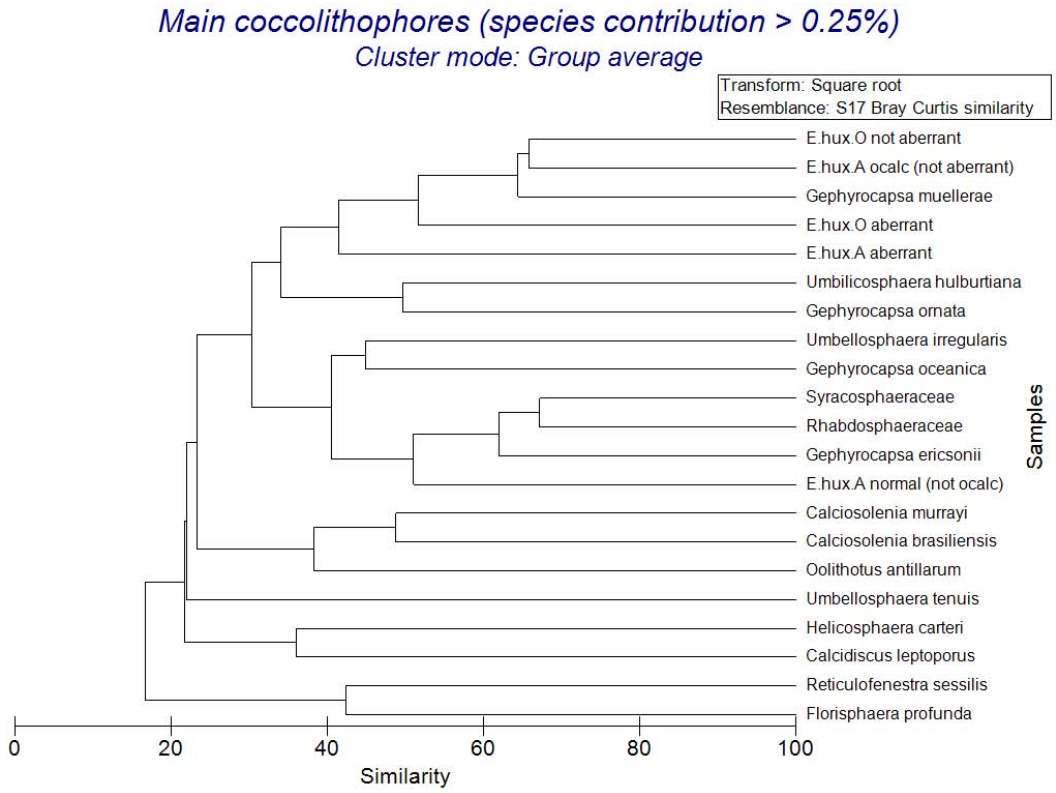

Figure C.17: Hierarchical cluster analysis on cell densities of the main taxa/morphologies (contributing more than 0.25% in the total cell standing stocks of the study). All species of the family Rhabdosphaeraceae are included in a single group. The analysis is based on the Bray-Curtis similarity using the group average method on square-root-transformed cell densities. All the results are significant according to the Simprof test, with a significance level of 5% (1000 permutations for mean profile and 999 simulation permutations).

C.2 Supplementary tables for Chapters 5 and 6

Table C.1: General information on samples analyzed at each station. Two casts (A and B) were used for each station to complete the biological and chemical profiles. CS: Coccospheres (cell density per morphotype and different morphologies); HC: Hydrographic conditions (temperature, salinity, density, chlorophyll, % transmission, photosynthetic active radiation, dissolved oxygen); NUTS: Nutrients (nitrate, nitrite, phosphate, ammonium and silicate); CSYS: Carbonate system (total alkalinity, dissolved inorganic carbon, CO_2, pCO_2, CO_3^{2-}, HCO_3^-, calcite saturation state). *Station 2 was sampled at two different dates, no data for the carbonate system was sampled for the second date, and hence it was taken out from the general results and the statistical analysis; it was used for some comparisons.

Station	*Lat [°N]*	*Lon [°W]*	*Depth of the sea floor [m]*	*Site and Cast (A)*	*Date (A)*	*Type of sampling (A)*	*Mixed layer depth [m]*	*Site and Cast (B)*	*Date (B)*	*Type of sampling (B)*
1	26.5	110.5	1400	01/01/16	07/11/08	CSYS,HC,CS	17	01/02/16	07/11/08	NUTS
2	24.5	109	2000	02/02/16	07/14/08	CS	4.4	02/01/16	07/14/08	HC, CSYS,NUTS
2*	24.5	109	2000	02/26/16	07/22/08	HC,CS	17.2	2-25	07/22/08	NUTS
8	20.5	106.5	3500	08/01/16	07/18/08	CS	8	08/01/16	07/18/08	HC, CSYS, NUTS
9	21.5	109.5	3000	09/21/16	07/27/08	HC, CS	15.3	09/01/16	07/25/08	CSYS, NUTS
10	24.7	113.3	3500	10/18/16	07/30/08	HC, CS	10.6	10/05/16	07/29/08	CSYS, NUTS
11	27.5	117.5	3750	11/13/16	08/02/08	HC, CS	22.3	11/01/16	08/01/08	CSYS, NUTS
12	32.5	120.5	3500	12-10	08/05/08	HC,CS	25.8	12/09/16	08/05/08	CSYS,NUTS

Table C.2: Groups of samples used in the SIMPER analysis. All the samples shown correspond to the samples used in the rest of multivariate analyses. G. Cal: Gulf of California; EPZ: euphotic zone; BPZ: below the euphotic zone.

G. Cal and Station 9 –EPZ–	Station 8	Stations 10-11 EPZ	Station 12 and BPZ of stations 9-12	Outlier
1-5	2-10	10-0	9-50	9-30
1-10	8-10	10-20	9-70	
1-15	8-20	10-30	9-100	
1-20	8-30	10-35	10-50	
1-30	8-40	10-40	10-70	
1-35	8-50	11-10	10-100	
2-20		11-20	12-5	
2-25		11-35	12-10	
2-30		11-50	12-20	
2-35		11-60	12-25	
2-50			12-30	
9-0			12-35	
9-10			12-40	
9-20			12-50	
9-25			12-70	
9-35				
9-40				
10-10				

Table C.3: (Part 1) Abiotic data: some environmental conditions and carbonate system data. T: temperature; DIC: dissolved inorganic carbon; TA: total alkalinity; Ω_{calc}: calcite saturation state. Only showing data from the samples used in the multivariate statistical analysis.

Station-Depth	*T °C*	*Salinity*	*DIC* $[\mu mol\,kg^{-1}]$	*TA* $[\mu mol\,kg^{-1}]$	*pH*	CO_2 $[\mu mol\,kg^{-1}]$	$pCO_2[\mu atm]$	HCO_3^- $[\mu mol\,kg^{-1}]$	CO_3^{2-} $[\mu mol\,kg^{-1}]$	Ω_{calc}
1-5	27.7	35.24	2050	2380	8.04	11.01	416	1802	236	5.7
1-10	27.7	35.24	2060	2366	8	12.19	461	1828	220	5.29
1-15	27.7	35.24	2054	2354	7.99	12.43	470	1827	215	5.18
1-20	26.4	35.19	2062	2360	8.01	12.27	450	1835	214	5.15
1-30	22.8	35.02	2086	2358	8.02	13.18	440	1877	196	4.68
1-35	20.3	34.82	2121	2321	7.92	18.05	562	1954	148	3.53
2-10	28	35.01	2030	2338	7.99	11.79	449	1798	221	5.32
2-20	26.7	34.94	2034	2334	8	11.93	441	1807	215	5.17
2-25	25.6	34.8	2037	2326	7.99	12.38	451	1818	207	4.98
2-30	25.1	34.8	2065	2306	7.92	15.19	538	1874	176	4.22
2-35	24.7	34.98	2067	2316	7.94	14.64	514	1872	181	4.33
2-50	21.3	34.64	2145	2300	7.79	23.59	764	2000	121	2.89
8-10	29	34.18	1944	2287	8.07	9.51	368	1692	243	5.92
8-20	28.5	34.31	1956	2271	8.02	10.75	414	1723	223	5.39
8-30	28	34.52	1976	2291	8.03	10.76	408	1741	224	5.43
8-40	27.6	34.68	1997	2300	8.01	11.48	431	1770	216	5.21
8-50	26.7	34.83	2016	2312	8.01	11.8	435	1791	212	5.09
9-0	28.7	34.31	2031	2331	7.98	12.28	474	1804	215	5.21
9-10	28.5	35.04	2037	2328	7.98	12.55	475	1815	209	5.06
9-20	27	34.87	2051	2328	8	12.88	452	1840	198	4.77
9-25	24	34.78	2069	2319	7.98	14.19	475	1874	181	4.33
9-30	21.8	34.6	2083	2311	7.97	15.46	492	1902	166	3.95
9-35	21.3	34.6	2120	2308	7.9	19.68	603	1960	141	3.36
9-40	20	34.5	2158	2306	7.83	23.91	715	2018	116	2.76
9-50	17.5	34.38	2171	2289	7.77	28.5	816	2045	98	2.32
9-70	15.7	34.54	2194	2304	7.76	31.03	838	2068	95	2.24
9-100	13.5	34.57	2230	2303	7.7	38.15	961	2118	73	1.72

Table C.4: (Part 2) Abiotic data: some environmental conditions and carbonate system data. T: temperature; DIC: dissolved inorganic carbon; TA: total alkalinity; Ω_{calc}: calcite saturation state. Only showing data from the samples used in the multivariate statistical analysis.

Station-Depth	$T\,^{\circ}C$	Salinity	$DIC\ [\mu mol\,kg^{-1}]$	$TA\ [\mu mol\,kg^{-1}]$	pH	$CO_2\ [\mu mol\,kg^{-1}]$	$pCO_2[\mu atm]$	$HCO_3^-\ [\mu mol\,kg^{-1}]$	$CO_3^{2-}\ [\mu mol\,kg^{-1}]$	Ω_{calc}
10-0	24.1	33.88	2006	2269	8.02	12.52	421	1805	189	4.58
10-10	23.7	33.88	2006	2267	8.02	12.66	426	1806	187	4.53
10-20	19.7	33.64	2004	2272	8.07	11.79	371	1801	191	4.6
10-30	17.7	33.67	2006	2237	8.05	13.28	380	1827	165	3.96
10-35	16.7	33.65	2018	2254	8.07	13.02	364	1837	168	4.03
10-40	16.3	33.66	2030	2270	8.09	12.77	349	1846	172	4.1
10-50	14.6	33.71	2083	2255	7.97	18.28	472	1936	128	3.05
10-70	13.5	33.75	2118	2243	7.87	24.58	605	1995	99	2.34
10-100	12.1	33.96	2175	2254	7.74	34.82	841	2066	74	1.75
11-10	20.8	33.62	1999	2245	8.03	12.91	405	1810	176	4.25
11-20	20.8	33.61	1995	2268	8.11	11.13	333	1790	194	4.67
11-35	17.2	33.46	2003	2270	8.13	11.13	311	1802	189	4.53
11-50	15.7	33.45	2021	2268	8.13	12.03	316	1833	176	4.19
11-60	14.6	33.43	2054	2244	8.02	16.13	410	1899	138	3.29
12-5	16.8	33.65	2009	2260	8.1	12.07	338	1819	179	4.29
12-10	16.8	33.65	2009	2261	8.1	12	336	1817	179	4.31
12-20	16.7	33.66	2022	2255	8.08	13.22	362	1842	167	3.99
12-25	16.4	33.66	2036	2248	8.05	14.51	390	1868	153	3.67
12-30	15.1	33.7	2046	2254	8.04	14.97	399	1881	150	3.59
12-35	13.9	33.7	2056	2259	8.03	15.43	407	1894	147	3.51
12-40	13.2	33.73	2079	2254	7.98	18.44	470	1930	130	3.1
12-50	11.8	33.78	2111	2254	7.92	21.91	542	1980	110	2.61
12-70	10.2	33.82	2172	2258	7.8	32.25	734	2061	78	1.84

Table C.5: (Part 1) Abiotic data: some environmental conditions and nutrient concentrations data. Chl-*a*: Chlorophyll-*a*; PAR: photosynthetic active radiation; DO: dissolved oxygen. Only showing data from the samples used in the multivariate statistical analysis.

Station-Depth	*Pressure [dbars]*	*Density [kg/m^3]*	*Chl-a [$\mu g\, l^{-1}$]*	*PAR [$\mu Ein\, m^{-2}\, s^{-1}$]*	*DO [$\mu mol\, kg^{-1}$]*	*Nitrate [$\mu g\, l^{-1}$]*	*Nitrite [$\mu g\, l^{-1}$]*	*Ammonium [$\mu g\, l^{-1}$]*	*Phosphate [$\mu g\, l^{-1}$]*	*Silicate [$\mu g\, l^{-1}$]*
1-5	4.93	1022.69	0.2	132.35	190.55	0	0.04	0	0.74	1.68
1-10	10.12	1022.71	0.2	86.53	190.47	0	0.05	0	0.75	1.72
1-15	15.08	1022.73	0.21	81.75	190.56	0.03	0.05	0	0.58	1.41
1-20	20.37	1023.13	0.22	99.76	200.7	0	0.04	14	0.8	2
1-30	29.88	1024.15	0.52	52.44	198.65	0.3	0.08	24	1	3.17
1-35	35.49	1024.71	0.51	22.32	159.21	4.45	0.38	195	1.28	5.19
2-10	10.22	1022.46	0.2	980.97	189.49	0.02	0	0	0.53	1.3
2-20	20.34	1022.86	0.3	431.72	193.7	0.06	0.03	2	0.51	1.13
2-25	25.59	1023.11	0.51	260.85	187.56	0.46	0.15	9	0.58	1.5
2-30	30.45	1023.3	0.43	166.1	180.36	3.49	0.35	5	0.83	2.59
2-35	35.31	1023.57	0.3	108.61	195.82	0.8	0.51	63	0.65	2.06
2-50	50.19	1024.36	0.22	29.42	78.56	11.77	0.08	2	1.52	8.74
8-10	9.98	1021.51	0.21	491.96	187.46	0	0.02	0	0.3	1.15
8-20	20.11	1021.78	0.26	212.21	187.06	0	0.02	0	0.32	1.2
8-30	29.8	1022.15	0.35	104.25	186.48	0.07	0.02	0	0.4	1.42
8-40	40.03	1022.46	0.29	52.5	189.93	0.01	0.03	0	0.37	1.47
8-50	50.68	1022.9	0.47	26.04	189.08	0.07	0.03	17	0.53	1.67
9-0	3.06	1021.66	0.06	1518.1	191.2	0.04	0.01	0	0.56	4.55
9-10	10.42	1022.3	0.06	632.73	193.04	0.03	0.01	3	0.63	1.59
9-20	20.14	1022.7	0.08	343.19	201.37	0.02	0.01	0	0.74	5.92
9-25	25.44	1023.59	0.14	233.71	212.18	0	0.04	3	0.7	5.17
9-30	30.55	1024.11	0.4	116.46	215.98	0.94	0.12	93	0.9	3.32
9-35	35.32	1024.26	0.53	53.69	203.14	5.23	0.48	167	1.23	6.03
9-40	40.01	1024.55	0.43	37.67	189.46	10.86	0.82	26	1.67	8.2
9-50	50.76	1025.13	0.28	15.51	134.51	14.29	0.49	3	1.76	12.91
9-70	70.77	1025.76	0.12	2.39	42.68	21.46	0.1	0	2.16	19.81
9-100	100.56	1026.4	0.05	0.45	19.06	14.88	0.07	0	1.87	16.51

Table C.6: (Part 2) Abiotic data: some environmental conditions and nutrient concentrations data. Chl-*a*: Chlorophyll-*a*; PAR: photosynthetic active radiation; DO: dissolved oxygen. Only showing data from the samples used in the multivariate statistical analysis.

Station-Depth	*Pressure [dbars]*	*Density [kg/m^3]*	*Chl-a [μg l^{-1}]*	*PAR [μEin m^{-2} s^{-1}]*	*DO [μmol kg^{-1}]*	*Nitrate [μg l^{-1}]*	*Nitrite [μg l^{-1}]*	*Ammonium [μg l^{-1}]*	*Phosphate [μg l^{-1}]*	*Silicate [μg l^{-1}]*
10-0	2.73	1022.79	0.05	1722.6	205.29	0.23	0.02	0	0.36	1.94
10-10	10.22	1022.93	0.07	817.28	207.65	0.05	0	0	0.34	2.43
10-20	20.25	1023.88	0.09	400.39	245.61	0.01	0	0	0.36	2.21
10-30	30.62	1024.46	0.12	196.94	249.95	0.03	0.01	1.15	0.49	4.3
10-35	36.34	1024.69	0.15	137.09	250.79	0.93	0.07	8.26	0.52	18.33
10-40	40.84	1024.82	0.15	101	248.65	6.36	0.37	11.55	0.72	7.82
10-50	50.75	1025.29	0.49	38.24	207.3	6.36	0.37	11.55	0.72	7.82
10-70	71.69	1025.65	0.28	5.9	157.25	14.55	0.03	23.16	1.3	14.53
10-100	101.92	1026.23	0.07	0.86	101.69	22.32	0.01	0	1.96	23.05
11-10	10.03	1023.53	0.05	363.65	217.35	0.08	0.03	0	0.29	2.7
11-20	20.2	1023.58	0.06	216.17	217.75	0.01	0.02	0	0.27	2.29
11-35	35.58	1024.45	0.11	86.77	252.35	0.03	0.01	0	0.32	2.74
11-50	50.48	1024.85	0.19	30.88	254.92	0.06	0.02	0	0.43	4.04
11-60	60.86	1025.13	0.44	14.28	248.29	4.55	0.37	3.87	0.69	5.74
12-5	5.25	1024.55	0.37	222.89	240.95	0.18	0	0.03	0.34	0.77
12-10	10.5	1024.59	0.45	126.15	241.26	0.26	0	0.03	0.34	0.79
12-20	19.87	1024.64	0.64	39.52	239.93	0.29	0	122.64	0.36	0.83
12-25	25.26	1024.73	0.82	41.04	238.45	3.95	0.21	122.64	0.67	4.05
12-30	30.28	1025.08	0.86	24.7	231.2	5.2	0.3	114.98	0.75	5.32
12-35	35.53	1025.37	0.66	13.61	215.04	5.9	0.37	0	0.81	5.87
12-40	40.53	1025.55	0.46	7.97	196.06	5.19	0.29	0	0.75	5.18
12-50	50.96	1025.9	0.14	4	166.48	24.49	0	0	1.89	25.14
12-70	71.01	1026.32	0.05	1.15	141.95	24.49	0	0	1.89	25.14

Table C.7: (PART 1) Cell densities (cells l^{-1}), at each sample, of the main morphotypes of *Emiliania huxleyi*, of the different species of the genus *Gephyrocapsa*, of the rest of coccolithophore species, and of the total number of coccolithophores. Only showing data from the samples used in the multivariate statistical analysis.

Station-Depth	*E. hux.* A	*E. hux.* O	*G. ericsonii*	*G. muellerae*	*G. oceanica*	*G. ornata*	Rest of spp.	TOTAL
1-5	10756	0	0	0	1388	0	4511	16655
1-10	4334	0	0	0	519	0	3075	7928
1-15	9000	0	0	0	433	0	6449	15882
1-20	20498	0	245	0	123	0	8960	29826
1-30	58225	0	177	0	177	0	4424	63003
1-35	39292	802	3495	0	1234	0	11925	56748
2-10	11867	0	0	0	31151	0	5933	48951
2-20	24931	0	4155	0	27008	0	10803	66897
2-25	34262	0	7252	0	20007	0	24509	86030
2-30	28499	0	7702	0	11554	0	44675	92430
2-35	15303	0	3601	0	3001	0	17403	39308
2-50	6603	892	4818	0	2498	0	5355	20166
8-10	717	0	0	0	25382	0	7725	33824
8-20	2178	0	0	0	30176	0	17732	50086
8-30	11758	574	574	0	34128	0	21795	68829
8-40	11690	0	0	0	24841	0	6819	43350
8-50	30959	0	4804	0	37365	0	13878	87006
9-0	1748	0	0	0	187	0	13730	15665
9-10	1890	0	0	222	1556	0	22569	26237
9-20	3464	0	41	0	1671	41	7132	12349
9-25	9617	0	558	186	4529	62	1489	16442
9-30	52447	1128	6203	0	3384	564	60342	124068
9-35	19588	1250	2378	0	1246	113	10759	35335
9-40	38949	5901	7082	0	1967	0	15343	69242
9-50	26113	14922	15252	363	2360	0	21426	80436
9-70	6182	5935	1860	168	672	60	11817	26694
9-100	1774	1774	431	0	152	0	5167	9298

Table C.8: (PART 2) Cell densities (cells l^{-1}), at each sample, of the main morphotypes of *Emiliania huxleyi*, of the different species of the genus *Gephyrocapsa*, of the rest of coccolithophore species, and of the total number of coccolithophores. Only showing data from the samples used in the multivariate statistical analysis.

Station-Depth	*E. hux.* A	*E. hux.* O	*G. ericsonii*	*G. muellerae*	*G. oceanica*	*G. ornata*	Rest of spp.	TOTAL
10-0	4323	480	314	97	0	83	338	5635
10-10	4527	181	2173	0	0	0	1630	8511
10-20	17977	0	1247	0	0	147	2201	21572
10-30	14339	2494	5923	935	0	1559	11845	37094
10-35	24732	3773	4501	429	0	1286	43936	78656
10-40	9698	2121	4567	806	0	940	15446	33578
10-50	21602	26933	942	6956	0	0	67037	123470
10-70	50620	91538	5906	3797	0	422	32482	184764
10-100	5365	4981	1046	116	0	232	23599	35340
11-10	8409	0	701	0	0	2453	12263	23825
11-20	12238	0	930	573	0	3077	12882	29700
11-35	50712	10142	8648	6085	0	10249	51246	137082
11-50	32255	1125	3632	7091	0	8993	25511	78607
11-60	53789	16947	5895	6631	0	3684	22842	109788
12-5	32553	11936	835	6511	0	0	2420	54254
12-10	65481	25465	742	12992	0	0	10765	115446
12-20	60166	16970	0	5343	0	0	2003	84482
12-25	44347	8492	548	5941	0	0	3833	63161
12-30	45929	20996	0	6561	0	0	9185	82671
12-35	15256	6185	0	4885	0	0	4479	30805
12-40	37003	12334	3084	8223	0	0	15419	76062
12-50	20248	8678	0	10606	0	0	10605	50137
12-70	15664	18137	0	7420	0	0	1648	42869

Table C.9: (Part 1) Cell densities (cells l^{-1}) of the different morphologies in *E. huxleyi* type A at each sample. u-calc: under-calcified; n-calc: normally calcified; o-calc: o-calc: over-calcified. Only showing data from the samples used in the multivariate statistical analysis.

Station-Depth	*E. hux. A* u-cal	*E. hux. A* n-cal	*E. hux. A* o-cal	*E. hux. A* mono- layered	*E. hux. A* multi-layered	*E. hux. A* normal	*E. hux. A* aberrant
1-5	2775	7980	0	6245	4510	9368	1388
1-10	656	3677	0	3152	1182	3940	394
1-15	4749	4249	0	6249	2749	5500	3500
1-20	7789	12708	0	15988	4509	20498	0
1-30	3295	48337	6591	50534	7690	57126	1099
1-35	2405	36886	0	30471	8820	39292	0
2-10	0	11867	0	2225	9641	11496	371
2-20	0	24930	0	12049	12880	24515	416
2-25	1370	30150	2740	16445	17816	30150	4111
2-30	3851	23877	770	14634	13864	27729	770
2-35	600	14703	0	9301	6001	15003	300
2-50	713	5710	178	3926	2676	6424	178
8-10	0	717	0	551	165	717	0
8-20	0	2177	0	933	1244	2178	0
8-30	0	11758	0	2294	9463	11758	0
8-40	11689	0	0	4140	7549	3410	8280
8-50	30959	0	0	13344	17614	30426	534
9-0	582	1165	0	1165	582	1748	0
9-10	135	1755	0	404	1485	1620	270
9-20	0	3464	0	989	2474	3217	247
9-25	630	8987	0	2135	7481	8326	1291
9-30	0	2255	50191	9023	43423	52447	0
9-35	3750	15420	416	10002	9585	19171	417
9-40	3934	30293	4721	9048	29900	35801	3147
9-50	932	16787	8393	18652	7460	26113	0
9-70	1483	3709	989	5440	741	6182	0
9-100	322	1290	161	1451	322	1774	0

Table C.10: (Part 2) Cell densities (cells l^{-1}) of the different morphologies in *E. huxleyi* type A at each sample. u-calc: under-calcified; n-calc: normally calcified; o-calc: o-calc: over-calcified. Only showing data from the samples used in the multivariate statistical analysis.

Station-Depth	*E. hux. A* u-cal	*E. hux. A* n-cal	*E. hux. A* o-cal	*E. hux. A* mono- layered	*E. hux. A* multi-layered	*E. hux. A* normal	*E. hux. A* aberrant
10-0	2642	1681	0	720	3602	4083	240
10-10	905	3621	0	2716	1810	3803	724
10-20	10272	7704	0	10272	7704	13354	4623
10-30	935	9974	3428	9974	4364	13715	623
10-35	5449	18863	419	21797	2934	23894	838
10-40	0	6667	3030	6970	2727	9698	0
10-50	0	19919	1683	18796	2805	21602	0
10-70	0	9702	40918	48089	2531	50198	422
10-100	0	3065	2299	5364	0	5365	0
11-10	350	8058	0	4905	3503	8058	350
11-20	1984	10253	0	2976	9261	12238	0
11-35	6454	44257	0	20284	30427	50712	0
11-50	6750	25128	375	18377	13876	26254	6001
11-60	1473	48630	3684	30210	23578	53052	737
12-5	6510	21701	4340	23871	8680	30383	2170
12-10	5456	50929	9094	50929	14551	63662	1819
12-20	3085	55537	1542	49366	10799	57081	3085
12-25	12266	30193	1887	36798	7548	37742	6605
12-30	9185	22308	14434	44616	1312	40680	5249
12-35	2061	7009	6184	14843	412	12782	2474
12-40	4111	5139	27752	35975	1027	37003	0
12-50	964	5785	13498	18319	1928	19283	964
12-70	824	4946	9892	15663	0	15664	0

Table C.11: (Part 1) Estimated calcite per liter of *Emiliania huxleyi* type A (*E. hux.* A) and type O (*E. hux.* O) at each sample, and of the different species of the genus *Gephyrocapsa*. *G.oc: G. oceanica; G.muel: G. muellerae; G.eric: G. ericsonii; G.orn: G. ornata.* Only showing data from the samples used in the multivariate statistical analysis.

Station-Depth	*E. hux. A calcite* [$\mu g l^{-1}$]	*E. hux. O calcite* [$\mu g l^{-1}$]	*G. oc calcite* [$\mu g l^{-1}$]	*G. muel calcite* [$\mu g l^{-1}$]	*G. eric calcite* [$\mu g l^{-1}$]	*G.orn calcite* [$\mu g l^{-1}$]	*E. hux calcite* [$\mu g l^{-1}$]	*Gephyrocapsa calcite* [$\mu g l^{-1}$]	*E. hux + G.oc calcite* [$\mu g l^{-1}$]	*E.hux + Gephyrocapsa calcite* [$\mu g l^{-1}$]
1-5	0.29	0	0.19	0	0	0	0.29	0.19	0.48	0.48
1-10	0.11	0	0.07	0	0	0	0.11	0.07	0.18	0.18
1-15	0.17	0	0.06	0	0	0	0.17	0.06	0.23	0.23
1-20	0.43	0	0.02	0	0.01	0	0.43	0.02	0.45	0.46
1-30	1.46	0	0.02	0	0	0	1.46	0.03	1.48	1.49
1-35	0.97	0	0.17	0	0.08	0	0.97	0.25	1.13	1.21
2-10	0.44	0	4.26	0	0	0	0.44	4.26	4.7	4.7
2-20	0.77	0	3.69	0	0.09	0	0.77	3.79	4.47	4.56
2-25	1.13	0	2.74	0	0.16	0	1.13	2.9	3.86	4.03
2-30	0.86	0	1.58	0	0.17	0	0.86	1.75	2.44	2.61
2-35	0.43	0	0.41	0	0.08	0	0.43	0.49	0.84	0.92
2-50	0.18	0	0.34	0	0.11	0	0.18	0.45	0.52	0.63
8-10	0.02	0	4.68	0	0	0	0.02	4.68	4.7	4.7
8-20	0.07	0	5.7	0	0	0	0.07	5.7	5.77	5.77
8-30	0.44	0	7.18	0	0.01	0	0.44	7.19	7.61	7.63
8-40	0.2	0	5.46	0	0	0	0.2	5.46	5.66	5.66
8-50	0.5	0	7.66	0	0.11	0	0.5	7.77	8.16	8.27
9-0	0.04	0	0.03	0	0	0	0.04	0.03	0.07	0.07
9-10	0.07	0	0.21	0.02	0	0	0.07	0.23	0.28	0.3
9-20	0.12	0	0.23	0	0	0	0.12	0.23	0.35	0.35
9-25	0.33	0	0.62	0.01	0.01	0	0.33	0.65	0.95	0.98
9-30	2	0	0.46	0	0.14	0.04	2	0.64	2.46	2.64
9-35	0.56	0	0.17	0	0.05	0.01	0.56	0.23	0.73	0.79
9-40	1.5	0.01	0.27	0	0.16	0	1.51	0.43	1.78	1.94
9-50	0.77	0.02	0.32	0.03	0.34	0	0.79	0.69	1.11	1.48
9-70	0.15	0.01	0.09	0.01	0.04	0	0.16	0.15	0.25	0.31
9-100	0.04	0	0.02	0	0.01	0	0.04	0.03	0.06	0.07

Table C.12: (Part 2) Estimated calcite per liter of *Emiliania huxleyi* type A (*E. hux.* A) and type O (*E. hux.* O) at each sample, and of the different species of the genus *Gephyrocapsa*. *G.oc: G. oceanica; G.muel: G. muellerae; G.eric: G. ericsonii; G.orn: G. ornata.* Only showing data from the samples used in the multivariate statistical analysis.

Station-Depth	*E. hux. A calcite* [$\mu g l^{-1}$]	*E. hux. O calcite* [$\mu g l^{-1}$]	*G. oc calcite* [$\mu g l^{-1}$]	*G. muel calcite* [$\mu g l^{-1}$]	*G. eric calcite* [$\mu g l^{-1}$]	*G. orn calcite* [$\mu g l^{-1}$]	*E. hux calcite* [$\mu g l^{-1}$]	*Gephyrocapsa calcite* [$\mu g l^{-1}$]	*E. hux + G. oc calcite* [$\mu g l^{-1}$]	*E. hux + Gephyrocapsa calcite* [$\mu g l^{-1}$]
10-0	0.11	0	0	0.01	0.01	0.01	0.11	0.02	0.11	0.13
10-10	0.12	0	0	0	0.05	0	0.12	0.05	0.12	0.16
10-20	0.42	0	0	0	0.03	0.01	0.42	0.04	0.42	0.46
10-30	0.58	0	0	0.07	0.13	0.1	0.58	0.3	0.58	0.89
10-35	0.52	0.01	0	0.03	0.1	0.08	0.53	0.22	0.53	0.74
10-40	0.45	0	0	0.06	0.1	0.06	0.45	0.22	0.45	0.68
10-50	0.57	0.04	0	0.53	0.02	0	0.6	0.55	0.6	1.16
10-70	1.98	0.13	0	0.29	0.13	0.03	2.11	0.45	2.11	2.56
10-100	0.16	0.01	0	0.01	0.02	0.02	0.16	0.05	0.16	0.21
11-10	0.24	0	0	0	0.02	0.16	0.24	0.18	0.24	0.42
11-20	0.41	0	0	0.04	0.02	0.2	0.41	0.27	0.41	0.67
11-35	1.57	0.01	0	0.47	0.19	0.67	1.58	1.33	1.58	2.91
11-50	0.78	0	0	0.54	0.08	0.59	0.79	1.21	0.79	1.99
11-60	1.65	0.02	0	0.51	0.13	0.24	1.68	0.88	1.68	2.56
12-5	0.88	0.02	0	0.5	0.02	0	0.9	0.52	0.9	1.42
12-10	1.83	0.03	0	0.99	0.02	0	1.87	1.01	1.87	2.88
12-20	1.41	0.02	0	0.41	0	0	1.44	0.41	1.44	1.85
12-25	0.92	0.01	0	0.45	0.01	0	0.93	0.47	0.93	1.4
12-30	1.19	0.03	0	0.5	0	0	1.22	0.5	1.22	1.72
12-35	0.42	0.01	0	0.37	0	0	0.43	0.37	0.43	0.81
12-40	1.33	0.02	0	0.63	0.07	0	1.35	0.7	1.35	2.05
12-50	0.76	0.01	0	0.81	0	0	0.78	0.81	0.78	1.59
12-70	0.52	0.02	0	0.57	0	0	0.54	0.57	0.54	1.11

Table C.13: Highly correlated abiotic variables ($r > 0.95; r < -0.95$), removed from multivariate analysis. DIC: dissolved inorganic carbon; Ω_{calc}: calcite saturation state.

Variable	Correlated variable (removed)	r
Temperature	Density	-0.961
pH	pCO_2	-0.99
DIC	HCO_3^-	0.968
CO_3^{2-}	Ω_{calc}	0.999
Nitrate	Nitrate + Nitrite	0.999
Ammonium	Nitrate + Nitrite + Ammonium	0.988

Table C.14: (PART 1) Spearmans rank correlation (r_S, $p < 0.03$) of *Emiliania huxleyi* type A and type O, *Emiliania huxleyi* type A morphological categories, *Gephyrocapsa oceanica, G. muellerae, G. ericsonii,* and *G. ornata,* versus the environmental variables. The morphological variability was standardized within each category. The six higher multivariate results with a BEST analysis of maximum 5 variables (r_S shown in the right column) and the six higher univariate results (r_S in brackets) are shown. G. Cal: Gulf of California; EZ: Entrance Zone. PAR: photosynthetic active radiation; Chl-*a*: chlorophyll-*a* concentration; DO: dissolved oxygen; CO_3^{2-}: carbonate ion concentration; CO_2: carbon dioxide concentration. When required is written if an environmental variable was excluded from the analysis, in these cases Table C.18, Table C.19, and C.20 show the analysis including the 14 variables.

A. *Emiliania huxleyi* type A (all data: stations 1 to 12; Chl-*a* excluded in the multivariate analysis)

Environmental variable	r_S
Temperature, PAR, DO, nitrate, ammonium	0.320
PAR, DO, nitrate, ammonium	0.313
Pressure, temperature, DO, nitrate, ammonium	0.311
Temperature, PAR, nitrate, ammonium	0.309
Pressure, PAR, DO, nitrate, ammonium	0.308
Pressure, temperature, PAR, nitrate, ammonium	0.307
Chl-*a* (0.232); PAR (0.206); pressure (0.184); ammonium (0.181); temperature (0.151); nitrate (0.140); CO_3^{2-} (0.107)	

B. *Emiliania huxleyi* type O (all data: stations 1 to 12)

Environmental variable	r_S
Temperature, salinity, nitrate	0.613
Temperature, nitrate	0.599
CO_3^{2-}, temperature, salinity, nitrate	0.571
Salinity, nitrate	0.563
Temperature, salinity, nitrate, ammonium	0.548
CO_3^{2-}, salinity, nitrate	0.533
Temperature (0.528); nitrate (0.430); salinity (0.392); CO_3^{2-} (0.248); silicate (0.079); PAR (0.057)	

C. *Emiliania huxleyi* type O (NE Pacific and station 9: stations 9 to 12)

Environmental variable	r_S
Temperature, nitrate	0.586
Temperature, salinity, nitrate	0.535
Temperature	0.521
Temperature, nitrate, ammonium	0.519
Temperature, salinity, nitrate, ammonium	0.513
Temperature, PAR, nitrate	0.498
Temperature (0.521); nitrate (0.420); salinity (0.240); PAR (0.207); CO_3^{2-} (0.125); pressure (0.054)	

Table C.15: PART 2 of table C.14

D. *Emiliania huxleyi* type A over-calcified standardized (all data: stations 1 to 12)

Environmental variable	r_S
Temperature, nitrate	0.576
Temperature, nitrate, ammonium	0.542
Nitrate	0.524
Temperature, salinity, nitrate, ammonium	0.523
Temperature, salinity, nitrate	0.510
CO_3^{2-},temperature, salinity, nitrate, ammonium	0.507
Nitrate (0.524); temperature (0.453);CO_3^{2-} (0.246); salinity (0.212); PAR (0.103); silicate (0.092)	

E. *Emiliania huxleyi* type A over-calcified standardized (NE Pacific and station 9: stations 9 to 12)

Environmental variable	r_S
Temperature, nitrate	0.655
Temperature, nitrate, ammonium	0.617
Temperature, PAR, nitrate, ammonium	0.567
Temperature, PAR, nitrate	0.563
CO_3^{2-}, temperature, nitrate, ammonium	0.557
Temperature, nitrate, phosphate, ammonium	0.557
Nitrate (0.534); temperature (0.530); PAR (0.275); CO_3^{2-} (0.209); salinity (0.181); phosphate (0.095)	

F. *Emiliania huxleyi* type A multi-layered standardized (all data, stations 1 to 12; Chl-*a* excluded from the multivariate analysis)

Environmental variable	r_S
CO_2, temperature, PAR	0.402
CO_2, temperature, PAR, silicate	0.399
CO_2, PAR	0.391
CO_2, temperature, PAR, silicate, ammonium	0.390
Temperature, PAR, silicate	0.390
CO_2, temperature	0.385
PAR (0.359); CO_2 (0.337); temperature (0.327); CO_3^{2-} (0.299); silicate (0.281); pressure (0.215)	

G. *Emiliania huxleyi* type A aberrant standardized (all data, stations 1 to 12)

Environmental variable	r_S
CO_2	0.302
CO_2, nitrate	0.269
pH, CO_2, nitrate	0.264
CO_2, nitrate, ammonium	0.264
pH, CO_2, CO_3^{2-}, nitrate	0.260
pH, CO_2	0.259
CO_2 (0.302);CO_3^{2-} (0.205); pH (0.188); DO (0.158); phosphate (0.154); pressure (0.151)	

Table C.16: PART 3 of table C.14

H. *Gephyrocapsa oceanica* (all data: stations 1 to 12)

Environmental variable	r_S
Salinity 0.746	
Temperature, salinity 0.691	
Salinity, nitrite	0.691
Temperature, salinity, nitrite	0.682
Temperature, salinity, Chl-*a*, nitrite	0.678
Temperature, salinity, Chl-*a*	0.670
Salinity (0.746); temperature (0.409); DO (321); Nitrite (0.210), Chl-*a* (148); Silicate (0.123)	

I. *Gephyrocapsa oceanica* (G. Cal and EZ: stations 1 to 9; salinity excluded in the multivariate analysis)

Environmental variable	r_S
Phosphate	0.247
Phosphate, silicate	0.235
Pressure, phosphate, silicate	0.232
Chl-*a*, phosphate	0.229
PAR, phosphate	0.226
Pressure, phosphate	0.221
Phosphate (0.247); silicate (0.176); PAR (0.086); temperature (0.061); Chl-*a* (0.060); salinity (0.058); pressure (0.041)	

J. *Gephyrocapsa muellerae* (all data, stations 1 to 12)

Environmental variable	r_S
Temperature, salinity 0.539	
Temperature, salinity, nitrate	0.503
Salinity 0.471	
CO_3^{2-}, temperature, salinity 0.466	
Temperature	0.460
Salinity, nitrate	0.458
Salinity (0.471); temperature (0.460); CO_3^{2-} (0.147); nitrate (0.138); DO (0.031); PAR (0.001)	

K. *Gephyrocapsa muellerae* (NE Pacific and station 9: stations 9 to 12)

Environmental variable	r_S
Temperature, salinity 0.508	
Temperature, salinity, PAR	0.454
Pressure, temperature, salinity 0.420	
Temperature, salinity, nitrate	0.420
Temperature, salinity, DO 0.409	
Salinity, PAR	0.404
Temperature (0.396); salinity (0.371); PAR (0.172); CO_3^{2-} (0.053); pressure (0.047); DO (0.042)	

Table C.17: Part 3 of table C.14

L. *Gephyrocapsa oceanica* and *G. muellerae* standardized (all data, stations 1 to 12)

Environmental variable	r_S
Salinity	0.793
Temperature, salinity	0.790
Temperature, salinity, Chl-*a*	0.665
Temperature, salinity, DO	0.661
Temperature, salinity, PAR	0.658
CO_3^{2-}, temperature, salinity	0.657
Salinity (0.793); temperature (0.575); DO (0.300); CO_3^{2-} (0.182); pH (0.110); silicate (0.103)	

M. *Gephyrocapsa ericsonii* (all data, stations 1 to 12)

Environmental variable	r_S
Temperature, Chl-*a*, nitrate, nitrite	0.350
Temperature, Chl-*a*, nitrate, nitrite, ammonium	0.347
Temperature, nitrate, nitrite, ammonium	0.342
Temperature, Chl-*a*, nitrate, ammonium	0.332
Temperature, Chl-*a*, nitrate	0.332
Temperature, nitrate, nitrite	0.322
Temperature (0.228); nitrate (0.213); CO_3^{2-} (0.132); nitrite (0.073); pressure (0.069); salinity (0.065)	

N. *Gephyrocapsa ornata* (all data, stations 1 to 12)

Environmental variable	r_S
Temperature, salinity, Chl-*a*, nitrite	0.330
Temperature, salinity, Chl-*a*, nitrite, silicate	0.319
CO_3^{2-}, temperature, salinity, Chl-*a*, nitrite	0.313
Salinity, Chl-*a*, nitrite, silicate	0.306
Temperature, salinity, Chl-*a*, nitrate, nitrite	0.305
CO_3^{2-}, salinity, Chl-*a*, nitrite	0.303
Chl-*a* (0.199); temperature (0.163); salinity(0.150); CO_3^{2-} (0.126); silicate (0.099); nitrite (0.088)	

O. *Gephyrocapsa ornata* (NE Pacific and station 9: stations 9 to 12)

Environmental variable	r_S
Temperature, Chl-*a*, nitrite	0.417
Chl-*a*, nitrite	0.395
pH, temperature, Chl-*a*, nitrite	0.388
Temperature, Chl-*a*, nitrite, silicate	0.380
CO_3^{2-}, Chl-*a*, nitrite	0.379
CO_3^{2-}, temperature, Chl-*a*, nitrite	0.370
CO_2, temperature, Chl-*a*, nitrite	0.370
Nitrite (0.268); Chl-*a* (0.249); CO_3^{2-} (0.103); silicate (0.086); PAR (0.073); DO (0.063); temperature (0.063)	

Table C.18: (PART 1) Extra Spearmans rank correlations (r_S, $p < 0.03$) of *Gephyrocapsa oceanica* and *Emiliania huxleyi* morphotypes (A and O) and morphological categories, versus the environmental variables. The six higher multivariate results with a BEST analysis of maximum 5 variables (r_S shown in the right column) and the six higher univariate results (r_S in brackets) are shown. G. Cal: Gulf of California; EZ: Entrance Zone. PAR: photosynthetic active radiation; Chl-*a*: chlorophyll-*a* concentration; DO: dissolved oxygen; CO_3^{2-}: carbonate ion concentration; CO_2: carbon dioxide concentration.

A. *Gephyrocapsa oceanica* (G. Cal and EZ: stations 1 to 9)

Environmental variable	r_S
Salinity, phosphate, silicate	0.269
Salinity, PAR, phosphate, silicate	0.265
Salinity, PAR, phosphate	0.264
Pressure, salinity, phosphate, silicate	0.261
Salinity, phosphate	0.254
Pressure, salinity, PAR, phosphate, silicate	0.253
Phosphate (0.247); silicate (0.176); PAR (0.086); temperature (0.061); Chl-*a* (0.060); salinity (0.058)	

B. *Emiliania huxleyi* type A (all data: stations 1 to 12)

Environmental variable	r_S
Temperature, Chl-*a*, DO, nitrate, ammonium	0.347
Chl-*a*, PAR, DO, nitrate, ammonium	0.338
Pressure, temperature, Chl-*a*, nitrate, ammonium	0.337
Pressure, Chl-*a*, DO, nitrate, ammonium	0.335
Pressure, Chl-*a*, nitrate, ammonium	0.334
Chl-*a*, DO, nitrate, ammonium	0.332
Chl-*a* (0.232); PAR (0.206); pressure (0.184); ammonium (0.181); temperature (0.151); nitrate (0.140)	

C. *Emiliania huxleyi* type A over-calcified (all data: stations 1 to 12)

Environmental variable	r_S
Temperature, nitrate	0.559
Temperature, nitrate, ammonium	0.525
Temperature, salinity, nitrate, ammonium	0.513
Nitrate	0.509
Temperature, salinity, nitrate	0.504
CO_3^{2-}, temperature, salinity, nitrate, ammonium	0.498
Nitrate (0.509); temperature (0.440);CO_3^{2-} (0.243); salinity (0.218); PAR (0.101); silicate (0.078)	

Table C.19: PART 2 of table C.18

D. *Emiliania huxleyi* type A over-calcified (NE Pacific and station 9: stations 9 to 12)

Environmental variable	r_S
Temperature, nitrate	0.623
Temperature, nitrate, ammonium	0.595
Temperature, PAR, nitrate, ammonium	0.563
Temperature, PAR, nitrate	0.558
Temperature, salinity, nitrate, ammonium	0.555
Temperature, salinity, PAR, nitrate, ammonium	0.546
Temperature (0.519); nitrate (0.493); PAR (0.293); salinity (0.214);CO_3^{2-} (0.209); pressure (0.080)	

E. *Emiliania huxleyi* type A under-calcified (all data: stations 1 to 12)

Environmental variable	r_S
Pressure, temperature, nitrate	0.118
CO_3^{2-}, pressure, temperature, nitrate	0.117
Pressure, temperature	0.114
Pressure, temperature, nitrate	0.111
CO_3^{2-}, pressure, temperature, PAR, nitrate	0.106
CO_3^{2-}, temperature	0.105
CO_3^{2-} (0.097);temperature (0.094);PAR (0.065); pressure (0.058);silicate (0.045);nitrate (0.043)	

F. *Emiliania huxleyi* type A multi-layered (all data, stations 1 to 12)

Environmental variable	r_S
CO_2, temperature, Chl-*a*, PAR, ammonium	0.340
CO_2, pressure, temperature, Chl-*a*, ammonium	0.336
CO_2, pressure, temperature, PAR, ammonium	0.334
CO_2, pressure, Chl-*a*, PAR, ammonium	0.333
CO_2, temperature, PAR, ammonium	0.332
CO_2, pressure, temperature, Chl-*a*, PAR	0.332
CO_2, temperature, Chl-*a*, PAR	0.332
CO_2 (0.319); PAR (0.317); pressure (0.266); CO_3^{2-} (0.253); pH (0.201); DO (0.175)	

Table C.20: PART 3 of table C.18

G. *Emiliania huxleyi* type A multi-layered standardized (all data, stations 1 to 12)

Environmental variable	r_S
CO_2, temperature, Chl-*a*, PAR, silicate	0.454
Temperature, Chl-*a*, PAR, silicate	0.454
CO_2, temperature, Chl-*a*, PAR	0.450
CO_2, temperature, Chl-*a*, silicate	0.447
Temperature, Chl-*a*, PAR	0.444
CO_2, temperature, Chl-*a*	0.440
PAR (0.359); CO_2 (0.337); temperature (0.327); CO_3^{2-} (0.299); silicate (0.281); pressure (0.215)	

H. *Emiliania huxleyi* type A aberrant (all data, stations 1 to 12)

Environmental variable	r_S
CO_2	0.283
pH, CO_2	0.267
pH, CO_2, nitrate	0.264
pH, CO_2, DO, nitrate	0.255
pH, CO_2, CO_3^{2-}	0.255
pH, CO_2, CO_3^{2-}, DO, nitrate	0.253
CO_2 (0.283); pH (0.209); DO (0.185); CO_3^{2-} (0.183); phosphate (0.149); PAR (0.137)	

I. *Emiliania huxleyi* and Gephyrocapsa spp. calcite (all data, stations 1 to 12)

Environmental variable	r_S
Pressure, temperature, PAR, ammonium	0.277
Pressure, temperature, PAR	0.273
Pressure, temperature, PAR, nitrate	0.273
Pressure, temperature, ammonium	0.269
Pressure, temperature, PAR, nitrate, ammonium	0.267
CO_3^{2-}, pressure, temperature, PAR, ammonium	0.266
Temperature, PAR	0.263
Pressure, temperature	0.262
PAR (0.208); pressure (0.207); temperature (0.165); CO_3^{2-} (0.151); Chl-*a* (0.139); nitrate (0.083)	

Table C.21: Linearly correlated hydrographic variables with all coccolithophores and with *Emiliania huxleyi* cell densities. Significant Pearson correlation coefficients (r, alpha = 0.05 (two-tailed test)) are given for all samples and for those in the euphotic zone of the Pacific margin (stations 10 to 12) and of the Gulf of California (G. Cal; stations 1 and 2) and Entrance Zone (EZ; stations 8 and 9).

	All data		Pacific (euphotic zone)		G. Cal and EZ (euphotic zone)	
Biological variable	Hydrographical variable	r	Hydrographical variable	r	Hydrographical variable	r
Coccolithophores	Chl-*a*	0.462	Temperature	-0.632	Chl-*a*	0.694
	Temperature	-0.351	Density	0.615	Depth	0.485
	Total alkalinity	-0.345	PAR %	-0.557		
	Salinity	-0.322	Salinity	-0.521		
	Density	0.322				
E. huxleyi	Chl-*a*	0.537	Chl-*a*	0.666	Chl-*a*	0.773
	Temperature	-0.511	Temperature	-0.574	Density	0.725
	Density	0.487	Density	0.55	Temperature	-0.706
	Salinity	-0.386	Ammonium	0.534	HCO_3^-	0.542
	TA	-0.374			DIC	0.534
	PAR %	-0.369			Depth	0.529
	CO_3^{2-}	-0.342			Phosphate	0.529
	Ammonium	0.31			CO_3^{2-}	-0.511
	N:P	0.299			Nitrite	0.498
					PAR %	-0.449
					CO_2	0.436
E. huxleyi calcite	Chl-*a*	0.541	Temperature	-0.518	Chl-*a*	0.705
	Temperature	-0.418	Chl-*a*	0.495	Density	0.639
	Density	0.412	pCO_2	-0.492	Temperature	-0.632
	PAR %	-0.358	Density	0.484	HCO_3^-	0.482
	Ammonium	0.323			Nitrite	0.475
	Salinity	-0.302			DIC	0.468
					CO_3^{2-}	-0.459
					Phosphate	0.448

Table C.22: Linearly correlated hydrographic variables with the proportion of *Emiliania huxleyi* type A versus type O. Significant Pearson correlation coefficients (r, alpha = 0.05 (two-tailed test))are given for samples from the Pacific margin (stations 10 to 12).

	Pacific (euphotic zone)		Pacific (all data)	
Biological variable	Hydrographical variable	r	Hydrographical variable	r
E.hux. A vs *E.hux.* O	HCO_3^-	-0.809	CO_3^{2-}	0.837
	DIC	-0.804	HCO_3^-	-0.834
	CO_3^{2-}	0.78	DIC	-0.82
	CO_2	-0.757	N:P	-0.781
	Density	-0.684	Density	-0.778
	Temperature	0.665	CO_2	-0.762
	N:P	-0.659	Temperature	0.749
	Nitrate	-0.651	pH	0.718
	Chl-*a*	-0.643	Nitrate	-0.706
	Nitrite	-0.616	Phosphate	-0.705
	Phosphate	-0.598	pCO_2	-0.695
			Depth	-0.67
			Silicate	-0.578

Table C.23: Linearly correlated hydrographic variables with *Gephyrocapsa oceanica* and with its proportion versus *Emiliania huxleyi*. Significant Pearson correlation coefficients (r, alpha = 0.05 (two-tailed test)) are given for samples in the euphotic zone from the Gulf of California (G. Cal; stations 1 and 2) and Entrance Zone (EZ; stations 8 and 9).

	G. Cal and EZ (euphotic zone)	
Biological variable	Hydrographical variable	r
G. oceanica	DIC	-0.689
	HCO_3^-	-0.617
	Phosphate	-0.585
	Density	-0.498
	Silicate	-0.475
	CO_3^{2-}	0.456
	Temperature	0.443
	CO_2	-0.44
	pCO_2	-0.435
	Total alkalinity	-0.427
	pH	0.406
G. oceanica vs *E. huxleyi*	DIC	-0.801
	HCO_3^-	-0.717
	Density	-0.673
	Phosphate	-0.662
	Temperature	0.584
	CO_3^{2-}	0.527
	Total alkalinity	-0.505
	CO_2	-0.502
	pCO_2	-0.481
	Silicate	-0.465
	pH	0.458
	Nitrite	-0.455

Table C.24: Linearly correlated hydrographic variables with the morphotypes of *Emiliania huxleyi* and the morphological levels of calcification of coccoliths. Significant Pearson correlation coefficients (r, alpha = 0.05 (two-tailed test)) are given for samples in the euphotic zone of the Pacific margin (considered as stations 10 to 12) and of the Gulf of California (G. Cal; stations 1 and 2) and Entrance Zone (EZ; stations 8 and 9).

	Pacific (euphotic zone)		G. Cal and EZ (euphotic zone)	
Biological variable	Hydrographical variable	r	Hydrographical variable	r
E. huxleyi type A	Ammonium	0.545	Temperature	-0.616
	Temperature	-0.517	Density	0.656
	Density	0.485	Depth	0.469
			DIC	0.449
			HCO_3^-	0.449
			Ammonium	0.434
			Phosphate	0.423
			Nitrite	0.413
			CO_3^{2-}	-0.405
E. huxleyi type O	HCO_3^-	0.572		
	Temperature	-0.571		
	Density	0.569		
	CO_3^{2-}	-0.563		
	DIC	0.559		
	CO_2	0.514		
% *E. huxleyi* type A under-calcified	PAR %	0.6		
	Density	-0.494		
	Temperature	0.492		
% *E. huxleyi* type A over-calcified	Phosphate	0.726	Temperature	-0.444
	Nitrite	0.672	Density	0.397
	Nitrate	0.672		
	N:P	0.637		
	Density	0.583		
	Temperature	-0.565		
	CO_3^{2-}	-0.514		
	HCO_3^-	0.512		
	DIC	0.487		

Table C.25: Linearly correlated hydrographic variables with the percentage of multi-layered cells of *Emiliania huxleyi* type A. Significant Pearson correlation coefficients (r, alpha = 0.05 (two-tailed test)) are given for samples from the Pacific margin (considered as stations 10 to 12) and from the Gulf of California (G. Cal; stations 1 and 2) and Entrance Zone (EZ; stations 8 and 9).

All data		Pacific (all data)		G. Cal and EZ (all data)	
Hydrographical variable	r	Hydrographical variable	r	Hydrographical variable	r
Temperature	0.629	Density	-0.803	Phosphate	-0.387
Density	-0.626	Temperature	0.785		
N:P	-0.571	CO_3^{2-}	0.721		
Silicate	-0.51	HCO_3^-	-0.698		
CO_3^{2-}	0.51	N:P	-0.676		
Nitrate	-0.493	DIC	-0.668		
HCO_3^-	-0.443	Phosphate	-0.619		
CO_2	-0.423	CO_2	-0.594		
Depth	-0.403	Nitrate	-0.579		
Phosphate	-0.386	Silicate	-0.553		
DIC	-0.361	Depth	-0.519		
Salinity	0.33	pCO_2	-0.516		
Total alkalinity	0.323	Chl-a	-0.456		
		Total alkalinity	0.47		
		pH	0.537		

Table C.26: (PART 1) Estimated particulate inorganic carbon (PIC) from the calcite estimated on the alkenone-producing coccolithophores (*E. huxleyi* and the *Gephyrocapsa* species), and the particulate organic carbon (POC) reported by Wolhowe et al. (2014) for the corresponding water samples. The depth reported by Wolhowe et al. (2014) for POC is shown, both with their reported standard deviations. *Station 2 was sampled at two different dates, as described in Table C.1.

Station-depth [m]	PIC [$\mu g\,L^{-1}$]	Depth [m]	SD	POC [$\mu g\,L^{-1}$]	SD	PIC : POC
1-5	0.06					
1-10	0.02					
1-15	0.03	15.76	3.33	68.10	12.53	0.000
1-20	0.05	25.41	5.09	85.16	16.11	0.001
1-30	0.18	29.97	4.49	125.66	23.77	0.001
1-35	0.15	35.32	6.02	175.67	33.22	0.001
1-40	0.19	40.41	6.50	123.85	23.42	0.002
1-50	0.07	49.77	6.62	85.75	16.22	0.001
1-70	0.03					
2-0	0.63	6.13	3.86	74.76	2.50	0.008
2-10	0.56	10.13	5.44	82.74	17.02	0.007
2-20	0.55	20.86	7.03	56.14	21.14	0.010
2-25	0.48	24.32	7.50	98.47	29.90	0.005
2-30	0.31	31.82	7.43	71.84	12.16	0.004
2-35	0.11	34.72	6.76	76.36	5.39	0.001
2-50	0.08	48.89	6.37	37.39	6.50	0.002
2*-0	0.24	8.29	1.85	59.17	8.57	0.004
2*-20	0.16	22.20	2.65	59.43	4.82	0.003
2*-35	0.37	35.65	2.40	103.05	3.29	0.004
2*-50	0.25	53.76	2.74	63.86	24.86	0.004
2*-70	0.10	68.28	3.59	42.66	8.87	0.002
2*-100	0.05	93.95	3.33	32.69	4.74	0.002
8-0	0.69	7.45	1.22	57.69	4.44	0.012
8-10	0.56	10.12	2.39	56.74	3.35	0.010
8-20	0.69	20.93	3.41	62.01	2.86	0.011
8-30	0.92	30.17	4.53	61.55	9.26	0.015
8-40	0.68	40.58	7.78	55.12	4.70	0.012
8-50	0.99	49.91	7.78	64.31	2.13	0.015
8-70	0.14	70.71	7.73	43.30	3.69	0.003
8-100	0.02	102.80	3.05	24.46	1.26	0.001
9-0	0.01	7.58	1.18	63.66	11.70	0.000
9-10	0.04	10.26	1.34	48.34	3.80	0.001
9-20	0.04	18.81	2.87	63.57	1.81	0.001
9-25	0.12	27.01	2.50	74.96	0.22	0.002
9-30	0.32	30.61	2.43	63.79	2.69	0.005
9-35	0.09	35.77	2.85	85.51	18.79	0.001
9-40	0.23	51.34	3.39	57.85	7.39	0.004
9-50	0.18	56.11	3.75	51.64	7.44	0.003
9-70	0.04	72.20	3.79	32.65	6.80	0.001
9-100	0.01					

Table C.27: (PART 2) Estimated particulate inorganic carbon (PIC) from the calcite estimated on the alkenone-producing coccolithophores (*E. huxleyi* and the *Gephyrocapsa* species), and the particulate organic carbon (POC) reported by Wolhowe et al. (2014) for the corresponding water samples. The depth reported by Wolhowe et al. (2014) for POC is shown, both with their reported standard deviations.

Station-depth [m]	PIC [μg L^{-1}]	Depth [m]	SD	POC [μg L^{-1}]	SD	PIC : POC
10-0	0.02	9.49	2.98	50.51	3.19	0.000
10-10	0.02	12.29	2.67	45.55	3.74	0.000
10-20	0.06	20.16	1.86	55.58	5.93	0.001
10-30	0.11	30.49	2.65	66.04	7.09	0.002
10-35	0.09	37.38	2.53	101.65	10.85	0.001
10-40	0.08	42.69	2.53	96.49	10.75	0.001
10-50	0.14	49.74	3.28	85.50	17.10	0.002
10-70	0.31	70.10	4.24	42.54	4.54	0.007
10-100	0.03	105.45	3.77	16.23	0.28	0.002
11-0	0.07	2.98	2.81	59.93	8.24	0.001
11-10	0.05	8.48	1.46	62.13	7.89	0.001
11-20	0.08	21.39	2.34	80.07	7.41	0.001
11-35	0.35	35.37	3.98	77.11	4.10	0.005
11-50	0.24	49.84	5.51	95.72	8.85	0.003
11-60	0.31	59.77	5.18	62.23	5.03	0.005
11-70	0.44	66.87	5.09	40.31	4.88	0.011
11-100	0.02	102.19	4.81	21.95	2.03	0.001
12-0	0.20					
12-5	0.17	8.06	3.85	134.61	16.20	0.001
12-10	0.35	14.97	4.44	134.22	13.23	0.003
12-20	0.22	21.49	3.57	129.35	12.89	0.002
12-25	0.17	26.24	4.04	178.88	7.92	0.001
12-30	0.21	30.21	4.76	126.71	10.86	0.002
12-35	0.10	35.48	3.55	98.66	8.55	0.001
12-40	0.25	40.43	3.18	76.17	7.21	0.003
12-50	0.19	52.73	3.94	42.13	2.08	0.005
12-70	0.13	72.05	3.97	33.12	7.69	0.004
12-100	0.09	90.91	3.54	27.47	2.97	0.003

Table C.28: Estimation of the particulate inorganic carbon production rate (PR PIC) using the scanning electronic microscope (SEM) results got from the attached coccoliths and using three different possible numbers of total coccoliths per cell for *E. huxleyi* (Rosas-Navarro et al., 2016); 40, 45, and 50 coccoliths per cell. The growth rates (μ) for the PR PIC were calculated from the cell production rate (data from Wolhowe et al. (2014) for the corresponding water samples) and the cell density of the alkenone-producing coccolithophores (*E. huxleyi* and the *Gephyrocapsa* species). Results were obtained for stations 1, 2, 8, and 12. The used depths from Wolhowe et al. (2014) are shown. The difference with the SEM results are shown in absolute numbers and in percentage. The total average with the standard deviation and standard error are shown.

Station-depth [m]	Depth (from Wolhowe et al. 2014)	μ (d^{-1})	PR PIC [$\mu g\ L^{-1}\ d^{-1}$] (SEM)	PR PIC (40)	PR PIC difference (40)	PR PIC % difference (40)	PR PIC (45)	PR PIC difference (45)	PR PIC % difference (45)	PR PIC (50)	PR PIC difference (50)	PR PIC % difference (50)
1-15	15.76	0.49	0.01	0.02	0.01	41%	0.03	0.01	47%	0.03	0.01	51%
1-20	25.41	0.48	0.03	0.05	0.03	51%	0.06	0.03	56%	0.07	0.04	61%
1-35	33.00	0.38	0.05	0.11	0.05	48%	0.12	0.06	53%	0.13	0.07	58%
1-40	42.64	0.20	0.04	0.06	0.02	33%	0.06	0.02	38%	0.07	0.03	42%
1-50	46.62	0.11	0.01	0.01	0.00	20%	0.01	0.00	24%	0.01	0.00	27%
2-10	10.13	0.17	0.10	0.10	0.00	4%	0.10	0.01	6%	0.11	0.01	7%
2-20	20.86	0.20	0.11	0.12	0.01	11%	0.12	0.02	14%	0.13	0.02	17%
2-30	31.82	0.27	0.08	0.11	0.02	21%	0.11	0.03	25%	0.12	0.03	29%
2-35	38.83	0.32	0.03	0.05	0.01	30%	0.05	0.02	35%	0.06	0.02	39%
2-50	46.72	0.23	0.02	0.02	0.00	21%	0.02	0.01	25%	0.02	0.01	29%
8-10	8.16	0.19	0.11	0.11	0.00	0%	0.11	0.00	1%	0.11	0.00	1%
8-20	20.74	0.17	0.12	0.12	0.00	1%	0.12	0.00	1%	0.12	0.00	1%
8-30	32.63	0.16	0.15	0.15	0.00	3%	0.15	0.01	4%	0.15	0.01	5%
8-40	37.39	0.14	0.09	0.10	0.00	2%	0.10	0.00	3%	0.10	0.00	3%
8-50	55.57	0.06	0.06	0.06	0.00	4%	0.06	0.00	5%	0.06	0.00	6%
12-5	8.06	0.36	0.06	0.10	0.04	41%	0.11	0.05	46%	0.12	0.06	50%
12-10	14.97	0.38	0.13	0.22	0.09	42%	0.25	0.12	47%	0.27	0.14	51%
12-20	21.49	0.09	0.02	0.04	0.02	50%	0.05	0.03	55%	0.05	0.03	59%
12-25	24.42	0.03	0.00	0.01	0.00	46%	0.01	0.01	51%	0.01	0.01	55%
12-30	27.85	0.05	0.01	0.02	0.01	52%	0.02	0.01	56%	0.02	0.01	60%
12-35	32.70	0.02	0.00	0.00	0.00	45%	0.00	0.00	50%	0.00	0.00	54%
12-40	40.64	0.01	0.00	0.00	0.00	51%	0.01	0.00	55%	0.01	0.00	59%
12-50	50.49	0.01	0.00	0.00	0.00	40%	0.00	0.00	45%	0.00	0.00	49%
AVE		0.20	0.05	0.07	0.02	29%	0.07	0.02	32%	0.08	0.02	35%
SD		0.15	0.05	0.06	0.02	19%	0.06	0.03	21%	0.06	0.03	22%
SDERR		0.03	0.01	0.01	0.00	4%	0.01	0.01	4%	0.01	0.01	5%

List of Figures

List of Tables

Bibliography

Acker, J. G. and Leptoukh, G.: Online analysis enhances use of NASA earth science data, Eos, Transactions American Geophysical Union, 88, 14–17, 2007.

Álvarez, M. C., Flores, J. A., Sierro, F. J., and Molina-Cruz, A.: Long-term upwelling evolution in tropical and equatorial Pacific during the last 800kyr as revealed by coccolithophore assemblages, Geobios, 43, 123–130, doi:10.1016/j.geobios.2009.07.001, URL http://linkinghub.elsevier.com/retrieve/pii/S0016699509000874, 2010a.

Álvarez, M. C., Flores, J. A., Sierro, F. J., and Molina-cruz, A.: The coccolithophore record for the last 11 000 years in the Gulf of California, Journal of Marine Systems, 80, 184–190, doi:10.1016/j.jmarsys.2009.10.008, URL http://linkinghub.elsevier.com/retrieve/pii/S0924796309002966http://dx.doi.org/10.1016/j.jmarsys.2009.10.008, 2010b.

Bach, L. T., Bauke, C., Meier, K. J. S., Riebesell, U., and Schulz, K. G.: Influence of changing carbonate chemistry on morphology and weight of coccoliths formed by *Emiliania huxleyi*, Biogeosciences, 9, 3449–3463, doi:10.5194/bg-9-3449-2012, URL http://www.biogeosciences.net/9/3449/2012/, 2012a.

Bach, L. T., Riebesell, U., Sett, S., Febiri, S., Rzepka, P., and Schulz, K. G.: An approach for particle sinking velocity measurements in the 3–400μm size range and considerations on the effect of temperature on sinking rates, Marine Biology, 159, 1853–1864, doi:10.1007/s00227-012-1945-2, URL http://dx.doi.org/10.1007/s00227-012-1945-2, 2012b.

Badan-Dangon, A.: Coastal circulation from the Galápagos to the Gulf of California, in: The Sea, edited by Robinson, A. R. and Brink, K. H., vol. 11, pp. 315–343, John Wiley and Sons, Inc., 1998.

Badan-Dangon, A., Robles, J., and Garcia, J.: Coastal and Estuarine Studies: Poleward Flows Along Eastern Ocean Boundaries, vol. 34, chap. Poleward flows off Mexico's Pacific coast, pp. 176–202, Springer, 1989.

Balch, W. M., Holligan, P. M., and Kilpatrick, K. A.: Calcification, photosynthesis and growth of the bloom-forming coccolithophore, *Emiliania huxleyi*, Conti-

nental Shelf Research, 12, 1353–1374, URL http://www.sciencedirect.com/science/article/pii/027843439290059S, 1992.

Barker, S., Higgins, J. A., and Elderfield, H.: The future of the carbon cycle: review, calcification response, ballast and feedback on atmospheric CO_2, Philosophical Transactions of the Royal Society of London Series A, 361, 1977–1999, doi:0.1098/rsta.2003.1238, 2003.

Baumann, F. G., Isenberg, H. D., and Gennaro, J.: The Inverse Relationship Between Nutrient Nitrogen Concentration and Coccolith Calcification in Cultures of the Coccolithophorid *Hymenomonas sp.*, Journal of Protozoology, 25, 253–256, doi:10.1111/j.1550-7408.1978.tb04408.x, URL http://doi.wiley.com/10.1111/j.1550-7408.1978.tb04408.x, 1978.

Baumann, K.-H., Čepek, M., and Kinkel, H.: Coccolithophores as indicators of ocean water masses, surface-water temperature, and paleoproductivityexamples from the South Atlantic, in: Use of Proxies in Paleoceanography: Examples from the South Atlantic, edited by Fischer, G. and Wefer, G., pp. 117–144, Springer-Verlag, Berlin Heidelberg, doi:10.1007/978-3-642-58646-0_4, URL http://dx.doi.org/10.1007/978-3-642-58646-0_4, 1999.

Beaufort, L.: Weight estimates of coccoliths using the optical properties (birefringence) of calcite, Micropaleontology, 51, 289–297, URL http://www.jstor.org/stable/4097062, 2005.

Beaufort, L. and Dollfus, D.: Automatic recognition of coccoliths by dynamical neural networks, Marine Micropaleontology, 51, 57–73, 2004.

Beaufort, L., Couapel, M., Buchet, N., Claustre, H., and Goyet, C.: Calcite production by coccolithophores in the south east Pacific Ocean, Biogeosciences, 5, 1101–1117, 2008.

Beaufort, L., Probert, I., de Garidel-Thoron, T., Bendif, E. M., Ruiz-Pino, D., Metzl, N., Goyet, C., Buchet, N., Coupel, P., Grelaud, M., Rost, B., Rickaby, R. E. M., and de Vargas, C.: Sensitivity of coccolithophores to carbonate chemistry and ocean acidification, Nature, 476, 80–83, doi:10.1038/nature10295, URL http://www.ncbi.nlm.nih.gov/pubmed/21814280, 2011.

Benner, I.: The utilization of organic nutrients in marine phytoplankton with emphasis on coccolithophores, Ph.D. thesis, University of Bremen, 2008.

Bollmann, J.: Morphology and biogeography of Gephyrocapsa coccoliths in Holocene sediments, Marine Micropaleontology, 29, 319–350, doi:10.1016/S0377-8398(96)00028-X, URL http://linkinghub.elsevier.com/retrieve/pii/S037783989600028X, 1997.

Bollmann, J., Cortés, M. Y., Haidar, A. T., Brabec, B., Close, A., Hofmann, R., Palma, S., Tupas, L., and Thierstein, H. R.: Techniques for quantitative analyses of calcareous marine phytoplankton, Marine Micropaleontology, 44, 163–185, 2002.

Bollmann, J., Herrle, J. O., Cortés, M., and Fielding, S. R.: The effect of sea water salinity on the morphology of *Emiliania huxleyi* in plankton and sediment samples, Earth and Planetary Science Letters, 284, 320–328, doi:10.1016/j.epsl.2009.05.003, URL http://linkinghub.elsevier.com/retrieve/pii/S0012821X0900274X, 2009.

Bolton, C. T., Hernández-Sánchez, M. T., Fuertes, M.-A., González-Lemos, S., Abrevaya, L., Mendez-Vicente, A., Flores, J.-A., Probert, I., Giosan, L., Johnson, J., et al.: Decrease in coccolithophore calcification and CO2 since the middle Miocene, Nature communications, 7, 10 284, 2016.

Bopp, L., Resplandy, L., Orr, J. C., Doney, S. C., Dunne, J. P., Gehlen, M., Halloran, P., Heinze, C., Ilyina, T., Seferian, R., et al.: Multiple stressors of ocean ecosystems in the 21st century: projections with CMIP5 models, Biogeosciences, 10, 6225–6245, 2013.

Bown, P.: Calcareous nannofossil biostratigraphy, British Micropalaeontological Society Publication Series. Chapman and Hall; Kluwer Academic: London., 1998.

Bown, P. R., Lees, J. A., and Young, J. R.: Calcareous nannoplankton evolution and diversity through time, in: Coccolithophores, pp. 481–508, Springer, 2004.

Boyd, P. W. and Doney, S. C.: Modelling regional responses by marine pelagic ecosystems to global climate change, Geophysical Research Letters, 29, 2002.

Bradshaw, A. L., Brewer, P. G., Shafer, D. K., and Williams, R. T.: Measurements of total carbon dioxide and alkalinity by potentiometric titration in the GEOSECS program, Earth and Planetary Science Letters, 55, 99–115, 1981.

Brewer, P., Bradshaw, A., and Williams, R.: Measurements of Total Carbon Dioxide and Alkalinity in the North Atlantic Ocean in 1981, in: The Changing Carbon Cycle, edited by Trabalka, J. and Reichle, D., pp. 348–370, Springer New York, doi:10.1007/978-1-4757-1915-4_18, URL http://dx.doi.org/10.1007/978-1-4757-1915-4_18, 1986.

Broerse, A., Ziveri, P., and Honjo, S.: Coccolithophore (–CaCO 3) flux in the Sea of Okhotsk: seasonality, settling and alteration processes, Marine Micropaleontology, 39, 179–200, 2000.

Brown, C.: Global Distribution of Coccolithophore Blooms, Oceanography, 8, 59–60, doi:10.5670/oceanog.1995.21, URL http://www.tos.org/oceanography/archive/8-2_brown.html, 1995.

Brown, C. W. and Yoder, J. A.: Coccolithophorid blooms in the global ocean, Journal of Geophysical Research: Oceans, 99, 7467–7482, 1994.

Brownlee, C. and Taylor, A.: Coccolithophores: From Molecular Processes to Global Impact, chap. Calcification in coccolithophores: A cellular perspective, pp. 31–49, Springer Berlin Heidelberg, Berlin, Heidelberg, doi:10.1007/978-3-662-06278-4_2, URL http://dx.doi.org/10.1007/978-3-662-06278-4_2, 2004.

Buitenhuis, E., Van Bleijswijk, J., Bakker, D., and Veldhuis, M.: Trends in inorganic and organic carbon in a bloom of *Emiliania huxleyi* in the North Sea, Marine Ecology Progress Series, 143, 271–282, 1996.

Buitenhuis, E. T., Pangerc, T., Franklin, D. J., Le Quéré, C., and Malin, G.: Growth rates of six coccolithophorid strains as a function of temperature, Limnology and Oceanography, 53, 1181–1185, doi:10.4319/lo.2008.53.3.1181, URL http://doi.wiley.com/10.4319/lo.2008.53.3.1181, 2008.

Burns, D. a.: Phenotypes and dissolution morphotypes of the genus Gephyrocapsa kamptner and *Emiliania huxleyi* (Lohmann), New Zealand Journal of Geology and Geophysics, 20, 143–155, doi:10.1080/00288306.1977.10431596, URL http://www.tandfonline.com/doi/abs/10.1080/00288306.1977.10431596, 1977.

Caldeira, K. and Wickett, M. E.: Oceanography: anthropogenic carbon and ocean pH, Nature, 425, 365–365, 2003.

Cermeño, P., Dutkiewicz, S., Harris, R. P., Follows, M., Schofield, O., and Falkowski, P. G.: The role of nutricline depth in regulating the ocean carbon cycle, Proceedings of the National Academy of Sciences, 105, 20 344–20 349, doi:10.1073/pnas.0811302106, URL http://www.pnas.org/content/105/51/20344.abstract, 2008.

Charalampopoulou, A., Poulton, A. J., Bakker, D. C., Lucas, M. I., Stinchcombe, M. C., and Tyrrell, T.: Environmental drivers of coccolithophore abundance and calcification across Drake Passage (Southern Ocean), Biogeosciences, 13, 5917, 2016.

Clarke, K. and Ainsworth, M.: A method of linking multivariate community, Marine ecology progress series, 92, 205–219, 1993.

Clarke, K. and Gorley, R.: PRIMER v6: user manual/tutorial (Plymouth routines in multivariate ecological research), Plymouth: Primer-E Ltd, 2006.

Collins, C., Ivanov, L., and Mel'nichenko, O.: Seasonal variability of the California Undercurrent: Statistical analysis based on the trajectories of floats with neutral buoyancy, Physical Oceanography, 13, 135–147, 2003.

Cros i Miguel, M. L.: Planktonic coccolithophores of the NW Mediterranean, Ph.D. thesis, Universitat de Barcelona, 2001.

Cubillos, J. C., Wright, S. W., Nash, G., de Salas, M. F., Griffiths, B., Tilbrook, B., Poisson, A., and Hallegraeff, G. M.: Calcification morphotypes of the coccolithophorid *Emiliania huxleyi* in the Southern Ocean: changes in 2001 to 2006 compared to historical data, Marine Ecology Progress Series, 348, 47–54, 2007.

De Bodt, C., Van Oostende, N., Harlay, J., Sabbe, K., and Chou, L.: Individual and interacting effects of pCO_2 and temperature on *Emiliania huxleyi* calcification: study of the calcite production, the coccolith morphology and the coccosphere size, Biogeosciences, 7, 1401–1412, doi:10.5194/bg-7-1401-2010, URL http://www.biogeosciences.net/7/1401/2010/, 2010.

de Vrind-de Jong, E. W. and de Vrind, J. P.: Algal deposition of carbonates and silicates, Reviews in Mineralogy and Geochemistry, 35, 267–307, 1997.

Dickson, A. and Millero, F.: A comparison of the equilibrium constants for the dissociation of carbonic acid in seawater media, Deep Sea Research Part A. Oceanographic Research Papers, 34, 1733–1743, doi:10.1016/0198-0149(87)90021-5, URL http://www.sciencedirect.com/science/article/pii/0198014987900215, 1987.

Dickson, A. and Riley, J.: The estimation of acid dissociation constants in seawater media from potentionmetric titrations with strong base. I. The ionic product of waterK w, Marine Chemistry, 7, 89–99, 1979.

Dimiza, M. D., Triantaphyllou, M. V., Malinverno, E., Psarra, S., Karatsolis, B., Mara, P., Lagaria, A., and Gogou, A.: The composition and distribution of living coccolithophores in the Aegean Sea (NE Mediterranean), Micropaleontology, 61, 521–540, 2015.

Dixon, H. H.: On the Structure of Coccospheres and the Origin of Coccoliths, Proceedings of the Royal Society of London, 66, 305–315, URL http://www.jstor.org/stable/116068, 1900.

Dollfus, D. and Beaufort, L.: Fat neural network for recognition of position-normalised objects, Neural Networks, 12, 553 – 560, doi:http://dx.doi.org/10.1016/S0893-6080(99)00011-8, URL http://www.sciencedirect.com/science/article/pii/S0893608099000118, 1999.

Doney, S. C., Fabry, V. J., Feely, R. a., and Kleypas, J. a.: Ocean acidification: the other CO_2 problem, Annual review of marine science, 1, 169–92, doi:10.1146/annurev.marine.010908.163834, URL http://www.ncbi.nlm.nih.gov/pubmed/21141034, 2009.

Edvardsen, B., Eikrem, W., Green, J., Andersen, R. A., Moon-van der Staay, S. Y., and Medlin, L. K.: Phylogenetic reconstructions of the Haptophyta inferred from 18S ribosomal DNA sequences and available morphological data, Phycologia, 39, 19–35, 2000.

Eppley, R. W., Rogers, J. N., and McCarthy, J. J.: Half-saturation constants for uptake of nitrate and ammonium by marine phytoplankton, Limnology and Oceanography, 14, 912–920, 1969.

Feely, R. A., Sabine, C. L., Hernandez-Ayon, J. M., Ianson, D., and Hales, B.: Evidence for upwelling of corrosive acidified water onto the continental shelf, Science, 320, 1490–1492, doi:10.1126/science.1155676, URL http://www.sciencemag.org/cgi/content/abstract/320/5882/1490, 2008.

Feng, Y., Warner, M. E., Zhan, Y., Sun, J., Fu, F., Rose, J. M., and Hutchins, D. A.: Interactive effects of increased pCO_2, temperature and irradiance on the marine coccolithophore *Emiliania huxleyi* (Prymnesiophyceae), European Journal of Phycology, 43, 87–98, doi:10.1080/09670260701664674, 2008.

Fichtinger-Schepman, A. M. J., Kamerling, J. P., Versluis, C., and Vliegenthart, J. F.: Structural studies of the methylated, acidic polysaccharide associated with coccoliths of *Emiliania huxleyi* (lohmann) kamptner, Carbohydrate research, 93, 105–123, 1981.

Findlay, C. and Giraudeau, J.: Extant calcareous nannoplankton in the Australian Sector of the Southern Ocean (austral summers 1994 and 1995), Marine Micropaleontology, 40, 417–439, doi:10.1016/S0377-8398(00)00046-3, URL http://www.sciencedirect.com/science/article/pii/S037783980000463http://linkinghub.elsevier.com/retrieve/pii/S0377839800000463, 2000.

Findlay, H. S., Calosi, P., and Crawfurd, K.: Determinants of the PIC : POC response in the coccolithophore *Emiliania huxleyi* under future ocean acidification scenarios, Limnology and Oceanography, 56, 1168–1178, doi:10.4319/lo.2011.56.3.1168, 2011.

Gerecht, A., Šupraha, L., Edvardsen, B., Langer, G., and Henderiks, J.: Phosphorus availability modifies carbon production in *Coccolithus pelagicus* (Haptophyta), Journal of Experimental Marine Biology and Ecology, 472, 24–31, 2015.

Gerecht, A. C., Šupraha, L., Edvardsen, B., Probert, I., and Henderiks, J.: High temperature decreases the PIC / POC ratio and increases phosphorus requirements in *Coccolithus pelagicus* (Haptophyta), Biogeosciences, 11, 3531–3545, 2014.

Gibbs, S. J., Poulton, A. J., Bown, P. R., Daniels, C. J., Hopkins, J., Young, J. R., Jones, H. L., Thiemann, G. J., O'Dea, S. A., and Newsam, C.: Species-specific growth response of coccolithophores to Palaeocene-Eocene environmental change, Nature Geoscience, 6, 218–222, doi:10.1038/ngeo1719, 2013.

Giraudeau, J., Monteiro, P. M., and Nikodemus, K.: Distribution and malformation of living coccolithophores in the northern Benguela upwelling system off Namibia, Marine Micropaleontology, 22, 93–110, doi:10.1016/0377-8398(93)90005-I, URL http://linkinghub.elsevier.com/retrieve/pii/037783989390005I, 1993.

Gran, G.: Determination of the equivalence point in potentiometric titrations of seawater with hydrochloric acid, Oceanol. Acta, 5, 209–218, 1952.

Gravalosa, J. M., Flores, J.-A., Sierro, F. J., and Gersonde, R.: Sea surface distribution of coccolithophores in the eastern Pacific sector of the Southern Ocean (Bellingshausen and Amundsen Seas) during the late austral summer of 2001, Marine Micropaleontology, 69, 16–25, doi:10.1016/j.marmicro.2007.11.006, URL http://linkinghub.elsevier.com/retrieve/pii/S037783980800042X, 2008.

Grelaud, M., Schimmelmann, A., and Beaufort, L.: Coccolithophore response to climate and surface hydrography in Santa Barbara Basin, California, AD 1917–2004, Biogeosciences, 6, 2025–2039, doi:10.5194/bg-6-2025-2009, URL http://www.biogeosciences.net/6/2025/2009/, 2009.

Guan, W. and Gao, K.: Enhanced calcification ameliorates the negative effects of UV radiation on photosynthesis in the calcifying phytoplankter *Emiliania huxleyi*, Chinese Science Bulletin, 55, 588–593–, URL http://dx.doi.org/10.1007/s11434-010-0042-5, 2010.

Guillard, R. R. and Ryther, J. H.: Studies of marine planktonic diatoms. I. Cyclotella nana Hustedt, and Detonula confervacea (cleve) Gran., Canadian journal of microbiology, 8, 229–239, 1962.

Hagino, K. and Okada, H.: Intra- and infra-specific morphological variation in selected coccolithophore species in the equatorial and subequatorial Pacific Ocean, Marine Micropaleontology, 58, 184–206, 2006.

Hagino, K., Okada, H., and Matsuoka, H.: Coccolithophore assemblages and morphotypes of *Emiliania huxleyi* in the boundary zone between the cold Oyashio and warm Kuroshio currents off the coast of Japan, Marine Micropaleontology, 55, 19–47, doi:10.1016/j.marmicro.2005.02.002, URL http://linkinghub.elsevier.com/retrieve/pii/S0377839805000149, 2005.

Hagino, K., Bendif, E. M., Young, J. R., Kogame, K., Probert, I., Takano, Y., Horiguchi, T., de Vargas, C., and Okada, H.: New evidence for morphological and genetic variation in the cosmopolitan coccolithophore *Emiliania huxleyi* (Prymnesiophyceae) from the COX1b-ATP4 GENES1, Journal of Phycology, 47, 1164–1176, doi:10.1111/j.1529-8817.2011.01053.x, URL http://doi.wiley.com/10.1111/j.1529-8817.2011.01053.x, 2011.

Harada, N., Sato, M., Oguri, K., Hagino, K., Okazaki, Y., Katsuki, K., Tsuji, Y., Shin, K.-H., Tadai, O., Saitoh, S.-I., Narita, H., Konno, S., Jordan, R. W., Shiraiwa, Y., and Grebmeier, J.: Enhancement of coccolithophorid blooms in the Bering Sea by recent environmental changes, Global Biogeochemical Cycles, 26, n/a–n/a, doi:10.1029/2011GB004177, URL http://dx.doi.org/10.1029/2011GB004177, gB2036, 2012.

Heinle, M.: The effects of light, temperature and nutrients on coccolithophores and implications for biogeochemical models, Ph.D. thesis, University of East Anglia, School of Environmental Sciences, Norwich, UK, 2014.

Henderiks, J., Winter, a., Elbrächter, M., Feistel, R., der Plas, A., Nausch, G., and Barlow, R.: Environmental controls on *Emiliania huxleyi* morphotypes in the Benguela coastal upwelling system (SE Atlantic), Marine Ecology Progress Series, 448, 51–66, doi:10.3354/meps09535, URL http://www.int-res.com/abstracts/meps/v448/p51-66/, 2012.

Henriksen, K., Stipp, S., Young, J., and Bown, P.: Tailoring calcite: Nanoscale AFM of coccolith biocrystals, American Mineralogist, 88, 2040–2044, 2003.

Henriksen, K., Stipp, S. L. S., Young, J. R., and Marsh, M. E.: Polysaccharides in coccolith biomineralization: Site-specific interaction with the calcite surface., Geochimica et Cosmochimica Acta, 68, A202, 2004.

Hernández-Becerril, D. U.: Vertical distribution of phytoplankton in the central and northern part of the Gulf of California (June 1982), Marine Ecology, 8, 237–251, 1987.

Hernández-Becerril, D. U., Bravo-Sierra, E., and Aké-Castillo, J. A.: Phytoplankton on the western coasts of Baja California in two different seasons in 1998, Scientia Marina, 71, 735–743, 2007.

Hickey, B. M.: Coastal oceanography of western North America from the tip of Baja California to Vancouver Island, in: The Global Coastal Ocean - Multiscale interdisciplinary processes, edited by Robinson, A. R. and Brink, K. H., vol. 11 Regional Studies and Synthesis, chap. 12, pp. 345–393, Harvard University Press, Cambridge, Massachusetts and London, 1998.

Hoffmann, R., Kirchlechner, C., Langer, G., Wochnik, A. S., Griesshaber, E., Schmahl, W. W., and Scheu, C.: Insight into *Emiliania huxleyi* coccospheres by focused ion beam sectioning, Biogeosciences, 12, 825–834, doi:10.5194/bg-12-825-2015, URL http://www.biogeosciences.net/12/825/2015/bg-12-825-2015.html, 2015.

Holligan, P. M., Fernández, E., Aiken, J., Balch, W. M., Boyd, P., Burkill, P. H., Finch, M., Groom, S. B., Malin, G., Muller, K., Purdie, D. A., Robinson, C., Trees, C. C., Turner, S. M., and van der Wal, P.: A biogeochemical study of the

coccolithophore, *Emiliania huxleyi*, in the North Atlantic, Global Biogeochem. Cycles, 7, 879–900, URL http://dx.doi.org/10.1029/93GB01731, 1993.

Holtz, L.-M., Langer, G., Rokitta, S., and Thoms, S.: Synthesis of nanostructured calcite particles in coccolithophores, unicellular algae, doi:10.1079/9781780642239.0132, 2013.

Honjo, S.: Coccoliths: Production, transportation and sedimentation, Marine Micropaleontology, 1, 65–79, doi:10.1016/0377-8398(76)90005-0, URL http://www.sciencedirect.com/science/article/pii/0377839876900050, 1976.

Hoppe, C. J. M., Langer, G., and Rost, B.: *Emiliania huxleyi* shows identical responses to elevated pCO_2 in TA and DIC manipulations, Journal of Experimental Marine Biology and Ecology, 406, 54–62, doi:10.1016/j.jembe.2011.06.008, URL http://linkinghub.elsevier.com/retrieve/pii/S002209811100267X, 2011.

Horigome, M. T., Ziveri, P., Grelaud, M., Baumann, K.-H., Marino, G., and Mortyn, P. G.: Environmental controls on the *Emiliania huxleyi* calcite mass, Biogeosciences, 11, 2295–2308, doi:10.5194/bg-11-2295-2014, URL http://www.biogeosciences.net/11/2295/2014/, 2014.

Hutchins, D. A.: Oceanography: forecasting the rain ratio, Nature, 476, 41, 2011.

Iglesias-Rodríguez, M. D., Schofield, O. M., Batley, J., Medlin, L. K., and Hayes, P. K.: Intraspecific genetic diversity in the marine coccolithophore *Emiliania huxleyi* (Prymnesiophyceae): The use of microsatellite analysis in marine phytoplankton population studies, Journal of Phycology, 42, 526–536, 2006.

IglesiasRodríguez, M. D., Sáez, A. G., Groben, R., Edwards, K. J., Batley, J., Medlin, L. K., and Hayes, P. K.: Polymorphic microsatellite loci in global populations of the marine coccolithophorid *Emiliania huxleyi*, Molecular Ecology Notes, 2, 495–497, 2002.

IPCC: Climate Change 2013: The Physical Science Basis. Contribution of Working Group I to the Fifth Assessment Report of the Intergovernmental Panel on Climate Change, 1535, Cambridge University Press, Cambridge, United Kingdom and New York, NY, USA, 2013.

Jin, P., Gao, K., and Beardall, J.: Evolutionary responses of a coccolithophorid *Gephyrocapsa oceanica* to ocean acidification, Evolution, 67, 1869–1878, doi:10.1111/evo.12112, URL http://dx.doi.org/10.1111/evo.12112, 2013.

Jordan, R. and Chamberlain, A.: Biodiversity among haptophyte algae, Biodiversity & Conservation, 6, 131–152, 1997.

Jordan, R. and Green, J.: A check-list of the extant Haptophyta of the world, Journal of the Marine Biological Association of the United Kingdom, 74, 149–174, 1994.

Jordan, R. and Kleijne, A.: Coccolithophores, chap. A classification system for living coccolithophores, pp. 83–105, Cambridge University Press, Cambridge, 1994.

Kang, L.-K., Lu, H.-M., Sung, P.-T., Chan, Y.-F., Lin, Y.-C., Gong, G.-C., and Chiang, K.-P.: The summer distribution of coccolithophores and its relationship to water masses in the East China Sea, Journal of Oceanography, 72, 883–893, 2016.

Kessler, W. S.: The circulation of the eastern tropical Pacific: A review, Progress in Oceanography, 69, 181–217, 2006.

Klaas, C. and Archer, D. E.: Association of sinking organic matter with various types of mineral ballast in the deep sea: Implications for the rain ratio, Global Biogeochem. Cycles, 16, 1116–, URL http://dx.doi.org/10.1029/2001GB001765, 2002.

Kleijne, A.: Distribution and malformation of extant calcareous nannoplankton in the Indonesian Seas, Marine Micropaleontology, 16, 293–316, 1990.

Langer, G. and Benner, I.: Effect of elevated nitrate concentration on calcification in *Emiliania huxleyi*, Journal of Nannoplankton Research, 30, 77–80, URL http://epic.awi.de/22502/, 2009.

Langer, G. and Bode, M.: CO_2 mediation of adverse effects of seawater acidification in *Calcidiscus leptoporus*, Geochemistry, Geophysics, Geosystems, 12, n/a–n/a, doi:10.1029/2010GC003393, URL http://dx.doi.org/10.1029/2010GC003393, q05001, 2011.

Langer, G., Geisen, M., Baumann, K.-H., Kläs, J., Riebesell, U., Thoms, S., and Young, J. R.: Species-specific responses of calcifying algae to changing seawater carbonate chemistry, Geochemistry, Geophysics, Geosystems, 7, n/a–n/a, doi:10.1029/2005GC001227, URL http://dx.doi.org/10.1029/2005GC001227, q09006, 2006.

Langer, G., Gussone, N., Nehrke, G., Riebesell, U., Eisenhauer, A., and Thoms, S.: Calcium isotope fractionation during coccolith formation in *Emiliania huxleyi*: Independence of growth and calcification rate, Geochemistry, Geophysics, Geosystems, 8, n/a–n/a, doi:10.1029/2006GC001422, URL http://doi.wiley.com/10.1029/2006GC001422, 2007.

Langer, G., Nehrke, G., Probert, I., Ly, J., and Ziveri, P.: Strain-specific responses of *Emiliania huxleyi* to changing seawater carbonate chemistry, Biogeosciences, 6, 2637–2646, URL http://www.biogeosciences.net/6/2637/2009/, 2009.

Langer, G., De Nooijer, L. J., and Oetjen, K.: On the role of the cytoskeleton in coccolith morphogenesis: The effect of cytoskeleton inhibitors, Journal of Phycology, 46, 1252–1256, 2010.

Langer, G., Probert, I., Nehrke, G., and Ziveri, P.: The morphological response of *Emiliania huxleyi* to seawater carbonate chemistry changes: an inter-strain comparison, Journal of Nannoplankton Research, 32, 29–34, 2011.

Langer, G., Oetjen, K., and Brenneis, T.: On culture artefacts in coccolith morphology, Helgoland Marine Research, 67, 359–369, doi: 10.1007/s10152-012-0328-x, URL http://link.springer.com/10.1007/s10152-012-0328-x, 2013.

Lavigne, H., Proye, A., and Gattuso, J.-P.: Package seacarb, Laboratoire d Océanographie de Villefranche (LOV) France., 2009.

Lecourt, M., Muggli, D. L., and Harrison, P. J.: Comparison of growth and sinking rates of non-coccolith- and coccolith-forming strains of *Emiliania huxleyi* (Prymnesiophyceae) grown under different irradiances and nitrogen sources, Journal of Phycology, 32, 17–21, doi:10.1111/j.0022-3646.1996.00017.x, URL http://dx.doi.org/10.1111/j.0022-3646.1996.00017.x, 1996.

Letelier, R. M., Karl, D. M., Abbott, M. R., and Bidigare, R. R.: Light driven seasonal patterns of chlorophyll and nitrate in the lower euphotic zone of the North Pacific Subtropical Gyre, Limnology and Oceanography, 49, 508–519, 2004.

Levitus, S., Antonov, J. I., Boyer, T. P., and Stephens, C.: Warming of the World Ocean, Science, 287, 2225–2229, doi:10.1126/science.287.5461.2225, URL http://science.sciencemag.org/content/287/5461/2225, 2000.

Lewis, E. and Wallace, D. W. R.: Program Developed for CO_2 System Calculations ORNL/CDIAC-105, Carbon Dioxide Information Analysis Centre, Oak Ridge National Laboratory, Laboratory, US Department of Energy, 1998.

Linschooten, C., Bleijswijk, J. D., Emburg, P. R., Vrind, J. P., Kempers, E. S., Westbroek, P., and Vrind-de Jong, E. W.: Role of the light-dark cycle and medium composition on the production of coccoliths by *Emiliania huxleyi* (Haptophyceae), Journal of Phycology, 27, 82–86, 1991.

Lueker, T. J., Dickson, A. G., and Keeling, C. D.: Ocean $p\mathrm{CO}_2$ calculated from dissolved inorganic carbon, alkalinity, and equations for K1 and K2: validation based on laboratory measurements of CO_2 in gas and seawater at equilibrium, Marine Chemistry, 70, 105–119, 2000.

Lyman, J. M., Good, S. A., Gouretski, V. V., Ishii, M., Johnson, G. C., Palmer, M. D., Smith, D. M., and Willis, J. K.: Robust warming of the global upper ocean, Nature, 465, 334–337, 2010.

Malinverno, E., Prahl, F., Popp, B., and Ziveri, P.: Alkenone abundance and its relationship to the coccolithophore assemblage in Gulf of California surface waters, Deep Sea Research Part I: Oceanographic Research Papers, 55, 1118–1130, doi:10.1016/j.dsr.2008.04.007, URL http://linkinghub.elsevier.com/retrieve/pii/S096706370800085X, 2008.

Malinverno, E., Maffioli, P., and Gariboldi, K.: Latitudinal distribution of extant fossilizable phytoplankton in the Southern Ocean: Planktonic provinces, hydrographic fronts and palaeoecological perspectives, Marine Micropaleontology, 123, 41–58, 2016.

Marsh, M.: Coccolith crystals ofPleurochrysis carterae: Crystallographic faces, organization, and development, Protoplasma, 207, 54–66–, URL http://dx.doi.org/10.1007/BF01294713, 1999.

Marsh, M., Ridall, A., Azadi, P., and Duke, P.: Galacturonomannan and Golgi-derived membrane linked to growth and shaping of biogenic calcite, Journal of Structural Biology, 139, 39–45, URL http://www.sciencedirect.com/science/article/pii/S1047847702005038, 2002.

Matsueda, H., Handa, N., Inoue, I., and Takano, H.: Ecological significance of salp fecal pellets collected by sediment traps in the eastern North Pacific, Marine Biology, 91, 421–431, 1986.

McIntyre, A. and Bé, A. W.: Modern coccolithophoridae of the atlantic ocean —I. Placoliths and cyrtoliths, 1967.

Medlin, L. K., Barker, G. L. A., Campbell, L., Green, J. C., Hayes, P. K., Marie, D., Wrieden, S., and Vaulot, D.: Genetic characterisation of *Emiliania huxleyi* (Haptophyta), Journal of Marine Systems, 9, 13–31, 1996.

Mehrbach, C., Culberson, C. H., Hawley, J. E., and Pytkowicz, R. M.: Measurement of the apparent dissociation constants of carbonic acid in seawater at atmospheric pressure, Limnology and Oceanography, 18, 897–907, doi:10.4319/lo.1973.18.6.0897, URL http://dx.doi.org/10.4319/lo.1973.18.6.0897, 1973.

Meier, K., Berger, C., and Kinkel, H.: Increasing coccolith calcification during CO2 rise of the penultimate deglaciation (Termination II), Marine Micropaleontology, 112, 1–12, 2014.

Menden-Deuer, S. and Lessard, E. J.: Carbon to volume relationships for dinoflagellates, diatoms, and other protist plankton, Limnology and Oceanography, 45, 569–579, 2000.

Millero, F. J., Chen, C.-T., Bradshaw, A., and Schleicher, K.: A new high pressure equation of state for seawater, Deep Sea Research Part A. Oceanographic Research Papers, 27, 255–264, doi:10.1016/0198-0149(80)90016-3, URL http://www.sciencedirect.com/science/article/pii/0198014980900163, 1980.

Milner, S., Langer, G., Grelaud, M., and Ziveri, P.: Ocean warming modulates the effects of acidification on *Emiliania huxleyi* calcification and sinking, Limnology and Oceanography, 61, 1322–1336, doi:10.1002/lno.10292, URL http://dx.doi.org/10.1002/lno.10292, 2016.

Monteiro, F. M., Bach, L. T., Brownlee, C., Bown, P., Rickaby, R. E. M., Poulton, A. J., Tyrrell, T., Beaufort, L., Dutkiewicz, S., Gibbs, S., Gutowska, M. A., Lee, R., Riebesell, U., Young, J., and Ridgwell, A.: Why marine phytoplankton calcify, Science Advances, 2, doi:10.1126/sciadv.1501822, URL http://advances.sciencemag.org/content/2/7/e1501822, 2016.

Müller, M. N., Antia, A. N., and La Roche, J.: Influence of cell cycle phase on calcification in the coccolithophore *Emiliania huxleyi*, Limnology and Oceanography, 53, 506–512, 2008.

Müller, M. N., Trull, T. W., and Hallegraeff, G. M.: Differing responses of three Southern Ocean Emiliania huxleyi ecotypes to changing seawater carbonate chemistry, Marine Ecology Progress Series, 531, 81–90, 2015.

Nielsen, M. V.: Growth, dark respiration and photosynthetic parameters of the coccolithophorid *Emiliania huxleyi* (Prymnesiophyceae) acclimated to different day lengthirradiance combinations, Journal of Phycology, 33, 818–822, doi:10.1111/j.0022-3646.1997.00818.x, URL http://dx.doi.org/10.1111/j.0022-3646.1997.00818.x, 1997.

Okada, H. and Honjo, S.: The distribution of oceanic coccolithophorids in the Pacific, Deep Sea Research and Oceanographic Abstracts, 20, 355 – 374, doi:https://doi.org/10.1016/0011-7471(73)90059-4, URL http://www.sciencedirect.com/science/article/pii/0011747173900594, 1973.

Okada, H. and Honjo, S.: Distribution of coccolithophores in marginal seas along the western Pacific Ocean and in the Red Sea, Marine Biology, 31, 271–285, 1975.

Okada, H. and McIntyre, A.: Seasonal distribution of modern coccolithophores in the western North Atlantic Ocean, Marine Biology, 54, 319–328, 1979.

Oviedo, A. M., Langer, G., and Ziveri, P.: Effect of phosphorus limitation on coccolith morphology and element ratios in Mediterranean strains of the coccolithophore *Emiliania huxleyi*, Journal of Experimental Marine Biology and Ecology, 459, 105–113, doi:10.1016/j.jembe.2014.04.021, URL http://www.sciencedirect.com/science/article/pii/S0022098114001142, 2014.

Paasche, E.: Roles of nitrogen and phosphorus in coccolith formation in *Emiliania huxleyi* (Prymnesiophyceae), European Journal of Phycology, 33, 33–42, doi:null, URL http://journals.cambridge.org/article_S0967026297001480, 1998.

Paasche, E.: A review of the coccolithophorid *Emiliania huxleyi* (Prymnesiophyceae), with particular reference to growth, coccolith formation, and calcification-photosynthesis interactions, Phycologia, 40, 503–529, URL http://dx.doi.org/10.2216/i0031-8884-40-6-503.1, 2001.

Paasche, E., Brubak, S., Skattebøl, S., Young, J. R., and Green, J. C.: Growth and calcification in the coccolithophorid *Emiliania huxleyi* (Haptophyceae) at low salinities, Phycologia, 35, 394–403, URL http://dx.doi.org/10.2216/i0031-8884-35-5-394.1, 1996.

Page, S., Hipkin, C. R., and Flynn, K. J.: Interactions between nitrate and ammonium in *Emiliania huxleyi*, Journal of Experimental Marine Biology and Ecology, 236, 307–319, URL http://www.sciencedirect.com/science/article/pii/S0022098198002123, 1999.

Pantorno, A., Holland, D. P., Stojkovic, S., and Beardall, J.: Impacts of nitrogen limitation on the sinking rate of the coccolithophorid *Emiliania huxleyi* (Prymnesiophyceae), Phycologia, 52, 288–294, 2013.

Pennington, J. T. and Chavez, F. P.: Seasonal fluctuations of temperature, salinity, nitrate, chlorophyll and primary production at station H3/M1 over 1989–1996 in Monterey Bay, California, Deep Sea Research Part II: Topical Studies in Oceanography, 47, 947–973, 2000.

Pierce, S., Smith, R., Kosro, P., Barth, J., and Wilson, C.: Continuity of the poleward undercurrent along the eastern boundary of the mid-latitude north Pacific, Deep Sea Research Part II: Topical Studies in Oceanography, 47, 811–829, 2000.

Popp, B. N., Prahl, F. G., Wallsgrove, R. J., and Tanimoto, J.: Seasonal patterns of alkenone production in the subtropical oligotrophic North Pacific, Paleoceanography, 21, 2006.

Prentice, K., Jones, T. D., Lees, J., Young, J., Bown, P., Langer, G., and Fearn, S.: Trace metal (Mg/Ca and Sr/Ca) analyses of single coccoliths by Secondary Ion Mass Spectrometry, Geochimica et Cosmochimica Acta, 146, 90–106, doi:10.1016/j.gca.2014.09.041, URL http://www.sciencedirect.com/science/article/pii/S0016703714005997, 2014.

Read, B. a., Kegel, J., Klute, M. J., Kuo, A., Lefebvre, S. C., Maumus, F., Mayer, C., Miller, J., Monier, A., Salamov, A., Young, J., Aguilar, M., Claverie, J.-M., Frickenhaus, S., Gonzalez, K., Herman, E. K., Lin, Y.-C., Napier, J., Ogata, H., Sarno, A. F., Shmutz, J., Schroeder, D., de Vargas, C., Verret, F., von Dassow, P., Valentin, K., Van de Peer, Y., Wheeler, G., Dacks, J. B., Delwiche, C. F., Dyhrman, S. T., Glöckner, G., John, U., Richards, T., Worden, A. Z., Zhang, X., and Grigoriev, I. V.: Pan genome of the phytoplankton Emiliania

underpins its global distribution, Nature, 499, 209–13, doi:10.1038/nature12221, URL http://www.ncbi.nlm.nih.gov/pubmed/23760476, 2013.

Richardson, K., Beardall, J., and Raven, J. A.: Adaptation of unicellular algae to irradiance: An analysis of strategies, New Phytologist, 93, 157–191, doi:10.1111/j.1469-8137.1983.tb03422.x, URL http://dx.doi.org/10.1111/j.1469-8137.1983.tb03422.x, 1983.

Ridgwell, A. and Zeebe, R. E.: The role of the global carbonate cycle in the regulation and evolution of the Earth system, Earth and Planetary Science Letters, 234, 299–315, doi:10.1016/j.epsl.2005.03.006, URL http://www.sciencedirect.com/science/article/pii/S0012821X05001883, 2005.

Robertson, J., Robinson, C., Turner, D., Holligan, P., Watson, A., Boyd, P., Fernandez, E., and Finch, M.: The impact of a coccolithophore bloom on oceanic carbon uptake in the northeast Atlantic during summer 1991, Deep Sea Research Part I: Oceanographic Research Papers, 41, 297 – 314, doi:http://dx.doi.org/10.1016/0967-0637(94)90005-1, URL http://www.sciencedirect.com/science/article/pii/0967063794900051, 1994.

Rosas-Navarro, A., Langer, G., and Ziveri, P.: Temperature affects the morphology and calcification of *Emiliania huxleyi* strains, Biogeosciences, 13, 2913–2926, doi:10.5194/bg-13-2913-2016, URL http://www.biogeosciences.net/13/2913/2016/, 2016.

Rosas-Navarro, A., Langer, G., and Ziveri, P.: Temperature effects on sinking velocity of different *Emiliania huxleyi* strains, PloS one, 13, e0194 386, URL https://doi.org/10.1371/journal.pone.0194386, 2018.

Rost, B. and Riebesell, U.: Coccolithophores and the biological pump: responses to environmental changes, in: Coccolithophores from molecular processes to global impact, edited by Thierstein, H. R. and Young, J. R., pp. 99–125, Springer-Verlag, Germany, 2004.

Rost, B., Zondervan, I., and Wolf-Gladrow, D.: Sensitivity of phytoplankton to future changes in ocean carbonate chemistry: current knowledge, contradictions and research directions, Marine ecology progress series, 373, 227–238, 2008.

Sáez, A. G., Probert, I., Geisen, M., Quinn, P., Young, J. R., and Medlin, L.: Pseudo-cryptic speciation in coccolithophores, Proceedings of the national academy of sciences of the united states of america, 100, 7163–7168, 2003.

Satoh, M., Iwamoto, K., Suzuki, I., and Shiraiwa, Y.: Cold stress stimulates intracellular calcification by the coccolithophore, *Emiliania huxleyi* (Haptophyceae) under phosphate-deficient conditions, Marine Biotechnology, 11, 327–333, 2009.

Schiebel, R., Brupbacher, U., Schmidtko, S., Nausch, G., Waniek, J. J., and Thierstein, H.-R.: Spring coccolithophore production and dispersion in the temperate eastern North Atlantic Ocean, Journal of Geophysical Research: Oceans, 116, doi:10.1029/2010JC006841, URL http://dx.doi.org/10.1029/2010JC006841, 2011.

Schlüter, L., Lohbeck, K. T., Gutowska, M. A., Gröger, J. P., Riebesell, U., and Reusch, T. B.: Adaptation of a globally important coccolithophore to ocean warming and acidification, Nature Climate Change, 4, 1024, 2014.

Schroeder, D. C., Biggi, G. F., Hall, M., Davy, J., Martinez, J. M., Richardson, A. J., Malin, G., and Wilson, W. H.: A genetic marker to separate *Emiliania huxleyi* (Prymnesiophyceae) morphotypes1, Journal of Phycology, 41, 874–879, doi:10.1111/j.1529-8817.2005.04188.x, URL http://doi.wiley.com/10.1111/j.1529-8817.2005.04188.x, 2005.

Sett, S., Bach, L. T., Schulz, K. G., Koch-Klavsen, S., Lebrato, M., and Riebesell, U.: Temperature modulates coccolithophorid sensitivity of growth, photosynthesis and calcification to increasing seawater pCO_2, PloS one, 9, e88 308, doi:10.1371/journal.pone.0088308, URL http://www.pubmedcentral.nih.gov/articlerender.fcgi?artid=3914986&tool=pmcentrez&rendertype=abstract, 2014.

Sharqawy, M. H., Lienhard, J. H., and Zubair, S. M.: Thermophysical properties of seawater: a review of existing correlations and data, Desalination and Water Treatment, 16, 354–380, doi:10.5004/dwt.2010.1079, URL http://www.tandfonline.com/doi/abs/10.5004/dwt.2010.1079, 2010.

Smith, H. E. K., Tyrrell, T., Charalampopoulou, A., Dumousseaud, C., Legge, O. J., Birchenough, S., Pettit, L. R., Garley, R., Hartman, S. E., Hartman, M. C., Sagoo, N., Daniels, C. J., Achterberg, E. P., and Hydes, D. J.: Predominance of heavily calcified coccolithophores at low $CaCO_3$ saturation during winter in the Bay of Biscay, Proceedings of the National Academy of Sciences of the U.S.A, 109, 8845–8849, 2012.

Smyth, T., Tyrrell, T., and Tarrant, B.: Time series of coccolithophore activity in the Barents Sea, from twenty years of satellite imagery, Geophysical Research Letters, 31, 2004.

Sorrosa, J. M., Satoh, M., and Shiraiwa, Y.: Low temperature stimulates cell enlargement and intracellular calcification of coccolithophorids, Marine biotechnology (New York, N.Y.), 7, 128–33, doi:10.1007/s10126-004-0478-1, URL http://www.ncbi.nlm.nih.gov/pubmed/15782289, 2005.

Stoll, H. M. and Schrag, D. P.: Coccolith Sr / Ca as a new indicator of coccolithophorid calcification and growth rate, Geochemistry, Geophysics, Geosys-

tems, 1, n/a–n/a, doi:10.1029/1999GC000015, URL http://dx.doi.org/10.1029/1999GC000015, 2000.

Stoll, H. M., Shimizu, N., Archer, D., and Ziveri, P.: Coccolithophore productivity response to greenhouse event of the Paleocene-Eocene Thermal Maximum, Earth and Planetary Science Letters, 258, 192–206, 2007.

Strickland, J. D. and Parsons, T. R.: A practical handbook of seawater analysis, Fisheries Research Board of Canada, 1972.

Thierstein, H. R. and Young, J. R.: Coccolithophores: from molecular processes to global impact, Springer Berlin Heidelberg, URL http://www.springer.com/978-3-540-21928-6, 2004.

Thunell, R., Pride, C., Ziveri, P., Muller-Karger, F., Sancetta, C., and Murray, D.: Plankton response to physical forcing in the Gulf of California, Journal of Plankton Research, 18, 2017–2026, 1996.

Triantaphyllou, M., Dimiza, M., Krasakopoulou, E., Malinverno, E., Lianou, V., and Souvermezoglou, E.: Seasonal variation in *Emiliania huxleyi* coccolith morphology and calcification in the Aegean Sea (Eastern Mediterranean), Geobios, 43, 99–110, URL http://www.sciencedirect.com/science/article/pii/S001669950900093X, 2010.

Tyrrell, T. and Young, J.: Coccolithophores, in: Encyclopedia of Ocean Sciences (Second Edition), edited by Steele, J. H., pp. 606 – 614, Academic Press, Oxford, second edition edn., doi:https://doi.org/10.1016/B978-012374473-9.00662-7, URL https://www.sciencedirect.com/science/article/pii/B9780123744739006627, 2009.

van Emburg, P., de Jong, E., and Daems, W.: Immunochemical localization of a polysaccharide from biomineral structures (coccoliths) of *Emiliania huxleyi*, Journal of Ultrastructure and Molecular Structure Research, 94, 246–259, URL http://www.sciencedirect.com/science/article/pii/0889160586900716, 1986.

Van Rijssel, M. and Gieskes, W. W. C.: Temperature, light, and the dimethylsulfoniopropionate (DMSP) content of *Emiliania huxleyi* (Prymnesiophyceae), Journal of Sea Research, 48, 17–27, 2002.

Verbeek, J. W.: Recent Calcareous Nannoplankton in the Southernmost Atlantic, Polarforschung, 59, 45–60, 1989.

von Dassow, P., Díaz-Rosas, F., Bendif, E. M., Gaitán-Espitia, J.-D., Mella-Flores, D., Rokitta, S., John, U., and Torres, R.: Overcalcified forms of the coccolithophore *Emiliania huxleyi* in high CO_2 waters are not pre-adapted to ocean acidification, Biogeosciences Discussions, 2017, 1–28, doi:10.5194/bg-2017-303, URL https://www.biogeosciences-discuss.net/bg-2017-303/, 2017.

Watabe, N. and Wilbur, K. M.: Effects of temperature on growth, calcification, and coccolith form in *Coccolithus huxleyi* (Coccolithineae), Limnology and Oceanography, 11, 567–575, doi:10.4319/lo.1966.11.4.0567, URL http://dx.doi.org/10.4319/lo.1966.11.4.0567, 1966.

Westbroek, P., Brown, C. W., van Bleijswijk, J., Brownlee, C., Brummer, G. J., Conte, M., Egge, J., Fernández, E., Jordan, R., Knappertsbusch, M., Stefels, J., Veldhuis, M., van der Wal, P., and Young, J.: A model system approach to biological climate forcing. The example of *Emiliania huxleyi*, Global and Planetary Change, 8, 27 – 46, doi:http://dx.doi.org/10.1016/0921-8181(93)90061-R, URL http://www.sciencedirect.com/science/article/pii/092181819390061R, 1993.

Winter, A. and Siesser, W. G.: Coccolithophores, Cambridge University Press, Cambridge, UK, 1994.

Winter, A., Henderiks, J., Beaufort, L., Rickaby, R. E. M., and Brown, C. W.: Poleward expansion of the coccolithophore Emiliania huxleyi, Journal of Plankton Research, 36, 316, doi:10.1093/plankt/fbt110, URL +http://dx.doi.org/10.1093/plankt/fbt110, 2014.

Wolhowe, M. D., Prahl, F. G., White, A. E., Popp, B. N., and Rosas-Navarro, A.: A biomarker perspective on coccolithophorid growth and export in a stratified sea, Progress in Oceanography, 122, 65 – 76, doi:10.1016/j.pocean.2013.12.001, URL http://www.sciencedirect.com/science/article/pii/S0079661113002292, 2014.

Young, J. R.: Variation in *Emiliania huxleyi* coccolith morphology in samples from the Norwegian EHUX experiment, 1992, Sarsia, 79, 417–425, doi:10.1080/00364827.1994.10413573, URL http://dx.doi.org/10.1080/00364827.1994.10413573, 1994.

Young, J. R. and Westbroek, P.: Genotypic variation in the coccolithophorid species *Emiliania huxleyi*, Marine Micropaleontology, 18, 5–23, URL http://www.sciencedirect.com/science/article/pii/037783989190004P, 1991.

Young, J. R. and Ziveri, P.: Calculation of coccolith volume and it use in calibration of carbonate flux estimates, Deep Sea Research Part II: Topical Studies in Oceanography, 47, 1679–1700, doi:10.1016/S0967-0645(00)00003-5, URL http://linkinghub.elsevier.com/retrieve/pii/S0967064500000035, 2000.

Young, J. R., Bergen, J. A., Bown, P. C., Burnett, J. A., Fiorentino, A., Jordan, R. W., Kleijne, A., Van Niel, B., Romein, A. T., and von Salts, K.: Guidelines for coccolith and calcareous nannofossil terminology, Palaeontology, 40, 875–912, 1997.

Young, J. R., Davis, S. A., Bown, P. R., and Mann, S.: Coccolith ultrastructure and biomineralisation, Journal of structural biology, 126, 195–215, 1999.

Young, J. R., Geisen, M., Cros, L., Kleijne, A., Sprengel, C., Probert, I., and Østergaard, J.: A guide to extant coccolithophore taxonomy, Journal of Nannoplankton Research, Special Issue 1, 1–125, 2003.

Young, J. R., Poulton, A. J., and Tyrrell, T.: Morphology of *Emiliania huxleyi* coccoliths on the North West European shelf – is there an influence of carbonate chemistry?, Biogeosciences Discussions, 11, 4531–4561, doi:10.5194/bgd-11-4531-2014, URL http://www.biogeosciences-discuss.net/11/4531/2014/, 2014.

Zeitzschel, B.: Primary productivity in the Gulf of California, Marine Biology, 3, 201–207, 1969.

Ziveri, P. and Thunell, R.: Coccolithophore export production in Guaymas Basin, Gulf of California: response to climate forcing, Deep Sea Research Part II: Topical Studies in Oceanography, 47, 2073–2100, doi:10.1016/S0967-0645(00)00017-5, URL http://linkinghub.elsevier.com/retrieve/pii/S0967064500000175, 2000.

Ziveri, P., Thunell, R. C., and Rio, D.: Export production of coccolithophores in an upwelling region: Results from San Pedro Basin, Southern California Borderlands, Marine Micropaleontology, 24, 335–358, 1995.

Ziveri, P., Baumann, K.-H., Böckel, B., Bollmann, J., and Young, J. R.: Coccolithophores: From Molecular Processes to Global Impact, chap. Biogeography of selected Holocene coccoliths in the Atlantic Ocean, pp. 403–428, Springer Berlin Heidelberg, Berlin, Heidelberg, doi:10.1007/978-3-662-06278-4_15, URL http://dx.doi.org/10.1007/978-3-662-06278-4_15, 2004.

Ziveri, P., de Bernardi, B., Baumann, K.-H., Stoll, H. M., and Mortyn, P. G.: Sinking of coccolith carbonate and potential contribution to organic carbon ballasting in the deep ocean, Deep Sea Research Part II: Topical Studies in Oceanography, 54, 659–675, URL http://www.sciencedirect.com/science/article/pii/S0967064507000409, 2007.

Ziveri, P., Passaro, M., Incarbona, A., Milazzo, M., Rodolfo-Metalpa, R., and Hall-Spencer, J. M.: Decline in coccolithophore diversity and impact on coccolith morphogenesis along a natural CO_2 gradient, The Biological Bulletin, 226, 282–290, URL http://www.biolbull.org/content/226/3/282.full, 2014.

Zondervan, I.: The effects of light, macronutrients, trace metals and CO2 on the production of calcium carbonate and organic carbon in coccolithophoresa review, Deep Sea Research Part II: Topical Studies in Oceanography, 54, 521–537, 2007.

Zondervan, I., Rost, B., and Riebesell, U.: Effect of CO_2 concentration on the PIC/POC ratio in the coccolithophore *Emiliania huxleyi* grown under light-limiting conditions and different daylengths, Journal of Experimental Marine Biology and Ecology, 272, 55–70, doi:10.1016/S0022-0981(02)00037-0, URL http://dx.doi.org/10.1016/S0022-0981(02)00037-0, 2002.